https://doi.org/10.15388/vu.thesis.352
https://orcid.org/0000-0002-8368-6188

VILNIUS UNIVERSITY

Mantas Žiaunys

Interaction of amyloidophilic molecules with protein amyloid fibrils

DOCTORAL DISSERTATION

Technological Sciences,
Chemical engineering (T 005)

VILNIUS 2022

This dissertation was written between 2018 and 2022 at Vilnius university.

Academic supervisor – Dr. Vytautas Smirnovas (Vilnius university, Technological sciences, Chemical engineering, T 005).

This doctoral dissertation will be defended in a public meeting of the Dissertation Defence Panel:

Chairman – Prof. Habil. Dr. Rolandas Meškys (Vilnius University, Technological sciences, Chemical engineering, T 005).
Members:
Dr. Rima Budvytytė (Vilnius University, Technological sciences, Chemical engineering, T 005).
Prof. Habil. Dr. Wojciech Dzwolak (University of Warsaw, Natural sciences, Chemistry, N 003).
Assoc. Prof. Dr. Vito Fodera (University of Copenhagen, Natural sciences, Biophysics, N 011).
Dr. Inga Matijošytė (Vilnius University, Technological sciences, Chemical engineering, T 005).

The dissertation shall be defended at a public meeting of the Dissertation Defence Panel at 10:00 on 29 September, 2022 in Room R401 of the Life Sciences Center (Vilnius University).
Address: Saulėtekio av. 7., Room No. R401, Vilnius, Lithuania
Tel. +370 607 14025; e-mail: mantas.ziaunys@gmc.vu.lt

The text of this dissertation can be accessed at the library of Vilnius University and on the website of Vilnius University:
www.vu.lt/lt/naujienos/ivykiu-kalendorius

https://doi.org/10.15388/vu.thesis.352
https://orcid.org/0000-0002-8368-6188

VILNIAUS UNIVERSITETAS

Mantas Žiaunys

Amiloidofilinių molekulių sąveika su baltymų amiloidinėmis fibrilėmis

DAKTARO DISERTACIJA

Technologijos mokslai,
Chemijos inžinerija (T 005)

VILNIUS 2022

Disertacija rengta 2018 – 2022 metais Vilniaus universitete.

Mokslinis vadovas – dr. Vytautas Smirnovas (Vilniaus universitetas, technologijos mokslai, chemijos inžinerija, T 005).

Gynimo taryba:
Pirmininkas – prof. dr. Rolandas Meškys (Vilniaus universitetas, technologijos mokslai, chemijos inžinerija, T 005).
Nariai:
Dr. Rima Budvytytė (Vilniaus universitetas, technologijos mokslai, chemijos inžinerija, T 005).
Prof. dr. Wojciech Dzwolak (Varšuvos universitetas, gamtos mokslai, chemija, N 003).
Dr. Vito Fodera (Kopenhagos universitetas, gamtos mokslai, biofizika, N 011).
Dr. Inga Matijošytė (Vilniaus universitetas, technologijos mokslai, chemijos inžinerija, T 005).

Disertacija ginama viešame Gynimo tarybos posėdyje 2022 m. rugsėjo mėn. 29 d. 10 val. Vilniaus universiteto Gyvybės mokslų centro R401 auditorijoje. Adresas: Saulėtekio al. 7, R401, Vilnius, Lietuva, tel. +370 607 14025; el. paštas mantas.ziaunys@gmc.vu.lt.

Disertaciją galima peržiūrėti Vilniaus universiteto bibliotekose ir VU interneto svetainėje adresu: https://www.vu.lt/naujienos/ivykiu-kalendorius

ACKNOWLEDGEMENTS

I would like to convey my appreciation to all people who have helped me throughout my PhD studies.

First, I would like to thank my supervisor Dr. Vytautas Smirnovas for the opportunity to work and grow my experience in the field of Amyloid research. During my studies he has provided an abundant amount of help and shared his experience and knowledge regarding all aspects of working with the complex system of protein aggregation.

I am also thankful to all my colleagues for their support throughout the years, especially Tomas Šneideris, Andrius Sakalauskas and Kamilė Mikalauskaitė. Their help has made it possible to achieve some seemingly impossible tasks and scientific results, as reflected by the sizable number of joint publications.

I would like to thank the entire Department of Biothermodynamics and Drug Design for a friendly atmosphere, as well as access and assistance in using several of their devices and equipment.

I am also thankful for all the collaborations, which have resulted in multiple joint publications, especially with Zigmantas Toleikis, Simona Strazdaitė, Martynas Talaikis, Gediminas Niaura, Lina Baranauskienė, Vytautas Petrauskas, Jekabs Fridmanis and Kristaps Jaudzems.

For the financial support I am grateful to Vilnius University and the Lithuanian Research Council.

Finally, my deepest gratitude goes to my family for their support and belief in me.

ABBREVIATIONS

Ab_{42}	Amyloid-beta (1-42)
AFM	Atomic force microscopy
ANS	8-anilino-1-naphthalenesulfonic acid
APP	Amyloid precursor protein
APTES	(3-aminopropyl)triethoxysilane
CR	Congo red
Dap	Dapoxyl
DMSO	Dimethyl sulfoxide
EEM	Excitation-emission matrix
FRET	Forster-resonance energy transfer
FTIR	Fourier-transform infrared spectroscopy
GPI	Glycosylphosphatydil inositol
GuHCl	Guanidine hydrochloride
GuSCN	Guanidine thiocyanate
HPLC	High-performance liquid chromatography
MB	Methylene blue
MoPrP	Mouse prion protein
PBS	Phosphate buffered saline
RPM	Rotations per minute
ThT	Thioflavin-T
TEM	Transmission electron microscopy
UV/Vis	Ultraviolet/Visible

CONTENTS/TURINYS

ABSTRACT

Amyloidogenic protein aggregation is linked with the onset and progression of multiple amyloidoses, including neurodegenerative Alzheimer‘s and Parkinson‘s diseases. Despite decades of intense research and countless experiments, there are still very few effective, disease-modifying drugs or treatments available. Coupled with the fact that the number of amyloid-related diseases is projected to further increase, this makes it vitally important to obtain a better understanding of the amyloid aggregation process, as well as search for potential anti-amyloid compounds.

In this work, the interaction between amyloidophilic molecules and protein amyloid fibrils was investigated using multiple approaches. First part of the study was dedicated towards understanding the relationship between environmental conditions and the resulting fibril types, as well as their affinity towards an aggregate-specific dye – thioflavin-T. The results indicated that amyloid proteins can form distinct fibrils even under identical conditions, with each type of aggregate having different ThT binding properties.

The second part of the study was dedicated towards understanding how different amyloidophilic molecules interact with protein aggregates. It was observed that there are multiple possible binding modes for such compounds, including ones not related to the surface of the amyloid fibril. Most importantly, the results displayed a correlation between fibril types, as well as solution ionic strength and the number of bound molecules. Lysozyme fibrils had the highest binding capacity and it was even further increased by raising the solution‘s ionic strength.

Using the knowledge obtained during these two approaches, it was investigated whether lysozyme amyloid fibrils could be used as a means of selectively separating anti-amyloid compounds from multiple complex mixtures. Analyzing the bound and non-bound compounds separately revealed that all molecules, which possess anti-amyloid properties, became bound to the lysozyme aggregates. These compounds could later be separated from the fibrils using three distinct methods and they were capable of inhibiting amyloid aggregation. This new method could potentially be used in future anti-amyloid drug screening protocols and aid in the discovery of potent, disease-modifying drugs.

Aim

To understand the interaction between amyloidophilic molecules and protein fibrils and apply this knowledge in screening of anti-amyloid compounds.

Objectives

1. To generate an array of different secondary structure and morphology fibrils from various amyloidogenic proteins.

2. To determine the relation between environmental conditions and resulting fibril type.

3. To examine different amyloid fibril and amyloidophilic molecule interaction affinities and binding modes.

4. To determine how environmental factors affect the interaction between amyloidophilic molecules and protein aggregates.

5. To examine the relationship between compound anti-amyloid activity and fibril-binding affinity.

6. To selectively separate potential anti-amyloid compounds from complex mixtures by utilizing compound-fibril interactions.

Scientific novelty

In this work, the complex mechanisms of amyloid formation and resulting fibril interactions with amyloidophilic compounds were investigated. Large scale protein aggregation assays were employed to determine the environmental condition and resulting fibril structure relationship. An extremely important observation during these screenings was the discovery of amyloid polymorphism existing even under identical environmental conditions. Both, prion protein (related to prionopathies), as well as alpha-synuclein (related to Parkinson‘s disease) were capable of forming structurally and morphologically distinct fibrils under a certain set of identical conditions and could be identified by differences in their amyloid-dye-binding properties. This provided new insight into the complex and unpredictable nature of amyloid aggregation.
Furthermore, it was investigated how the environmental conditions (both during fibril formation, as well as post-aggregation) determine amyloidophilic

molecules interactions with protein aggregates. It was observed that fibrils possess multiple possible binding sites for various compounds, with some binding modes only accessible during the aggregation process. The environment was also shown to be extremely important in modulating the compound-fibril affinity of certain amyloidophilic molecules, with ionic strength having the most significant effect.
Finally, it was observed that compounds, which possess anti-amyloid properties, have a high binding affinity towards the surface of amyloid fibrils. This specific binding was utilized to separate anti-amyloid compounds from varying complexity mixtures via the surface of lysozyme aggregates. The novel method proved to be exceptionally efficient at removing all aggregation-inhibiting molecules from each tested solution, which could then be separated by destabilizing the fibrils. This new method, based on fibril-compound interactions, opens up possibilities for large scale anti-amyloid drug screenings by separating effective molecules from various high complexity mixtures.

Defending statements:

1. The same sequence protein can form structurally distinct fibrils under identical experimental conditions.

2. Different structure amyloid fibrils have specific affinities towards amyloidophilic molecules.

3. Ionic strength has a significant effect on amyloid aggregation and fibril-compound interactions.

4. There are compound binding modes not specific to the amyloid surface structure.

5. Protein aggregation inhibitor molecules can be separated from complex solutions by utilizing their binding to the surface of amyloid fibrils.

1. LITERATURE OVERVIEW

1.1. Brief history of amyloids

The first recorded cases of amyloid-related disorders date back to the XVII century, where isolated instances of strange animal behaviour or peculiar starch-like deposits in tissues were observed. However, the true nature of these disorders was not discovered for a long time, with multiple hypotheses being raised and disproven, such as parasites, bacteria or viruses being the cause of the observed diseases. In 1854, Rudolph Virchow treated infected tissue with iodine and noted that these deposits obtained a pale blue colour, which was associated with the presence of starch/cellulose. These accumulations were then termed as "amyloid", based on the latin and greek words "amylum, amylon", which directly translate to "starch" [1]. In 1859, Friedreich and Kekule stated that amyloids do not possess carbohydrates and instead contain proteins. In 1922, H. Benhold discovered that amyloids could be stained with Congo red – a water soluble azo dye, which later became a standart for amyloid-disease diagnosis [2]. In 1927, the combination of Congo red and light microscopy revealed amyloid deposits in muscle tissue [1]. A couple of decades later, it was observed that low pH insulin solutions formed spherite precipitated, composed of radially oriented fibrils with lengths up to 400 nm [3]. In 1959, electron microscopy imaging displayed fibrous components in tissues obtained from different parts of the body, suggesting that amyloid aggregates may have diverse origins [4].

Over the past few decades, amyloids have received considerable attention and multiple revelations were made regarding their structure and function. In 1969, amyloid aggregate X-ray diffraction analysis revealed that such deposits consist of fibrous protein aggregates, which have beta-sheets arranged along the fibril axis, while the beta-strands which form them are perpendicular to it ("cross-beta" diffraction pattern) [2]. It was also shown that these aggregates are partially resistant to detergents and proteinases [5]. In 2006, a comprehensive review by Chiti and Dobson of a wide range of protein/peptide aggregation studies suggested a generic nature of amyloid fibril formation and their link to many human diseases [6]. In 2009, Knowles *et al.* proposed a unified theoretical framework describing the aggregation of proteins/peptides, which included nucleation, linear growth and secondary nucleation events [7]. In recent years even more progress has been made regarding amyloid formation tracking and resulting structure, including various staining and detection methods [8], reports of distinct secondary structures, as well as strain-specific morphological features and surface patterns [9,10]. A better

understanding of amyloids has also resulted in the discovery of potential drugs and treatment modalities [11], with over a hundred compounds currently undergoing clinical trials [12]. The first anti-amyloid drug for the treatment of transthyretin-related cardiomyopathy (Tafamidis) was approved by the FDA in 2019 [11] and the newest FDA-approved addition to anti-amyloid medications was Aduhelm, a monoclonal antibody directed to aggregated forms of Alzheimer's disease-related amyloid-beta [13].

1.2. Amyloid-related disorders

Currently, there are over 30 known disease-related amyloid proteins/peptides, whose aggregation leads to a wide variety of amyloidoses, including neurodegenerative Alzheimer‘s or Parkinson‘s diseases (Table 1) [14,15]. Despite forming similar fibrillar structures, there is no definitive amino acid sequence that can be linked with certain protein tendencies to form fibrillar aggregates [16]. As an example, the Alzheimer‘s disease-related amyloid-beta peptide is composed out of 42 amino acid residues, while the microtubule-associated Tau protein, which is implicated in Alzheimer‘s disease and tauopathies, has a 10-fold higher number of residues [14]. The initial native structure of amyloidogenic proteins also does not appear to be a determining factor, as they can be intrinsically disordered (amyloid-beta, tau, alpha-synuclein), have a high alpha-helical (insulin, prion protein) or beta-sheet (immunoglobulin light chain, transthyretin) content and have a mix of secondary structures (lysozyme, lactoferrin) [14]. It has even been reported that short peptides can form amyloid-like aggregates [17], with some being as little as dipeptides (diphenylalanine) [18]. It was also hypothesized that every single protein/peptide may be able to aggregate into fibrils if placed under specific conditions and that this process may be a global intrinsic property [16].

Similarly to the high variety of protein/peptide sequences and structures, the aggregates cause a wide variety of disorders, which differ in type of onset or transmission, localization and symptom severity [14]. Amyloid-related diseases can be divided into sporadic (Alzheimer‘s disease [19], Parkinson‘s disease [20]), hereditary (Huntington disease [21], fatal insomnia [22]), transmissible (kuru [23]) or iatrogenic (injection-localized amyloidosis [24]). Certain disorders require years for the symptoms to emerge (Alzheimer‘s disease, Parkinson‘s disease [19,20]), others are relatively fast-acting (Creutzfeldt-Jakob disease [25]), while some are localized and do not pose significant life-threatening complications (injection-localized amyloidosis [24]). However, despite years of research and countless studies, there are still

very few drugs or cures available, with only symptomatic treatments for certain disorders [26].

Table 1. Examples of amyloidogenic proteins/peptides, number of their respective amino acid residues, secondary structures and associated diseases (based on [14]).

Protein/peptide	Number of residues	Structure	Associated diseases
Amyloid-beta	40 or 42	Intrinsically disordered	Alzheimer‘s disease
Alpha-synuclein	140	Intrinsically disordered	Parkinson‘s disease Multiple system atrophy
Prion protein	208	Intrinsically disordered N-terminus, three alpha-helices and one short beta-sheet	Creutzfeldt-Jakob disease Fatal insomnia Gerstmann-Straussler-Scheinker disease
Tau protein	352-441	Intrinsically disordered	Pick disease Progressive supranuclear palsy Corticobasal degeneration
Transthyretin	127	Beta-sheets	Senile systemic amyloidosis
Immunoglobulin light chain	~100	Beta-sheets	Light-chain amyloidosis
Lysozyme	130	Alpha helices and beta-sheets	Lysozyme amyloidosis
Insulin	51	Alpha-helices	Injection-localized amyloidosis

1.3. Cures and treatments

The search for anti-amyloid compounds has led to a wide variety of candidates, with various mechanisms of action, including direct aggregation inhibition, neuroprotection, anti-inflammation and others [12]. The compounds in question range from small molecules [27,28] all the way to monoclonal antibodies [29] or complex drug mixtures [12]. However, despite over a hundred possible treatments being in various stages of clinical trials, very few are able to pass them, with most ending as a failure [26,30,31] (Figure 1). This, in turn, has not allowed to slow down the ever-increasing number of patients afflicted with amyloid-related disorders [32,33], which makes it vitally important to find an effective treatment or cure.

Currently, many natural compounds are being investigated for their anti-amyloid activity, with many successful demonstrations of significantly reduced aggregation rates or resulting aggregate toxicity [34–36]. Multiple classes of compounds found in various plant species or their derivatives were reported to have either a direct or indirect effect on amyloid formation and accumulation. Acetylcholinesterase inhibition (related to the cholinergic hypothesis in Alzheimer's disease) was achieved with alkaloids (physostigmine, galantamine, huperzine), terpenoids (1,8-cineole, α-pinene) and shikimate-derived compounds (linarin, tilianin). Inhibition of proteolytic enzymes, involved in the formation of amyloid-beta peptides was observed with polyketides (hispidin, xestosaprol), terpenoids (withanolide, asiatic acid) and alkaloids (dictazole A, bastadin 9). Molecules promoting anti-aggregation and aggregate clearance included shikimate-derived compounds (curcumin, fisetin, chrysin), terpenoids (retinol, β-carotene) and alkaloids (nicotine, melatonin) [28]. Several of these molecules were also shown to possess antioxidant, as well as neuro-regenerative properties, which help in reducing amyloid-related neuronal damage [28]. Despite this large range of potential anti-amyloid compounds, only a few are currently FDA-approved for treatment of amyloidoses (tafamidis, daratumumab, patisiran and inotersen) (source: U.S. Food and Drug Administration).

One of the many possible reasons for such a high level of failed clinical trials is the difference between conditions during anti-amyloid compound screenings *in vitro* and the environment *in vivo*. A factor that has received minimal attention is the solution's ionic strength, which is known to modulate both the rate of amyloid formation, as well as the structure of formed aggregates [37–39]. Due to this reason, part of my work was dedicated towards obtaining a better understanding of how the solution's ionic strength modulates the effectiveness of a well-known anti-aggregation compound - epigallocatechin-3-gallate (Appendix Publication 6).

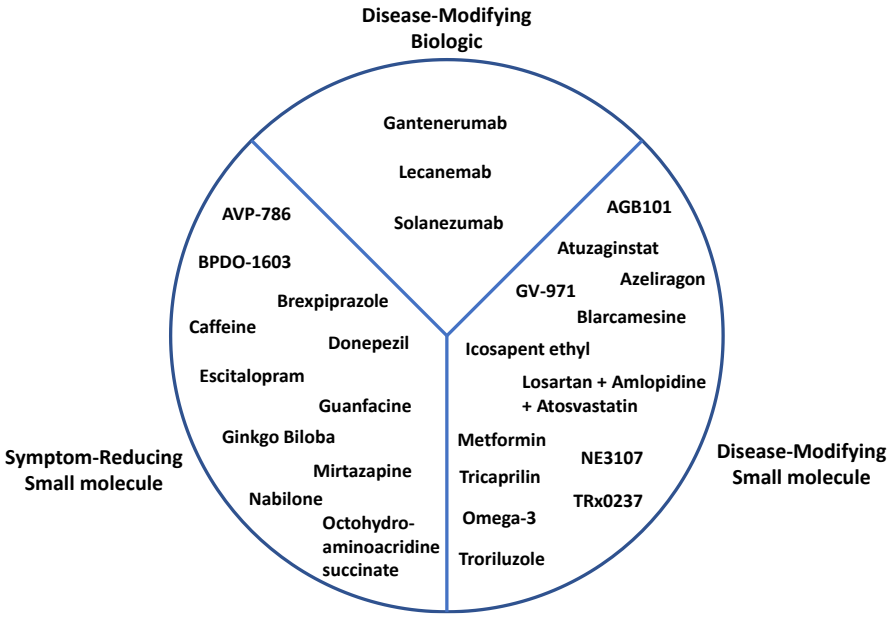

Figure 1. Agents in phase 3 clinical trials for treatment of Alzheimer's disease (based on [31]).

1.4. Mechanism of amyloid formation

Protein/peptide misfolding and association into fibrillar structures proceeds through multiple stages (Figure 2). The first step in amyloid aggregation is primary nucleation – a process during which native protein/peptide molecules misfold and assemble into a stable, β-sheet-rich nucleus [40,41]. The probability of such a transition depends on both the environment, as well as the protein/peptide itself. Factors which increase the likelihood of misfolding (higher temperature [42], presence of denaturants [43], point mutations in the amino acid sequence [44]), as well as conditions which facilitate a higher probability of protein/peptide interactions (agitation/mixing [45], higher protein/peptide concentration [46], charge-shielding by ions [47]) reduce the lag time of primary nucleation. The formation of an amyloid nucleus also depends on the minimum number of proteins/peptides, at which it becomes stable. This number has been reported to range from two to several dozen and depends highly on the protein/peptide in question [48–50].

Once a stable nucleus is formed, it can then incorporate other, homologous protein/peptide molecules into its structure and elongate into a protofibrillar aggregate. The process of elongation occurs at the ends of the fibrillar structure, which act as both a catalyst and template for the conversion of native

protein/peptide molecules [51–53]. This step proceeds at a considerably faster rate than primary nucleation and is also modulated by factors, which decrease the energy barrier required for protein/peptide misfolding and which increase the probability of interactions between fibril ends and protein/peptide molecules [43]. The elongated protofibril strands then associate into a mature fibril and the number of such strands and how they intertwine determine the fibril‘s morphological properties [54–56].

When amyloid fibrils reach a critical length, they can experience fragmentation – a process during which the aggregate breaks into two shorter fibrils, each with its own aggregation-catalysing ends. The incidence of fragmentation depends on both the structural stability of the aggregate, as well as the environmental conditions [57]. In some cases, they can reach lengths up to several micrometers, if the protein/peptide is capable of forming highly stable fibrillar structures and they are not affected by agitation or shear forces. In other cases, the aggregates have such a low level of stability that they readily fragment even under quiescent conditions [58]. This process is a substantial contributing factor to the exponential growth phase in amyloid formation, as each fragmentation event essentially doubles the number of available fibril ends for the same number of aggregated protein/peptide molecules. This event may also play a role in the overall toxicity of amyloids, as a higher fragmentation rate can lead to shorter fibrils, which can both migrate easier and may potentially be more toxic than their highly elongated counterparts [59].

Another process, which occurs once amyloid fibrils form, is surface-mediated nucleation (also referred to as secondary nucleation) [60–62]. During this step, the surface of aggregates acts as a catalyst for the formation of new amyloid nuclei. Unlike elongation at fibril ends, this process does not template the aggregate‘s structure onto the nuclei, but only increase their probability of formation [63]. The type of nuclei that forms is governed by the environmental conditions, similarly to that of primary nucleation [41,64,65]. This process gains prevalence as more fibrils form and is also a substantial contributing factor during the exponential growth phase in amyloid formation.

In addition to this basic mechanism of amyloid formation, there is also a complex transitory step between the native protein and stable amyloid nuclei. It is presumed that these intermediate species form through several misfolding and association steps, however, their unstable and relatively quick structural transition has not allowed to gain a deeper insight into this process [66–68]. In some cases, such as with insulin, it was even shown that some forms of these intermediate species were capable of binding amyloid-specific dye molecules [69]. Due to an insufficient understanding of such an important

transitory step in amyloid formation, part of my work was dedicated towards obtaining a better understanding of insulin aggregation intermediate species and their effect on the final fibril structure (Appendix Publication 1).

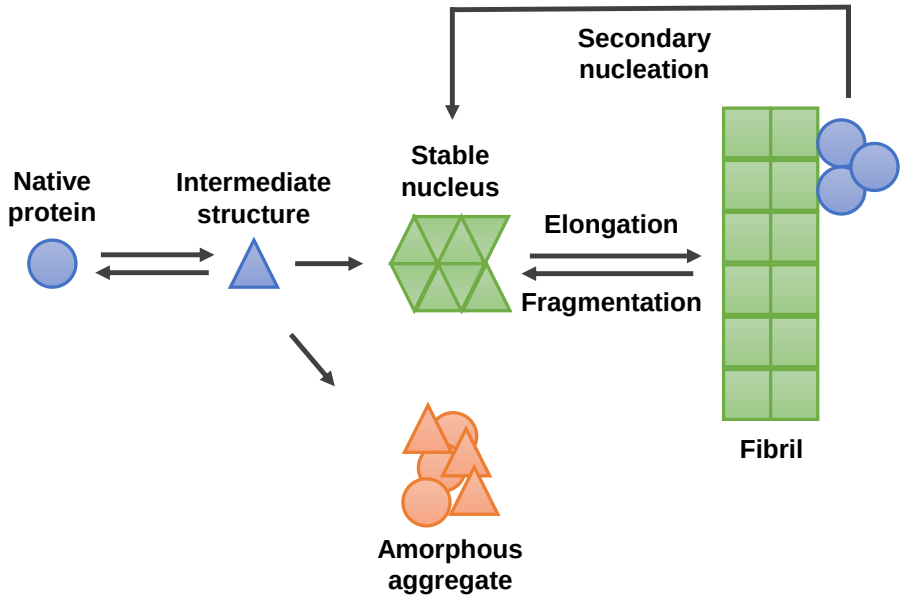

Figure 2. Basic mechanism of amyloid fibril formation from native state proteins and secondary aggregation processes.

1.5. Fibril secondary structure and morphology

In general, the secondary structure of amyloid fibrils is considered to be composed out of intermolecular beta-sheets and unstructured parts, regardless of the initial structure of the native precursor protein. However, the length of the beta-strands and their placement in the structure of amyloid fibrils is a highly variable parameter. For most proteins, only a specific section of the amino acid sequence is included in the highly-structured beta-sheet core [5,70–73]. The sequence and size of this beta-sheet core depends on the fibril-forming protein and can range from several amino acids to over a hundred [72,74].

Analysis of amyloid fibril secondary structures by Fourier-transform infrared spectroscopy has revealed that there exists a diverse distribution of possible hydrogen bonding types, as well as various turn/loop motifs [75,76]. It has even been reported on a few occasions that certain fibril aggregates may have cross-alpha [77], or beta-solenoid [78,79] motives in their structure.

Overall, the varying fibril core size, different secondary structure motifs and their distribution in relation to one another cause the high structural diversity of amyloid fibrils, which makes amyloid research a complex task [80].

Apart from the highly diverse secondary structure of amyloid fibrils, they also possess specific morphological features. The aggregates can be completely linear or have branches, they can be twisting or straight and have varying lengths from nanometers to micrometers [81,82]. Clumping into large clusters by binding to one another at segments or lateral association are also a common feature of amyloid fibrils, especially *in vivo* where they form massive deposits [83,84]. The fibril structure itself can have periodicity, arising from twisting between protofilaments [85] or be completely crystalline and have no discernible pattern [86]. As with amyloid secondary structures, fibril morphology does not have a set relation to the initial precursor protein [87].

Over the course of amyloid studies, it has been observed that amyloidogenic proteins/peptides are capable of forming multiple distinct fibrillar structures from the same initial protein/peptide, depending on the environmental conditions or point mutations in the amino acid sequence [85,87,88]. This polymorphism is associated with different onset times, rates of propagation and cytotoxic effects during different amyloid-related disorders. As an example, the aggregation of prion proteins can cause multiple distinct disorders, including Creutzfeldt-Jakob disease, Gerstmann–Sträussler–Scheinker syndrome, fatal familial insomnia and Kuru [89,90].

Interestingly, while the formation of structurally and morphologically distinct aggregates under different conditions is a widely reported and well-known fact, there have recently been reports indicating that this event may occur under identical conditions. It has been shown that amyloid-beta can form up to eleven morphologically different fibrils under the same conditions (Figure 3) [87], which have specific periodicity patterns. It was also reported that alpha-synuclein forms a mixture of different morphology aggregates *in vitro* (Figure 3) [86]. Considering that two of the most prevalent disease-related proteins/peptides display polymorphism under identical conditions, it is possible that this feature extends to other amyloidogenic proteins as well.

Since this phenomenon was identified in only a few experiments, it is still unclear as to how far such polymorphism extends to other amyloid proteins. In addition, these observations were made on a limited number of environmental conditions, further emphasizing a need for additional examinations. For this reason, a significant part of my work was committed to explore prion protein and alpha-synuclein polymorphism under identical

conditions, using a range of different temperature, protein concentration and solution ionic strength conditions. (Appendix Publications 3, 4 and 7).

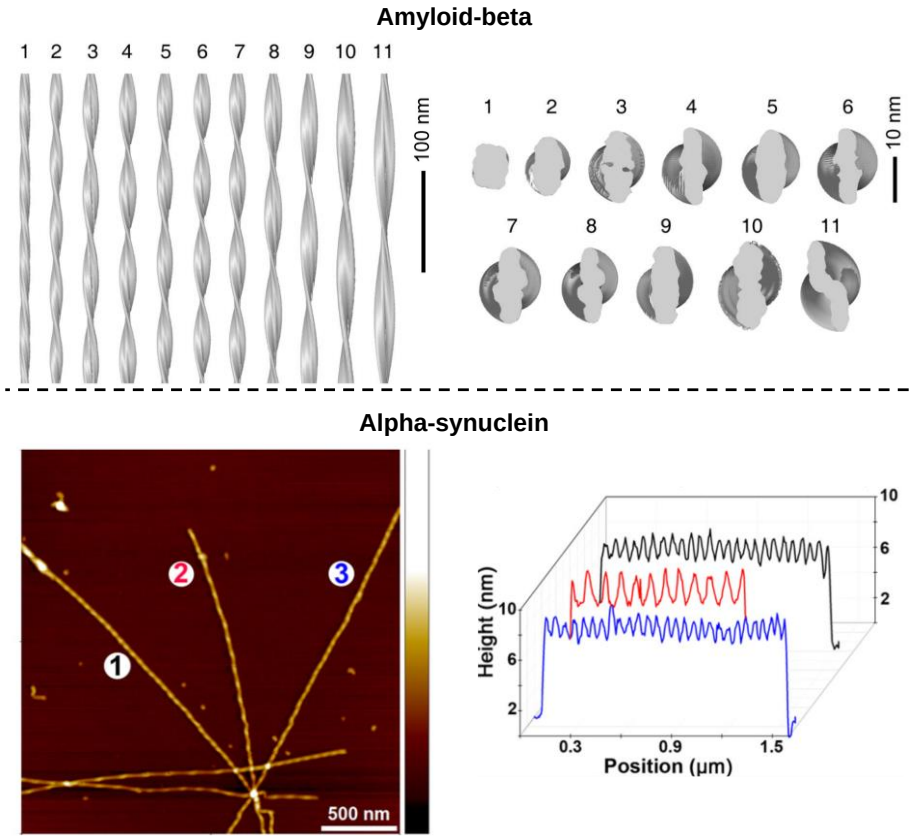

Figure 3. Amyloid-beta (1-40) and alpha-synuclein amyloid fibril polymorphism (adapted from [87] and [86]).

1.6. Fibril stability

One parameter that is prevalent for most amyloid fibrils is their relatively extreme stability against multiple environmental factors. Certain conditions which would result in a complete denaturation of the initial native protein appear completely ineffective at altering the state of their corresponding amyloid fibrils. These aggregates have been shown to withstand temperatures above the boiling point of water [91], high concentrations of salts and denaturants [43,92], various forms of agitation, including sonication [93], as well as pressures ranging to several megapascals [69]. The beta-sheet cores of such aggregates are also immune to digestion by proteinase K, which only affects the unstructured parts of the fibrils [5].

All of these factors taken together make it extremely difficult to eliminate aggregates that have already formed. *In vitro*, the materials and methods used to disassemble amyloid fibrils are highly concentrated denaturant solutions (Figure 4) [63] (urea, guanidinium hydrochloride or guanidinium thiocyanate), significant changes to solution pH value [55,94] or organic solvents [95]. Since none of these methods can be applied *in vivo*, there is an ongoing effort to find compounds to either destabilize the structure of amyloid fibrils [96,97] or to prevent their further growth and propagation [98]. There are also several non-invasive techniques being developed, such as scanning ultrasound, light therapy and electric fields, that may disrupt the high-stability aggregates, cause their disassembly or prevent their formation [99].

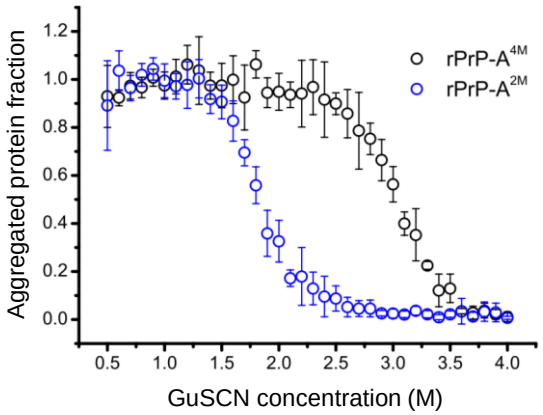

Figure 4. Prion protein fibril stability against denaturation by GuSCN, when the fibrils are prepared under two different denaturant concentrations (2 M (blue) or 4 M (black) guanidine hydrochloride) (adapted from [63]).

1.7. Amyloid proteins used in this work

Amyloid-beta (1-42) is a peptide associated with the onset and progression of Alzheimer's disease. It is considered that the short peptide is the result of proteolytic processing of the amyloid precursor protein (APP) [100]. In its native state, it is reported to play several possible physiological functions, including protection from infections, blood-brain barrier maintenance and synaptic function regulation [101]. However, its aggregates are implicated in causing the loss of synaptic signaling, production of reactive oxygen species and mitochondria dysfunction, as well as neuroinflammation and neuronal loss [102]. *In vitro*, its aggregation into amyloid fibrils is very rapid and can occur even under room temperature, at physiological conditions with no

agitation [103,104]. This is both a positive and negative during experimental procedures involving amyloid-beta. On one hand, the aggregation reactions can be completed under a relatively short time and monitored without the need to use non-physiological conditions, such as elevated temperatures or denaturants. On the other hand, both the purification and handling of the peptide are quite complicated, as these procedures have to account for its rapid spontaneous aggregation [105].

Alpha-synuclein fibrillar aggregates are related to the second most common neurodegenerative disease in humans (Parkinson's disease). The 140-residue presynaptic protein, which is typically found in soluble or membrane-associated fractions in the brain, aggregates into structures termed Lewy bodies and Lewy neurites [85]. The relative abundance of such structures in patients suffering from Parkinson's disease has implicated the protein and its aggregates as one of the major causes of the disease [106]. *In vitro*, alpha-synuclein readily forms fibrils with multiple distinct morphological and secondary structure features, depending on the environmental conditions and point mutations [107]. Compared to amyloid-beta, its aggregation under physiological conditions is significantly slower and requires a considerably higher protein concentration [108]. Alpha-synuclein can also undergo liquid-liquid phase separation, which affects the nucleation process [109] and its aggregation is influenced heavily by liquid-air, as well as liquid-hydrophobic-surface interfaces [110].

Prion proteins are cell-surface glycoproteins, attached to the plasma membrane through a glycosylphosphatydil inositol (GPI) anchor. It is considered to play a role in several physiological functions, such as copper homeostasis, neuroprotection, stem cell renewal and certain memory mechanisms [111]. Its aggregation into fibrils with distinct morphological and structural features (strains) is associated with multiple disorders (Creutzfeldt-Jakob disease, Gerstmann–Straussler–Scheinker syndrome, fatal familial insomnia, kuru [23,25]), including one of the first discovered animal neurodegenerative diseases – scrapie [112]. *In vitro*, spontaneous prion protein aggregation is carried out with the use of denaturants, such as urea [113] or guanidine hydrochloride [114], which differs from both previously described amyloid-beta and alpha-synuclein. It has also been observed that prion protein aggregates, isolated from infected animals, have a significantly larger beta-sheet core when compared to fibrils generated *in vitro* [5]. This suggests that there may be a correlation between protein aggregate infectivity and their secondary structure or that there are certain unknown factors necessary for infective fibril generation.

Insulin is a small polypeptide hormone, composed of two 21 and 30 amino acid chains, connected by two disulfide bridges. *In vivo* it acts as a hormone for the regulatory function of carbohydrate, fat and protein metabolism [115]. Its aggregation into amyloid fibrils is associated with localized amyloidosis at the site of repeat insulin injections [14]. Unlike with the previously mentioned neurodegenerative-disease related proteins/peptides, insulin aggregation in patients is a very rare occurrence and does not cause fatal complications [116]. Its aggregation *in vitro* is usually induced by elevated temperatures, low or neutral pH conditions and/or agitation [117,118]. Depending on the environmental conditions, it can exist in a number of oligomeric states, which affect both the mechanism of aggregation and the resulting aggregate types [119,120]. Due to its wide availability, it is often used in amyloid studies to gain mechanistic insight [121], as well as to test potential anti-amyloid compounds [98,122,123].

Lysozyme is a single chain, 129 amino acid antimicrobial protein, which is abundantly (up to 1 mg/mL) found in the blood, liver, tears, saliva and mucosal surfaces. It is also present in macrophages, neutrophils and dendritic cells and plays a critical role in the host‘s defence [124]. The structure and certain functions of lysozyme, such as the ability to hydrolyze bacterial cell wall peptidoglycans, is conserved among various species in the animal kingdom [124]. Its aggregation is linked with a slow progressing and rare hereditary lysozyme amyloidosis, which causes multiple organ dysfunction [125]. Due to its wide availability, relatively low purification costs and close relation to human lysozyme, hen egg-white lysozyme (HEWL) is often used in amyloid studies [126]. *In vitro*, it can form aggregates in the presence of high denaturant concentrations, low pH values and in certain organic solvents, such as ethanol [92,127].

1.8. Amyloidophilic molecules

From the initial observation of amyloid fibrils binding specific compounds, such as iodine or Congo red [2], there have been many discoveries of molecules that associate with protein fibril structures. Arguably the two most important amyloidophilic molecules is the aforementioned Congo red – a benzidine-based anionic diazo dye [128] and thioflavin – a benzothiazole salt [129]. Their interaction with amyloid fibrils results in changes to their absorbance and fluorescence spectra, which have been used as a hallmark in protein aggregation studies [8,130]. Considering the vastly different structures of Congo Red and thioflavin-T (ThT), as well as other molecules that are known to bind to amyloids, such as Methylene blue [131] or Dapoxyl [132],

it is quite clear that amyloid aggregates possess a range of possible binding modes towards various distinct compounds (Figure 5).

Molecular docking studies have shown that many aggregation-inhibiting compounds are also capable of binding to aggregation intermediates or the fibrils themselves [133–135]. Even ThT and Congo red were proposed to have several unique binding modes, with some reports suggesting up to six distinct sites on the fibril surface [136–138]. It was even hypothesized that fibrils may have certain binding sites or cavities [138], which are only accessible during the aggregation process. ThT has also been shown to have distinct affinity towards different amyloid fibrils, formed from the same precursor protein [139]. Taken together, this suggests that amyloid fibrils can facilitate a vast array of different structure molecule binding and this factor relates to their secondary structure and morphology.

Despite reports of such a significant number of binding modes and fibril associations with different molecules, there is limited information on how the environmental conditions affect these interactions. There is also a lack of knowledge regarding the relationship between amyloid fibril surface structural motifs and their ability/capacity to bind different types of compounds. Since this information would be beneficial to both the application of amyloid-specific dyes, as well as for the search of potential anti-aggregation compounds, a significant portion of my work was dedicated towards this particular area of research (Appendix Publications 2, 5, 8 – 10).

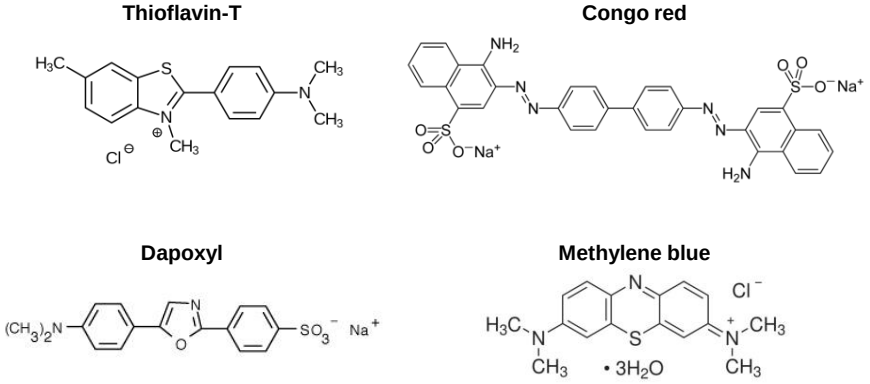

Figure 5. Structures of thioflavin-T, Congo red, Dapoxyl and Methylene blue.

2. METHOD OVERVIEW

2.1. Induction of fibrillization

In order to induce amyloid fibril formation from native state proteins/peptides in a reasonable time frame, it is necessary to create conditions, which destabilize the structure of the protein/peptide and increase its chance of misfolding. There are multiple conditions which can achieve this and they usually depend on the protein/peptide in question, as they each have specific pI values, stabilities and solubilities. In the case of insulin, acidic environments and elevated temperatures are typically used [118]. For lysozyme, denaturing agents, such as guanidine hydrochloride are employed to destabilize its highly stable structure [127]. Prion proteins also require similar conditions as lysozyme [63]. Intrinsically disordered alpha-synuclein and amyloid-beta, on the other hand, readily undergo aggregation without denaturants and at physiological conditions [87,140]. In all cases, agitation can be used to speed up the reaction, as it both causes protein/peptide destabilization and also fragments the formed fibrils, creating new aggregation centers.

2.2. Fibrillization tracking

One of the most commonly used means of tracking amyloid fibril formation is thioflavin-T. When protein aggregates are formed, ThT binds to their surface and attains a locked conformation, which significantly increases its fluorescence quantum yield and red-shifts the excitation and emission wavelengths [141]. Usually the dye concentration used is in the range from 10 to 100 μM, depending on the reaction length (as ThT can undergo hydroxylation at neutral or basic pH and higher temperatures [142]) and the concentration of protein used. An insufficient concentration of ThT can skew the experimental results, if there are no non-bound molecules available while aggregation is still proceeding, while a large surplus of the dye might cause an inner filter effect and reduce the fluorescence signal intensity. Bound-ThT excitation wavelength is 440 – 450 nm, with emission being monitored at 480 – 490 nm, although the maximum excitation and emission wavelengths can vary based on the binding modes present on the fibril surface. In general, if the solution contains a relatively homogenous distribution of aggregates, ThT fluorescence intensity correlates to the concentration of aggregates linearly and can be used as a quantitative measure of the concentration of proteins in their aggregated state.

2.3. Kinetic data analysis

Data collected during fibrillization tracking has to be analyzed in order to obtain information regarding the aggregation reaction, which includes lag time, aggregation half-time and rate of fibrillization. In this work, kinetic data was analyzed using Origin software by applying either a Boltzmann sigmoidal fit or a linear fit. In cases when aggregation proceeded spontaneously, the aggregation reaction curves were sigmoidal. For this type of data, a Boltzmann sigmoidal fit was used, which provided parameters that could then be used to calculate the lag time (time required for the protein to form the first nuclei, which can be detected with a ThT-assay), the half-time of aggregation (a point in time where the quantity of aggregated and non-aggregated proteins is equal) and the apparent rate constant at the half-time point). If aggregation proceeded without a lag phase, the half-times and apparent rate constants were calculated by applying a linear fit between the 40% and 60% of maximum signal intensity values and extrapolating the 50% time and slope values.

2.4. Fourier-transform infrared spectroscopy

Fourier-transform infrared spectroscopy is used to get insight into the secondary structure of amyloid fibrils by analyzing the Amide I/I' band of the infrared spectrum [143,144]. In order to achieve a high quality spectrum and to prevent a H_2O-specific band from overlapping with the Amide I/I' band, the generated aggregates are centrifuged and resuspended into D_2O multiple times to remove H_2O and to reach a relatively high protein concentration. After collecting a sufficient number of interferograms, the Amide I/I' band can be analyzed for fibril structural features. The peaks present in the region provide information about the presence of different types of hydrogen bonding, which allows us to identify nuances in secondary structures. The spectra can then be used to compare distinct samples for structural similarities and differences.

2.5. Atomic force microscopy

Atomic force microscopy (AFM) is used as a means of identifying amyloid aggregate morphological features, such as height, width, length and periodicity patterns [144]. Due to its high sensitivity, it can detect nanometer sized differences on the surface of aggregates and thus can be applied to detect and categorize distinct amyloid fibrils. Scanning a relatively large mica surface with adsorbed aggregates can provide a global overview on the variety

of fibrils present in the sample and allow to calculate the values and distributions of the aforementioned parameters. It can also be used to determine if fibrils have a tendency to form large fibrillar clusters or if the aggregates are prone towards lateral association. Unlike ThT or FTIR assays, which give an average overview of the sample as a whole, AFM provides single-molecule data, which allows to determine the heterogeneity of the fibrils present in the sample.

2.6. Fluorescence and absorbance spectroscopy

Changes in sample fluorescence emission intensity or the maximum positions of excitation and emission wavelengths, as well as differences in absorbance spectra can be used as a means of determining if the compound in question interacts with other molecules or binds to amyloid fibrils [8]. To compare if such interactions exist, sample excitation-emission matrices and absorbance spectra can be scanned before and after combining one compound with another or with amyloid fibrils. If a shift in the signal or maximum positions is detected, it can be assumed that there is an interaction between the combined molecules. It is also possible to detect if such interactions cause molecule sedimentation or aggregate clumping by measuring the changes to solution optical density or right-angle light scattering at 600 nm.

2.7. Amyloid fibril destabilization

Amyloid fibrils can be destabilized using several approaches, all of which include drastically changing the fibril environmental conditions. One commonly used method is to resuspend the aggregates into a concentrated denaturant solution. In this case, high molarity urea, guanidine hydrochloride or guanidine thiocyanate are used. This method is also used as an assay to determine amyloid fibril stability [63], by resuspending the aggregates into a range of denaturant concentrations and determining the point at which they break apart into monomers. Another method is to drastically change the solution's pH value to a point where fibrils begin to disassemble. As an example, insulin aggregates easily dissociate when the pH is changed from acidic to neutral/basic [55,94]. A third method is resuspension into organic solvents. It has been shown that both insulin and lysozyme fibrils become destabilized in the presence of a high concentration of DMSO [95,145].

2.8. Compound separation

Solutions containing amyloidophilic molecules are combined with lysozyme amyloid fibrils and the non-bound compounds are removed by multiple rounds of centrifugation and resuspension of the fibril-compound pellets in a buffer solution. In order to separate fibril-bound compounds, two approaches can be used, namely diffusion and fibril destabilization. In the case of diffusion, the aggregate-compound solution is centrifuged and the pellet is resuspended into a small volume of buffer solution, which is then periodically mixed for several hours or days. The highly-concentrated molecules diffuse into the buffer solution, based on their binding affinity and can then be separated by centrifuging the solution and collecting the supernatant. Alternatively, the fibrils can be destabilized as described previously and then separated from the compounds (that were released due to the loss of the amyloid structure) using protein concentrators. In this case, the compound solution will also contain the chosen destabilizing agent, which is either a denaturant (GuSCN) or organic solvent (DMSO).

Examples of methods described in this section and representative examples of data obtained are presented in Figure 6.

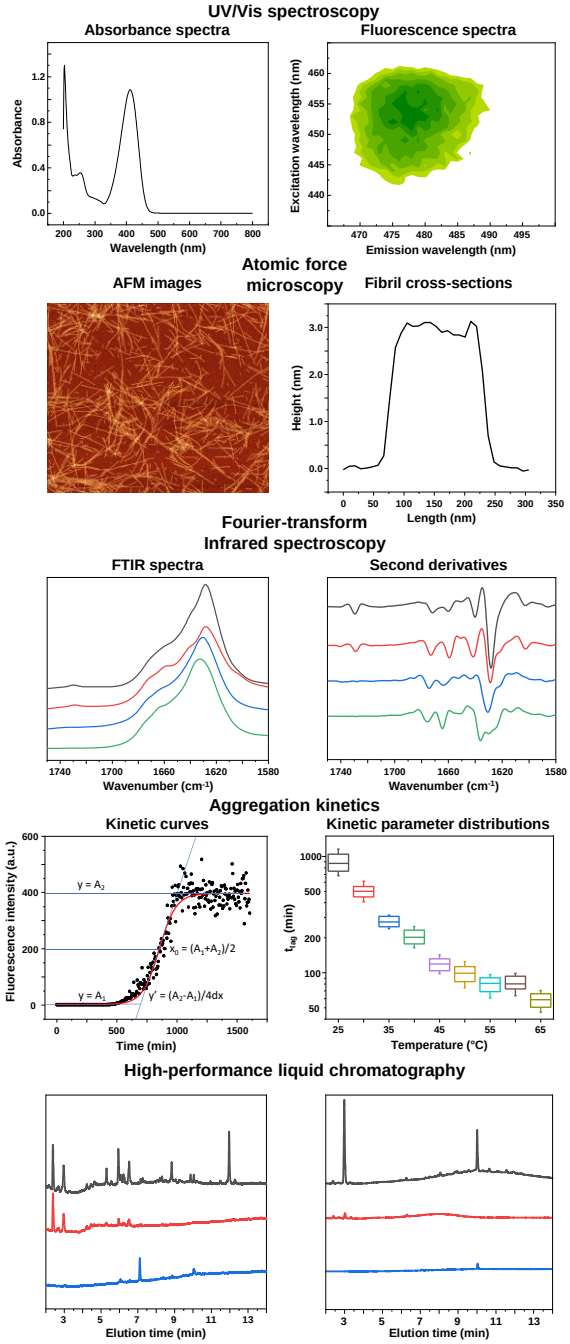

Figure 6. Summary of methods used in this work and representative examples of obtained data.

3. RESULT OVERVIEW

Articles:

3.1. Article 1

Exploring the occurrence of thioflavin-T-positive insulin amyloid aggregation intermediates

Aim of the study – to analyze an anomalous and random occurrence of double-sigmoidal insulin aggregation kinetics, where an initial ThT fluorescence emission signal is detected prior to the main fibril growth phase.

Results – due to the random and relatively rare occurrence of double sigmoidal insulin aggregation kinetic curves, a total of one thousand low volume insulin samples were analyzed. It was observed that roughly 5% of all aggregation curves had a double-sigmoidal profile and 7% had an intermediate profile, where the double-sigmoidal profile was not clearly expressed. Both groups of normal and double-sigmoidal kinetic profile samples were separated and analyzed by AFM, FTIR and reseeding. The double-sigmoidal aggregation was also tracked by scanning the sample excitation-emission matrices (EEM).

The results showed that the double-sigmoidal aggregation did not influence the end-point fibril structure, morphology or seeding potential. However, the EEM data revealed that there are significant maximum positions and intensity shifts during the anomalous aggregation phase. After the first increase in the double-sigmoidal phase ended, there were no longer any significant variations in either the maximum position or its intensity, suggesting that the variability was caused by possible ThT-positive intermediate species. The sudden changes could be related to quick formation and dissociation of intermediate insulin aggregation species, which can trap ThT within their structure and cause an increase in fluorescence emission quantum yield, without actually binding ThT to beta-sheet grooves.

Conclusions – double-sigmoidal insulin aggregation does not affect the end-point fibril secondary structure, morphology or seeding potential. The first signal increase during such anomalous aggregation is most likely related to the assembly and disassembly of intermediate aggregate species with non-specific ThT binding modes.

Identifying insulin fibril conformational differences by thioflavin-T binding characteristics

Aim of the study – to investigate if it is possible to differentiate between different conformation insulin amyloid fibrils, based on their thioflavin-T binding characteristics.

Results - to generate conformationally distinct insulin amyloid fibrils, four environmental conditions were used. These included insulin aggregation in PBS (pH 7.4) with constant 600 RPM agitation, 100 mM sodium phosphate (pH 2.4) with 100 mM NaCl, 100 mM sodium phosphate (pH 2.0) buffers, as well as a 20% acetic acid with 100 mM NaCl solution. The generated aggregates were then examined using FTIR and AFM to confirm that they were significantly different from one another. Both methods revealed that the fibrils had distinct length, width and height, as well as hydrogen bond strength and turn/loop motif regions.

Afterwards, all four fibril types were combined with a range of different concentration thioflavin-T solutions, from as little as 0.1 μM to 100 μM. The resulting solutions were then examined by scanning their excitation-emission matrices and fibril-ThT absorbance spectra. The fibrils with bound ThT molecules were then separated from solution by centrifugation and the non-bound ThT absorbance spectra were scanned in order to determine their concentrations. The results indicated that all four fibril types had distinct bound-ThT fluorescence quantum yields under the entire range of ThT concentrations. The EEM analysis also yielded unique maximum ThT fluorescence excitation-emission maximum positions, which shifted quite significantly under the entire ThT concentration range, indicating multiple possible dye-binding modes. By combining both of these parameters, it was possible to differentiate between all four fibril types, despite them being resuspended into identical solutions prior to analysis.

Conclusions – distinct conformation insulin amyloid fibrils can be distinguished based on their ThT-binding and fluorescence parameters. These include the quantum yield of bound-ThT molecules, as well as the maximum fluorescence excitation-emission positions and this method may be used as an alternative to FTIR or AFM assays.

3.3. Article 3

Formation of distinct prion protein amyloid fibrils under identical experimental conditions

Aim of the study – to investigate if independent prion protein samples, aggregated under identical environmental conditions, yielded fibrils with identical secondary structures and morphologies.

Results - three sets of 20 identical mouse prion protein fragment 89-230 samples, prepared from the same batch of initial protein, were aggregated under identical conditions (2 M GuHCl, 37°C and 600 RPM agitation). After aggregation, each sample was cooled down to room temperature and their fluorescence emission was scanned using a Varian Cary eclipse spectrofluorometer. The resulting sample bound-ThT fluorescence intensity had a significant variation in each of the sets, which was used as a means of separating the samples into three groups (low, medium and high fluorescence intensity). Each group was then analyzed using FTIR, AFM, stability and ThT-binding assays.

The FTIR assay revealed that the secondary structure of low (LI) and medium intensity (MI) samples shared many similarities, while both of them differed from the high intensity (HI) sample, which had a higher content of weaker hydrogen-bonding in the beta-sheet structure. Contrary to this observation, the AFM images revealed that the LI sample was the most distinct from the rest, with most of its fibrils forming clusters and having slightly different length, width and height values. Both MI and HI samples had highly dispersed aggregates and the samples were visually almost completely transparent. The ThT-binding assay data showed that the HI fibrils likely had a different mode of ThT-binding, which could explain the significantly higher fluorescence value. Finally, the stability assay did not display any significant variation between all three groups, suggesting that the structural differences were related to the fibril surface.

Conclusions – these findings show that prion protein can misfold into at least two distinct amyloid conformations even under identical conditions and can be quickly distinguished by comparing their ThT fluorescence emission intensities, FTIR spectra or cluster formation tendencies.

3.4. Article 4

Temperature-dependent structural variability of prion protein amyloid fibrils

Aim of the study – to determine if the initial folded/unfolded state of prion proteins dictates the structural variability of their amyloid fibrils.

Results – a large number of identical prion protein samples were aggregated under a range of temperatures from 25°C to 65°C. The resulting samples were analyzed by scanning their excitation-emission matrices and eight from each temperature set were chosen based on their EEM maximum positions (4 cluster samples with significantly different fluorescence intensities and 4 outlier samples with significantly different EEM maximum positions). Each of them were replicated and analysed by FTIR spectroscopy. Fibrils with unique FTIR spectra were then examined by AFM.

The results showed that the cluster samples had three different fibril types, with one type being dominant at lower temperatures, another - at higher temperatures and the third type present under most conditions. Matters were significantly more complicated when examining the outlier samples. In this case, most temperature sets resulted in multiple samples with distinct FTIR spectra. These fibrils also had unique morphological features, with ones forming long intertwined aggregate networks, while others were short and clumped into clusters. Analysing the aggregation lag time dependence on reaction temperature in an Arrhenius plot also revealed a shift in activation energy at 45°C, the point where the prion protein molecules transition from mostly folded to mostly unfolded. The existence of different fibril types above and below this point suggest that the state of the initial protein molecules is important in determining the end-point aggregate structure. It is also worth noting that none of the tested conditions resulted in a homogenous distribution of fibril types.

Conclusions – the initial folded/unfolded state of prion proteins is important in determining the structural variability of their resulting fibril secondary structures and morphologies. In addition, not a single temperature condition resulted in a homogenous set of amyloid fibrils, suggesting that prion protein polymorphism may be present under various environmental conditions.

3.5. Article 5

Effect of ionic strength on thioflavin-T affinity to amyloid fibrils and its fluorescence intensity

Aim of the study – to determine if the solution's ionic strength has an effect on thioflavin-T binding to different amyloid fibrils and the resulting fluorescence intensity.

Results – for this study, amyloid fibrils of insulin, lysozyme, prion protein and alpha-synuclein were generated. The resulting fibrils were then centrifuged and resuspended into solutions containing a range of sodium chloride (from 0 to 2 M) and ThT (from 0 to 100 μM) concentrations. The resulting solution excitation-emission matrices and absorbance spectra were scanned. Afterwards, the fibrils with bound ThT molecules were separated from solution by centrifugation and the supernatant absorbance spectra were scanned to determine the quantity of non-bound ThT molecules.

The first interesting result is that each protein fibrils had a specific ionic strength, at which they gained significant self-association properties. In all cases, low ionic strength caused the aggregates to remain in the supernatant even after extensive centrifugation. For some fibrils, a small concentration of NaCl was enough to trigger a high level of self-association and an increase in the sample's optical density. For others, the ionic strength had to be increased to near-physiological levels to trigger a similar level of association. The results also revealed that each fibril had a specific ThT-binding capacity, with lysozyme fibrils having the highest number of ThT-binding positions. Finally, it was evident that ionic strength had an extremely large effect on the concentration of fibril-bound ThT molecules, with the number being 10-fold larger at high ionic strength, as opposed to low NaCl concentrations. The global effect that NaCl had on fibril self-association tendencies and ThT binding suggest this feature may exist for other amyloid protein aggregates as well.

Conclusions – solution ionic strength is a highly important factor in fibril self-association events, as well as ThT binding affinity and the resulting dye fluorescence intensity. All four tested protein fibrils experienced a massive increase in bound-ThT molecules at higher NaCl concentrations.

Interplay between epigallocatechin-3-gallate and ionic strength during amyloid aggregation

Aim of the study – to examine how the solution's ionic strength affects the inhibitory potential of epigallocatechin-3-gallate on insulin, alpha-synuclein and amyloid-beta aggregation.

Results – insulin, alpha-synuclein and amyloid-beta were aggregated in the presence of pre-oxidized EGCG (oxidation was achieved by incubating EGCG for 72 h at 60°C in a pH 7.4 potassium phopshate buffer solution) and a range of NaCl concentrations. The aggregation kinetic curves were analyzed to determine how the inhibitor affects the reaction's lag time, half-time and rate values. After fibrillization had completed, the samples were collected and their FTIR spectra were scanned in order to examine if the interplay between NaCl and EGCG had an effect on their structure.

Surprisingly, an increase in solution ionic strength had a strong negative effect on the efficiency of EGCG anti-amyloid properties for insulin an alpha-synuclein. In both cases, the inhibitory potential was reduced to being almost completely ineffective at 800 mM NaCl. Oppositely, amyloid-beta aggregation was minimally affected by the change in NaCl concentration. In all three cases, the most potent inhibition was observed at lower ionic strength conditions, suggesting that there may be optimal conditions to test these types of inhibitors. The FTIR analysis revealed that both NaCl and EGCG were responsible for secondary structure changes in insulin and alpha-synuclein fibrils. This suggests that there is an interplay between ionic strength and EGCG in determining the resulting fibril structure. For amyloid-beta, it was not possible to obtain a sufficient concentration of fibrils for an accurate FTIR analysis.

Conclusions – EGCG anti-amyloid potential was the strongest at low ionic strength conditions, while high NaCl concentrations had a large negative impact on its inhibitory effect. There was also a clear interplay between both ionic strength and EGCG on determining the resulting fibril secondary structure for insulin and alpha-synuclein amyloid aggregates.

3.7. Article 7

Polymorphism of alpha-synuclein amyloid fibrils depends on ionic strength and protein concentration

Aim of the study – to analyze the structural variability of alpha-synuclein amyloid fibrils when they are generated under a range of different ionic strength and protein concentration conditions.

Results – sets of 96 identical alpha-synuclein samples were aggregated under a range of NaCl (0 – 500 mM) and protein concentrations (50 – 250 μM). The resulting fibril solutions were combined with 500 mM and 650 mM NaCl solutions to result in all samples having 10 μM protein, 500 mM NaCl and 100 μM ThT. This was done to equalize the ionic strength and protein concentration between all samples, for an accurate comparison. The resulting sample excitation-emission matrices were then scanned and compared. Samples from EEM maxima clusters with different emission intensities, as well as outliers (samples with distinct EEM maximum positions) were chosen for further analysis by FTIR and AFM.

FTIR analysis revealed that throughout the entire 30 different condition samples, there were eight different fibril types. This was further confirmed by obtaining their atomic force microscopy images, which revealed different morphologies and self-association tendencies. Interestingly, low ionic strength conditions yielded a significantly higher variability of EEM maximum positions, as well as sample FTIR spectra and fibril morphology. Certain conditions resulted in up to four distinct fibril types present among the 96 repeats. At higher ionic strength and protein concentration conditions, the level of polymorphism was significantly reduced, with some conditions yielding a single type of alpha-synuclein aggregate.

Conclusions – alpha-synuclein amyloid fibril structural variability is most prevalent at low ionic strength conditions and, to a smaller extent, at low protein concentrations. This structural variability is significantly diminished once solution ionic strength surpasses 200 mM NaCl, where only one or two types of fibrils are present. These results suggest that both ionic strength and protein concentration are important factors governing the final structure of alpha-synuclein amyloid aggregates.

3.8. Article 8

Additional thioflavin-T binding mode in insulin fibril inner core region

Aim of the study – to determine if insulin amyloid fibrils can have an additional, non-surface binding mode of thioflavin-T, as was hypothesized in a previously reported *in silico* model.

Results – insulin amyloid fibrils were generated under identical protein and solution conditions, with one variation. In one case, a range of ThT concentration solutions were added prior to aggregation and in the other case – after aggregation. After both fibrillization reactions, both solutions contained an identical protein and dye concentration. The resulting aggregates were then examined by scanning their excitation-emission matrices and the concentrations of non-bound ThT was determined by separating the fibrils with bound ThT from solutions by centrifugation and scanning the absorbance spectra of the supernatants.

Interestingly, there was only a minimal difference between the concentration of bound ThT molecules, however, the fluorescence intensity value was ~30% higher in the samples that had ThT added prior to aggregation. Examining the quantum yields of bound-ThT at low dye concentrations revealed that there was likely a small population of bound ThT molecules that were responsible for the significant difference in the total fluorescence intensity. The EEM maxima positions also suggested that there was an additional ThT binding mode when the dye was added prior to aggregation. This position likely becomes inaccessible once the fibrils are fully formed, which is why when the dye was added after aggregation, the fluorescence intensity and quantum yield was significantly lower. Sample sonication also did not allow ThT to enter this position, further supporting an inner core binding mode.

Conclusions – insulin amyloid fibrils most likely have a non-surface related binding mode of ThT, which is only accessible during the fibril formation process. This binding mode is responsible for a significant increase in fluorescence emission intensity, while only binding a minimal concentration of ThT.

3.9. Article 9

Amyloidophilic molecule interactions on the surface of insulin fibrils: cooperative binding and fluorescence quenching

Aim of the study – to examine how different amyloidophilic molecules interact with one another in solution and on the surface of amyloid fibrils.

Results – five amyloidophilic molecules, which are associated with amyloid aggregation studies, were chosen to examine their cross-interactions in solution and on the surface of insulin amyloid fibrils. The molecules chosen were thioflavin-T (ThT), Congo red (CR), 8-anilinonaphthalene-1-sulfonic acid (ANS), dapoxyl (Dap) and methylene blue (MB). These molecules were then combined in pairs and examined both with and without fibrils using UV/Vis spectroscopy. Their cross-interactions were determined by changes in absorbance and fluorescence spectra maximum positions and intensity.

The results showed that certain amyloidophilic molecule pairs interacted with each other in solution, even without the presence of fibrils. Contrary to what may be expected, in most cases when the compound pairs were combined with insulin aggregates, they experienced cooperative binding, rather than preventing each other's association with the fibril's surface. This was most prevalent in the case with CR and ThT, where it had a substantial effect at increasing the concentration of bound ThT molecules. Further investigation revealed that one CR molecule can, on average, cause an additional binding of 1.3 ThT molecules. It was also observed that many amyloidophilic molecule pairs inhibited each other's fluorescence intensity when bound to insulin fibrils, with the only exception being ANS and Dap, which have similar excitation and emission intensities. An explanation for the diminished fluorescence intensity can be the overlap between one molecule's emission and another's excitation wavelengths. Other possibilities include direct interaction/chemical modifications or non-conjugated Forster-resonance energy transfer (FRET) due to their close proximity on the aggregate.

Conclusions – most amyloidophilic molecules are able to assist one another in binding to insulin amyloid fibrils and only certain pairings interfere with each other. However, additional binding does not result in an increased fluorescence emission intensity, as most pairs inhibiting each other's fluorescence properties either by inner filter effects, direct interaction or possibly by non-conjugated FRET.

3.10. Article 10

Using lysozyme amyloid fibrils as a means of scavenging aggregation-inhibiting compounds

Aim of the study – to determine if it is possible to bind anti-amyloid compounds to lysozyme fibrils, wash away the non-effective compounds and then separate the inhibitors from the amyloid aggregates.

Results – to test whether it is possible to use lysozyme amyloid fibrils as a means of selectively scavenging anti-amyloid compounds, four varying complexity inhibitor solutions were prepared, namely oxidized gallic acid, oxidized EGCG, green tea extra and incubated green tea extract. The four solutions were then combined with a concentrated mass of lysozyme fibrils, after which the fibrils were washed multiple times. To separate the bound compounds, three different methods were used. The compounds were separated by diffusion, fibril denaturation with GuSCN and fibril destabilization by resuspension into DMSO. The initial inhibitors, non-binding compounds and separated molecules were analyzed by HPLC and by examining their effect on insulin aggregation.

The non-binding compounds were completely ineffective at inhibiting insulin aggregation, suggesting that all inhibitor molecules became bound to lysozyme fibrils. The molecules that were later separated from the fibrils were all effective at inhibiting insulin fibrillization. HPLC analysis also revealed that more than one type of compound became bound to the fibrils, hinting at the possibility of multiple potential inhibitor molecules. These results display the possibility of using lysozyme amyloid fibrils as a means of scavenging anti-amyloid compounds from complex mixtures.

Conclusions – all molecules that could inhibit aggregation became bound to lysozyme amyloid fibrils in all four cases, suggesting that this is a viable method of separating the effective molecules from ones that do not inhibit amyloid aggregation. Diffusion, denaturation and destabilization were all efficient methods at removing the anti-amyloid compounds from lysozyme fibrils.

A timeline of all experimental procedures, results and conclusions are presented in Figure 7.

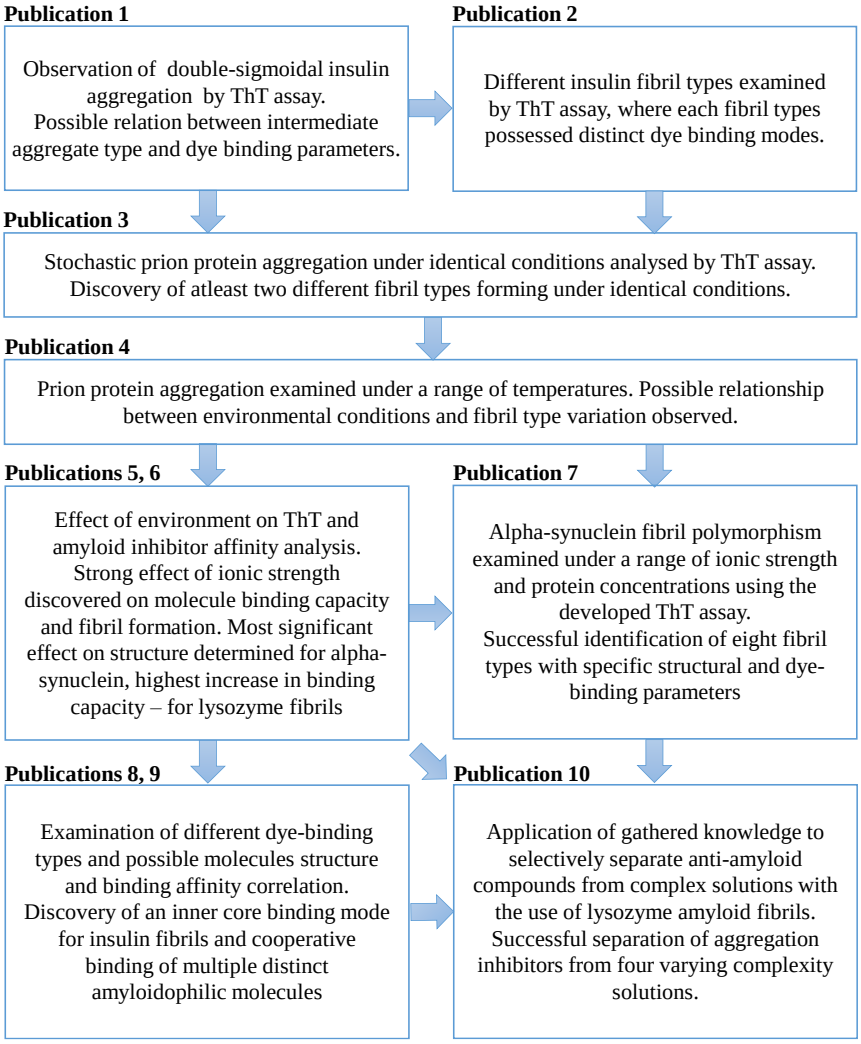

Figure 7. Timeline of experimental procedures, results and conclusions.

4. DISCUSSION

4.1. Amyloid structure and dye binding

During amyloid protein aggregation studies, there is often the appearance of peculiar deviations in signal intensity, arising from fibril-bound thioflavin-T (ThT) molecules. These include double-sigmoidal fluorescence intensity changes [146], as well as highly distinct end-point signal values from identical samples [43]. Since these factors have a negative effect on reproducibility and may or may not influence the conclusions drawn from experimental results, a deeper investigation into the matter was necessary.

In the case of insulin amyloid aggregation, it was reported that certain conditions resulted in a reproducible appearance of double-sigmoidal kinetic curves, when using ThT as a fluorescent probe [69]. The first increase during this double-sigmoidal aggregation was proposed to be due to the appearance of insulin aggregate intermediate species, capable of binding the dye molecule [69]. The issue with examining how this factor influences the aggregation of insulin is the processes' high sensitivity towards environmental conditions. It is known that even a small change in solution pH value or an increase in ionic strength can modulate the lag phase, rate of aggregation, as well as resulting fibril structure [120,147]. This makes it difficult to determine if any observed structural or morphological differences are due to different conditions or the double-sigmoidal aggregation process.

When conducting insulin aggregation studies under pH 2.4 conditions, we observed both regular and double-sigmoidal kinetic curves even from the same sample batch. This created an opportunity to examine if and how the unusual fibrillization influenced the kinetic parameters, as well as end-point fibril structure. Surprisingly, the apparent rate of elongation, aggregation half-time and even end-point fluorescence intensity values were within margin of error. The resulting fibril secondary structures and morphologies were also nearly indistinguishable. This suggested that the appearance of such ThT-positive aggregation intermediates did not have any significant influence on the aggregation of insulin, however, their random appearance was quite puzzling. Observing the double-sigmoidal aggregation of insulin by scanning the sample's excitation-emission matrices (EEM) revealed that the intermediate species formed and dissociated quickly. This was evident by high intensity lines in the EEMs, which were caused by a sudden appearance of ThT-binding structures. Calculating the EEM intensity centers of mass displayed a significant excitation and emission wavelength maximum position deviation from values, which were determined for bound-ThT at the end of

the aggregation reaction. This implied that the intermediate structures had a different mode of incorporating the dye molecules [148]. It was also possible that ThT did not bind to the surface of these structures, but its fluorescence quantum yield was enhanced when they were “trapped” in the structure of such intermediates [149].

Since it is known that distinct fibril types may have specific bound-ThT fluorescence intensities [139] and the previously described experiment displayed the dye’s sensitivity towards different insulin aggregates, this relationship was examined further. Four different insulin fibril types were subjected to a range of ThT concentrations and their dye-binding, as well as fluorescence parameters were examined. Interestingly, all four fibril types had very distinct dye-binding properties, with unique quantum yields, EEM maxima positions and fluorescence intensities. In fact, these parameters were so distinct for each fibril type that they could potentially be used to identify different insulin fibril types. Considering that this method is relatively fast, requires only a minimal amount of aggregates, it could be used as an alternative to other fibril polymorphism identification methods, such as Fourier-transform infrared spectroscopy (FTIR) and atomic force microscopy (AFM).

Since there was such a strong relationship between insulin aggregate types and their ThT-binding properties, it was interesting to examine whether this factor carried over to other protein fibrils as well. Prion proteins have long been established as being capable of forming many distinct structure aggregates (strains), depending on point mutations or environmental conditions [63,150,151]. Prion protein aggregation studies *in vitro* have also often resulted in very diverse bound-ThT fluorescence intensities and this was observed even for similar or identical samples [43,152,153]. As with the peculiar double-sigmoidal aggregation of insulin, this high level of signal variability made prion proteins a suitable candidate for examination via the previously described dye binding method.

During the initial prion protein aggregate examinations in this work, a peculiar anomaly was observed. Several identically prepared fibril samples displayed a very significant variation in their bound-ThT fluorescence intensity signal, even up to a point where the difference was 3-fold. Based on the previously established relationship between fibril conformation and dye-binding properties, this suggested that the identically prepared fibril samples contained distinct aggregate types. Further examination by FTIR and AFM confirmed this hypothesis, which meant that the selected aggregation conditions could randomly yield two different prion protein fibril conformations or heterogenous mixtures. Combined with their unique ThT-

binding modes, this could explain the previously observed variations in signal intensity during aggregation kinetic studies.

Since there existed the possibility of the selected conditions being on the "border" between two environments, which favour either one type of aggregate or another [154], further analysis into the phenomenon was necessary. Prion proteins were aggregated under a range of different temperature conditions, from ones where most prion protein molecules were in their folded state, to ones where they were unfolded. Surprisingly, all conditions yielded samples with distinct ThT-binding parameters and more than four types of different fibril types were observed. The structure and ThT-binding relationship also made it possible to detect a small number of outlier samples, which had very distinct secondary structures and morphologies. Considering that dye-binding could be used to identify different amyloid aggregate structures for both insulin and prion proteins, it suggested that this may extend towards other amyloidogenic proteins/peptides as well.

4.2. Effect of ionic strength

Amyloid aggregation studies are carried out under a broad range of conditions, with distinct pH, temperature, ionic strength, and protein concentrations. While there were multiple reports indicating how these factors influence the aggregation process, as well as amyloidophilic molecule interactions with fibrils [142,155], there was limited information regarding the effect of ionic strength. A few studies have shown that the solution's ionic strength modulated ThT binding to prion protein [156], amyloid-beta [157] and lysozyme fibrils [37], where higher NaCl concentrations resulted in a significant increase in the dye's fluorescence intensity. It was also demonstrated that ionic strength can influence the structure of amyloid aggregates [158]. Taking into consideration that the modest number of reports displayed such a profound effect of ionic strength, it prompted the need for additional studies. Analysis of the effect of ionic strength on amyloid fibril formation, their interaction with ThT and how it modulates the inhibitory effect of epigallocatechin-3-gallate (EGCG) revealed that this factor is a far greater influence than previously thought. Its effect on multiple different proteins/peptides, such as amyloid-beta, alpha-synuclein, insulin, lysozyme and prion protein suggested that solution ionic strength may have a global effect on amyloid fibril formation, structure, as well as their interaction with amyloidophilic molecules.

The first unexpected, yet important factor was ionic strength's influence on fibril self-association tendencies. Different proteins had a critical

concentration of NaCl at which they began to accumulate into larger clusters. This observed effect may be due to different surface charges on the fibril's surface [159], which, when not shielded by salt ions, prevent fibrils from forming larger, self-associated structures. If this is the case, then even minor variations in solution ionic strength could significantly alter amyloid fibril aggregation kinetics, as well as their superstructural motifs.

The second observation was the massive influence that ionic strength had on ThT binding and fluorescence intensity. While it has been reported that low and high ionic strength solutions can result in different ThT signal intensities [37,156,157], the data obtained in this work shows that even a minor change in NaCl concentration can have a drastic impact on both the concentration of bound ThT molecules, as well as their fluorescence intensity. This was especially true at lower ionic strength conditions, where even a 10 mM increase in NaCl concentration yielded a doubling of the signal intensity. Taking into consideration that during many amyloid studies, ThT fluorescence intensity is often considered to be proportional to the concentration of aggregates present in the sample [160,161], such a significant signal intensity and ionic strength relationship may have a sizeable impact on the results and conclusions.

Another interesting aspect of ionic strength was its effect on the inhibitory properties of EGCG. Depending on the concentration of NaCl in solution, EGCG inhibition potential ranged from significant (4-fold higher lag times at low ionic strength) to weak or non-existent (at high ionic strength). The interplay between ionic strength and EGCG also had an effect on the resulting fibril secondary structures. Considering that amyloid aggregation studies *in vitro* are carried out under a broad range of ionic strength conditions [134,162] and the possibility of this effect being present for other compounds, this may lead to false-negative results. This is especially true for instances where amyloid aggregation *in vitro* employs relatively high concentrations of denaturants, such as prion protein [43] or lysozyme fibrillization [92].

4.3. Ionic strength and alpha-synuclein aggregation

During the aforementioned examinations, a peculiar relationship was observed between the structural and amyloidophilic molecule interaction properties of alpha-synuclein and the solution's ionic strength. The concentration of NaCl determined not only the secondary structure of aggregates, but also induced its change after aggregation had already occurred. This structural transition was also evident in the change of bound-ThT quantum yield. Similar observations have also been previously reported,

where alpha-synuclein formed two distinct fibril types under low and high ionic strength [85]. This prompted a need for a deeper investigation into the complex relationship between ionic strength and alpha-synuclein amyloid aggregation.

Alpha-synuclein was aggregated under a range of protein concentrations and ionic strength conditions. The resulting aggregates were then analyzed using the previously established ThT binding and fluorescence assays. After different structure samples were identified by their specific ThT-binding parameters, they were further investigated using FTIR and AFM. This revealed that there was a transition between two main fibril types, occurring between 100 mM and 200 mM of NaCl, which coincided with the report of two aggregate structures forming at low and high ionic strength [85]. However, the ThT assays revealed that the ionic-strength and alpha-synuclein relationship was considerably more complex than previously thought. At low ionic strength conditions, alpha-synuclein was capable of forming up to four distinct secondary structure and morphology aggregates. This variability was significantly reduced when the concentration of NaCl was increased to 200 mM and was even completely diminished under certain sets of conditions. In total, these ThT assays allowed the identification of eight distinct secondary structure and morphology fibrils, which implied a similar or even higher level of polymorphism than prion proteins. Many studies involving alpha-synuclein are conducted at near-physiological conditions [108] and this transition between high and low variability appears amid this specific ionic strength. Due to the high variance in resulting fibril type, this factor may affect both the reproducibility, as well as conclusions drawn from the experiment results.

4.4. Alternative modes of binding

During aggregation studies with ThT, it was observed that the binding of this dye molecule may depend on the stage at which it is added to solution. In the case of insulin aggregation at pH 1.6, it was reported that there were no differences in dye binding, regardless whether ThT was added before or after aggregation [148]. However, a model of ThT binding to amyloid fibrils displayed the possibility of inner core binding modes [163], which would be inaccessible after aggregation had occurred. In order to examine this phenomenon, a ThT binding assay was performed with insulin fibrils, which were prepared under conditions yielding a different type of aggregate (pH 2.4) [120].

When ThT was added before aggregation, the end-point fluorescence intensity was roughly 50% higher than in samples, where it was added after

aggregation. The same conclusion was reached even after samples were sonicated, in order to minimize the possibility of large clusters preventing effective dye binding. Surprisingly, the actual concentration of bound ThT was similar in both samples. Since such a significant difference in signal intensity would have to be the result of a small number of bound dye molecules, their quantum yield had to be considerably higher. This could be achieved if the dye molecules were shielded from contact with the solution molecules or placed in a densely crowded position [149,164]. Both of these factors could be achieved by an inner core binding mode, as shown in theoretical models [163]. The observation that fibrils prepared at pH 1.6 [148] and pH 2.4 differ in the existence of such a binding mode suggest that it is not a universal structural property of amyloid aggregates and may depend highly on the fibril's secondary structure and morphology.

Another peculiar and unexpected interaction between amyloidophilic molecules was observed during their cross-interaction examination. In a study by Girych *et al.* it was shown that ThT and Congo red can interact with one another on the surface of amyloid fibrils and affect each other's fluorescence or absorbance parameters [8]. Due to the possibility of other amyloidophilic molecule interactions, we examined pairs of ThT, Congo red, 8-anilino-1-naftalenesulfonic acid (ANS), dapoxyl and methylene blue (molecules which have shown affinity towards amyloid aggregates [132,165,166]). Surprisingly, in most cases, the compounds aided each other's binding to the surface of insulin aggregates and the effect was most apparent with Congo red. In the case of the ThT and Congo red pair, the concentration of bound ThT molecules increased over 2-fold. However, the actual fluorescence intensity value decreased, even after it was corrected for both the primary and secondary inner filter effects. The change in ThT and CR absorbance spectra also suggested the formation of a complex, even in the absence of insulin fibrils. Both of these observations lead to the conclusion that ThT may not associate with the aggregate in a regular binding mode, but rather forms a complex with the fibril-bound Congo red.

4.5. Anti-amyloid compound separation

Taking into consideration the different chemical structures of the tested amyloidophilic molecules (ThT, Congo red, ANS, dapoxyl, methylene blue) and how they were all capable of binding to amyloid fibrils in ample concentrations, it is possible that the same factor applies to potential aggregation-inhibiting compounds as well. During the previously described fibrillization assays with EGCG, it was observed that the autoxidation

products of this inhibitor molecule (yellow, light brown color) bind to amyloid fibrils and precipitate together to the bottom of the test-tube. The remaining solution retains a significantly reduced color, which suggested that this interaction may be used to separate anti-amyloid compounds using protein aggregates. In order to conduct such an experiment, it was first necessary to choose which type of amyloid fibril to use. Based on the previous observations in this work, it seemed that lysozyme aggregates had the highest capacity for binding amyloid-specific molecules. It also required the lowest ionic strength to both begin self-associating and have a considerable number of bound molecules (after resuspension into a H_2O and NaCl solution). It was also an amyloidogenic protein with a simple aggregation protocol and a relatively low cost [167], which was ideal, as this assay would require significant amounts of aggregates. Based on all these factors, lysozyme was chosen to examine its potential in separating anti-amyloid compounds.

The second part involved choosing inhibitors, which have been documented to modulate the aggregation of amyloidogenic proteins. For this reason, gallic acid and EGCG were chosen, as they have been shown to inhibit multiple different amyloidogenic proteins/peptides [27,98,122,168–170]. In order to test how selective the anti-amyloid compound binding is, it was necessary to obtain complex mixtures, from which the potent compounds could be separated from. For this task, green tea was chosen, since it contains a plethora of components and has been the subject of numerous anti-amyloid studies [36,171,172]. In addition, it has been demonstrated that autoxidation improves the aggregation-inhibiting properties of both gallic acid [170] and EGCG [173]. Due to this, both the small molecular weight compounds, as well as green tea were incubated at an elevated temperature, which also increased their complexity via the formation of multiple autoxidation products [174].

The lysozyme fibril and inhibitor solutions were then combined and separated by centrifugation. To prevent any residual lysozyme aggregates from initiating its own aggregation, insulin fibrillization was used to test the supernatant solutions. In all four cases (gallic acid, EGCG, green tea, incubated green tea), the supernatant was incapable of altering insulin aggregation, while the control samples were all effective at increasing the process lag time 2 – 4-fold. This leads to the conclusion that all compounds, which possess anti-amyloid properties, became bound to the lysozyme aggregates and were separated from the solution by centrifugation. Given the fact that the tested inhibitor mixtures contained some of the most prominent compounds used in amyloid studies, it is possible that this amyloid-binding property extends to other aggregation-inhibiting compounds as well.

4.6. Anti-amyloid compound retrieval

While it was certain that anti-amyloid compounds became bound to lysozyme fibril aggregates, it was still necessary to retrieve them from the fibril-compound solution. For this reason, the bound compounds had to be separated from the fibrils and then removed from the protein solution. To achieve this, three different methods were employed, which relied on fibril destabilization and reversible binding of the anti-amyloid compounds.

The first and the simplest method used was diffusion, where the fibril-compound solution was centrifuged and the pellet was placed in a small volume of buffer solution. After some time, the bound molecules diffused into the buffer solution and could then be separated by centrifugation and filtration. The obtained compounds were then capable of inhibiting amyloid aggregation; however, the gallic acid solution molecules displayed a minimal effect. This method did not require the addition of any destabilizing agents, which would then have to be separated again during subsequent purification steps.

While diffusion was sufficient enough to remove certain anti-amyloid compounds, it was clearly evident that there was a substantial concentration of molecules still bound to the fibrils (dark yellow color of the fibril pellets). For this reason, it was necessary to use destabilizing agents, in order to disrupt the fibril surface and eliminate compound binding modes. Both concentrated guanidine thiocyanate (GuSCN), as well as dimethyl sulfoxide (DMSO) proved to be extremely efficient at this task and substantial concentrations of bound compounds were separated from the lysozyme fibrils/monomers. Molecules separated by these methods were also efficient at inhibiting amyloid aggregation, however, unlike in the case of diffusion, the anti-amyloid solutions contained GuSCN or DMSO.

Analysis of both the initial and separated inhibitor solutions with HPLC revealed that there were several binding and non-binding components in each case. This proved that it is possible to separate anti-amyloid compounds from ineffective ones, however, the number of different binding molecules was an unexpected and interesting result. It is possible that the complex inhibitor mixtures contain several molecules with aggregation inhibiting properties. However, it is also likely that some of these components only associate with the aggregates without actually altering their rate of formation or propagation. It was also observed that certain molecules did not become separated from lysozyme, even after its denaturation in concentrated GuSCN, which suggests that they may become covalently bound to the protein, as was shown with EGCG autoxidation products [175].

Taking all of these results into consideration, it appears that the relationship between amyloidophilic molecules and the surface of amyloid fibrils is extremely complex. However, it can be applied as a means of not only identifying different types of aggregates, but also used to separate anti-amyloid compounds. This work presents the initial steps in such practices, which will hopefully be applied in future amyloid polymorphism studies and potential aggregation inhibitor screenings.

CONCLUSIONS

By analysing differences in thioflavin-T binding characteristics, it was determined that prion proteins, as well as alpha-synuclein can aggregate into different types of amyloid fibrils even under identical conditions. Examining this phenomenon under a range of different environments revealed that the level of aggregate structural variability correlated with the fibrillization conditions. Low ionic strength resulted in the most significant variation of alpha-synuclein aggregates, while prion proteins yielded a diverse set of fibrils under all tested environments. Taking into account the differences between both of these proteins, it is possible that this type of polymorphism is a generic feature of amyloid proteins and likely extends to other proteins/peptides as well.

An examination of how different amyloidophilic molecules interact with each other and in combination with amyloid fibrils revealed an unexpected result. In most cases, the combined pairs of compounds were able to assist each other in binding to the surface of protein aggregates, with Congo Red and thioflavin-T demonstrating the most effective cooperation. This observation suggested that the fibril surface may contain a wide range of distinct binding modes and that different structure molecules may not compete for a position, but rather help each other‘s binding by inducing minor fibril structural variations or shielding its surface charge.

Examining how the environment affects protein aggregate and amyloidophilic molecule interactions revealed that ionic strength was an extremely important factor. An increase in this parameter caused a 10-fold higher number of bound thioflavin-T molecules and it was observed that lysozyme fibrils had the highest binding capacity out of all the tested aggregates. It was also demonstrated that certain protein fibrils may possess a binding mode within their structure, which is not accessible after aggregation occurs.

Based on the combined results of the binding studies, it was hypothesized that anti-amyloid compounds could be selectively removed from complex mixtures by utilizing their affinity to lysozyme fibrils. All molecules which did not inhibit amyloid aggregation were not capable of binding to lysozyme aggregates, while everything that could slow down the fibrillization reaction became associated with the fibril surface. After diffusion and lysozyme aggregate destabilization, the bound compounds could be removed from solution. This method appeared to be effective on all tested complex inhibitor solutions and could potentially be used in future drug screenings.

SANTRAUKA

SANTRUMPOS

Ab_{42}	Amiloidas beta (1-42)
AJM	Atominės jėgos mikroskopija
ANS	8-Anilino-1-naftalensulfoninė rūgštis
APP	Amiloido beta pirmtakas
APTES	(3-aminopropil)trietoksisilanas
CR	Kongo raudonasis
Dap	Dapoksilas
DMSO	Dimetilsulfoksidas
EEM	Sužadinimo-emisijos matrica
FRET	Forsterio-rezonanso energijos perdavimas
FTIR	Furjė-transformacijos infraraudonoji spektroskopija
GPI	Glikozilfosfatidil inozitolis
GuHCl	Guanidino hidrochloridas
GuSCN	Guanidino tiocianatas
HPLC	Aukšto efektyvumo skysčių chromatografija
MB	Metileno mėlis
MoPrP	Pelės prioninis baltymas
PBS	Fosfato buferinis fiziologinis tirpalas
Aps.	Apsisukimai
ThT	Tioflavinas-T
TEM	Transmisinė elektroninė mikroskopija
UV/Vis	Ultravioletinė/regima

Tikslas

Suprasti sąveiką tarp amiloidofilinių molekulių ir baltymų fibrilių bei pritaikyti šias žinias anti-amiloidinių junginių paieškoje.

Uždaviniai

1. Pagaminti daug skirtingos antrinės struktūros ir morfologijos fibrilių iš įvairių amiloidogeninių baltymų;

2. Nustatyti ryšį tarp aplinkos sąlygų ir susidarančių fibrilių tipų;

3. Ištirti afiniškumą tarp skirtingų amiloidofilinių molekulių ir amiloidinių fibrilių bei nustatyti jų jungimosi būdus;

4. Nustatyti kokią įtaką turi aplinkos sąlygos amiloidofilinių molekulių ir baltymų agregatų tarpusavio sąveikai;

5. Ištirti ryšį tarp junginių anti-amiloidinio aktyvumo ir jų jungimosi prie fibrilių afiniškumo;

6. Remiantis junginių-fibrilių sąveika, selektyviai atskirti potencialius anti-amiloidinius junginius iš sudėtingų mišinių.

5. ĮVADAS

5.1. Amiloidų atradimas ir istorija

Pirmieji su amiloidų agregacija susiję sutrikimai nustatyti XVII amžiuje, kai buvo pastebėti pavieniai keisti gyvūnų elgsenos atvejai arba neįprastos, panašios į krakmolą sankaupos nerviniuose audiniuose. Šios sankaupos buvo pavadintos „amiloidais“, remiantis lotyniškais ir graikiškais žodžiais „amylum, amylon“, kurie lietuviškai reiškia „krakmolas“ [1]. Tačiau tikrasis su amiloidais susijusių sutrikimų pobūdis nebuvo atrastas ilgą laiką. Per šį laikotarpį buvo iškeltos ir paneigtos kelios hipotezės, kad parazitai, bakterijos ar virusai yra šių ligų sukėlėjai [2]. 1859 metais Friedreich ir Kekule parodė, kad amiloidinės struktūros yra sudarytos iš baltymų, o ne angliavandenių, kaip buvo manyta anksčiau. 1922 metais Benhold atrado, kad amiloidus galima dažyti Kongo raudonuoju – vandenyje tirpiu dažu, kuris vėliau buvo naudojamas kaip standartas amiloidinių ligų nustatymui [2]. 1927 metais, naudojant šį dažą ir poliarizuotos šviesos mikroskopiją, buvo nustatytos amiloidų sankaupos raumeniniame audinyje. Po poros dešimtmečių pastebėta, kad esant žemam pH, insulinas geba formuoti sferines struktūras, sudarytas iš fibrilių [3]. 1959 metais, naudojant elektroninę mikroskopiją, buvo parodyta, kad amiloidinės fibrilės gali susidaryti įvairiuose organuose ir audiniuose [4].

Per paskutinius kelis dešimtmečius amiloidams buvo skiriamas didelis dėmesys ir buvo padaryta daug atradimų, susijusių su jų struktūra ir funkcija. Rentgeno spindulių difrakcijos tyrimas parodė, kad amiloidinės sankaupos sudarytos iš fibrilių, turinčių beta-klosčių struktūras [2]. Taip pat pranešta, kad fibriliniai agregatai yra iš dalies atsparūs detergentams ir skaidymui proteinaze-K [5]. 2009 metais Knowles ir kt. pasiūlė teorinį modelį, apibūdinantį baltymų/peptidų agregaciją, kuris apima branduolių susidarymą, linijinį fibrilių augimą ir antrinius branduolių susidarymo procesus [7]. Intensyvūs amiloidų tyrimai leido geriau suprasti baltymų agregacijos procesus, todėl buvo atrasta daug potencialių anti-amiloidinių junginių, iš kurių daugiau nei šimtas yra įtraukti į klinikinius tyrimus [12]. Vieną iš šių preparatų Jungtinių Valstijų Maisto ir vaistų administracija (FDA) 2019 metais patvirtino su transtiretinu susijusios kardiomiopatijos gydymui (Tafamidis) [11], o 2021 metais buvo patvirtintas Alzheimerio ligos vaistas – monokloninis antikūnas (Aduhelm), nutaikytas prieš amiloido-beta agregatus [13].

5.2. Amiloidinės ligos

Šiuo metu yra žinoma daugiau nei 30 su ligomis susijusių amiloidinių baltymų/peptidų, kurių agregacija sukelia daugybę amiloidozių, įskaitant neurodegeneracines Alzheimerio ar Parkinsono ligas [14,15]. Nepaisant to, kad susidaro panašios fibrilinės struktūros, nėra specifinės aminorūgščių sekos, kurią būtų galima susieti su tam tikromis baltymų tendencijomis formuoti fibrilinius agregatus [16]. Pavyzdžiui, su Alzheimerio liga susijęs amiloido-beta peptidas sudarytas iš 42 aminorūgščių, o su mikrovamzdeliais asocijuoto Tau baltymo, kuris yra susijęs su Alzheimerio liga ir tauopatijomis, aminorūgščių skaičius yra 10 kartų didesnis [14]. Pradinė natyvi amiloidogeninių baltymų struktūra taip pat nėra lemiamas veiksnys, nes jie gali būti bestruktūriai (amiloidas-beta, tau, alfa-sinukleinas), turėti daug alfa-spiralių (insulinas, prioninis baltymas) arba beta-klosčių (imunoglobulino lengvoji grandinė, transtiretinas) ir turėti antrinių struktūrų mišinį (lizocimas, laktoferinas) [14]. Net buvo parodyta, kad trumpi peptidai gali sudaryti į amiloidus panašius agregatus (difenilalaninas) [18]. Taip pat buvo iškelta hipotezė, kad kiekvienas baltymas/peptidas gali agreguoti į fibriles, jei yra sudaromos tam tikros specifinės sąlygos, ir kad šis procesas gali būti bendra baltymams/peptidams būdinga savybė [16].

Ši didelė baltymų/peptidų sekų ir struktūrų įvairovė nulemia tai, kad jų agregatai sukelia daug įvairių sutrikimų, kurie skiriasi atsiradimo ar perdavimo tipu, lokalizacija ir simptomų sunkumu. Su amiloidais susijusias ligas galima suskirstyti į spontanines (Alzheimerio liga [19], Parkinsono liga [20]), paveldimas (Huntingtono liga [21], mirtina nemiga [22]), užkrečiamas (kuru [23]) arba jatrogenines (injekcijų vietų lokalizuota amiloidozė [24]). Kai kuriems sutrikimų simptomams atsirasti reikia kelių metų (Alzheimerio liga, Parkinsono liga [19,20]), kiti veikia gana greitai (Creutzfeldt-Jakob liga [25]), o kai kurie yra lokalizuoti ir nesukelia rimtų, gyvybei pavojingų komplikacijų (injekcijų vietų lokalizuota amiloidozė [24]). Tačiau, nepaisant daugybės tyrimų, vis dar nėra veiksmingų vaistų ar gydymo būdų, o tik tam tikrų sutrikimų simptomų gydymas [26].

Viena iš daugelio galimų priežasčių kodėl tokia didelė dalis klinikinių tyrimų baigiasi nesėkme yra sąlygų skirtumas tarp anti-amiloidinių junginių tyrimų *in vitro* ir *in vivo*. Vienas veiksnys, kuris mažai tyrinėjamas, yra tirpalo joninės jėgos skirtumai, kurie gali turėti įtakos amiloidinių agregatų formavimuisi [37–39]. Dėl šios priežasties, dalis mano tyrimų buvo skirta geriau suprasti kaip joninė jėga veikia anti-amiloidinių junginių efektyvumą (Priedo 6 publikacija).

5.3. Anti-amiloidiniai vaistai

Ieškant anti-amiloidinių junginių, buvo atrasta daug įvairių kandidatų, turinčių skirtingus veikimo mechanizmus, įskaitant tiesioginį agregacijos slopinimą, neuroprotekciją, priešuždegiminį poveikį ir kt [12]. Šie junginiai turi įvairias struktūras nuo mažų molekulių iki monokloninių antikūnų ar sudėtingų vaistų mišinių [27–29]. Tačiau nepaisant didelio kiekio potencialių junginių, daugumos klinikiniai tyrimai yra pasibaigę nesėkmingai [26,30]. Tai savo ruožtu neleidžia sumažinti vis didėjančio skaičiaus pacientų, kenčiančių nuo su amiloidais susijusių sutrikimų. Dėl šios priežasties labai svarbu rasti veiksmingą gydymo būdą ar amiloidų plitimą slopinantį metodą [32,33].

Šiuo metu yra tiriamas daugelio natūralių junginių anti-amiloidinis aktyvumas ir yra parodyta, kad šios molekulės geba žymiai sumažinti agregacijos greitį arba atsirandančių agregatų toksiškumą. Buvo nustatyta, kad kelios natūraliai randamų junginių klasės gali tiesiogiai arba netiesiogiai paveikti amiloidinių fibrilių susidarymą ir kaupimąsi. Acetilcholinesterazės (susijusios su Alzheimerio ligos cholinergine hipoteze), proteolitinių fermentų (fermentai atsakingi už amiloido-beta peptidų susidarymą) bei amiloidinės agregacijos slopinimas buvo pasiektas naudojant įvairius alkaloidus, terpenoidus ir poliketidus. Dalis šių junginių taip pat pasižymėjo neuro-regeneraciniu ir antioksidaciniu poveikiu, padedančiu sumažinti amiloidinių ligų sukeltas pažaidas ir simptomus [28].

5.4. Agregacijos mechanizmas

Baltymų/peptidų agregacija į fibrilines struktūras vyksta keliais etapais (1 pav.). Pradinis amiloidinės agregacijos žingsnis yra branduolių susidarymas (pirminė nukleacija) – procesas, kurio metu natyvių baltymų/peptidų molekulės susirenka į stabilų β-klosčių turintį branduolį [40,41]. Tokio perėjimo tikimybė priklauso ir nuo aplinkos, ir nuo paties baltymo/peptido. Veiksniai, didinantys agregacijos tikimybę (aukštesnė temperatūra [42], denatūrantai [43], taškinės mutacijos aminorūgščių sekoje [44]), taip pat sąlygos, kurios palengvina didesnę baltymų ir peptidų sąveikos tikimybę (mėginio maišymas ar purtymas [45], didesnė baltymų/peptidų koncentracija [46], krūvio ekranavimas jonais [47]) sutrumpina branduolių susidarymo laiką. Amiloidinio branduolio susidarymas taip pat priklauso nuo minimalaus baltymų/peptidų skaičiaus, kuriam esant jis tampa stabilus. Yra nustatyta, kad šis skaičius gali svyruoti nuo dviejų iki kelių dešimčių ir labai priklauso nuo pačio baltymo/peptido [48–50].

Kai susidaro stabilus branduolys, jis gali į savo struktūrą prijungti kitas homologines baltymų/peptidų molekules ir pailgėti į protofibrilinį agregatą. Šis ilgėjimo procesas vyksta fibrilinės struktūros galuose, kurie veikia ir kaip katalizatorius, ir kaip natyvių baltymų/peptidų konversijos šablonas [51–53]. Šis etapas vyksta daug greičiau nei pirminis branduolių susidarymas ir jam įtakos turi veiksniai, kurie sumažina proceso energetinį barjerą ir padidina fibrilių galų ir baltymų/peptidų molekulių sąveikos tikimybę [43]. Pailgėjusios protofibrilinės gijos tada susijungia į subrendusią fibrilę ir tokių gijų skaičius bei jų persipynimas lemia agregato morfologiją [54–56].

Kai amiloidinės fibrilės pasiekia kritinį ilgį, jos gali skilti – tai fragmentacijos procesas, kurio metu agregatas pasidalina į dvi trumpesnes fibriles, kurių kiekviena turi savo agregaciją katalizuojančius galus. Fragmentacijos dažnis priklauso ir nuo agregato struktūrinio stabilumo, ir nuo aplinkos sąlygų [57]. Kai kuriais atvejais fibrilės gali būti kelių mikrometrų ilgio, jei baltymas/peptidas gali sudaryti labai stabilias struktūras ir fibrilė nėra veikiama maišymo ar tempimo jėgų. Kitais atvejais agregatai turi tokį žemą stabilumo lygį, kad jie lengvai skyla net ramybės sąlygomis [58]. Šis procesas yra svarbus veiksnys, skatinantis amiloidinių agregatų kiekio eksponentinį augimą, nes kiekvienas skilimo įvykis iš esmės padvigubina turimų fibrilių galų skaičių. Fragmentacija taip pat gali turėti įtakos bendram amiloidų toksiškumui, nes dėl didesnio suskaidymo greičio gali susidaryti trumpesnės fibrilės, kurios gali lengviau migruoti ir būti toksiškesnės nei ilgesni jų variantai [59].

Kitas procesas, vykstantis susiformavus amiloidinėms fibrilėms, yra paviršiaus-sąlygojamas branduolių susidarymas (taip pat vadinamas antrine nukleacija) [60–62]. Šio etapo metu agregatų paviršius veikia kaip naujų amiloido branduolių susidarymo katalizatorius. Skirtingai nuo pailgėjimo fibrilės galuose, fibrilių paviršius neveikia kaip šablonas naujai susidarančių branduolių struktūrai, o tik padidina jų susidarymo tikimybę [63]. Susiformuojančių branduolių tipą lemia aplinkos sąlygos, panašiai kaip ir pirminės nukleacijos atveju [41,64,65]. Šis procesas tampa vis labiau reikšmingas, kai atsiranda didesnė koncentracija fibrilių, ir taip pat yra svarbus veiksnys skatinantis amiloidinių agregatų kiekio eksponentinį augimą.

Be šių pagrindinių agregacijos mechanizmo žingsnių egzistuoja kompleksiškas natyvios baltymo struktūros perėjimo į amiloidinį branduolį etapas. Manoma, kad šio proceso metu formuojasi kelios nestabilios tarpinės agregatų formos, kurių greiti pokyčiai neleidžia tiksliai nustatyti jų struktūros [66–68]. Kadangi vis dar mažai žinoma apie šį amiloidų formavimosi etapą, dalis mano darbo buvo skirta geriau suprasti tarpinių agregatų atsiradimą ir kokią įtaką tai turi fibrilių formavimuisi (Priedo 1 publikacija).

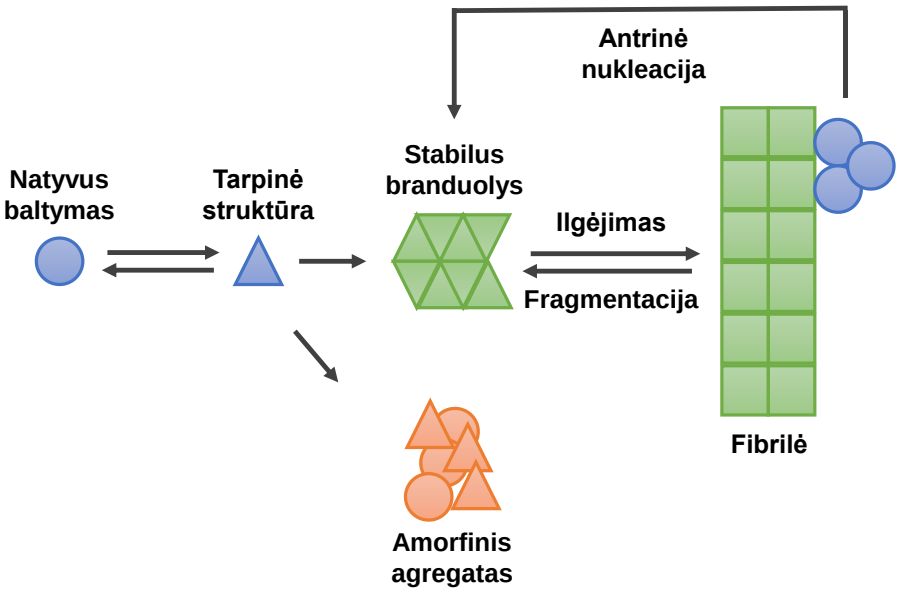

1 pav. Amiloidinių fibrilių susidarymo ir antrinių agregacijos procesų mechanizmas.

5.5. Fibrilių struktūra ir morfologija

Amiloidinių fibrilių antrinių struktūrų analizė Furjė-transformacijos infraraudonųjų spindulių spektroskopija atskleidė, kad egzistuoja įvairus galimų vandenilinių jungčių tipų pasiskirstymas, taip pat skirtingi linkių/kilpų motyvai [75,76]. Netgi buvo pranešta apie galimybę, kad tam tikrų fibrilių agregatų struktūroje gali būti "cross-alfa" arba beta-solenoido motyvų [77–79]. Bendrai, įvairūs fibrilių branduolio dydžiai, skirtingi antrinės struktūros motyvai ir jų pasiskirstymas vienas kito atžvilgiu lemia didelę amiloidinių fibrilių struktūrinę įvairovę, o tai sukelia problemų atliekant amiloidų tyrimus.

Be amiloidinių fibrilių antrinės struktūros skirtumų, jos taip pat turi specifinių morfologinių savybių. Agregatai gali būti visiškai linijiniai arba turėti atšakas, jie gali būti besisukantys arba tiesūs ir įvairaus ilgio – nuo nanometrų iki mikrometrų [81,82]. Sulipimas į dideles grupes, jungiantis vienas prie kito segmentuose arba šoninis susiejimas, taip pat yra bendras amiloidinių fibrilių bruožas (ypač dažnai matomas *in vivo*, kai susidaro didžiulės sankaupos) [83,84]. Pati fibrilių struktūra gali būti periodiška, atsirandanti dėl susisukimo tarp protofilamentų, [85] arba visiškai kristališka ir neturėti jokio pastebimo periodiškumo [86]. Kaip ir amiloidų antrinių struktūrų atveju, fibrilių morfologija neturi nustatyto sąryšio su pradiniu natyviu baltymu. Buvo nustatyta, kad vienas baltymas/peptidas gali sudaryti

morfologiškai skirtingų fibrilių rinkinį su specifiniais ilgiais, pločiais ir periodiškumais [85,87,88].

Šis polimorfizmas yra susijęs su skirtingu branduolių susidarymo laiku, plitimo greičiu ir citotoksiniu poveikiu įvairių su amiloidais susijusių sutrikimų metu. Pavyzdžiui, prioninių baltymų agregacija gali sukelti daugybę skirtingų sutrikimų, įskaitant Creutzfeldt-Jakob ligą, Gerstmann-Sträussler-Scheinker sindromą, mirtiną šeimyninę nemigą ir kuru [89,90]. Nepaisant daugybės duomenų apie tokius struktūrinius skirtumus, vis dar nėra aiškaus supratimo kaip aplinkos veiksniai (temperatūra, pH, maišymas, baltymų koncentracija, druskos koncentracija ir kt.) arba aminorūgščių sekos mutacijos lemia specifinių agregatų susidarymą.

Įdomu tai, kad nors struktūriškai ir morfologiškai skirtingų agregatų susidarymas įvairiomis sąlygomis yra plačiai ištirtas, neseniai buvo parodyta, kad šis reiškinys gali įvykti identiškomis sąlygomis. Nustatyta, kad amiloidas-beta tomis pačiomis sąlygomis gali sudaryti iki vienuolikos skirtingų tipų fibrilių (2 pav.), turinčių specifinių morfologinių savybių [87]. Taip pat buvo aprašytas atvejis, kai alfa-sinukleinas sudarė skirtingų agregatų mišinį *in vitro* (2 pav.) [86]. Atsižvelgiant į tai, kad du labiausiai paplitę ir su neurodegeneracinėmis ligomis susiję baltymai/peptidai pasižymi polimorfizmu identiškomis sąlygomis, gali būti, kad ši savybė taip pat galioja ir kitiems amiloidogeniniams baltymams.

Kadangi tokia baltymų savybė formuoti skirtingus agregatus identiškomis sąlygomis yra vis dar mažai ištyrinėta sritis, didelė mano darbo dalis buvo skirta išsiaiškinti kokią įtaką aplinkos sąlygos turi prioninio baltymo ir alfa-sinukleino polimorfizmui (Priedo 3, 4 ir 7 publikacijos).

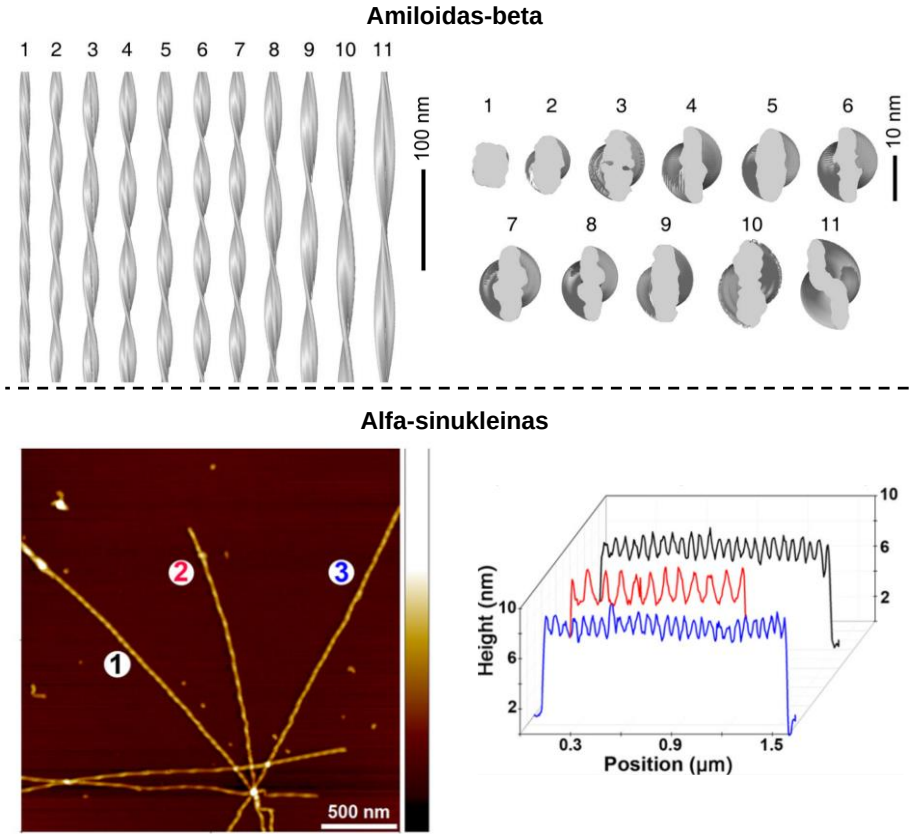

2 pav. Amiloido-beta ir alfa-sinukleino fibrilių polimorfizmas (pagal [87] ir [86])

5.6. Amiloidofilinės molekulės

Nuo tada, kai buvo atrasta, kad amiloidinės fibrilės geba prijungti specifines molekules, tokias kaip jodas ar Kongo raudonasis [2], buvo atrasta ir daugiau su fibrilėmis sąveikaujančių molekulių. Neabejotinai dvi svarbiausios amiloidofilinės molekulės yra minėtas Kongo raudonasis – anijoninis diazo-benzidino dažiklis [128] ir tioflavinas – benzotiazolo druska [129]. Dėl jų sąveikos su amiloidinėmis fibrilėmis pasikeičia jų sugerties ir fluorescencijos spektrai, kurie naudojami kaip daugybės baltymų agregacijos požymis [8,130]. Atsižvelgiant į labai skirtingas Kongo raudonojo ir tioflavino-T (ThT) struktūras, taip pat kitas molekules, kurios jungiasi prie amiloidų (metileno mėlynasis [131] arba dapoksilas [132]) (3 pav.), galima daryti išvadą, kad amiloidiniai agregatai neturi specifiškumo konkrečiai molekulinei struktūrai, bet veikiau geba jungti įvairių struktūrų molekules.

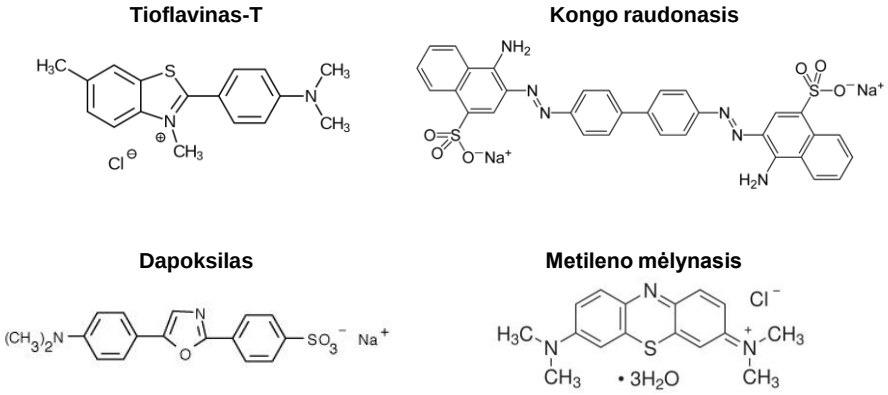

3 pav. Tioflavino-T, Kongo raudonojo, dapoksilo ir metileno mėlio molekulinė struktūra.

Molekulinio jungimosi tyrimai parodė, kad daugelis agregaciją slopinančių medžiagų taip pat gali prisijungti prie agregacijos tarpinių produktų arba pačių fibrilių [133–135]. Net ThT ir Kongo raudonojo atvejais buvo pasiūlyti keli skirtingi dažų surišimo būdai ir yra tyrimų, rodančių, kad fibrilės paviršiuje yra iki šešių skirtingų ThT jungimosi vietų [136–138]. Net buvo iškelta hipotezė, kad fibrilės gali turėti tam tikras surišimo vietas arba ertmes, kurios pasiekiamos tik agregacijos proceso metu [138]. Taip pat nustatyta, kad ThT turi skirtingą afiniškumą skirtingoms amiloidinėms fibrilėms, susidariusioms iš to paties pirmtako baltymo [139]. Tai parodo, kad šis veiksnys gali būti susijęs su jų antrine struktūra ir morfologija.

Nors yra daug tyrimų parodančių skirtingas amiloidofilinių molekulių jungimo sritis ant baltymų agregatų, vis dar mažai žinoma apie aplinkos poveikį šioms sąveikoms. Taip pat nėra nustatyta tiksli korealiacija tarp molekulių struktūros ir jų gebėjimo jungtis prie fibrilių paviršiaus. Kadangi tokios žinios stipriai prisidėtų prie amiloidų tyrimų ir potencialių agregacijos slopiklių paieškoje, didelė dalis mano darbo buvo skirta šios srities tyrimams (Priedo 2, 5, 8 – 10 publikacijos)

6. METODAI

6.1. Fibrilių susidarymas

Norint per santykinai trumpą laiką sukelti amiloidinių fibrilių susidarymą iš natyvios būsenos baltymų/peptidų, būtina sudaryti sąlygas, kurios destabilizuotų baltymo/peptido struktūrą ir padidintų jo agregacijos tikimybę. Yra daug aplinkos sąlygų, kurios turi įtakos amiloidinių fibrilių susidarymui. Dažniausiai jos parenkamos atsižvelgus į patį baltymą/peptidą, kadangi jie skiriasi savo struktūriniu stabilumu, tirpumu ir pI vertėmis. Insulino atveju paprastai naudojama rūgštinė aplinka ir aukštesnė temperatūra [118]. Lizocimui ir prioniniams baltymams dažnai naudojami denatūrantai, tokie kaip guanidino hidrochloridas [63,127]. Natyviai bestruktūriai alfa-sinukleinas bei amiloidas-beta gali agreguoti esant fiziologinėms sąlygoms [87,140]. Visais atvejais reakcijai paspartinti gali būti naudojamas maišymas, nes jis padidina baltymų/peptidų tarpusavio sąveikos tikimybę ir skatina susidariusių fibrilių fragmentaciją, taip sukuriant naujus agregacijos centrus.

6.2. Agregatų susidarymo sekimas

Viena iš dažniausiai naudojamų amiloidinių fibrilių susidarymo sekimo priemonių yra tioflavinas-T (ThT). Kai susidaro baltymų agregatai, ThT prisijungia prie jų paviršiaus ir įgauna “užrakintą” konformaciją, o tai žymiai padidina jo fluorescencijos kvantinę išeigą ir sukelia sužadinimo ir emisijos bangų ilgių raudonąjį poslinkį [141]. Paprastai naudojama dažų koncentracija yra nuo 10 iki 100 μM, priklausomai nuo reakcijos trukmės (kadangi ThT gali būti hidroksilinamas esant neutraliam arba baziniam pH ir aukštesnei temperatūrai [142]) ir naudojamo baltymo koncentracijos. Nepakankama ThT koncentracija gali iškreipti eksperimento rezultatus, jei dar vykstant agregacijai nebelieka nesurištų molekulių, o didelis dažų perteklius gali sukelti vidinio filtro efektą ir sumažinti fluorescencijos signalo intensyvumą. Prisijungusio ThT sužadinimo bangos ilgis yra 440–450 nm, o emisija stebima esant 480–490 nm, nors maksimalūs sužadinimo ir emisijos bangos ilgiai gali skirtis dėl fibrilės paviršiuje esančių dažo jungimosi pozicijų variacijos. Jei tirpale yra santykinai homogeniškas agregatų pasiskirstymas, ThT fluorescencijos intensyvumas tiesiškai koreliuoja su agregatų koncentracija ir gali būti naudojamas kiekybiniam fibrilių koncentracijos nustatymui.

6.3. Kinetinių duomenų analizė

Duomenys, gauti fibrilių susidarymo metu, turi būti išanalizuoti, siekiant gauti informacijos apie agregacijos reakciją (lag laikas, agregacijos puslaikis ir ilgėjimo greičio konstanta). Duomenys analizuojami naudojant „Origin“ programinę įrangą, taikant Boltzmann'o sigmoidinį arba tiesinį gluodinimą. Tais atvejais, kai agregacija vyko spontaniškai, agregacijos reakcijos kreivės buvo sigmoidinės. Šio tipo duomenims naudotas Boltzmann'o sigmoidinis gluodinimas, pagal kurio parametrus buvo galima apskaičiuoti reakcijos lag laiką (laiką, kurio reikia baltymui suformuoti pirmuosius agregatus, kuriuos galima aptikti naudojant ThT), agregacijos puslaikį (laiko momentą, kai agreguotų ir neagreguotų baltymų kiekis yra lygus) ir ilgėjimo greičio konstantą (agregatų augimo greitis pusėjimo taške). Jei agregacija vyko be lag fazės, agregacijos vidurio taško laikas ir ilgėjimo greičio konstanta apskaičiuoti taikant tiesinį gluodinimą tarp 40% ir 60% didžiausio signalo intensyvumo verčių ir ekstrapoliuojant 50% laiko reikšmę ir krypties koeficientą.

6.4. Furjė-transformacijos infraraudonoji spektroskopija

Furjė-transformacijos infraraudonųjų spindulių spektroskopija naudojama norint gauti informacijos apie amiloidinių fibrilių antrinę struktūrą, analizuojant infraraudonųjų spindulių spektro [143,144] amido I/I' sritį. Norint gauti aukštos kokybės spektrą ir panaikinti H_2O-specifinę sugertį (kuri persidengia su amido I/I' sritimi), susidarę agregatai kelis kartus centrifuguojami ir resuspenduojami į D_2O, kad būtų pašalintas H_2O ir būtų pasiekta santykinai didelė baltymų koncentracija. Agregatų suspensijos patalpinamos tarp dviejų CaF_2 langelių ir nuskenuojamos bei suvidurkinamos 256 interferogramos. Iš gauto spektro atimami D_2O ir vandens garų spektrai. Amido I/I' srityje esančios smailės suteikia informacijos apie fibrilių antrinės struktūros niuansus ir leidžia palyginti atskirus amiloidinių fibrilių mėginius.

6.5. Atominės jėgos mikroskopija

Atominės jėgos mikroskopija (AJM) naudojama nustatyti amiloidinių agregatų morfologines savybes, tokias kaip aukštis, plotis, ilgis ir paviršiaus periodiškumai [144]. Dėl didelio jautrumo, šis metodas gali aptikti nanometrų dydžio skirtumus agregatų paviršiuje ir tai leidžia nesunkiai kategorizuoti susidarančius fibrilinius agregatus. Skirtingai nei ThT arba FTIR tyrimai, kurie suteikia vidutinę viso mėginio apžvalgą, AJM naudojamas įvertinti

kiekvienos atskiros fibrilės parametrus ir yra puikus metodus tirti heterogeninius mėginius. Santykinai didelio žėručio paviršiaus nuskaitymas su adsorbuotais agregatais leidžia sudaryti bendrą pavyzdyje esančių fibrilių įvairovės vaizdą ir apskaičiuoti anksčiau minėtų parametrų reikšmes bei pasiskirstymą. Šis metodas taip pat gali būti naudojamas norint nustatyti, ar fibrilės turi tendenciją asocijuoti tarpusavyje, formuojant dideles sankaupas.

6.6. Fluorescencinė ir šviesos sugerties spektroskopija

Mėginių fluorescencijos emisijos intensyvumo arba sužadinimo ir emisijos bangų ilgių maksimumo padėčių pokyčiai, taip pat sugerties spektrų skirtumai gali būti naudojami kaip priemonė nustatyti, ar atitinkamas junginys sąveikauja su kitomis molekulėmis bei jungiasi su amiloidinėmis fibrilėmis [8]. Norint patikrinti, ar tokios sąveikos egzistuoja, skenuojamos mėginių sužadinimo-emisijos matricos bei sugerties spektrai. Jeigu aptinkamas signalo arba sugerties maksimumo pozicijų pokytis, galima daryti prielaidą, kad tarp tiriamų molekulių yra sąveika. Taip pat galima nustatyti, ar tokia sąveika sukelia molekulių nusėdimą arba agregatų sulipimą, matuojant tirpalo optinio tankio pokyčius naudojant 600 nm bangos ilgio šviesą.

6.7. Amiloidinių fibrilių destabilizacija

Amiloidinės fibrilės gali būti destabilizuojamos stipriai pakeičiant aplinkos sąlygas. Vienas iš dažniausiai naudojamų metodų yra agregatų tirpinimas koncentruotame denatūranto tirpale. Šiuo atveju naudojamas karbamidas, guanidino hidrochloridas arba guanidino tiocianatas. Tirpinimas denatūrantuose taip pat gali būti naudojamas nustatyti amiloidinių agregatų stabilumą [63]. Fibrilės yra sumaišomos su ruožu skirtingos koncentracijos denatūrantų tirpalų ir nustatoma, kokioje koncentracijoje agregatai pradeda skilti į monomerus. Kitas būdas yra tirpalo pH padidinimas iki vertės, kurioje fibrilės praranda struktūrinį stabilumą. Kaip pavyzdys, insulino agregatai skyla į monomerus, kai pH pakeičiamas iš rūgštinio į neutralų arba bazinį [55,94]. Trečias agregatų destabilizavimo būdas yra tirpinimas organiniuose tirpikliuose. Nustatyta, kad tiek insulino, tiek lizocimo amiloidinės fibrilės praranda stabilumą esant didelei DMSO [95,145] koncentracijai.

6.8. Junginių atskyrimas

Amiloidofilinių molekulių mišiniai sumaišomi su koncentruotu lizocimo amiloidinių fibrilių tirpalu. Prie fibrilių neprisijungusios molekulės atplaunamos kelis kartus centrifuguojant mišinį ir pakeičiant supernatantą buferiniu tirpalu. Norint atskirti su fibrilėmis surištus junginius, naudojami trys metodai: difuzija, denatūracija arba destabilizacija. Difuzijos atveju agregato-junginio tirpalas centrifuguojamas, o nuosėdos resuspenduojamos buferiniame tirpale, kuris vėliau periodiškai maišomas keletą valandų. Prisijungusios molekulės difunduoja į buferinį tirpalą ir tada gali būti atskirtos centrifuguojant mišinį ir surenkant supernatantą. Kitu atveju, fibriles galima tirpinti koncentruotame guanidino tiocianato tirpale (denatūracija) arba dimetilsulfokside (destabilizacija). Atsiskyrę junginiai filtruojami per 10 kDa koncentratorių, siekiant pašalinti lizocimo monomerus ar fibrilių fragmentus. Priešingai nei difuzijos metodu, junginius reikia papildomai atskirti nuo denatūranto arba dimetilsulfoksido.

7. REZULTATAI

7.1. Publikacija 1

Tioflaviną-T jungiančių insulino amiloidinės agregacijos tarpinių agregatų atsiradimo tyrimas

Darbo tikslas – išanalizuoti tarpinių insulino amiloidinių agregatų, gebančių jungti tioflaviną-T, atsiradimo tikimybę, struktūrą ir poveikį fibrilių formavimosi kinetikai.

Rezultatai – dėl atsitiktinių ir gana retų dvigubos sigmoidinės formos insulino agregacijos kinetinių kreivių atsiradimo, iš viso buvo ištirta tūkstantis insulino mėginių. Pastebėta, kad maždaug 5% visų agregacijos kreivių turėjo dvigubą sigmoidinį profilį, o 7% - tarpinį profilį. Rezultatai parodė, kad atsitiktinai atsirandantys, tioflaviną-T rišantys tarpiniai agregatai, neturėjo įtakos susidariusių fibrilių struktūrai, morfologijai ar savireplikacijos efektyvumui. Tačiau EEM duomenys atskleidė, kad anomalios agregacijos fazės metu yra reikšmingų maksimalių sužadinimo/emisijos bangos ilgių pozicijų poslinkių ir intensyvumo pokyčių. Pasibaigus pirmajam tioflavino-T intensyvumo pakilimui, šie pokyčiai nebebuvo matomi, o tai rodo, kad signalo pokyčius galėjo lemti ThT jungiančios tarpinės insulino agregatų rūšys.

Išvados – atsitiktinai atsirandantys insulino tarpiniai agregatai neturi įtakos fibrilių antrinei struktūrai, morfologijai ar savireplikacijos potencialui. Pirmasis signalo padidėjimas tokios anomalios agregacijos metu gali būti susijęs su tarpinių agregatų susidarymu, kurie geba nespecifiškai rišti ThT.

7.2. Publikacija 2

Insulino amiloidinių fibrilių konformacinių skirtumų nustatymas pagal tioflavino-T jungimosi charakteristiką

Darbo tikslas – ištirti, ar galima atskirti skirtingos konformacijos insulino amiloidines fibriles pagal jų tioflavino-T jungimosi charakteristikas.

Rezultatai – keturi fibrilių tipai buvo sumaišyti su įvairių koncentracijų tioflavino-T tirpalais. Tada gauti tirpalai buvo tiriami nuskaitant jų sužadinimo-emisijos matricas ir fibrilių-ThT sugerties spektrus. Fibrilės su surištomis ThT molekulėmis buvo atskirtos nuo tirpalo, buvo nuskenuoti neprisirišusio ThT sugerties spektrai, siekiant nustatyti jų koncentracijas. Rezultatai parodė, kad visi keturi fibrilių tipai turėjo unikalias surišto ThT fluorescencijos kvantines išeigas visame ThT koncentracijų ruože. EEM

analizė taip pat atskleidė skirtingas maksimalias ThT fluorescencijos sužadinimo ir emisijos pozicijas, kurios gana reikšmingai keitėsi visame ThT koncentracijų ruože. Tai rodo kelis galimus dažo surišimo būdus. Atsižvelgiant į abu šiuos parametrus, buvo galima atskirti visus keturis fibrilių tipus, nepaisant to, kad prieš analizę jie buvo resuspenduoti į identiškus tirpalus.

Išvados – pagal ThT jungimosi ir fluorescencijos parametrus (fluorescencijos kvantinė išeiga, EEM maksimumo pozicija) galima atskirti skirtingos konformacijos insulino amiloidines fibriles. Šis metodas gali būti naudojamas kaip alternatyva FTIR arba AJM tyrimams.

7.3. Publikacija 3

Skirtingų prioninių baltymų amiloidinių fibrilių susidarymas identiškomis eksperimentinėmis sąlygomis

Darbo tikslas – ištirti, ar nepriklausomi prioninių baltymų mėginiai, agreguoti identiškomis aplinkos sąlygomis, sudaro identiškų antrinių struktūrų ir morfologijų fibriles.

Rezultatai – FTIR tyrimas atskleidė, kad žemo (LI) ir vidutinio intensyvumo (MI) mėginių antrinė struktūra turėjo daug panašumų ir abu skyrėsi nuo didelio intensyvumo (HI) mėginių, kurių beta-klosčių vandeniliniai ryšiai buvo silpnesni. AJM analizė atskleidė, kad LI mėginys labiausiai skyrėsi nuo kitų, o dauguma jo fibrilių sudarė sankaupas ir turėjo skirtingas ilgio, pločio ir aukščio vertes. ThT surišimo tyrimo duomenys parodė, kad HI fibrilės turėjo skirtingą ThT jungimo būdą, o tai gali paaiškinti žymiai didesnę fluorescencijos signalo vertę. Stabilumo tyrimas neparodė jokių reikšmingų skirtumų tarp visų trijų grupių.

Išvados – šie rezultatai parodo, kad prioninis baltymas, net esant identiškoms sąlygoms, gali suformuoti bent dviejų skirtingų tipų amiloidines fibriles, kurios gali būti greitai identifikuojamos palyginant jų ThT fluorescencijos emisijos intensyvumą, FTIR spektrus ar sankaupų formavimo tendencijas.

7.4. Publikacija 4

Prioninių baltymų amiloidinių fibrilių struktūrinio variabilumo priklausomybė nuo temperatūros

Darbo tikslas – nustatyti, ar pradinė prioninių baltymų būsena nulemia jų amiloidinių fibrilių struktūrinį variabilumą.

Rezultatai – analizuojant agregacijos kinetikos lag laiko priklausomybę nuo reakcijos temperatūros Arrhenius koordinatėse, buvo nustatytas aktyvacijos energijos pokytis 45°C temperatūroje, kur prioninių baltymų molekulės pereina iš sulankstytos būsenos į nesulankstytą. Susidariusių agregatų EEM klasterių mėginiai turėjo tris skirtingus fibrilių tipus, kurių vienas tipas dominavo žemesnėje nei 45°C temperatūroje, kitas - aukštesnėje temperatūroje, o trečiasis egzistavo daugelyje sąlygų. Nagrinėjant stipriai išsiskiriančius mėginius, struktūrinis variabilumas buvo žymiai didesnis. Šiuo atveju dauguma temperatūros rinkinių turėjo kelis mėginius su skirtingais FTIR spektrais. Šios fibrilės taip pat turėjo unikalių morfologinių ypatybių: vienos sudarė ilgus susipynusius agregatų tinklus, o kitos buvo trumpos ir sulipusios į sankaupas.

Išvados – pradinė prioninių baltymų būsena yra svarbus parametras, nulemiantis susidarančių fibrilių antrinių struktūrų ir morfologijų variabilumą. Šis variabilumas buvo nustatytas visame tirtame temperatūrų ruože ir nei vienas mėginių rinkinys nebuvo homogeniškas.

7.5. Publikacija 5

Joninės jėgos poveikis tioflavino-T afiniškumui amiloidinėms fibrilėms ir jo fluorescencijos intensyvumui

Darbo tikslas – nustatyti, ar tirpalo joninė jėga turi įtakos tioflavino-T prisijungimui prie skirtingų amiloidinių fibrilių ir atsirandančiam fluorescencijos intensyvumui.

Rezultatai – pirmasis įdomus rezultatas yra tai, kad skirtingų baltymų fibrilės turėjo joms specifinę joninę jėgą, kuriai esant jos pradėjo asocijuoti į didesnes sankaupas. Visais atvejais kai buvo maža joninė jėga, agregatai liko supernatante net ir po intensyvaus centrifugavimo. Rezultatai taip pat atskleidė, kad skirtingų rūšių fibrilės turėjo specifinį ThT surišimo pajėgumą, o lizocimo fibrilės turėjo daugiausiai ThT surišimo pozicijų. Galiausiai buvo nustatyta, kad joninės jėgos stiprumas turėjo labai didelį poveikį surištų ThT

molekulių koncentracijai, kurių skaičius buvo 10 kartų didesnis esant didelei joninei jėgai, lyginant su mažomis NaCl koncentracijomis.

Išvados – tirpalo joninė jėga yra labai svarbus faktorius fibrilių tarpusavio asocijacijai, taip pat ThT surišimo pajėgumui ir dėl to atsirandančiam dažo fluorescencijos intensyvumui.

7.6. Publikacija 6

Epigalokatechin-3-galato ir joninės jėgos sąveika amiloidinės agregacijos metu

Darbo tikslas – ištirti, kaip tirpalo joninė jėga veikia epigalokatechin-3-galato (EGCG) efektyvumą insulino, alfa-sinukleino ir amiloido-beta agregacijos metu.

Rezultatai – nustatyta, kad tirpalo joninės jėgos padidėjimas gali stipriai paveikti EGCG anti-amiloidines savybes. Insulino ir alfa-sinukleino agregacijos metu, EGCG poveikis stipriai sumažėjo, kai tirpale buvo didesnė NaCl koncentracija. Amiloido-beta atveju, skirtinga tirpalo NaCl koncentracija turėjo žymiai mažesnį poveikį. Visais trimis atvejais stipriausias slopinimas buvo pastebėtas esant mažesnei tirpalo joninei jėgai ir šios sąlygos buvo optimalios tikrinant EGCG savybes. FTIR analizė parodė, kad ir NaCl, ir EGCG buvo atsakingi už insulino ir alfa-sinukleino fibrilių antrinės struktūros pokyčius. Amiloido-beta atveju nebuvo įmanoma gauti pakankamos fibrilių koncentracijos, kad būtų galima atlikti tikslią FTIR analizę ir šių veiksnių poveikis nebuvo ištirtas.

Išvados – EGCG anti-amiloidinis potencialas buvo stipriausias esant mažai tirpalo joninei jėgai, o didelės NaCl koncentracijos turėjo neigiamą įtaką jo efektyvumui. Tirpalo joninė jėga, kartu su EGCG, nulėmė insulino ir alfa-sinukleino fibrilių antrinę struktūrą.

7.7. Publikacija 7

Alfa-sinukleino amiloidinių fibrilių polimorfizmo priklausomybė nuo tirpalo joninės jėgos ir baltymo koncentracijos

Darbo tikslas – išanalizuoti alfa-sinukleino amiloidinių fibrilių struktūrinį variabilumą, kai jos susidaro skirtingomis tirpalo joninės jėgos ir baltymo koncentracijos sąlygomis.

Rezultatai – FTIR analizės metu, tarp visų 30 skirtingų sąlygų mėginių buvo nustatyti aštuoni unikalūs fibrilių tipai. Tai buvo patvirtinta nuskenavus jų atominės jėgos mikroskopijos vaizdus, kurie atskleidė skirtingas morfologijas ir fibrilių tarpusavio asociacijos tendencijas. Įdomu tai, kad žemos joninės jėgos sąlygos lėmė žymiai didesnį EEM maksimumo pozicijų, taip pat mėginių FTIR spektrų ir fibrilių morfologijos variabilumą. Tam tikromis sąlygomis tarp 96 pakartojimų buvo iki keturių skirtingų fibrilių tipų. Didesnės joninės jėgos ir baltymo koncentracijos sąlygomis polimorfizmo lygis buvo žymiai mažesnis, o kai kuriomis sąlygomis susidarė tik vieno tipo alfa-sinukleino agregatai.

Išvados – alfa-sinukleino amiloidinių fibrilių struktūrų polimorfizmas labiausiai vyrauja esant mažai tirpalo joninei jėgai ir baltymo koncentracijai. Šis struktūrinis variabilumas tampa žymiai mažesnis, kai tirpale esančio NaCl koncentracija būna 200 mM ar didesnė.

7.8. Publikacija 8

Papildoma tioflavino-T surišimo pozicija insulino fibrilių vidinėje dalyje

Darbo tikslas – nustatyti, ar insulino amiloidinės fibrilės gali turėti papildomą, ne paviršinę, tioflavino-T surišimo poziciją.

Rezultatai – nustatyta, kad surištų ThT molekulių koncentracijos skirtumas buvo minimalus tarp šių sąlygų, tačiau fluorescencijos intensyvumo vertė buvo ~ 30% didesnė mėginiuose, į kuriuos ThT buvo pridėtas prieš agregaciją. Ištyrus surišto ThT kvantinę išeigą esant mažoms dažų koncentracijoms, paaiškėjo, kad fibrilėse buvo nedidelė surištų ThT molekulių populiacija, kuri buvo atsakinga už reikšmingą bendro fluorescencijos intensyvumo skirtumą. EEM maksimumų pozicijos taip pat parodė, kad yra papildoma ThT surišimo pozicija, į kurią dažas pakliūna, kai jis pridedamas prieš agregaciją. Kai susiformuoja fibrilės, ši pozicija tampa neprieinama ir tai lemia žymiai mažesnę bendrą fluorescencijos signalo intensyvumą.

Išvados – insulino amiloidinės fibrilės turi ThT surišimo poziciją vidinėje dalyje, kuri yra pasiekiama tik agregatų formavimosi metu. Ši pozicija yra atsakinga už reikšmingą ThT fluorescencijos emisijos intensyvumo padidėjimą.

7.9. Publikacija 9

Amiloidofilinių molekulių sąveika ant insulino fibrilių paviršiaus: kooperacinis surišimas ir fluorescencijos gesinimas

Darbo tikslas – ištirti, kaip skirtingos amiloidofilinės molekulės sąveikauja viena su kita tirpale ir ant amiloidinių fibrilių paviršiaus.

Rezultatai – penkių amiloidofilinių molekulių tyrimas parodė, kad tam tikros junginių poros sąveikavo viena su kita tirpale, net ir be fibrilių. Priešingai nei buvo galima tikėtis, dauguma šių porų su insulino fibrilėmis sąveikavo kooperatyviai, o ne trukdė viena kitos prisijungimui. Tai buvo geriausiai matoma CR ir ThT atveju, kai CR turėjo didžiulį poveikį didinant surištų ThT molekulių koncentraciją. Išsamesnis tyrimas atskleidė, kad vidutiniškai, viena CR molekulė sąlygoja papildomą 1,3 ThT molekulių prisijungimą. Taip pat buvo pastebėta, kad daugelis amiloidofilinių molekulių porų slopino viena kitos fluorescencijos intensyvumą, išskyrus ANS ir Dap, kurių sužadinimo ir emisijos bangos ilgiai buvo panašūs.

Išvados – dauguma tirtų amiloidofilinių molekulių padėjo viena kitai prisijungti prie insulino amiloidinių fibrilių ir tik maža dalis molekulių trukdė viena kitai. Tačiau papildomai prijungtos molekulės sumažino mėginių fluorescencijos intensyvumą dėl vidinio filtro efektų, tiesioginės sąveikos arba nekonjuguoto FRET.

7.10. Publikacija 10

Amiloidinę agregaciją slopinančių junginių atskyrimas per fibrilių paviršių

Darbo tikslas – nustatyti, ar galima prie lizocimo fibrilių prijungti anti-amiloidinius junginius, pašalinti neveiksmingas molekules ir atskirti šiuos slopiklius nuo agregatų.

Rezultatai – su lizocimo fibrilėmis nesusirišantys junginiai buvo visiškai neveiksmingi slopinant insulino agregaciją. Molekulės, kurios vėliau buvo atskirtos nuo fibrilių, veiksmingai slopino insulino agregaciją. HPLC analizė taip pat atskleidė, kad prie fibrilių prisijungė daugiau nei vieno tipo molekulė. Šie rezultatai rodo, kad galima naudoti lizocimo amiloidines fibriles kaip priemonę pašalinti anti-amiloidinius junginius iš sudėtingų mišinių.

Išvados – visos molekulės, kurios gebėjo slopinti baltymų agregaciją, prisijungė prie lizocimo amiloidinių fibrilių paviršiaus. Šios anti-amiloidinės

molekulės buvo sėkmingai atskirtos nuo fibrilių paviršiaus naudojant difuziją, agregatų denatūraciją ar destabilizaciją.

IŠVADOS

Analizuojant tioflavino-T surišimo parametrų skirtumus, nustatyta, kad net ir identiškomis sąlygomis, prioniniai baltymai ir alfa-sinukleinas gali agreguoti į skirtingų tipų amiloidines fibriles. Išnagrinėjus šį reiškinį įvairiose skirtingose aplinkos sąlygose, paaiškėjo, kad struktūrinio variabilumo lygis koreliuoja su agregacijos sąlygomis. Esant mažai joninei jėgai alfa-sinukleino agregatų variabilumas buvo didžiausias, o prioninių baltymų atveju šis polimorfizmas buvo stebimas visose tirtose sąlygose. Atsižvelgiant į tai, kad šie baltymai stipriai skiriasi savo pirmine ir antrine struktūromis, galima daryti prielaidą, kad toks polimorfizmas būdingas ir kitų amiloidinių baltymų atveju.

Ištyrus, kaip skirtingos amiloidofilinės molekulės sąveikauja tarpusavyje ir kartu su amiloidinėmis fibrilėmis, buvo pastebėtas netikėtas rezultatas. Daugeliu atvejų kombinuotos junginių poros padėjo viena kitai prisijungti prie baltymų agregatų paviršiaus, o Kongo raudonasis ir tioflavinas-T turėjo veiksmingiausią tarpusavio sąveiką. Šis pastebėjimas leido manyti, kad fibrilės paviršiuje gali būti daug skirtingų surišimo būdų ir kad skirtingos struktūros molekulės gali nekonkuruoti dėl padėties, o padėti viena kitai prisijungti, sukeldamos nedidelius fibrilės struktūrinius pokyčius arba ekranuodamos jos paviršiaus krūvį.

Atlikus tyrimus kaip aplinka veikia baltymų agregatų ir amiloidofilinių molekulių sąveiką, paaiškėjo, kad joninė jėga buvo itin svarbus veiksnys. Tirpale esant didesnei NaCl koncentracijai, lizocimo fibrilės gebėjo prijungti net 10 kartų didesnį kiekį tioflavino-T molekulių. Kitų tirtų amiloidinių baltymų atveju (insulinas, prioninis baltymas, alfa-sinukleinas) taip pat buvo stebimas padidėjęs tioflavino-T jungimo efektas. Taip pat buvo įrodyta, kad tam tikros baltymų fibrilės savo vidinėje struktūroje gali turėti surišimo būdą, kuris nėra pasiekiamas po to, kai įvyksta agregacija.

Remiantis bendrais fibrilių-molekulių jungimosi tyrimų rezultatais, buvo iškelta hipotezė, kad anti-amiloidiniai junginiai gali būti selektyviai atskiriami iš sudėtingų junginių mišinių, panaudojant jų jungimąsi su lizocimo fibrilėmis. Visos molekulės, kurios neslopino amiloidinės agregacijos, negalėjo prisijungti prie lizocimo agregatų, o viskas, kas galėjo sulėtinti fibrilizacijos reakciją, susijungė su fibrilių paviršiumi. Po difuzijos ir lizocimo agregatų destabilizavimo, surišti junginiai galėjo būti atskirti iš tirpalo. Šis metodas pasirodė esąs veiksmingas naudojant visus, skirtingo kompleksiškumo, inhibitorių tirpalus ir gali būti pritaikomas potencialių vaistų paieškoje.

REFERENCES/BIBLIOGRAFIJA

[1] Sipe JD, Cohen AS. Review: History of the amyloid fibril. J Struct Biol 2000;130:88–98. https://doi.org/10.1006/jsbi.2000.4221.

[2] Nizhnikov AA, Antonets KS, Inge-Vechtomov SG. Amyloids: from pathogenesis to function. Biochem 2015;80:1127–44. https://doi.org/10.1134/S0006297915090047.

[3] Waugh DF, Thompson RE, Weimer RJ. Assay of insulin in vitro by fibril elongation and precipitation. J Biol Chem 1950;185:85–95. https://doi.org/10.1016/S0021-9258(18)56396-1.

[4] Cohen AS, Calkins E. Electron Microscopic Observations on a Fibrous Component in Amyloid of Diverse Origins. Nature 1959;183:1202–3. https://doi.org/10.1038/1831202a0.

[5] Kushnirov V V., Dergalev AA, Alexandrov AI. Proteinase K resistant cores of prions and amyloids. Prion 2020;14:11–9. https://doi.org/10.1080/19336896.2019.1704612.

[6] Chiti F, Dobson CM. Protein Misfolding, Functional Amyloid, and Human Disease. Annu Rev Biochem 2006;75:333–66. https://doi.org/10.1146/annurev.biochem.75.101304.123901.

[7] Knowles TPJ, Waudby CA, Devlin GL, Cohen SIA, Aguzzi A, Vendruscolo M, et al. An analytical solution to the kinetics of breakable filament assembly. Science (80-) 2009;326:1533–7. https://doi.org/10.1126/science.1178250.

[8] Girych M, Gorbenko G, Maliyov I, Trusova V, Mizuguchi C, Saito H, et al. Combined thioflavin T–Congo red fluorescence assay for amyloid fibril detection. Methods Appl Fluoresc 2016;4:034010. https://doi.org/10.1088/2050-6120/4/3/034010.

[9] Heise H, Hoyer W, Becker S, Andronesi OC, Riedel D, Baldus M. Molecular-level secondary structure, polymorphism, and dynamics of full-length -synuclein fibrils studied by solid-state NMR. Proc Natl Acad Sci 2005;102:15871–6. https://doi.org/10.1073/pnas.0506109102.

[10] Fitzpatrick AWP, Debelouchina GT, Bayro MJ, Clare DK, Caporini MA, Bajaj VS, et al. Atomic structure and hierarchical assembly of a cross- amyloid fibril. Proc Natl Acad Sci 2013;110:5468–73. https://doi.org/10.1073/pnas.1219476110.

[11] Park J, Egolum U, Parker S, Andrews E, Ombengi D, Ling H. Tafamidis: A First-in-Class Transthyretin Stabilizer for Transthyretin Amyloid Cardiomyopathy. Ann Pharmacother 2020;54:470–7. https://doi.org/10.1177/1060028019888489.

[12] Cummings J, Lee G, Ritter A, Sabbagh M, Zhong K. Alzheimer's disease drug development pipeline: 2020. Alzheimer's Dement Transl Res Clin Interv 2020;6:1–29. https://doi.org/10.1002/trc2.12050.

[13] Abyadeh M, Gupta V, Gupta V, Chitranshi N, Wu Y, Meyfour A, et al. Comparative Analysis of Aducanumab , Zagotenemab and

Pioglitazone as Targeted Treatment Strategies for Alzheimer ' s Disease 2021;12:1–13.
[14] Chiti F, Dobson CM. Protein Misfolding, Amyloid Formation, and Human Disease: A Summary of Progress Over the Last Decade. Annu Rev Biochem 2017;86:27–68. https://doi.org/10.1146/annurev-biochem- 061516-045115.
[15] Baker KR, Rice L. The Amyloidoses: Clinical Features, Diagnosis And Treatment. Methodist Debakey Cardiovasc J 2012;8:3–7. https://doi.org/10.14797/mdcj-8-3-3.
[16] Monsellier E, Ramazzotti M, Taddei N, Chiti F. Aggregation propensity of the human proteome. PLoS Comput Biol 2008;4. https://doi.org/10.1371/journal.pcbi.1000199.
[17] Al-garawi ZS, Morris KL, Marshall KE, Eichler J, Serpell LC, Serpell LC. The diversity and utility of amyloid fibrils formed by short amyloidogenic peptides 2017.
[18] Reches M, Gazit E. Formation of Closed-Cage Nanostructures by Self-Assembly of Aromatic Dipeptides. Nano Lett 2004;4:581–5. https://doi.org/10.1021/nl035159z.
[19] Chakrabarti S, Kumar Khemka V, Banerjee A, Chatterjee G, Ganguly A, Biswas A. Metabolic Risk Factors of Sporadic Alzheimer's Disease: Implications in the Pathology, Pathogenesis and Treatment. Aging Dis 2015;6:282. https://doi.org/10.14336/AD.2014.002.
[20] Chai C, Lim K. Genetic Insights into Sporadic Parkinson's Disease Pathogenesis. Curr Genomics 2014;14:486–501. https://doi.org/10.2174/1389202914666131210195808.
[21] Myers RH. Huntington's Disease Genetics. NeuroRx 2004;1:255–62. https://doi.org/10.1602/neurorx.1.2.255.
[22] Cortelli P, Gambetti P, Montagna P, Lugaresi E. Fatal familial insomnia: Clinical features and molecular genetics. J Sleep Res 1999;8:23–9. https://doi.org/10.1046/j.1365-2869.1999.00005.x.
[23] Baldwin KJ, Correll CM. Prion Disease. Semin Neurol 2019;39:428–39. https://doi.org/10.1055/s-0039-1687841.
[24] Shikama Y, Kitazawa JI, Yagihashi N, Uehara O, Murata Y, Yajima N, et al. Localized amyloidosis at the site of repeated insulin injection in a diabetic patient. Intern Med 2010;49:397–401. https://doi.org/10.2169/internalmedicine.49.2633.
[25] Collinge J. Variant Creutzfeldt-Jakob disease. Lancet 1999;354:317–23. https://doi.org/10.1016/S0140-6736(99)05128-4.
[26] Mehta D, Jackson R, Paul G, Shi J, Sabbagh M. Why do trials for Alzheimer's disease drugs keep failing? A discontinued drug perspective for 2010-2015. Expert Opin Investig Drugs 2017;26:735–9. https://doi.org/10.1080/13543784.2017.1323868.
[27] Yu M, Chen X, Liu J, Ma Q, Zhuo Z, Chen H, et al. Gallic acid disruption of Aβ1–42 aggregation rescues cognitive decline of APP/PS1 double transgenic mouse. Neurobiol Dis 2019;124:67–80.

https://doi.org/10.1016/j.nbd.2018.11.009.
[28] Williams P, Sorribas A, Howes M-JR. Natural products as a source of Alzheimer's drug leads. Nat Prod Rep 2011;28:48–77. https://doi.org/10.1039/C0NP00027B.
[29] Prins ND, Scheltens P. Treating Alzheimer's disease with monoclonal antibodies: Current status and outlook for the future. Alzheimer's Res Ther 2013;5. https://doi.org/10.1186/alzrt220.
[30] Doig AJ, del Castillo-Frias MP, Berthoumieu O, Tarus B, Nasica-Labouze J, Sterpone F, et al. Why Is Research on Amyloid-β Failing to Give New Drugs for Alzheimer's Disease? ACS Chem Neurosci 2017;8:1435–7. https://doi.org/10.1021/acschemneuro.7b00188.
[31] Cummings J, Lee G, Zhong K, Fonseca J, Taghva K. Alzheimer's disease drug development pipeline: 2021. Alzheimer's Dement Transl Res Clin Interv 2021;7:1–24. https://doi.org/10.1002/trc2.12179.
[32] Brookmeyer R, Gray S, Kawas C. Projections of Alzheimer's disease in the United States and the public health impact of delaying disease onset. Am J Public Health 1998;88:1337–42. https://doi.org/10.2105/AJPH.88.9.1337.
[33] Arthur KC, Calvo A, Price TR, Geiger JT, Chiò A, Traynor BJ. Projected increase in amyotrophic lateral sclerosis from 2015 to 2040. Nat Commun 2016;7:12408. https://doi.org/10.1038/ncomms12408.
[34] Ferreira N, Saraiva MJ, Almeida MR. Natural polyphenols inhibit different steps of the process of transthyretin (TTR) amyloid fibril formation. FEBS Lett 2011;585:2424–30. https://doi.org/10.1016/j.febslet.2011.06.030.
[35] Siposova K, Kozar T, Huntosova V, Tomkova S, Musatov A. Inhibition of amyloid fibril formation and disassembly of pre-formed fibrils by natural polyphenol rottlerin. Biochim Biophys Acta - Proteins Proteomics 2019;1867:259–74. https://doi.org/10.1016/j.bbapap.2018.10.002.
[36] Andrich K, Bieschke J. Natural Compounds as Therapeutic Agents for Amyloidogenic Diseases. vol. 863. Cham: Springer International Publishing; 2015. https://doi.org/10.1007/978-3-319-18365-7.
[37] Wawer J, Szociński M, Olszewski M, Piątek R, Naczk M, Krakowiak J. Influence of the ionic strength on the amyloid fibrillogenesis of hen egg white lysozyme. Int J Biol Macromol 2019;121:63–70. https://doi.org/10.1016/j.ijbiomac.2018.09.165.
[38] Gaspar R, Lund M, Sparr E, Linse S. Anomalous Salt Dependence Reveals an Interplay of Attractive and Repulsive Electrostatic Interactions in α-synuclein Fibril Formation. QRB Discov 2020;1. https://doi.org/10.1017/qrd.2020.7.
[39] Bousset L, Pieri L, Ruiz-Arlandis G, Gath J, Jensen PH, Habenstein B, et al. Structural and functional characterization of two alpha-synuclein strains. Nat Commun 2013;4. https://doi.org/10.1038/ncomms3575.
[40] Meisl G, Yang X, Hellstrand E, Frohm B, Kirkegaard JB, Cohen SIA,

et al. Differences in nucleation behavior underlie the contrasting aggregation kinetics of the Aβ40 and Aβ42 peptides. Proc Natl Acad Sci 2014;111:9384–9. https://doi.org/10.1073/pnas.1401564111.

[41] Buell AK, Galvagnion C, Gaspar R, Sparr E, Vendruscolo M, Knowles TPJ, et al. Solution conditions determine the relative importance of nucleation and growth processes in -synuclein aggregation. Proc Natl Acad Sci 2014;111:7671–6. https://doi.org/10.1073/pnas.1315346111.

[42] Chamachi NG, Chakrabarty S. Temperature-Induced Misfolding in Prion Protein: Evidence of Multiple Partially Disordered States Stabilized by Non-Native Hydrogen Bonds. Biochemistry 2017;56:833–44. https://doi.org/10.1021/acs.biochem.6b01042.

[43] Milto K, Michailova K, Smirnovas V. Elongation of Mouse Prion Protein Amyloid-Like Fibrils: Effect of Temperature and Denaturant Concentration. PLoS One 2014;9:e94469. https://doi.org/10.1371/journal.pone.0094469.

[44] Hafner-Bratkovič I, Gaedtke L, Ondracka A, Veranič P, Vorberg I, Jerala R. Effect of Hydrophobic Mutations in the H2-H3 Subdomain of Prion Protein on Stability and Conversion In Vitro and In Vivo. PLoS One 2011;6:e24238. https://doi.org/10.1371/journal.pone.0024238.

[45] Batzli KM, Love BJ. Agitation of amyloid proteins to speed aggregation measured by ThT fluorescence: A call for standardization. Mater Sci Eng C 2015;48:359–64. https://doi.org/10.1016/j.msec.2014.09.015.

[46] Hellstrand E, Boland B, Walsh DM, Linse S. Amyloid β-protein aggregation produces highly reproducible kinetic data and occurs by a two-phase process. ACS Chem Neurosci 2010;1:13–8. https://doi.org/10.1021/cn900015v.

[47] Perez-Jimenez R, Godoy-Ruiz R, Ibarra-Molero B, Sanchez-Ruiz JM. The Efficiency of Different Salts to Screen Charge Interactions in Proteins: A Hofmeister Effect? Biophys J 2004;86:2414–29. https://doi.org/10.1016/S0006-3495(04)74298-8.

[48] Ghosh P, Vaidya A, Kumar A, Rangachari V. Determination of critical nucleation number for a single nucleation amyloid-β aggregation model. Math Biosci 2016;273:70–9. https://doi.org/10.1016/j.mbs.2015.12.004.

[49] Villali J, Dark J, Brechtel TM, Pei F, Sindi SS, Serio TR. Nucleation seed size determines amyloid clearance and establishes a barrier to prion appearance in yeast. Nat Struct Mol Biol 2020;27:540–9. https://doi.org/10.1038/s41594-020-0416-6.

[50] Grigorashvili EI, Selivanova OM, Dovidchenko N V., Dzhus UF, Mikhailina AO, Suvorina MY, et al. Determination of size of folding nuclei of fibrils formed from recombinant Aβ(1-40) peptide. Biochem 2016;81:538–47. https://doi.org/10.1134/S0006297916050114.

[51] Gurry T, Stultz CM. Mechanism of amyloid-β fibril elongation. Biochemistry 2014;53:6981–91. https://doi.org/10.1021/bi500695g.
[52] Milto K, Botyriute A, Smirnovas V. Amyloid-Like Fibril Elongation Follows Michaelis-Menten Kinetics. PLoS One 2013;8:8–11. https://doi.org/10.1371/journal.pone.0068684.
[53] Rodriguez RA, Chen LY, Plascencia-Villa G, Perry G. Thermodynamics of Amyloid-β Fibril Elongation: Atomistic Details of the Transition State. ACS Chem Neurosci 2018;9:783–9. https://doi.org/10.1021/acschemneuro.7b00409.
[54] Ghosh P, Kumar A, Datta B, Rangachari V. Dynamics of protofibril elongation and association involved in Aβ42 peptide aggregation in Alzheimer's disease. BMC Bioinformatics 2010;11:1–19. https://doi.org/10.1186/1471-2105-11-24.
[55] Darussalam EY, Peterfi O, Deckert-Gaudig T, Roussille L, Deckert V. pH-dependent disintegration of insulin amyloid fibrils monitored with atomic force microscopy and surface-enhanced Raman spectroscopy. Spectrochim Acta - Part A Mol Biomol Spectrosc 2021;256:119672. https://doi.org/10.1016/j.saa.2021.119672.
[56] Van Gestel J, De Leeuw SW. The formation of fibrils by intertwining of filaments: Model and application to amyloid Aβ protein. Biophys J 2007;92:1157–63. https://doi.org/10.1529/biophysj.106.097535.
[57] Nicoud L, Lazzari S, Balderas Barragán D, Morbidelli M. Fragmentation of Amyloid Fibrils Occurs in Preferential Positions Depending on the Environmental Conditions. J Phys Chem B 2015;119:4644–52. https://doi.org/10.1021/acs.jpcb.5b01160.
[58] Sun Y, Makarava N, Lee C-I, Laksanalamai P, Robb FT, Baskakov I V. Conformational Stability of PrP Amyloid Fibrils Controls Their Smallest Possible Fragment Size. J Mol Biol 2008;376:1155–67. https://doi.org/10.1016/j.jmb.2007.12.053.
[59] Taneja V, Verma M, Vats A. Toxic species in amyloid disorders: Oligomers or mature fibrils. Ann Indian Acad Neurol 2015;18:138. https://doi.org/10.4103/0972-2327.144284.
[60] Törnquist M, Michaels TCT, Sanagavarapu K, Yang X, Meisl G, Cohen SIA, et al. Secondary nucleation in amyloid formation. Chem Commun 2018;54:8667–84. https://doi.org/10.1039/C8CC02204F.
[61] Foderà V, Librizzi F, Groenning M, Van De Weert M, Leone M. Secondary nucleation and accessible surface in insulin amyloid fibril formation. J Phys Chem B 2008;112:3853–8. https://doi.org/10.1021/jp710131u.
[62] Gaspar R, Meisl G, Buell AK, Young L, Kaminski CF, Knowles TPJ, et al. Secondary nucleation of monomers on fibril surface dominates α-synuclein aggregation and provides autocatalytic amyloid amplification. Q Rev Biophys 2017;50. https://doi.org/10.1017/S0033583516000172.
[63] Sneideris T, Milto K, Smirnovas V. Polymorphism of amyloid-like

fibrils can be defined by the concentration of seeds. PeerJ 2015;3:e1207. https://doi.org/10.7717/peerj.1207.
[64] Scheidt T, Łapińska U, Kumita JR, Whiten DR, Klenerman D, Wilson MR, et al. Secondary nucleation and elongation occur at different sites on Alzheimer's amyloid-β aggregates. Sci Adv 2019;5:eaau3112. https://doi.org/10.1126/sciadv.aau3112.
[65] Jeong JS, Ansaloni A, Mezzenga R, Lashuel HA, Dietler G. Novel mechanistic insight into the molecular basis of amyloid polymorphism and secondary nucleation during amyloid formation. J Mol Biol 2013;425:1765–81. https://doi.org/10.1016/j.jmb.2013.02.005.
[66] Langkilde AE, Vestergaard B. Methods for structural characterization of prefibrillar intermediates and amyloid fibrils. FEBS Lett 2009;583:2600–9. https://doi.org/10.1016/j.febslet.2009.05.040.
[67] Stohr J, Weinmann N, Wille H, Kaimann T, Nagel-Steger L, Birkmann E, et al. Mechanisms of prion protein assembly into amyloid. Proc Natl Acad Sci 2008;105:2409–14. https://doi.org/10.1073/pnas.0712036105.
[68] Dolui S, Roy A, Pal U, Saha A, Maiti NC. Structural Insight of Amyloidogenic Intermediates of Human Insulin. ACS Omega 2018;3:2452–62. https://doi.org/10.1021/acsomega.7b01776.
[69] Grudzielanek S, Smirnovas V, Winter R. Solvation-assisted Pressure Tuning of Insulin Fibrillation: From Novel Aggregation Pathways to Biotechnological Applications. J Mol Biol 2006;356:497–509. https://doi.org/10.1016/j.jmb.2005.11.075.
[70] Saiki M, Shiba K, Okumura M. Structural stability of amyloid fibrils depends on the existence of the peripheral sequence near the core cross-β region. FEBS Lett 2015;589:3541–7. https://doi.org/10.1016/j.febslet.2015.10.015.
[71] Zandomeneghi G, Krebs MRH, McCammon MG, Fändrich M. FTIR reveals structural differences between native β-sheet proteins and amyloid fibrils. Protein Sci 2009;13:3314–21. https://doi.org/10.1110/ps.041024904.
[72] Cobb NJ, Apostol MI, Chen S, Smirnovas V, Surewicz WK. Conformational Stability of Mammalian Prion Protein Amyloid Fibrils Is Dictated by a Packing Polymorphism within the Core Region. J Biol Chem 2014;289:2643–50. https://doi.org/10.1016/j.jmb.2010.05.051.
[73] Shigeto S, Chang C, Hiramatsu H. Directly Probing Intermolecular Structural Change of a Core Fragment of β 2 -Microglobulin Amyloid Fibrils with Low-Frequency Raman Spectroscopy. J Phys Chem B 2017;121:490–6. https://doi.org/10.1021/acs.jpcb.6b10779.
[74] Dregni AJ, Wang HK, Wu H, Duan P, Jin J, Degrado WF, et al. Inclusion of the C-Terminal Domain in the β-Sheet Core of Heparin-Fibrillized Three-Repeat Tau Protein Revealed by Solid-State Nuclear Magnetic Resonance Spectroscopy. J Am Chem Soc 2021;143:7839–51. https://doi.org/10.1021/jacs.1c03314.

[75] Nilsson M. Techniques to study amyloid fibril formation in vitro. Methods 2004;34:151–60. https://doi.org/10.1016/j.ymeth.2004.03.012.
[76] Dzwolak W, Smirnovas V, Jansen R, Winter R. Insulin forms amyloid in a strain-dependent manner: An FT-IR spectroscopic study. Protein Sci 2004;13:1927–32. https://doi.org/10.1110/ps.03607204.
[77] Tayeb-fligelman E, Tabachnikov O, Moshe A, Goldshmidt-tran O, Sawaya MR, Coquelle N, et al. The cytotoxic Staphylococcus aureus. Science 2017;355:21–4.
[78] Toyama BH, Weissman JS. Amyloid structure: Conformational diversity and consequences. Annu Rev Biochem 2011;80:557–85. https://doi.org/10.1146/annurev-biochem-090908-120656.
[79] Zhang S-Q, Huang H, Yang J, Kratochvil HT, Lolicato M, Liu Y, et al. Designed peptides that assemble into cross-α amyloid-like structures. Nat Chem Biol 2018;14:870–5. https://doi.org/10.1038/s41589-018-0105-5.
[80] Giorgetti S, Greco C, Tortora P, Aprile F. Targeting Amyloid Aggregation: An Overview of Strategies and Mechanisms. Int J Mol Sci 2018;19:2677. https://doi.org/10.3390/ijms19092677.
[81] Jansen R, Grudzielanek S, Dzwolak W, Winter R. High Pressure Promotes Circularly Shaped Insulin Amyloid. J Mol Biol 2004;338:203–6. https://doi.org/10.1016/j.jmb.2004.02.056.
[82] Andersen CB, Yagi H, Manno M, Martorana V, Ban T, Christiansen G, et al. Branching in amyloid fibril growth. Biophys J 2009;96:1529–36. https://doi.org/10.1016/j.bpj.2008.11.024.
[83] Fujiwara S, Matsumoto F, Yonezawa Y. Effects of salt concentration on association of the amyloid protofilaments of Hen egg white lysozyme studied by time-resolved neutron scattering. J Mol Biol 2003;331:21–8. https://doi.org/10.1016/S0022-2836(03)00722-8.
[84] Okamura N, Mori M, Furumoto S, Yoshikawa T, Harada R, Ito S, et al. In vivo detection of amyloid plaques in the mouse brain using the near-infrared fluorescence probe THK-265. J Alzheimer's Dis 2011;23:37–48. https://doi.org/10.3233/JAD-2010-100270.
[85] Bousset L, Pieri L, Ruiz-Arlandis G, Gath J, Jensen PH, Habenstein B, et al. Structural and functional characterization of two alpha-synuclein strains. Nat Commun 2013;4:2575. https://doi.org/10.1038/ncomms3575.
[86] Sidhu A, Segers-Nolten I, Raussens V, Claessens MMAE, Subramaniam V. Distinct Mechanisms Determine α-Synuclein Fibril Morphology during Growth and Maturation. ACS Chem Neurosci 2017;8:538–47. https://doi.org/10.1021/acschemneuro.6b00287.
[87] Fändrich M, Meinhardt J, Grigorieff N. Structural polymorphism of Alzheimer Aβ and other amyloid fibrils. Prion 2009;3:89–93. https://doi.org/10.4161/pri.3.2.8859.
[88] Yang S, Thackray AM, Hopkins L, Monie TP, Burke DF, Bujdoso R.

Polymorphisms at amino acid residues 141 and 154 influence conformational variation in ovine PrP. Biomed Res Int 2014;2014:372491. https://doi.org/10.1155/2014/372491.
[89] Collinge J. Molecular neurology of prion disease. J Neurol Neurosurg Psychiatry 2005;76:906–19. https://doi.org/10.1136/jnnp.2004.048660.
[90] Tixador P, Herzog L, Reine F, Jaumain E, Chapuis J, Le Dur A, et al. The physical relationship between infectivity and prion protein aggregates is strain-dependent. PLoS Pathog 2010;6:e1000859. https://doi.org/10.1371/journal.ppat.1000859.
[91] Arora A, Ha C, Park CB. Insulin amyloid fibrillation at above 100°C: New insights into protein folding under extreme temperatures. Protein Sci 2004;13:2429–36. https://doi.org/10.1110/ps.04823504.
[92] Vernaglia BA, Huang J, Clark ED. Guanidine Hydrochloride Can Induce Amyloid Fibril Formation from Hen Egg-White Lysozyme. Biomacromolecules 2004;5:1362–70. https://doi.org/10.1021/bm0498979.
[93] Surmacz-Chwedoruk W, Babenko V, Dec R, Szymczak P, Dzwolak W. The emergence of superstructural order in insulin amyloid fibrils upon multiple rounds of self-seeding 2016. https://doi.org/10.1038/srep32022.
[94] Shammas SL, Knowles TPJ, Baldwin AJ, MacPhee CE, Welland ME, Dobson CM, et al. Perturbation of the Stability of Amyloid Fibrils through Alteration of Electrostatic Interactions. Biophys J 2011;100:2783–91. https://doi.org/10.1016/j.bpj.2011.04.039.
[95] Voets IK, Cruz WA, Moitzi C, Lindner P, Arêas EPG, Schurtenberger P. DMSO-induced denaturation of hen egg white lysozyme. J Phys Chem B 2010;114:11875–83. https://doi.org/10.1021/jp103515b.
[96] Ono K, Hirohata M, Yamada M. Ferulic acid destabilizes preformed β-amyloid fibrils in vitro. Biochem Biophys Res Commun 2005;336:444–9. https://doi.org/10.1016/j.bbrc.2005.08.148.
[97] Ono K, Yoshiike Y, Takashima A, Hasegawa K, Naiki H, Yamada M. Potent anti-amyloidogenic and fibril-destabilizing effects of polyphenols in vitro: implications for the prevention and therapeutics of Alzheimer's disease. J Neurochem 2003;87:172–81. https://doi.org/10.1046/j.1471-4159.2003.01976.x.
[98] Jayamani J, Shanmugam G. Gallic acid, one of the components in many plant tissues, is a potential inhibitor for insulin amyloid fibril formation. Eur J Med Chem 2014;85:352–8. https://doi.org/10.1016/j.ejmech.2014.07.111.
[99] Pandey G, Ramakrishnan V. Invasive and non-invasive therapies for Alzheimer's disease and other amyloidosis. Biophys Rev 2020;12:1175–86. https://doi.org/10.1007/s12551-020-00752-y.
[100] Findeis MA. The role of amyloid β peptide 42 in Alzheimer's disease. Pharmacol Ther 2007;116:266–86.

https://doi.org/10.1016/j.pharmthera.2007.06.006.
[101] Brothers HM, Gosztyla ML, Robinson SR. The physiological roles of amyloid-β peptide hint at new ways to treat Alzheimer's disease. Front Aging Neurosci 2018;10:1–16. https://doi.org/10.3389/fnagi.2018.00118.
[102] Cataldi R, Chia S, Pisani K, Ruggeri FS, Xu CK, Šneideris T, et al. A dopamine metabolite stabilizes neurotoxic amyloid-β oligomers. Commun Biol 2021;4:1–10. https://doi.org/10.1038/s42003-020-01490-3.
[103] Fibers U, Nichols MR, Moss MA, Reed DK, Hoh JH, Rosenberry TL. Rapid Assembly of Amyloid- Peptide at a Liquid / Liquid Interface Produces. Society 2005:165–73.
[104] Morel B, Carrasco-Jiménez MP, Jurado S, Conejero-Lara F. Rapid conversion of amyloid-beta 1-40 oligomers to mature fibrils through a self-catalytic bimolecular process. Int J Mol Sci 2021;22:1–21. https://doi.org/10.3390/ijms22126370.
[105] Šneideris T, Baranauskienė L, Cannon JG, Rutkienė R, Meškys R, Smirnovas V. Looking for a generic inhibitor of amyloid-like fibril formation among flavone derivatives. PeerJ 2015;3:e1271. https://doi.org/10.7717/peerj.1271.
[106] Bendor JT, Logan TP, Edwards RH. The function of α-synuclein. Neuron 2013;79:1044–66. https://doi.org/10.1016/j.neuron.2013.09.004.
[107] Mehra S, Gadhe L, Bera R, Sawner AS, Maji SK. Structural and functional insights into α-synuclein fibril polymorphism. Biomolecules 2021;11. https://doi.org/10.3390/biom11101419.
[108] Giehm L, Lorenzen N, Otzen DE. Assays for α-synuclein aggregation. Methods 2011;53:295–305. https://doi.org/10.1016/j.ymeth.2010.12.008.
[109] Ray S, Singh N, Kumar R, Patel K, Pandey S, Datta D, et al. α-Synuclein aggregation nucleates through liquid–liquid phase separation. Nat Chem 2020;12:705–16. https://doi.org/10.1038/s41557-020-0465-9.
[110] Campioni S, Carret G, Jordens S, Nicoud L, Mezzenga R, Riek R. The presence of an air-water interface affects formation and elongation of α-synuclein fibrils. J Am Chem Soc 2014;136:2866–75. https://doi.org/10.1021/ja412105t.
[111] Linden R. The biological function of the prion protein: A cell surface scaffold of signaling modules. Front Mol Neurosci 2017;10:1–19. https://doi.org/10.3389/fnmol.2017.00077.
[112] Atkinson CJ, Zhang K, Munn AL, Wiegmans A, Wei MQ. Prion protein scrapie and the normal cellular prion protein. Prion 2016;10:63–82. https://doi.org/10.1080/19336896.2015.1110293.
[113] Baskakov I, Disterer P, Breydo L, Shaw M, Gill A, James W, et al. The presence of valine at residue 129 in human prion protein accelerates

amyloid formation. FEBS Lett 2005;579:2589–96. https://doi.org/10.1016/j.febslet.2005.03.075.
[114] Wang F, Wang X, Orrú CD, Groveman BR, Surewicz K, Abskharon R, et al. Self-propagating, protease-resistant, recombinant prion protein conformers with or without in vivo pathogenicity. PLoS Pathog 2017;13:1–23. https://doi.org/10.1371/journal.ppat.1006491.
[115] Tokarz VL, MacDonald PE, Klip A. The cell biology of systemic insulin function. J Cell Biol 2018;217:2273–89. https://doi.org/10.1083/jcb.201802095.
[116] Gupta Y, Singla G, Singla R. Insulin-derived amyloidosis. Indian J Endocrinol Metab 2015;19:174–7. https://doi.org/10.4103/2230-8210.146879.
[117] Iannuzzi C, Borriello M, Portaccio M, Irace G, Sirangelo I. Insights into insulin fibril assembly at physiological and acidic ph and related amyloid intrinsic fluorescence. Int J Mol Sci 2017;18. https://doi.org/10.3390/ijms18122551.
[118] Noormägi A, Valmsen K, Tõugu V, Palumaa P. Insulin Fibrillization at Acidic and Physiological pH Values is Controlled by Different Molecular Mechanisms. Protein J 2015;34:398–403. https://doi.org/10.1007/s10930-015-9634-x.
[119] Nettleton EJ, Tito P, Sunde M, Bouchard M, Dobson CM, Robinson C V. Characterization of the Oligomeric States of Insulin in Self-Assembly and Amyloid Fibril Formation by Mass Spectrometry. Biophys J 2000;79:1053–65. https://doi.org/10.1016/S0006-3495(00)76359-4.
[120] Sneideris T, Darguzis D, Botyriute A, Grigaliunas M, Winter R, Smirnovas V. pH-Driven Polymorphism of Insulin Amyloid-Like Fibrils. PLoS One 2015;10:e0136602. https://doi.org/10.1371/journal.pone.0136602.
[121] Nielsen L, Khurana R, Coats A, Frokjaer S, Brange J, Vyas S, et al. Effect of environmental factors on the kinetics of insulin fibril formation: Elucidation of the molecular mechanism. Biochemistry 2001;40:6036–46. https://doi.org/10.1021/bi002555c.
[122] Nie R, Zhu W, Peng J, Ge Z, Li C. A-type dimeric epigallocatechin-3-gallate (EGCG) is a more potent inhibitor against the formation of insulin amyloid fibril than EGCG monomer. Biochimie 2016;125:204–12. https://doi.org/10.1016/j.biochi.2016.03.011.
[123] Wang J-B, Wang Y-M, Zeng C-M. Quercetin inhibits amyloid fibrillation of bovine insulin and destabilizes preformed fibrils. Biochem Biophys Res Commun 2011;415:675–9. https://doi.org/10.1016/j.bbrc.2011.10.135.
[124] Ragland SA, Criss AK. From bacterial killing to immune modulation: Recent insights into the functions of lysozyme. PLoS Pathog 2017;13:1–22. https://doi.org/10.1371/journal.ppat.1006512.
[125] Pleyer C, Flesche J, Saeed F. Lysozyme amyloidosis – a case report

and review of the literature. Clin Nephrol Case Stud 2015;3:2015–8. https://doi.org/10.5414/cncs108538.
[126] Yonezawa Y, Tanaka S, Kubota T, Wakabayashi K, Yutani K, Fujiwara S. An insight into the pathway of the amyloid fibril formation of hen egg white lysozyme obtained from a small-angle X-ray and neutron scattering study. J Mol Biol 2002;323:237–51. https://doi.org/10.1016/S0022-2836(02)00941-5.
[127] Swaminathan R, Ravi VK, Kumar S, Kumar MVS, Chandra N. Lysozyme: a model protein for amyloid research. Adv. Protein Chem. Struct. Biol., vol. 84, 2011, p. 63–111. https://doi.org/10.1016/B978-0-12-386483-3.00003-3.
[128] Klunk WE, Pettegrew JW, Abraham DJ. Quantitative evaluation of congo red binding to amyloid-like proteins with a beta-pleated sheet conformation. J Histochem Cytochem 1989;37:1273–81. https://doi.org/10.1177/37.8.2666510.
[129] Gade Malmos K, Blancas-Mejia LM, Weber B, Buchner J, Ramirez-Alvarado M, Naiki H, et al. ThT 101: a primer on the use of thioflavin T to investigate amyloid formation. Amyloid 2017;24:1–16. https://doi.org/10.1080/13506129.2017.1304905.
[130] Krebs MRH, Bromley EHC, Donald AM. The binding of thioflavin-T to amyloid fibrils: localisation and implications. J Struct Biol 2005;149:30–7. https://doi.org/10.1016/j.jsb.2004.08.002.
[131] Saha B, Chowdhury S, Sanyal D, Chattopadhyay K, Suresh Kumar G. Comparative Study of Toluidine Blue O and Methylene Blue Binding to Lysozyme and Their Inhibitory Effects on Protein Aggregation. ACS Omega 2018;3:2588–601. https://doi.org/10.1021/acsomega.7b01991.
[132] Yates E V., Meisl G, Knowles TPJ, Dobson CM. An Environmentally Sensitive Fluorescent Dye as a Multidimensional Probe of Amyloid Formation. J Phys Chem B 2016;120:2087–94. https://doi.org/10.1021/acs.jpcb.5b09663.
[133] Srinivasan E, Rajasekaran R. Probing the inhibitory activity of epigallocatechin-gallate on toxic aggregates of mutant (L84F) SOD1 protein through geometry based sampling and steered molecular dynamics. J Mol Graph Model 2017;74:288–95. https://doi.org/10.1016/j.jmgm.2017.04.019.
[134] Zheng Q, Lazo ND. Mechanistic Studies of the Inhibition of Insulin Fibril Formation by Rosmarinic Acid. J Phys Chem B 2018;122:2323–31. https://doi.org/10.1021/acs.jpcb.8b00689.
[135] How S-C, Cheng Y-H, Lo C-H, Lai J-T, Lin T-H, Bednarikova Z, et al. Exploring the effects of methylene blue on amyloid fibrillogenesis of lysozyme. Int J Biol Macromol 2018;119:1059–67. https://doi.org/10.1016/j.ijbiomac.2018.08.038.
[136] Kuznetsova IM, Sulatskaya AI, Uversky VN, Turoverov KK. Analyzing Thioflavin T Binding to Amyloid Fibrils by an Equilibrium

Microdialysis-Based Technique. PLoS One 2012;7:e30724. https://doi.org/10.1371/journal.pone.0030724.
[137] Freire S, De Araujo MH, Al-Soufi W, Novo M. Photophysical study of Thioflavin T as fluorescence marker of amyloid fibrils. Dye Pigment 2014;110:97–105. https://doi.org/10.1016/j.dyepig.2014.05.004.
[138] Kawai R, Araki M, Yoshimura M, Kamiya N, Ono M, Saji H, et al. Core Binding Site of a Thioflavin-T-Derived Imaging Probe on Amyloid β Fibrils Predicted by Computational Methods. ACS Chem Neurosci 2018;9:957–66. https://doi.org/10.1021/acschemneuro.7b00389.
[139] Sidhu A, Vaneyck J, Blum C, Segers-Nolten I, Subramaniam V. Polymorph-specific distribution of binding sites determines thioflavin-T fluorescence intensity in α-synuclein fibrils. Amyloid 2018;25:189–96. https://doi.org/10.1080/13506129.2018.1517736.
[140] Peduzzo A, Linse S, Buell A. The Properties of α-Synuclein Secondary Nuclei are Dominated by the Solution Conditions Rather than the Seed Fibril Strain 2019. https://doi.org/10.26434/chemrxiv.9757778.v1.
[141] Xue C, Lin TY, Chang D, Guo Z. Thioflavin T as an amyloid dye: fibril quantification, optimal concentration and effect on aggregation. R Soc Open Sci 2017;4:160696. https://doi.org/10.1098/rsos.160696.
[142] Foderà V, Groenning M, Vetri V, Librizzi F, Spagnolo S, Cornett C, et al. Thioflavin T Hydroxylation at Basic pH and Its Effect on Amyloid Fibril Detection. J Phys Chem B 2008;112:15174–81. https://doi.org/10.1021/jp805560c.
[143] Barth A. Infrared spectroscopy of proteins. Biochim Biophys Acta - Bioenerg 2007;1767:1073–101. https://doi.org/10.1016/j.bbabio.2007.06.004.
[144] Moran SD, Zanni MT. How to Get Insight into Amyloid Structure and Formation from Infrared Spectroscopy. J Phys Chem Lett 2014;5:1984–93. https://doi.org/10.1021/jz500794d.
[145] Zhang G, Babenko V, Dzwolak W, Keiderling TA. Dimethyl Sulfoxide Induced Destabilization and Disassembly of Various Structural Variants of Insulin Fibrils Monitored by Vibrational Circular Dichroism. Biochemistry 2015;54:7193–202. https://doi.org/10.1021/acs.biochem.5b00809.
[146] Foderà V, Cataldo S, Librizzi F, Pignataro B, Spiccia P, Leone M. Self-Organization Pathways and Spatial Heterogeneity in Insulin Amyloid Fibril Formation. J Phys Chem B 2009;113:10830–7. https://doi.org/10.1021/jp810972y.
[147] Kutsch M, Hortmann P, Herrmann C, Weibels S, Weingärtner H. Dissecting ion-specific from electrostatic salt effects on amyloid fibrillation: A case study of insulin. Biointerphases 2016;11:019008. https://doi.org/10.1116/1.4941008.
[148] Groenning M, Norrman M, Flink JM, van de Weert M, Bukrinsky JT, Schluckebier G, et al. Binding mode of Thioflavin T in insulin amyloid

fibrils. J Struct Biol 2007;159:483–97. https://doi.org/10.1016/j.jsb.2007.06.004.
[149] Rodina NP, Sulatsky MI, Sulatskaya AI, Kuznetsova IM, Uversky VN, Turoverov KK. Photophysical Properties of Fluorescent Probe Thioflavin T in Crowded Milieu. J Spectrosc 2017;2017. https://doi.org/10.1155/2017/2365746.
[150] Zampieri M, Legname G, Altafini C. Investigating the Conformational Stability of Prion Strains through a Kinetic Replication Model. PLoS Comput Biol 2009;5:e1000420. https://doi.org/10.1371/journal.pcbi.1000420.
[151] Morales R, Hu PP, Duran-Aniotz C, Moda F, Diaz-Espinoza R, Chen B, et al. Strain-dependent profile of misfolded prion protein aggregates. Sci Rep 2016;6:20526. https://doi.org/10.1038/srep20526.
[152] Green AJE. Prion protein aggregation assays in the diagnosis of human prion diseases. Future Neurol 2015;10:217–28. https://doi.org/10.2217/fnl.15.10.
[153] Almstedt K, Nyström S, Nilsson KPR, Hammarström P. Amyloid fibrils of human prion protein are spun and woven from morphologically disordered aggregates. Prion 2009;3. https://doi.org/10.4161/pri.3.4.10112.
[154] Fridmanis J, Toleikis Z, Sneideris T, Ziaunys M, Bobrovs R, Smirnovas V, et al. Aggregation Condition–Structure Relationship of Mouse Prion Protein Fibrils. Int J Mol Sci 2021;22:9635. https://doi.org/10.3390/ijms22179635.
[155] Morel B, Varela L, Azuaga AI, Conejero-Lara F. Environmental Conditions Affect the Kinetics of Nucleation of Amyloid Fibrils and Determine Their Morphology. Biophys J 2010;99:3801–10. https://doi.org/10.1016/j.bpj.2010.10.039.
[156] Sabaté R, Lascu I, Saupe SJ. On the binding of Thioflavin-T to HET-s amyloid fibrils assembled at pH 2. J Struct Biol 2008;162:387–96. https://doi.org/10.1016/j.jsb.2008.02.002.
[157] LeVine H. Stopped-flow kinetics reveal multiple phases of thioflavin T binding to Alzheimer β(140) amyloid fibrils. Arch Biochem Biophys 1997;342:306–16. https://doi.org/10.1006/abbi.1997.0137.
[158] Flynn JD, McGlinchey RP, Walker RL, Lee JC. Structural features of α-synuclein amyloid fibrils revealed by Raman spectroscopy. J Biol Chem 2018;293:767–76. https://doi.org/10.1074/jbc.M117.812388.
[159] Lee G, Lee W, Lee H, Woo Lee S, Sung Yoon D, Eom K, et al. Mapping the surface charge distribution of amyloid fibril. Appl Phys Lett 2012;101. https://doi.org/10.1063/1.4739494.
[160] Roy S, Bhat R. Suppression, disaggregation, and modulation of γ-Synuclein fibrillation pathway by green tea polyphenol EGCG. Protein Sci 2019;28:382–402. https://doi.org/10.1002/pro.3549.
[161] Manno M, Craparo EF, Martorana V, Bulone D, San Biagio PL. Kinetics of Insulin Aggregation: Disentanglement of Amyloid

Fibrillation from Large-Size Cluster Formation. Biophys J 2006;90:4585–91. https://doi.org/10.1529/biophysj.105.077636.
[162] Saha S, Deep S. Glycerol inhibits the primary pathways and transforms the secondary pathway of insulin aggregation. Phys Chem Chem Phys 2016;18:18934–48. https://doi.org/10.1039/C6CP02906J.
[163] Rodríguez-Rodríguez C, Rimola A, Rodríguez-Santiago L, Ugliengo P, Álvarez-Larena Á, Gutiérrez-de-Terán H, et al. Crystal structure of thioflavin-T and its binding to amyloid fibrils: insights at the molecular level. Chem Commun 2010;46:1156. https://doi.org/10.1039/b912396b.
[164] Sulatskaya AI, Maskevich AA, Kuznetsova IM, Uversky VN, Turoverov KK. Fluorescence Quantum Yield of Thioflavin T in Rigid Isotropic Solution and Incorporated into the Amyloid Fibrils. PLoS One 2010;5:e15385. https://doi.org/10.1371/journal.pone.0015385.
[165] Musteikyte G, Ziaunys M, Smirnovas V. Methylene blue inhibits nucleation and elongation of SOD1 amyloid fibrils. PeerJ 2020;8:e9719. https://doi.org/10.7717/peerj.9719.
[166] Chatani E, Yagi H, Naiki H, Goto Y. Polymorphism of β 2 - Microglobulin Amyloid Fibrils Manifested by Ultrasonication-enhanced Fibril Formation in Trifluoroethanol. J Biol Chem 2012;287:22827–37. https://doi.org/10.1074/jbc.M111.333310.
[167] Swaminathan R, Ravi VK, Kumar S, Kumar MVS, Chandra N. Lysozyme: A model protein for amyloid research. Adv. Protein Chem. Struct. Biol., vol. 84, 2011, p. 63–111. https://doi.org/10.1016/B978-0-12-386483-3.00003-3.
[168] Xu Y, Zhang Y, Quan Z, Wong W, Guo J, Zhang R, et al. Epigallocatechin Gallate (EGCG) Inhibits Alpha-Synuclein Aggregation: A Potential Agent for Parkinson's Disease. Neurochem Res 2016;41:2788–96. https://doi.org/10.1007/s11064-016-1995-9.
[169] Ngo ST, Truong DT, Tam NM, Nguyen MT. EGCG inhibits the oligomerization of amyloid beta (16-22) hexamer: Theoretical studies. J Mol Graph Model 2017;76:1–10. https://doi.org/10.1016/j.jmgm.2017.06.018.
[170] Konar M, Bag S, Roy P, Dasgupta S. Gallic acid induced dose dependent inhibition of lysozyme fibrillation. Int J Biol Macromol 2017;103:1224–31. https://doi.org/10.1016/j.ijbiomac.2017.05.158.
[171] Lee L-S, Kim S-H, Kim Y-B, Kim Y-C. Quantitative Analysis of Major Constituents in Green Tea with Different Plucking Periods and Their Antioxidant Activity. Molecules 2014;19:9173–86. https://doi.org/10.3390/molecules19079173.
[172] Bastianetto S, Yao Z-X, Papadopoulos V, Quirion R. Neuroprotective effects of green and black teas and their catechin gallate esters against β-amyloid-induced toxicity. Eur J Neurosci 2006;23:55–64. https://doi.org/10.1111/j.1460-9568.2005.04532.x.
[173] Sneideris T, Sakalauskas A, Sternke-Hoffmann R, Peduzzo A, Ziaunys

M, Buell AK, et al. The Environment Is a Key Factor in Determining the Anti-Amyloid Efficacy of EGCG. Biomolecules 2019;9:1–17. https://doi.org/10.3390/biom9120855.

[174] Wei Y, Chen P, Ling T, Wang Y, Dong R, Zhang C, et al. Certain (-)-epigallocatechin-3-gallate (EGCG) auto-oxidation products (EAOPs) retain the cytotoxic activities of EGCG. Food Chem 2016;204:218–26. https://doi.org/10.1016/j.foodchem.2016.02.134.

[175] Ishii T, Mori T, Tanaka T, Mizuno D, Yamaji R, Kumazawa S, et al. Covalent modification of proteins by green tea polyphenol (-)-epigallocatechin-3-gallate through autoxidation. Free Radic Biol Med 2008;45:1384–94. https://doi.org/10.1016/j.freeradbiomed.2008.07.023.

CURRICULUM VITAE

EDUCATION:

2012 - 2016: Bachelor's degree in Biochemistry, Vilnius University, Vilnius, Lithuania.
2016 - 2018: Master's degree in Biochemistry, Vilnius University, Vilnius, Lithuania.
2018 - 2022: PhD studies in Chemical Engineering, Vilnius University, Vilnius, Lithuania

WORK EXPERIENCE:

2015 Intern at „ThermoFisher Scientific Baltics", Vilnius, Lithuania
2015 – 2017 Intern at Department of Biothermodynamics and Drug Design, Institute of Biotechnology, Vilnius University, Vilnius, Lithuania.
2017 – 2018: Technician at Department of Biothermodynamics and Drug Design, Institute of Biotechnology, Vilnius University, Vilnius, Lithuania.
2018 – current: Junior researcher at Department of Biothermodynamics and Drug Design, Institute of Biotechnology, Vilnius University, Vilnius, Lithuania.

PARTICIPATION IN PROJECTS

1. Vilnius university research promotion fund project „Examination of amyloid fibril surface affinity for organic fluorescent dyes (MSF-JM-3)" 2019-2020;
2. RCL National Research Programme „Healthy Ageing" „Cross-interactions in amyloid fibril formation: from mechanisms to inhibition" (P-SEN-20-3) 2020-2021;
3. European Social Fund project operated by Central Project Management Agency „Exploring drug candidates for cancer and neurodegenerative diseases" (01.2.2-CPVA-K-703-03-0006) 2020-2023;
4. European Structural Fund project „Screening for new methods for treatment of neurodegenerative disorders" (01.2.2-LMT-K-718-03-0021) 2020-2023;
5. European Structural Fund project „Design of anti-Alzheimer's Drug Candidates that Inhibit BACE1 Enzymatic Activity and Aggregation of Aβ Peptide" (01.2.2-LMT-K-718-03-0003) 2020-2023.

Science promotion activities
Invited lecturer in an event organized by The COINS "Scientific article writing ABC"

LIST OF PUBLICATIONS

Publications included in the dissertation

1. **Ziaunys M**, Sakalauskas A, Mikalauskaite K, Smirnovas V. Exploring the occurrence of thioflavin-T-positive insulin amyloid aggregation intermediates. PeerJ. 2021;9:e10918. https://peerj.com/articles/10918/
Author contribution – I have devised the idea, planned the experiments, performed excitation-emission matrix scanning assays, analyzed the data and prepared the first draft of the publication.

2. **Ziaunys M**, Sakalauskas A, Smirnovas V. Identifying Insulin Fibril Conformational Differences by Thioflavin-T Binding Characteristics. Biomacromolecules. 2020 Dec 14;21(12):4989–97. https://pubs.acs.org/doi/10.1021/acs.biomac.0c01178
Author contribution – I have devised the idea, planned the experiments, performed dye binding assays and analyzed the data from all experiments. I prepared the initial draft of the publication.

3. **Ziaunys M**, Sneideris T, Smirnovas V. Formation of distinct prion protein amyloid fibrils under identical experimental conditions. Sci Rep. 2020 Dec 12;10(1):4572.http://www.nature.com/articles/s41598-020-61663-2
Author contribution – I have planned the experiments, performed aggregation kinetic, dye binding and fibril stability assays and analyzed the results from these experiments. I prepared all parts of the initial draft of the publication, apart from sections related to AFM.

4. **Ziaunys M**, Sakalauskas A, Mikalauskaite K, Snieckute R, Smirnovas V. Temperature-dependent structural variability of prion protein amyloid fibrils. Int J Mol Sci 2021;22. https://doi.org/10.3390/ijms22105075
Author contribution – I have devised the idea, planned the experiments, performed aggregation kinetic and dye binding assays and analyzed the data from all experiments. I prepared the initial draft of the publication.

5. Mikalauskaite K, **Ziaunys M**, Sneideris T, Smirnovas V. Effect of Ionic Strength on Thioflavin-T Affinity to Amyloid Fibrils and Its

Fluorescence Intensity. Int J Mol Sci. 2020 Nov 24;21(23):8916. https://www.mdpi.com/1422-0067/21/23/8916
Author contribution – I have devised the idea, planned the experiments, analyzed the data and prepared the initial draft of the publication.

6. **Ziaunys M**, Mikalauskaite K, Sakalauskas A, Smirnovas V. Interplay between epigallocatechin-3-gallate and ionic strength during amyloid aggregation. PeerJ 2021;9:e12381. https://doi.org/10.7717/peerj.12381
Author contribution – I have devised the idea, planned the experiments, performed the aggregation kinetic assays, analyzed the data and prepared the initial draft of the publication.

7. **Ziaunys M**, Sakalauskas A, Mikalauskaite K, Smirnovas V. Polymorphism of Alpha-Synuclein Amyloid Fibrils Depends on Ionic Strength and Protein Concentration. Int J Mol Sci 2021;22:12382. https://doi.org/10.3390/ijms222212382
Author contribution – I have devised the idea, planned the experiments, performed aggregation kinetic and dye binding assays and analyzed the data from all experiments. I prepared the initial draft of the publication.

8. **Ziaunys M**, Smirnovas V. Additional Thioflavin-T Binding Mode in Insulin Fibril Inner Core Region. J Phys Chem B. 2019 Oct 17;123(41):8727–32. https://pubs.acs.org/doi/10.1021/acs.jpcb.9b08652
Author contribution – I have devised the idea, planned the experiments, performed all the assays, analyzed the data and prepared the first draft of the publication.

9. **Ziaunys M**, Mikalauskaite K, Smirnovas V. Amyloidophilic Molecule Interactions on the Surface of Insulin Fibrils : Cooperative Binding and Fluorescence Quenching. Sci Rep. 2019;1–10. http://dx.doi.org/10.1038/s41598-019-56788-y
Author contribution – I have devised the idea, planned the experiments, performed dye binding assays, analyzed the data and prepared the first draft of the publication.

10. **Ziaunys M**, Mikalauskaite K, Sakalauskas A, Smirnovas V. Using lysozyme amyloid fibrils as a means of scavenging aggregation-inhibiting compounds. Biotechnol J 2021:2100138. https://doi.org/10.1002/biot.202100138

Author contribution – I have devised the idea, planned the experiments, performed aggregation kinetic assays, analyzed the data and prepared the first draft of the publication.

8. Publications not included in the dissertation

1. **Ziaunys M**, Sneideris T, Smirnovas V. Self-inhibition of insulin amyloid-like aggregation. Phys Chem Chem Phys. 2018;20(43):27638–45. https://pubs.rsc.org/en/content/articlelanding/2018/CP/C8CP04838J#!div Abstract

2. **Ziaunys M**, Smirnovas V. Emergence of visible light optical properties of L-phenylalanine aggregates. PeerJ. 2019 Feb 25;7:e6518. https://peerj.com/articles/6518

3. **Ziaunys M**, Sneideris T, Smirnovas V. Exploring the potential of deep-blue autofluorescence for monitoring amyloid fibril formation and dissociation. PeerJ. 2019 Aug 16;7:e7554. https://peerj.com/articles/7554

4. Sneideris T, Sakalauskas A, Sternke-Hoffmann R, Peduzzo A, **Ziaunys M**, Buell AK, et al. The Environment Is a Key Factor in Determining the Anti-Amyloid Efficacy of EGCG. Biomolecules. 2019;9(12):1–17. https://www.mdpi.com/2218-273X/9/12/855

5. Sakalauskas A, **Ziaunys M**, Smirnovas V. Concentration-dependent polymorphism of insulin amyloid fibrils. PeerJ. 2019 Dec 10;7(12):e8208. https://peerj.com/articles/8208

6. Martins PM, Navarro S, Silva A, Pinto MF, Sárkány Z, Figueiredo F, et al. MIRRAGGE – Minimum Information Required for Reproducible AGGregation Experiments. Front Mol Neurosci. 2020;13(November):1–18. https://www.frontiersin.org/articles/10.3389/fnmol.2020.582488/full

7. Sakalauskas A, **Ziaunys M**, Smirnovas V. Gallic acid oxidation products alter the formation pathway of insulin amyloid fibrils. Sci Rep. 2020;10(1):1–9. https://doi.org/10.1038/s41598-020-70982-3

8. Sneideris T, **Ziaunys M**, Chu BKY, Chen RPY, Smirnovas V. Self-Replication of Prion Protein Fragment 89-230 Amyloid Fibrils Accelerated

by Prion Protein Fragment 107-143 Aggregates. Int J Mol Sci. 2020 Oct 8;21(19):7410. https://www.mdpi.com/1422-0067/21/19/7410

9. Musteikyte G, **Ziaunys M**, Smirnovas V. Methylene blue inhibits nucleation and elongation of SOD1 amyloid fibrils. PeerJ. 2020 Aug 14;8:e9719. https://peerj.com/articles/9719

10. Talaikis M, Strazdaitė S, **Žiaunys M**, Niaura G. Far-Off Resonance: Multiwavelength Raman Spectroscopy Probing Amide Bands of Amyloid-β-(37–42) Peptide. Molecules. 2020 Aug 4;25(15):3556. https://www.mdpi.com/1420-3049/25/15/3556

11. **Ziaunys M**, Sakalauskas A, Sneideris T, Smirnovas V. Lysozyme fibrils alter the mechanism of insulin amyloid aggregation. Int J Mol Sci. 2021;22(4):1–12. https://www.mdpi.com/1422-0067/22/4/1775

12. Toleikis Z, **Ziaunys M**, Baranauskiene L, Petrauskas V, Jaudzems K, Smirnovas V. S100A9 Alters the Pathway of Alpha-Synuclein Amyloid Aggregation. Int J Mol Sci 2021;22:7972. https://doi.org/10.3390/ijms22157972

13. Fridmanis J, Toleikis Z, Sneideris T, **Ziaunys M**, Bobrovs R, Smirnovas V, et al. Aggregation Condition–Structure Relationship of Mouse Prion Protein Fibrils. Int J Mol Sci 2021;22:9635. https://doi.org/10.3390/ijms22179635

14. Sakalauskas A, **Ziaunys M**, Snieckute R, Smirnovas V. Autoxidation Enhances Anti-Amyloid Potential of Flavone Derivatives. Antioxidants 2021;10:1428. https://doi.org/10.3390/antiox10091428

15. **Ziaunys M**, Mikalauskaite K, Veiveris D, Sakalauskas A. Superoxide dismutase-1 alters the rate of prion protein aggregation and resulting fibril conformation. Arch Biochem Biophys 2022;715:109096. https://doi.org/10.1016/j.abb.2021.109096.

16. Mikalauskaite K, **Ziaunys M**, Smirnovas V. Lysozyme Amyloid Fibril Structural Variability Dependence on Initial Protein Folding State. Int J Mol Sci 2022;23:5421. https://doi.org/10.3390/ijms23105421.

17. Toleikis Z, Bobrovs R, Janoniene A, Lends A, **Ziaunys M**, Baronaite I, et al. Interactions between S100A9 and Alpha-Synuclein: Insight from NMR Spectroscopy. Int J Mol Sci 2022;23:6781. https://doi.org/10.3390/ijms23126781.

LIST OF SCIENTIFIC EVENTS

Results of the dissertation research were presented in scientific events:

1. „Temperature Dependent Changes in Structure and Seeding Potential of Amyloid Fibrils“. Authors: M. Žiaunys, V. Smirnovas. The COINS, Lithuania, 2019.

2. „Temperature Dependent Changes in Structure and Seeding Potential of Amyloid Fibrils.“ Authors: M. Žiaunys, V. Smirnovas. Strategies and tools for modulating pathologic protein self-assembly, Portugal, 2019.

3. „Exploring the potential of deep-blue autofluorescence for monitoring amyloid fibril formation and conformational stability.“ Authors: M. Žiaunys, T. Šneideris, V. Smirnovas. 8th Scandinavian Conference, Amyloid Diseases and Amyloid Mechanisms, Sweden, 2019.

4. „Additional Thioflavin-T Binding Mode in Insulin Amyloid Fibrils.“ Authors: M. Ziaunys, V. Smirnovas. The COINS, Lithuania, 2020.

5. „Additional Thioflavin-T Binding Mode in Insulin Amyloid Fibrils.“ Authors: M. Ziaunys, V. Smirnovas. Vita Scientia, Lithuania, 2020.

6. „Identifying Insulin Fibril Conformational Differences by Thioflavin-T Binding Characteristics“. Authors: M. Ziaunys, A. Sakalauskas, V. Smirnovas. Open readings, Lithuania, 2021.

7. „Identifying Insulin Fibril Conformational Differences by Thioflavin-T Binding Characteristics“. Authors: M. Ziaunys, A. Sakalauskas, V. Smirnovas. The COINS 2021, Lithuania, 2021.

COPIES OF PUBLICATIONS/PUBLIKACIJŲ KOPIJOS

Exploring the occurrence of thioflavin-T-positive insulin amyloid aggregation intermediates

Mantas Ziaunys, Andrius Sakalauskas, Kamile Mikalauskaite and Vytautas Smirnovas

Institute of Biotechnology, Life Sciences Center, Vilnius University, Vilnius, Lithuania

ABSTRACT

The aggregation of proteins is considered to be the main cause of several neurodegenerative diseases. Despite much progress in amyloid research, the process of fibrillization is still not fully understood, which is one of the main reasons why there are still very few effective treatments available. When the aggregation of insulin, a model amyloidogenic protein, is tracked using thioflavin-T (ThT), an amyloid specific dye, there is an anomalous occurrence of double-sigmoidal aggregation kinetics. Such an event is likely related to the formation of ThT-positive intermediates, which may affect the outcome of both aggregation kinetic data, as well as final fibril structure. In this work we explore insulin fibrillization under conditions, where both normal and double-sigmoidal kinetics are observed and show that, despite their dye-binding properties and random occurrence, the ThT-positive intermediates do not significantly alter the overall aggregation process.

Subjects Biochemistry, Biophysics

Keywords Insulin aggregation, Thioflavin-T, Amyloid aggregation, Aggregation intermediates, Double-sigmoidal kinetics

Submitted 5 November 2020
Accepted 18 January 2021
Published 10 February 2021

Corresponding author
Mantas Ziaunys,
mantas.ziaunys@gmc.vu.lt,
mantas.ziaunys@gmail.com

Academic editor
Eugene Permyakov

Additional Information and Declarations can be found on page 11

DOI **10.7717/peerj.10918**

INTRODUCTION

Protein aggregation into amyloid fibrils is linked to multiple neurodegenerative disorders, such as Alzheimer's, Parkinson's or prion diseases (*Knowles, Vendruscolo & Dobson, 2014*; *Chiti & Dobson, 2017*), affecting millions of people worldwide (*Isik, 2010*). Such protein assembly into insoluble aggregates is still not fully understood, despite the significant effort put into figuring out both the mechanism of aggregation (*Meisl et al., 2016*; *Castello et al., 2017*; *Biza et al., 2017*; *Giorgetti et al., 2018*; *Linse, 2019*), as well as the resulting fibril structural aspects (*Makin & Serpell, 2005*; *Fitzpatrick et al., 2013*). As a consequence, there are still very few disease modifying drugs available (*Mehta et al., 2017*; *Cummings et al., 2019*; *Maurer et al., 2018*; *Park et al., 2020*).

The process of amyloid fibril formation consists of multiple microscopic events. The first one being nucleation, a process during which proteins lose their native structure and form a primary aggregation center (*Chatani & Yamamoto, 2018*). This structure then passes several growth phases, such as elongation (*Gurry & Stultz, 2014*), assembly into protofibrils (*Dolui et al., 2018*) and subsequent maturation into fully formed fibrils (*Ma et al., 2013*; *Sidhu et al., 2017*). The resulting aggregates are then capable of acting

as catalysts for surface-mediated secondary nucleation (*Törnquist et al., 2018*), as well as fragmenting into smaller fibrils (*Nicoud et al., 2015*), thus creating new aggregation centers. Different proteins have also been shown to form specific oligomeric species prior to further aggregation processes (*Nettleton et al., 2000*; *Chiti & Dobson, 2006*; *Danzer et al., 2007*; *Selivanova & Galzitskaya, 2012*; *Sengupta, Nilson & Kayed, 2016*). Such a large number of possible steps involved in the aggregation process significantly complicates matters and requires extensive research in order to understand and prevent the progress of amyloid-related diseases.

In order to study aggregation reactions in vitro, insulin is often used as a model amyloidogenic protein (*Brange et al., 1997*). Despite its main application as a treatment for diabetes, insulin is capable of forming amyloid fibrils under acidic or neutral pH at an elevated temperature (*Nielsen et al., 2001*). This, coupled with its availability, has made it a widely used protein to study both the mechanisms of amyloid formation (*Ahmad et al., 2003*; *Podestà et al., 2006*; *Malik & Roy, 2011*), as well as possible inhibitory compounds (*Wang, Dong & Sun, 2012*; *Malisauskas et al., 2015*; *Zheng & Lazo, 2018*). Even though a large number of experiments have been conducted with insulin under various conditions, new information regarding its fibrillation continues to arise, such as new possible aggregation mechanisms or structural polymorphisms (*Sakalauskas, Ziaunys & Smirnovas, 2019*; *Ratha et al., 2020*). A factor that requires further attention is the seemingly random appearance of double-sigmoidal aggregation kinetics when examining the fibrillization of insulin with a fluorescent probe—thioflavin-T (ThT). This phenomenon was examined by *Smirnovas & Winter (2008)*, *Grudzielanek, Smirnovas & Winter (2006)* and *Foderà et al. (2009)*, where it was shown that the first increase in the double-sigmoidal curve is likely related to the formation of oligomeric intermediate species capable of binding ThT and this event was consistently reproducible only under certain environmental conditions.

ThT is a benzothiazole dye that binds to the beta-sheet grooves of amyloid fibrils and attains a locked conformation (*Robbins et al., 2012*). This causes a red shift of its excitation and emission wavelengths, as well as a significant increase in fluorescence quantum yield (*Gade Malmos et al., 2017*; *Xue et al., 2017*). The fluorescence intensity, binding affinity and maximum excitation/emission wavelengths are highly dependent on the conformation of fibrils and there are even reports of multiple types of binding modes on the same type of aggregate (*Sidhu et al., 2018*; *Ziaunys, Sneideris & Smirnovas, 2020*). Despite being widely used as a probe to track amyloid formation, the dye's fluorescence is not exclusively tied to such fibrillar aggregates, as it has been shown to increase in fluorescence upon binding or being trapped in non-amyloid structures (*Singh et al., 2010*; *Sulatskaya et al., 2018*). This, in turn, does not rule out the possibility of the double-sigmoidal kinetics being the result of structures that are not amyloid in nature.

In our research we observed that when human recombinant insulin is aggregated at pH 2.4, there exist both regular sigmoidal fibrilization kinetic curves, as well as double-sigmoidal ones under the same aggregation conditions. Unlike in the previously reported cases (*Grudzielanek, Smirnovas & Winter, 2006*; *Smirnovas & Winter, 2008*; *Foderà et al., 2009*), this occurrence appears to be random even when the same batch of protein is used.

The double-sigmoidal curves also possess a different ThT fluorescence intensity at the end of the reaction, which begs the question whether the formation of these anomalous ThT-positive intermediates could yield differently structured fibrils. Small variations in insulin aggregation conditions, such as pH value or protein concentration (*Sneideris et al., 2015*; *Sakalauskas, Ziaunys & Smirnovas, 2019*) can cause the formation of distinct conformation aggregates. Since both regular and double-sigmoidal aggregation types exist under the same conditions, this creates an opportunity to explore any possible differences during the whole fibrillization process. In this work we examine a large sample size of insulin aggregation kinetic curves, isolate the double-sigmoidal kinetic samples from regular ones and determine whether there are secondary structure, morphology, ThT binding and seeding propensity differences between them. In addition, both regular and double-sigmoidal aggregation reactions are tracked by scanning ThT fluorescence excitation-emission matrices in order to determine if there are aggregate structural differences from distinct dye binding, such as specific maximum excitation and emission wavelengths or bound-ThT fluorescence intensity (*Groenning et al., 2007*; *Ziaunys & Smirnovas, 2019b*; *Ziaunys, Sakalauskas & Smirnovas, 2020*).

MATERIALS AND METHODS

Insulin aggregation

Human recombinant insulin powder (Sigma-Aldrich cat. No. 91077C) was dissolved in a 100 mM sodium phosphate buffer (pH 2.4) containing 100 mM NaCl (reaction buffer). ThT (Sigma-Aldrich cat. No. T3516) was dissolved in H_2O to a final concentration of ~12 mM and mixed for 10 min using vigorous agitation, after which the dye solution was filtered through a 0.22 μm pore syringe filter. An aliquot of the ThT stock solution was diluted 200 times and the exact dye concentration was determined by measuring the solution's absorbance at 412 nm ($\varepsilon_{412} = 23250\ M^{-1}cm^{-1}$). The ThT stock solution was then diluted to a final concentration of 10 mM. The protein solution was then combined with the reaction buffer and a 10 mM ThTsolution to a final protein and ThT concentration of 100 μM (insulin $\varepsilon_{280} = 6{,}335\ M^{-1}cm^{-1}$, MW=5808 Da) and distributed into 200 μL test tubes (20 μL final volume). These conditions result in both types of aggregation, with a random appearance of double-sigmoidal kinetic curves.

The aggregation kinetics were tracked as previously described (*Milto, Michailova & Smirnovas, 2014*). In short, sample ThT fluorescence intensity was monitored using a Qiagen Rotorgene Q real-time analyzer at a constant 60 °C temperature with measurements taken every minute. A total of one thousand samples were measured in batches of 36. After the aggregation reaction, the samples were stored at 4 °C.

For seeded aggregation, fibril samples were sonicated for 10 min using a Bandelin Sonopuls ultrasonic homogenizer with a MS73 tip (40% power, with 30 s sonication/30 s rest intervals). Then insulin, ThT and fibril solutions were combined to a final protein concentration of 100 μM, ThT concentration of 100 μM and 1% or 10^{-5}% fibrils (% of total protein mass in solution). The reaction was monitored as in the non-seeded aggregation experiment.

Kinetic data analysis

A first-order derivative was calculated for each sample's kinetic data, using a 40-point averaging range. The maximum value of the derivative curve corresponds to the rate of aggregation, while its position—to the time at which the rate is highest (t_r). Samples which had one clear peak in the first-order derivative were regarded as normal, while ones which were composed of two peaks (regular, high-rate peak and a small, low-rate peak preceding it)—as double-sigmoidal. Data processing was done using Origin 2018 software.

Fluorescence measurements

Each sample was diluted 5 times to 100 μL with the reaction buffer containing 100 μM of ThT and their fluorescence intensity was measured using a Varian Cary Eclipse Fluorescence Spectrophotometer with 440 nm excitation (slit width—5 nm) and 480 nm emission (slit width—5 nm) wavelengths. For each case, three measurements were taken and averaged.

Atomic force microscopy

The samples were separated into two groups based on their aggregation kinetic profiles and mixed to result in a homogenous solution. 30 μL aliquots were deposited on freshly cleaved mica, incubated for 1 min, washed with 1 mL of MilliQ water and dried under airflow. In the case of intermediate aggregates during the double-sigmoidal aggregation, the real-time analyzer was stopped when the aggregation curve reached the first minor plateau. Then the samples were quickly removed and placed on freshly cleaved mica as mentioned earlier. For each condition, three 10 × 10 μm AFM images were recorded as previously described (*Sneideris et al., 2019*) using a Dimension Icon (Bruker) atomic force microscope, operating in tapping mode with a silicon cantilever Tap300AI-G (40 N m^{-1}, Budget Sensors). High resolution (1,024 × 1,024 pixels) images were flattened and analyzed using Gwyddion 2.5.5 and SPIP 6.7.8. Each fibril's height was determined by tracing lines perpendicular to the fibril's axis. Height statistical analysis was conducted by taking into consideration all three repeats for each condition, i.e., a similar number of aggregates were examined in every image.

Fourier-transform infrared spectroscopy

The two sample groups were centrifuged at 10,000 g for 30 min and resuspended in 1 mL of D_2O. The centrifugation and resuspension step was repeated 3 times and the final resuspension volume was 0.25 mL. Before measurements, both samples were sonicated using a Bandelin Sonopuls ultrasonic homogenizer with a MS72 tip (20% power and constant sonication for 30 s). Sonication helps to break fibril clumps, which leads to less scattering effects and better-quality FTIR spectra. During sample preparation and measurement, H-D exchange is insignificant, as in the case of insulin fibrils it is very slow (*Dzwolak, Loksztejn & Smirnovas, 2006*). The spectra were recorded as previously described (*Sneideris et al., 2019*). In short, the concentrated fibril samples were scanned in near-vacuum conditions (~2 mbar) at room temperature using a Vertex 80v (Bruker) IR spectrometer. 256 interferograms were averaged for each spectrum. A D_2O spectrum was subtracted and the resulting spectra were normalized to the same area of amide I/I' band (1,700–1,595 cm^{-1}). Data processing was performed using GRAMS software.

ThT fluorescence excitation-emission matrices

The aggregation solution was prepared as described in the insulin aggregation section to a final volume of 3 mL. The solution was then placed in a 10 mm pathlength cuvette, sealed with a plug cap to prevent evaporation and incubated at 60 °C without agitation. EEMs were scanned every 5 min using a Varian Cary Eclipse fluorescence spectrophotometer using an excitation range from 440 to 465 nm and emission range from 475 to 500 nm (excitation and emission slit widths—5 nm, wavelength step—1 nm, scan rate—600 points/min). Due to the analysis being conducted on a transitioning system, the EEM size was optimized to be as minimal as possible to lower the impact of an intensity drift, which results from different concentrations of aggregates present at the start and finish of each scan cycle. This was done by first acquiring a larger EEM, which encompassed the maximum ThT fluorescence zone, then it was narrowed down as much as possible to reduce scan time.

Each EEM was corrected for the inner filter effect caused by 100 μM of ThT as described previously (*Ziaunys & Smirnovas, 2019b*). In short, the correction was made by using the absorbance spectra of 100 μM non-bound ThT, as it is extremely difficult to account for absorbance changes throughout the entire reaction resulting from ThT becoming bound to fibrils and because the majority of ThT remains non-bound even when all insulin is aggregated (*Ziaunys & Smirnovas, 2019b*). The EEM "center of mass" was then calculated for the entire EEM after the inner filter correction. This was done to prevent signal noise, caused by light scattering, from affecting the maximum intensity position.

RESULTS

Aggregation kinetics

A large number ($n = 1{,}000$) of low volume insulin samples were aggregated under the exact same conditions and their kinetics were tracked by monitoring changes in ThT fluorescence intensity. Analysis of all the data revealed that a majority of samples experienced normal, sigmoidal spontaneous aggregation kinetics, with one rate maximum seen in the first order derivative (Figs. 1A and 1C). A fraction of samples displayed double-sigmoidal kinetics, with two peaks in the first order derivative curve (Figs. 1B and 1D). The first increase in fluorescence intensity of the double-sigmoidal aggregation kinetics occurred roughly 100 min before the second increase and its rate was, on average, nearly 10-fold lower.

A total of 55 samples possessed such unusual aggregation kinetics, constituting a probability of such an occurrence being at least 5.5% under the tested conditions. 77 samples had a mixed kinetic profile (very small first peak or a large overlap between both peaks), which could not be accurately attributed to either type of aggregation. The normal and double-sigmoidal samples were then separated for further analysis.

In order to determine if there are any links between the rate of aggregation, the time at which this rate is highest and the resulting fluorescence intensity of fibrils, all three factor dependencies were examined. We can see that all three parameters are mostly independent from one another (Figs. 2A–2C). The time at which the aggregation rate is highest, does not influence the rate at which fibril elongation occurs, neither does it change the final fluorescence intensity of the formed fibrils. When we compare these three

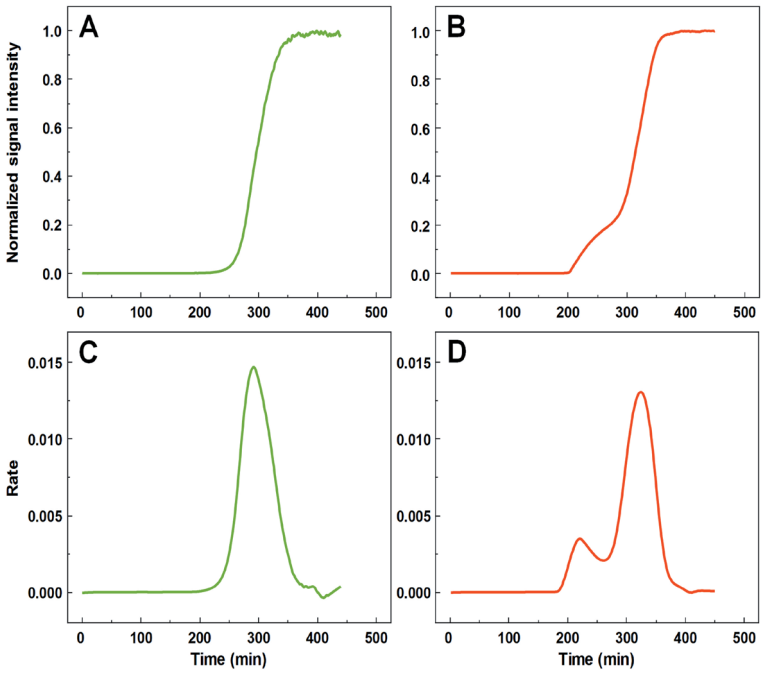

Figure 1 Insulin aggregation curves and their derivatives. Normal, sigmoidal (A) and anomalous, double-sigmoidal (B) insulin aggregation kinetics and their first order derivatives (C, D respectively).
Full-size DOI: 10.7717/peerj.10918/fig-1

factors between the normal and double-sigmoidal samples (Figs. 2D–2I), it appears that the double-sigmoidal fibrillization has a slightly lower time at which the maximum aggregation rate is reached (Figs. 2D and 2G) and it has no effect on the rate itself (Figs. 2E and 2H). There is, however, a considerable difference in the final fluorescence intensity distribution (Figs. 2F and 2I). The distribution maximum is more than 10% lower when the aggregation kinetics are double-sigmoidal, suggesting that there are either off-pathway aggregates or a fraction of fibrils possess a different ThT binding mode. Despite this distinction in average fluorescence intensity, a large portion of all three data sets overlap with one another due to a large spread caused by the stochastic nature of non-seeded insulin aggregation (*Foderà et al., 2008*).

Fibril structure and seeding properties

The fibril samples were examined using atomic force microscopy (AFM), Fourier-transform infrared spectroscopy (FTIR) and used as seeds to examine their rate of self-replication. In the AFM images acquired during the first increase in signal intensity during double-sigmoidal kinetics, we observe small, round oligomeric aggregate species (with most having a height of 1–2 nm) and short protofibrils (0.1–0.5 μm in length) (Fig. 3A, Fig. S1). When compared to a sample obtained before an increase in dye fluorescence is observed

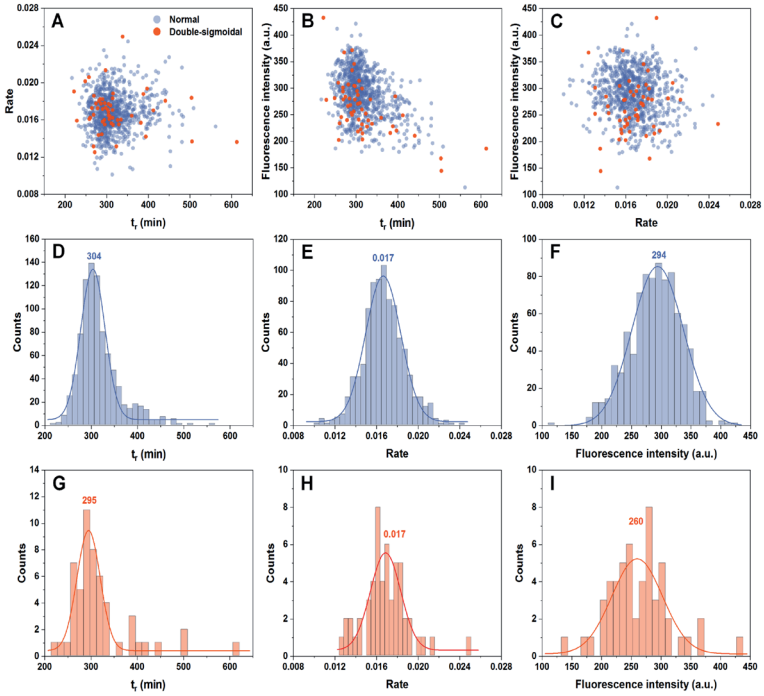

Figure 2 Distribution of maximum insulin aggregation rate, the time at which it is reached (t_r) and final fibril fluorescence intensity. Dependence of aggregation rate on t_r (A), fluorescence intensity on t_r (B) and aggregation rate on fluorescence intensity (C). Distribution of t_r (D, G), aggregation rate (E, H) and fluorescence intensity (F, I) for normal and double-sigmoidal samples respectively. Color-coded numbers, displayed above peak-fit curves, indicate peak maximum values.

Full-size DOI: 10.7717/peerj.10918/fig-2

(Fig. S1), there are far more aggregates present in the case of ThT-positive intermediates. The ThT-negative samples also contain a higher number of 0.5–1.5 nm height assemblies and very few elongated structures (Figs. S2A–S2C). When the aggregation reactions are concluded, the fibrils are considerably longer and have a greater height, however, there do not seem to be any major differences between both cases, neither visually nor by their height distribution (Figs. 3B–3D, Fig. S1). Due to formation of large aggregate clumps, the fibrils were sonicated to better examine any possible differences in their height. While the height distribution average values are similar, there is a wider spread in the case of the sonicated double-sigmoidal sample (Fig. S3), likely caused by the existence of several smaller fibrils or amorphous aggregates. The FTIR second derivative spectra (Fig. 3E) and seeding kinetics (Fig. 3F) are also nearly identical for both cases, indicating that the double-sigmoidal aggregation does not have a significant influence on the final fibril secondary structure or self-replication properties.

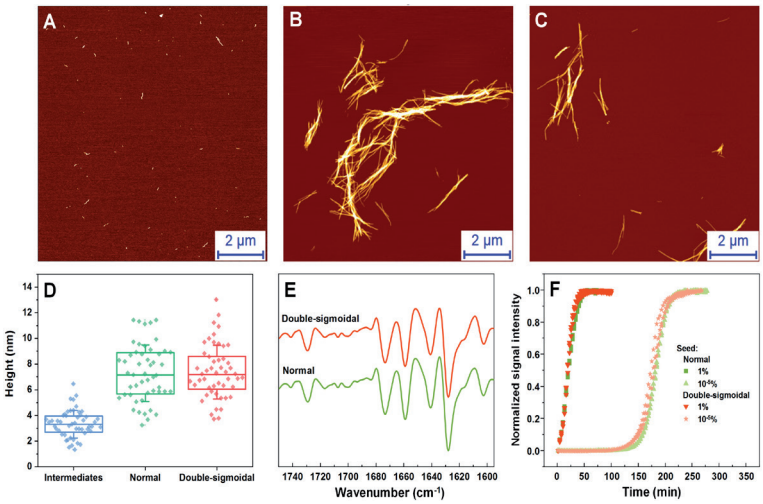

Figure 3 Normal, intermediate and double-sigmoidal sample AFM images, fibril height distributions, second order FTIR spectra and seeding kinetics. AFM images of insulin aggregates during the first part of the double-sigmoidal kinetics (A) and at the end of normal (B) and double-sigmoidal (C) aggregation. Height distribution of double-sigmoidal aggregation intermediates and fibrils after normal and double-sigmoidal aggregation (D), where box plots indicate the interquartile range and error bars are one standard deviation. Second order FTIR spectra (E) and seeded aggregation kinetics (F).

Full-size DOI: 10.7717/peerj.10918/fig-3

ThT-positive intermediates

The normal and double-sigmoidal aggregation reactions were examined by scanning excitation-emission matrices of ThT fluorescence during aggregation. The kinetic curves were plotted as the maximum EEM signal intensity over time. When examining the kinetics of double-sigmoidal aggregation, we see that the lag phase is followed by a slow increase in ThT fluorescence intensity, then a sudden jump in intensity (marked as *), which then quickly returns to a low value and is continued by the second growth phase (Fig. 4A). Such a jump is not visible in the normal aggregation data (Fig. 4A), nor in any of the previous experiments, where samples were only scanned once a minute. This indicates that it may only be visible for a very short time during the EEM scan. When the excitation and emission wavelengths of the EEM "center of mass" are calculated (Figs. 4B and 4C), we see that there are significant changes in both of these parameters during the first, anomalous increase in ThT intensity, as compared to relatively minor variations in the normal aggregation. The excitation wavelength shifts from 457 nm to 453 nm and then rises back to 454 nm, while the emission intensity shifts between 489 nm and 487 nm and gradually reaches 488 nm. Both wavelengths reach a constant value at roughly the same time after the sudden increase in ThT fluorescence intensity, marking the end of the anomalous phase.

If we examine the top fluorescence intensity value distributions in the EEMs before and after the sudden signal jump (Fig. 4D), there are both significant shifts in the top value positions during the anomalous phase, as well as single, high intensity lines. Such lines can

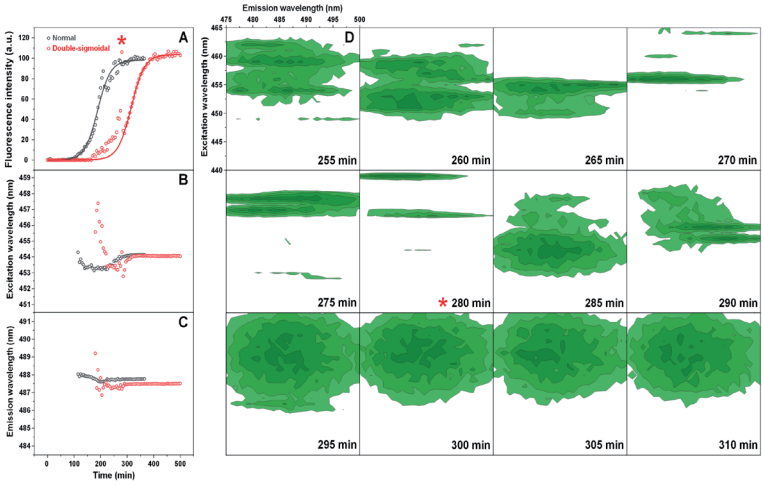

Figure 4 Insulin aggregation kinetics and bound ThT fluorescence EEMs. Insulin aggregation kinetics monitored by scanning ThT fluorescence EEMs (A), where each data point is the maximum value in the recorded EEM. EEM "center of mass" excitation (B) and emission (C) wavelengths over the course of aggregation. Top intensity values present in the ThT EEMs at different aggregation time points (D) during the first double-sigmoidal increase (darker green areas represent higher intensity zones). The red * symbol indicates the point where there is a sudden jump in ThT fluorescence intensity. Data in part (A) was fit using a Boltzmann's sigmoidal equation with the anomalous aggregation phase data points omitted from the fitting procedure.

Full-size DOI: 10.7717/peerj.10918/fig-4

be caused by either a large particle floating past the optical path during a scan or by sudden association and dissociation of a ThT-positive aggregate. After the high intensity jump, once the signal returns to normal, these lines are no longer present in any of the EEMs (as seen after 290 min (Fig. 4D)) and they become nearly identical. Such an occurrence has been observed multiple times throughout the study and it ranged from being mild (Fig. S4) to very extreme (Fig. S5).

DISCUSSION

The large sample size of aggregation reactions shows that under these conditions, the occurrence of such anomalous, double-sigmoidal fibrilization kinetics is both relatively rare (5.5%) and seemingly random. This is unlike the previously reported cases, where a certain set of conditions caused all of the kinetic curves to be double-sigmoidal (*Grudzielanek, Smirnovas & Winter, 2006*; *Smirnovas & Winter, 2008*; *Foderà et al., 2009*). The conditions used in this work allowed to examine how such peculiar kinetics affected the overall aggregation reaction, as both types of fibrillizations were observed. When compared to normal aggregation, this anomalous event occurs roughly 100 min before the second increase, however it does not influence the time at which maximum aggregation rate is reached nor the rate of aggregation and the resulting fibrils have an identical morphology, secondary structure and seeding properties. It is possible that it generates a small population

of small, amorphous structures, as hinted by the fibril height range, AFM images and the lower ThT fluorescence intensity distribution. The fact that this anomaly does not influence the overall kinetic parameters (apart from lag time) or fibril structure is a positive aspect, considering that these values are often used to determine the effectiveness of anti-amyloid compounds. However, the random formation of different intermediate species does raise concerns. If these structures can appear in any reaction solution and there is minimal connection between their existence and the overall aggregation process, then there is essentially no way of controlling this event.

Judging from the ThT fluorescence EEMs, it appears that during the anomalous aggregation phase, there exists the formation of ThT-positive intermediates or structures that are capable of trapping and conformationally "locking" the dye molecules, unlike during a normal fibrilization process. AFM images acquired during this phase show small and round aggregates, as well as short protofibril species, with an average height that is much lower than observed for fully formed fibrils. Their ability to bind ThT in a different mode (as identified by the higher excitation and emission wavelengths) suggests that they possess a structure that is distinct from both normal intermediate species, as well as the fully formed fibrils. The differences in these parameters could also be an indicator that there is no actual surface-dye interaction, but rather an entrapment of ThT in the oligomeric structure. The lower ThT fluorescence intensity distribution at the end of the reaction and AFM images also hint at a possibility that some of these structures remain in solution and do not become incorporated into the amyloid structure of normal fibrils.

A possible explanation for the ThT-binding ability of these intermediates may stem from the high intensity lines seen in the ThT fluorescence EEMs. When the sample is continuously scanned to generate an EEM, such lines can only result from either a larger particle floating past the optical path or by a quick association and dissociation of a ThT positive aggregate. Considering that during fibrilization the concentration of large aggregates increases, an event which results in enhanced light scattering and signal noise, we would expect to observe an increasing amount of such high intensity lines, however, this is not the case. Once the first phase of the double-sigmoidal kinetics is concluded, they are no longer seen, which means that they are likely not the result of light scattering from larger aggregate particles. This leaves the hypothesis that ThT-positive intermediates quickly associate and dissociate during this time period. If these intermediates are capable of trapping ThT molecules within their structure, they may not even require a similarity to amyloids, as it has been shown that ThT immobilization can cause an increase in fluorescence intensity (*Hutter et al., 2011*; *Ziaunys & Smirnovas, 2019a*). This would also explain the significantly different excitation and emission wavelengths, as these parameters depend highly on the dye's binding mode.

While these ThT-positive intermediates do not have any major effect on the final fibril structure and most kinetic parameters, they could become an issue when testing potential anti-amyloid compounds. If an inhibitor targets the process of primary nucleation and is specific towards a certain type of intermediate structure, the formation of a different type of aggregate, which incorporates ThT but is not amyloid-like, may not be affected at all and result in an increase in ThT fluorescence intensity. This would then lead to a false

interpretation on the effectiveness of the tested compound and negatively affect the drug screening process.

CONCLUSIONS

The occurrence of double-sigmoidal kinetics during insulin amyloid aggregation does not influence the final fibril structure or morphology, nor does it change the rate of the main reaction. However, it does result in a lower ThT fluorescence intensity and may be related to the formation of a different type of aggregates. The random variability observed during intermediate oligomer formation may also have a negative impact during potential anti-amyloid drug screenings and lead to false interpretations.

ADDITIONAL INFORMATION AND DECLARATIONS

Funding

This research is funded by Vilnius University, grant No. MSF-JM-3. The funders had no role in study design, data collection and analysis, decision to publish, or preparation of the manuscript.

Grant Disclosures

The following grant information was disclosed by the authors:
Vilnius University: MSF-JM-3.

Competing Interests

The authors declare there are no competing interests.

Author Contributions

- Mantas Ziaunys conceived and designed the experiments, performed the experiments, analyzed the data, prepared figures and/or tables, authored or reviewed drafts of the paper, and approved the final draft.
- Andrius Sakalauskas and Kamile Mikalauskaite performed the experiments, authored or reviewed drafts of the paper, and approved the final draft.
- Vytautas Smirnovas conceived and designed the experiments, analyzed the data, authored or reviewed drafts of the paper, and approved the final draft.

Data Availability

The following information was supplied regarding data availability:

Data, including spontaneous and seeded aggregation kinetic data, Fourier-transform infrared spectra and excitation-emission matrix files, atomic force microscopy images, are available in the Supplemental Files.

Supplemental Information

Supplemental information for this article can be found online at http://dx.doi.org/10.7717/peerj.10918#supplemental-information.

REFERENCES

Ahmad A, Millett IS, Doniach S, Uversky VN, Fink AL. 2003. Partially folded intermediates in insulin fibrillation. *Biochemistry* **42**:11404–11416 DOI 10.1021/bi034868o.

Biza KV, Nastou KC, Tsiolaki PL, Mastrokalou CV, Hamodrakas SJ, Iconomidou VA. 2017. The amyloid interactome: exploring protein aggregation. *PLOS ONE* **12**:e0173163 DOI 10.1371/journal.pone.0173163.

Brange J, Andersen L, Laursen ED, Meyn G, Rasmussen E. 1997. Toward understanding insulin fibrillation. *Journal of Pharmaceutical Sciences* **86**:517–525 DOI 10.1021/js960297s.

Castello F, Paredes JM, Ruedas-Rama MJ, Martin M, Roldan M, Casares S, Orte A. 2017. Two-step amyloid aggregation: sequential lag phase intermediates. *Scientific Reports* **7**:40065 DOI 10.1038/srep40065.

Chatani E, Yamamoto N. 2018. Recent progress on understanding the mechanisms of amyloid nucleation. *Biophysical Reviews* **10**:527–534 DOI 10.1007/s12551-017-0353-8.

Chiti F, Dobson CM. 2006. Protein misfolding, functional amyloid, and human disease. *Annual Review of Biochemistry* **75**:333–366 DOI 10.1146/annurev.biochem.75.101304.123901.

Chiti F, Dobson CM. 2017. Protein misfolding, amyloid formation, and human disease: a summary of progress over the last decade. *Annual Review of Biochemistry* **86**:27–68 DOI 10.1146/annurev-biochem-061516-045115.

Cummings J, Lee G, Ritter A, Sabbagh M, Zhong K. 2019. Alzheimer's disease drug development pipeline: 2019. *Alzheimer's & Dementia: Translational Research & Clinical Interventions* **5**:272–293 DOI 10.1016/j.trci.2019.05.008.

Danzer KM, Haasen D, Karow AR, Moussaud S, Habeck M, Giese A, Kretzschmar H, Hengerer B, Kostka M. 2007. Different species of α-synuclein oligomers induce calcium influx and seeding. *Journal of Neuroscience* **27**:9220–9232 DOI 10.1523/JNEUROSCI.2617-07.2007.

Dolui S, Roy A, Pal U, Saha A, Maiti NC. 2018. Structural insight of amyloidogenic intermediates of human insulin. *ACS Omega* **3**:2452–2462 DOI 10.1021/acsomega.7b01776.

Dzwolak W, Loksztejn A, Smirnovas V. 2006. New insights into the self-assembly of insulin amyloid fibrils: an H-D exchange FT-IR study. *Biochemistry* **45**:8143–8151 DOI 10.1021/bi060341a.

Fitzpatrick AWP, Debelouchina GT, Bayro MJ, Clare DK, Caporini MA, Bajaj VS, Jaroniec CP, Wang L, Ladizhansky V, Muller SA, MacPhee CE, Waudby CA, Mott HR, De Simone A, Knowles TPJ, Saibil HR, Vendruscolo M, Orlova EV, Griffin RG, Dobson CM. 2013. Atomic structure and hierarchical assembly of a cross- β amyloid fibril. *Proceedings of the National Academy of Sciences of the United States of America* **110**:5468–5473 DOI 10.1073/pnas.1219476110.

Foderà V, Cataldo S, Librizzi F, Pignataro B, Spiccia P, Leone M. 2009. Self-organization pathways and spatial heterogeneity in insulin amyloid fibril formation. *The Journal of Physical Chemistry B* **113**:10830–10837 DOI 10.1021/jp810972y.

Foderà V, Librizzi F, Groenning M, Van De Weert M, Leone M. 2008. Secondary nucleation and accessible surface in insulin amyloid fibril formation. *Journal of Physical Chemistry B* **112**:3853–3858 DOI 10.1021/jp710131u.

Gade Malmos K, Blancas-Mejia LM, Weber B, Buchner J, Ramirez-Alvarado M, Naiki H, Otzen D. 2017. ThT 101: a primer on the use of thioflavin T to investigate amyloid formation. *Amyloid* **24**:1–16 DOI 10.1080/13506129.2017.1304905.

Giorgetti S, Greco C, Tortora P, Aprile F. 2018. Targeting Amyloid aggregation: an overview of strategies and mechanisms. *International Journal of Molecular Sciences* **19**:2677 DOI 10.3390/ijms19092677.

Groenning M, Norrman M, Flink JM, Van de Weert M, Bukrinsky JT, Schluckebier G, Frokjaer S. 2007. Binding mode of Thioflavin T in insulin amyloid fibrils. *Journal of Structural Biology* **159**:483–497 DOI 10.1016/j.jsb.2007.06.004.

Grudzielanek S, Smirnovas V, Winter R. 2006. Solvation-assisted pressure tuning of insulin fibrillation: from novel aggregation pathways to biotechnological applications. *Journal of Molecular Biology* **356**:497–509 DOI 10.1016/j.jmb.2005.11.075.

Gurry T, Stultz CM. 2014. Mechanism of amyloid- β fibril elongation. *Biochemistry* **53**:6981–6991 DOI 10.1021/bi500695g.

Hutter T, Amdursky N, Gepshtein R, Elliott SR, Huppert D. 2011. Study of Thioflavin-T immobilized in porous silicon and the effect of different organic vapors on the fluorescence lifetime. *Langmuir* **27**:7587–7594 DOI 10.1021/la200875k.

Isik AT. 2010. Late onset Alzheimer's disease in older people. *Clinical Interventions in Aging* **5**:307–311 DOI 10.2147/CIA.S11718.

Knowles TPJ, Vendruscolo M, Dobson CM. 2014. The amyloid state and its association with protein misfolding diseases. *Nature Reviews Molecular Cell Biology* **15**:384–396 DOI 10.1038/nrm3810.

Linse S. 2019. Mechanism of amyloid protein aggregation and the role of inhibitors. *Pure and Applied Chemistry* **91**:211–229 DOI 10.1515/pac-2018-1017.

Ma J, Komatsu H, Kim YS, Liu L, Hochstrasser RM, Axelsen PH. 2013. Intrinsic structural heterogeneity and long-term maturation of amyloid β peptide fibrils. *ACS Chemical Neuroscience* **4**:1236–1243 DOI 10.1021/cn400092v.

Makin OS, Serpell LC. 2005. Structures for amyloid fibrils. *FEBS Journal* **272**:5950–5961 DOI 10.1111/j.1742-4658.2005.05025.x.

Malik R, Roy I. 2011. Probing the mechanism of insulin aggregation during agitation. *International Journal of Pharmaceutics* **413**:73–80 DOI 10.1016/j.ijpharm.2011.04.024.

Malisauskas R, Botyriute A, Cannon JG, Smirnovas V. 2015. Flavone derivatives as inhibitors of insulin amyloid-like fibril formation. *PLOS ONE* **10**:e0121231 DOI 10.1371/journal.pone.0121231.

Maurer MS, Schwartz JH, Gundapaneni B, Elliott PM, Merlini G, Waddington-Cruz M, Kristen AV, Grogan M, Witteles R, Damy T, Drachman BM, Shah SJ, Hanna M, Judge DP, Barsdorf AI, Huber P, Patterson TA, Riley S, Schumacher J, Stewart M,

Sultan MB, Rapezzi C. 2018. Tafamidis Treatment for Patients with Transthyretin Amyloid Cardiomyopathy. *New England Journal of Medicine* **379**:1007–1016 DOI 10.1056/NEJMoa1805689.

Mehta D, Jackson R, Paul G, Shi J, Sabbagh M. 2017. Why do trials for Alzheimer's disease drugs keep failing? A discontinued drug perspective for 2010–2015. *Expert Opinion on Investigational Drugs* **26**:735–739 DOI 10.1080/13543784.2017.1323868.

Meisl G, Kirkegaard JB, Arosio P, Michaels TCT, Vendruscolo M, Dobson CM, Linse S, Knowles TPJ. 2016. Molecular mechanisms of protein aggregation from global fitting of kinetic models. *Nature Protocols* **11**:252–272 DOI 10.1038/nprot.2016.010.

Milto K, Michailova K, Smirnovas V. 2014. Elongation of mouse prion protein amyloid-like fibrils: effect of temperature and denaturant concentration. *PLOS ONE* **9**:e94469 DOI 10.1371/journal.pone.0094469.

Nettleton EJ, Tito P, Sunde M, Bouchard M, Dobson CM, Robinson CV. 2000. Characterization of the oligomeric states of insulin in self-assembly and amyloid fibril formation by mass spectrometry. *Biophysical Journal* **79**:1053–1065 DOI 10.1016/S0006-3495(00)76359-4.

Nicoud L, Lazzari S, Balderas Barragán D, Morbidelli M. 2015. Fragmentation of amyloid fibrils occurs in preferential positions depending on the environmental conditions. *The Journal of Physical Chemistry B* **119**:4644–4652 DOI 10.1021/acs.jpcb.5b01160.

Nielsen L, Khurana R, Coats A, Frokjaer S, Brange J, Vyas S, Uversky VN, Fink AL. 2001. Effect of environmental factors on the kinetics of insulin fibril formation: elucidation of the molecular mechanism. *Biochemistry* **40**:6036–6046 DOI 10.1021/bi002555c.

Park J, Egolum U, Parker S, Andrews E, Ombengi D, Ling H. 2020. Tafamidis: a first-in-class transthyretin stabilizer for transthyretin amyloid cardiomyopathy. *Annals of Pharmacotherapy* **54**:470–477 DOI 10.1177/1060028019888489.

Podestà A, Tiana G, Milani P, Manno M. 2006. Early events in insulin fibrillization studied by time-lapse atomic force microscopy. *Biophysical Journal* **90**:589–597 DOI 10.1529/biophysj.105.068833.

Ratha BN, Kar RK, Bednarikova Z, Gazova Z, Kotler SA, Raha S, De S, Maiti NC, Bhunia A. 2020. Molecular details of a salt bridge and its role in insulin fibrillation by NMR and Raman spectroscopic analysis. *The Journal of Physical Chemistry B* **124**:1125–1136 DOI 10.1021/acs.jpcb.9b10349.

Robbins KJ, Liu G, Selmani V, Lazo ND. 2012. Conformational analysis of thioflavin T bound to the surface of amyloid fibrils. *Langmuir* **28**:16490–16495 DOI 10.1021/la303677t.

Sakalauskas A, Ziaunys M, Smirnovas V. 2019. Concentration-dependent polymorphism of insulin amyloid fibrils. *PeerJ* **7**:e8208 DOI 10.7717/peerj.8208.

Selivanova OM, Galzitskaya OV. 2012. Structural polymorphism and possible pathways of amyloid fibril formation on the example of insulin protein. *Biochemistry* **77**:1237–1247 DOI 10.1134/S0006297912110028.

Sengupta U, Nilson AN, Kayed R. 2016. The role of Amyloid- β oligomers in toxicity, propagation, and immunotherapy. *EBioMedicine* **6**:42–49 DOI 10.1016/j.ebiom.2016.03.035.

Sidhu A, Segers-Nolten I, Raussens V, Claessens MMAE, Subramaniam V. 2017. Distinct mechanisms determine α-synuclein fibril morphology during growth and maturation. *ACS Chemical Neuroscience* **8**:538–547 DOI 10.1021/acschemneuro.6b00287.

Sidhu A, Vaneyck J, Blum C, Segers-Nolten I, Subramaniam V. 2018. Polymorph-specific distribution of binding sites determines thioflavin-T fluorescence intensity in α-synuclein fibrils. *Amyloid* **25**:189–196 DOI 10.1080/13506129.2018.1517736.

Singh PK, Kumbhakar M, Pal H, Nath S. 2010. Viscosity effect on the ultrafast bond twisting dynamics in an amyloid fibril sensor: thioflavin-T. *The Journal of Physical Chemistry B* **114**:5920–5927 DOI 10.1021/jp100371s.

Smirnovas V, Winter R. 2008. Revealing different aggregation pathways of amyloidogenic proteins by ultrasound velocimetry. *Biophysical Journal* **94**:3241–3246 DOI 10.1529/biophysj.107.123133.

Sneideris T, Darguzis D, Botyriute A, Grigaliunas M, Winter R, Smirnovas V. 2015. pH-driven polymorphism of insulin amyloid-like fibrils. *PLOS ONE* **10**:e0136602 DOI 10.1371/journal.pone.0136602.

Sneideris T, Sakalauskas A, Sternke-Hoffmann R, Peduzzo A, Ziaunys M, Buell AK, Smirnovas V. 2019. The environment is a key factor in determining the anti-amyloid efficacy of EGCG. *Biomolecules* **9**:1–17 DOI 10.3390/biom9120855.

Sulatskaya AI, Rychkov GN, Sulatsky MI, Rodina NP, Kuznetsova IM, Turoverov KK. 2018. Thioflavin T interaction with acetylcholinesterase: new evidence of 1:1 binding stoichiometry obtained with samples prepared by equilibrium microdialysis. *ACS Chemical Neuroscience* **9**:1793–1801 DOI 10.1021/acschemneuro.8b00111.

Törnquist M, Michaels TCT, Sanagavarapu K, Yang X, Meisl G, Cohen SIA, Knowles TPJ, Linse S. 2018. Secondary nucleation in amyloid formation. *Chemical Communications* **54**:8667–8684 DOI 10.1039/C8CC02204F.

Wang S-H, Dong X-Y, Sun Y. 2012. Effect of (−)-epigallocatechin-3-gallate on human insulin fibrillation/aggregation kinetics. *Biochemical Engineering Journal* **63**:38–49 DOI 10.1016/j.bej.2012.02.002.

Xue C, Lin TY, Chang D, Guo Z. 2017. Thioflavin T as an amyloid dye: fibril quantification, optimal concentration and effect on aggregation. *Royal Society Open Science* **4**:160696 DOI 10.1098/rsos.160696.

Zheng Q, Lazo ND. 2018. Mechanistic studies of the inhibition of insulin fibril formation by rosmarinic acid. *The Journal of Physical Chemistry B* **122**:2323–2331 DOI 10.1021/acs.jpcb.8b00689.

Ziaunys M, Sakalauskas A, Smirnovas V. 2020. Identifying insulin fibril conformational differences by Thioflavin-T binding characteristics. *Biomacromolecules* **21**:4989–4997 DOI 10.1021/acs.biomac.0c01178.

Ziaunys M, Smirnovas V. 2019a. Emergence of visible light optical properties of L-phenylalanine aggregates. *PeerJ* **7**:e6518 DOI 10.7717/peerj.6518.

Ziaunys M, Smirnovas V. 2019b. Additional Thioflavin-T binding mode in insulin fibril inner core region. *The Journal of Physical Chemistry B* **123**:8727–8732 DOI 10.1021/acs.jpcb.9b08652.

Ziaunys M, Sneideris T, Smirnovas V. 2020. Formation of distinct prion protein amyloid fibrils under identical experimental conditions. *Scientific Reports* **10**:4572 DOI 10.1038/s41598-020-61663-2.

BIOMACROMOLECULES

pubs.acs.org/Biomac

Article

Identifying Insulin Fibril Conformational Differences by Thioflavin-T Binding Characteristics

Mantas Ziaunys, Andrius Sakalauskas, and Vytautas Smirnovas*

Cite This: *Biomacromolecules* 2020, 21, 4989−4997

Read Online

ACCESS | Metrics & More | Article Recommendations | Supporting Information

ABSTRACT: Amyloidogenic protein aggregation into highly structured fibrils is linked to more than 30 amyloidoses, including several neurodegenerative disorders. Despite significant progress in trying to understand the process of amyloid formation, there is still no cure or effective treatment available. A number of studies involving potential anti-amyloid compounds rely on the use of a fluorescent probe—thioflavin-T—to track the appearance, growth, or disassembly of these cytotoxic aggregates. Despite the wide application of this dye molecule, its interaction with amyloid fibrils is still poorly understood. Recent reports have shown it may possess distinct binding modes and fluorescence intensities based on the conformation of the examined fibrils. In this work, we generate insulin fibrils under four different conditions and attempt to identify distinct conformations using both classic methods, such as atomic force microscopy and Fourier-transform infrared spectroscopy, as well as their ThT binding ability and fluorescence quantum yield. We show that there is a significant variance of ThT fluorescence quantum yields, excitation/emission maxima positions, and binding modes between distinct insulin fibril conformations.

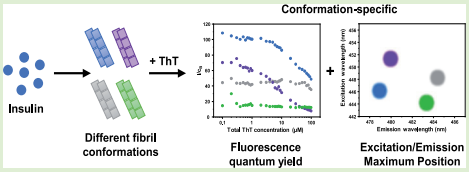

INTRODUCTION

Protein misfolding and association into amyloid fibrils is linked with more than 30 amyloidoses, which lead to organ dysfunction, including neurodegenerative disorders, such as Alzheimer's or Parkinson's disease.[1−3] These afflictions affect millions of people worldwide,[4] and the number is projected to increase further as the average human lifespan continues to increase.[5,6] Currently, both the mechanism[7,8] and the resulting structure[9,10] of such aggregates are still not fully understood, which is one of the main reasons why there is still no effective cure or treatment available.[11]

To better understand the process of how these fibrils form, what their resulting structure is, and how potential drug molecules are able to alter the aggregation process, countless experiments are conducted *in vitro* using amyloidogenic proteins.[12−16] To track this process and determine whether there are amyloids present in the sample, multiple techniques are used. These include atomic force microscopy (AFM),[17,18] light scattering,[19] Fourier-transform infrared (FTIR) spectroscopy,[20] and fluorescence spectroscopy.[21] One common fluorescent probe used to investigate the kinetics of fibrilization, as well as to quantify the concentration of fibrils, is thioflavin-T (ThT).[22,23] Upon binding to β-sheet grooves located on the surface of amyloids, the conformation of ThT becomes locked, which results in both a red shift of its excitation/emission wavelengths and a significant increase in its fluorescence quantum yield.[24]

Despite the relatively simple structure and specific affinity toward amyloid fibrils, this dye molecule has been proven to be far more complex than initially perceived. One interesting aspect of ThT is its ability to bind to fibrils in more than one mode,[25] with distinct modes having specific excitation and emission wavelength maximum positions and fluorescence quantum yields.[26,27] Multiple experimental and computational reports have shown that the number of binding modes for ThT can vary from one to six,[25,28−32] depending on the protein that the fibril is composed of. It was also demonstrated that α-synuclein[33] and prion proteins[34] can form two distinct conformations that differ by their ThT fluorescence intensity. In addition to this, we have also recently observed distinct fluorescence intensities for two insulin conformations generated at different protein concentrations,[35] as well as a massive increase in ThT fluorescence when EGCG was used to alter the aggregation reaction.[36]

Insulin is a peptide hormone that regulates carbohydrate, fat, and protein metabolism. Its aggregation is associated with insulin-derived amyloidosis, localized at injection sites in patients with diabetes.[37] Considering that insulin is also a model protein used to study fibril formation,[38] as well as to screen potential anti-amyloid drugs,[39−41] such conformation-specific variation in the ThT fluorescence intensity could significantly alter the experimental results. If a compound is

Received: August 10, 2020
Revised: October 6, 2020
Published: November 17, 2020

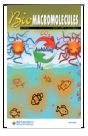

https://dx.doi.org/10.1021/acs.biomac.0c01178
Biomacromolecules 2020, 21, 4989−4997

capable of slightly altering the structure of fibrils, which results in a different or additional ThT binding mode, this would, in turn, cause an increase or decrease in the signal's intensity, leading to a conclusion that the molecule worked as an aggregation enhancer or inhibitor. The occurrence of such an event is not unlikely, as it is known that variations in pH[42] or concentration[35] can have a sizeable impact on the resulting structure of insulin fibrils. On the other hand, if the differences in ThT signal intensities or excitation/emission maxima positions are conformation-specific, then this factor could also be used as a quick and simple way of distinguishing between insulin fibril conformations and may be applied to other amyloidogenic proteins, such as the previously mentioned α-synuclein[33] and prion proteins.[34]

MATERIALS AND METHODS

Human recombinant insulin (Sigma-Aldrich, Cat. No. 91077C) was dissolved in either 20% acetic acid solution (AC), containing 100 mM NaCl, 100 mM sodium phosphate buffer (pH 2.0), 100 mM sodium phosphate buffer, containing 100 mM NaCl (pH 2.4) or phosphate buffer saline (pH 7.4) to a final protein concentration of 200 μM and placed into 1.5 mL test tubes (Fisher, Cat. No. 15432545) to a final volume of 1 mL (Table 1). The samples were incubated at 60 °C for 24 h in a Ditabis Thermomixer. The phosphate-buffered saline (PBS) samples also contained two glass beads each (Merck, Cat. No. 104015) and were agitated at 600 rpm throughout the incubation period.

Table 1. Insulin Sample Aggregation Reaction Conditions

sample name	reaction solution	agitation
AC	20% acetic acid	none
	100 mM NaCl	
PH20	100 mM sodium phosphate buffer (pH 2.0)	none
PH24	100 mM sodium phosphate buffer (pH 2.4)	none
	100 mM NaCl	
PH74	phosphate buffer saline (pH 7.4)	600 rpm + 2 glass beads

Atomic Force Microscopy. Each sample (30 μL) was deposited on mica disks, left to adsorb for 1 min, gently washed with 1 mL of H_2O, and dried using airflow. AFM images were scanned using a Dimension Icon (Bruker) atomic force microscope (tapping mode), equipped with a silicon cantilever (40 N/m, Budget Sensors). The 1024 × 1024 pixel resolution images were acquired using a scan rate of 0.5 Hz. AFM images were analyzed using Gwyddion 2.5.5 software. The fibril height and width were determined by tracing a line perpendicular to the fibril axis, while the fibril length was determined by tracing parallel to the fibril axis. The height, width, and length distributions were calculated from 50 traces for each sample.

Fourier-Transform Infrared Spectroscopy. Each sample was centrifuged at 10 000g for 30 min, after which the supernatant was removed and fibrils were resuspended in D_2O. The centrifugation and resuspension steps were repeated four times. Finally, the fibrils were resuspended in a small volume of D_2O (final fibril concentration ~10 mg/mL). The fibril samples were sonicated for 1 min using a Bandelin Sonopuls ultrasonic homogenizer with an MS 73 tip (40% total power). The FTIR spectra were recorded using a Vertex 80v (Bruker) IR spectrometer with a mercury cadmium telluride detector at room temperature under near-vacuum conditions. A total of 256 interferograms with 2 cm^{-1} resolution were averaged. The spectrum of D_2O was subtracted from each sample's spectrum. All spectra were normalized to the same area of amide I/I' band (1700−1580 cm^{-1}) using GRAMS software. To calculate the amide I/I' band's width at its half-height (HHBW),[43] the spectra were baseline-corrected between 1700 and 1580 cm^{-1} before normalization.

Sample Preparation for ThT Binding Assays. Each sample was centrifuged at 10 000g for 30 min, after which the supernatant was removed and the fibrils were resuspended in MilliQ H_2O. The centrifugation and resuspension procedure was repeated five times. Each sample was then sonicated for 1 min using a Bandelin Sonopuls ultrasonic homogenizer with an MS 73 tip (40% total power). The samples were then combined to a final protein concentration of 200 μM. The combined solution was then further sonicated for 10 min using the previously described method with 30 s sonication/rest intervals. The resuspension and sonication procedure resulted in highly dispersed and fragmented aggregates (Figure S1A−D), with a greatly reduced average fibril length (Figure S2A,B). The four fibril samples had similar width, and the height distribution remained comparable to the untreated fibrils (Figure S1E,F).

ThT (Sigma-Aldrich, Cat. No. T3516) was dissolved in MilliQ water to a final concentration of 10 mM. The exact concentration was determined by taking an aliquot of the dye solution, diluting it 200 times with MilliQ water and scanning its absorbance at 412 nm (ε_{412} = 23 250 M^{-1} cm^{-1}). The ThT solution was then diluted to prepare 200, 20, and 2 μM stock solutions. The sonicated fibrils were mixed with ThT stock solutions and H_2O to a range of ThT concentrations (final protein concentration was 100 μM in all cases).

ThT Excitation−Emission Matrix (EEM) Analysis. Each fibril−ThT solution (100 μL) was placed in a 3 mm pathlength cuvette, and its excitation−emission matrix was scanned using a Varian Cary Eclipse fluorescence spectrophotometer (excitation range was 435−465 nm with 1 nm steps and 5 nm slit width, emission range was 460−500 nm with 1 nm steps and 2.5 nm slit width; all other device parameters were kept the same for all sample scans). Three EEMs were scanned for every sample, the background spectrum was subtracted, and the resulting matrices were averaged. Due to slightly different fibril cross-interactions in the presence of ThT, the EEM areas where light scattering is prevalent cannot be accurately subtracted. Therefore, for further data analysis, the EEM region present 7 nm or less away from the excitation wavelength was not taken into account.

To correct for the inner filter effect caused by ThT, the absorbance spectra of each sample were scanned from 300 to 600 nm using 1 nm steps (each spectrum was the average of three repeats). The spectrum of fibrils without ThT was subtracted from each fibril−ThT spectrum. Because of ThT-induced differences in fibril association, the fibril spectrum could not be subtracted by a factor of 1 in certain cases (light absorbance differences induced by fibril clumping). The fibril spectrum was therefore subtracted by multiplying it by a certain factor (usually between 0.9 and 1.1) until there was no slope observed in the 550−600 nm range in the resulting spectrum.

The inner filter effect was corrected for every EEM point by using the following equation

$$I_m = I_c \times 10^{-(AEx+AEm)/2} \quad (1)$$

where AEx is the sample's absorbance at the excitation wavelength, AEm is the sample's absorbance at the emission wavelength, I_m is the signal intensity observed during measurement, and I_c is the corrected signal intensity.

The EEM intensity "center of mass" was calculated by selecting the top 10% intensity values and using the following equation

$$\lambda = \left(\sum \left(\lambda_n \times \sum I_n\right)\right) / \sum I_a \quad (2)$$

where λ is the wavelength of either the excitation or emission center of mass, λ_n is the excitation or emission wavelength, $\sum I_n$ is the sum of all signal intensities at λ_n, and $\sum I_a$ is the sum of all signal intensities.

This method helps avoiding the discrepancy caused by variations in light scattering at emission wavelengths close to the excitation wavelength, as well as EEM maxima position deviations due to background noise.

https://dx.doi.org/10.1021/acs.biomac.0c01178
Biomacromolecules 2020, 21, 4989−4997

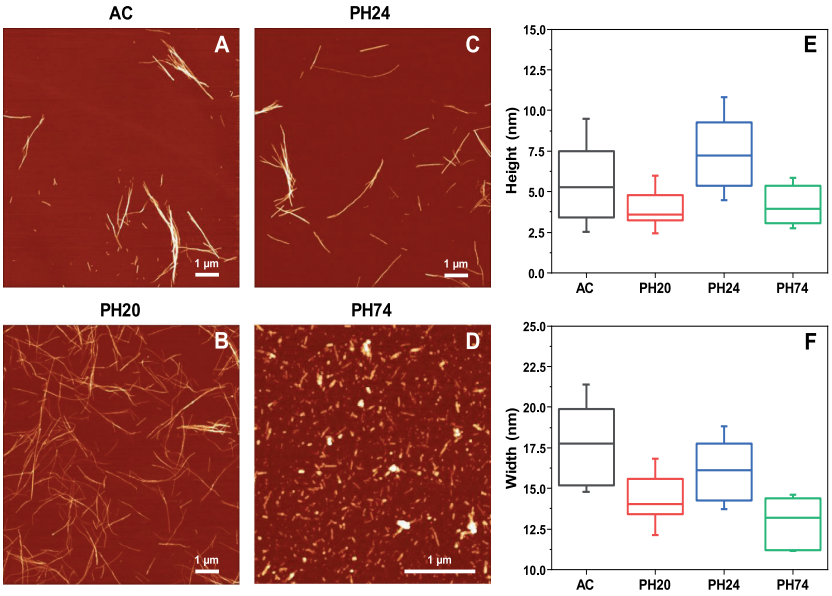

Figure 1. Atomic force microscopy images and fibril height and width distributions of insulin samples prepared under different conditions. Insulin fibrils were prepared under AC (A), PH20 (B), PH24 (C), and PH74 (D) conditions. Fibril height (E) and width (F) distribution (n = 50), where box plots indicate the interquartile range and error bars are 1 standard deviation.

Bound ThT Concentration Determination. Two methods used to determine the concentration of fibril-bound ThT include sample centrifugation[26] or sample dialysis.[29] Since each sample is sonicated, certain fibril types become difficult to separate from solution by centrifugation. Microdialysis techniques can lack accuracy at low ThT concentrations due to dye−membrane association and the relatively long time needed that can result in fibril clumping. To determine the concentration of bound ThT, a different method was devised based on two ThT−fibril interaction factors. First, based on the reported dye binding constants,[29] when the sample contains 100 μM insulin aggregates and 1 μM or less ThT, the majority of it should be bound to fibrils. Second, the difference between the absorbance spectra of free and bound ThT is much greater than the difference between spectra of ThT bound in distinct binding modes.

In this case, the absorbance spectra of ThT in the range from 0.1 to 1.0 μM should be the result of bound ThT molecules. By taking the absorbance values at 412 nm (free ThT spectrum maximum position) and 450 nm (bound ThT absorbance spectrum shifts toward higher wavelengths), we can calculate the extinction coefficients of bound ThT at these two wavelengths (ε_{412} and ε_{450}) for all four fibril samples. Since the ε_{412} and ε_{450} values are known for free ThT (23 250 and 5880 M^{-1} cm^{-1} respectively), the concentration of bound ThT can be calculated using the following system of equations

$$c_F \times 23\,250 + c_B \times \varepsilon_{412} = A_{412} \quad (3)$$

$$c_F \times 5880 + c_B \times \varepsilon_{450} = A_{450} \quad (4)$$

where c_F is the concentration of free ThT, c_B is the concentration of bound ThT, ε_{412} and ε_{450} are the extinction coefficients of bound ThT, and A_{412} and A_{450} are sample absorbance values at 412 and 450 nm, determined by subtracting the fibril absorbance spectrum from the fibril−ThT spectrum, as described previously.

The concentration of bound ThT determined using this method may lose accuracy if distinct binding modes have vastly different ε_{412} and ε_{450} values; however, the calculated total ThT concentration has a linear dependence on total ThT present in the sample (Figure S3), which indicates that there are no drastic changes to bound ThT extinction coefficients.

RESULTS

Four distinct conformation insulin amyloid fibrils were generated by aggregating the protein under four different environmental conditions: 20% acetic acid solution (further referred to as AC),[35] pH 2.0 and pH 2.4 sodium phosphate buffers (PH20 and PH24, respectively),[42] as well as pH 7.4 phosphate buffer saline (PH74).[44] To evaluate the effectiveness of identifying insulin amyloid fibrils with different conformations, control experiments had to be carried out using well-established methods, such as Fourier-transform infrared spectroscopy and atomic force microscopy.

Atomic Force Microscopy. The four fibril samples were first evaluated based on their AFM images, as well as by comparing the height and width of aggregates. The AC (Figure 1A), PH20 (Figure 1B), and PH24 (Figure 1C) samples contain long, linear fibrils, with some self-association observed in the case of AC and PH24 conditions. The PH74 sample (Figure 1D), on the other hand, contains highly fragmented and short aggregates. When considering the height distribution (Figure 1E), PH20 and PH74 aggregates have the smallest height (average value is 4 nm). The AC fibril height is slightly bigger—5 nm—and the pH 2.4 sample contains the highest fibrils—7 nm. Based on the width of aggregates (Figure 1F), all four samples have different values, with PH74 having the lowest (13 nm), PH20 (14 nm), pH 2.4 (16 nm), and AC (18 nm). By combining the height and width measurements and the visual inspection of AFM images, the PH20 and PH74 samples are easy to differentiate from the rest, while AC and PH24 are quite similar to one another.

https://dx.doi.org/10.1021/acs.biomac.0c01178
Biomacromolecules 2020, 21, 4989−4997

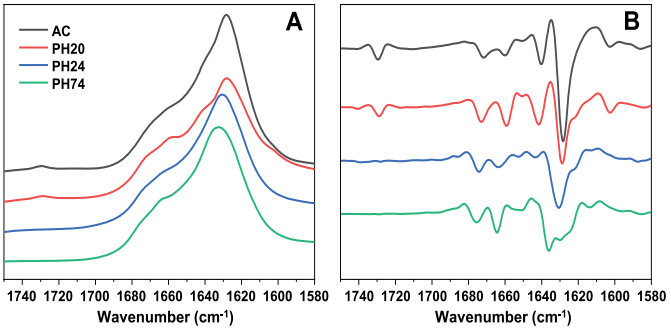

Sample	Beta-sheets	Turns/loops	Carboxyl groups	HHBW (cm^{-1})
AC	1628/1640	1660/1671	1729	33
PH20	1628/1641	1659/1673	1729	38
PH24	1630	1664/1674	-	35
PH74	1630/1636	1664/1675	-	38

Figure 2. Insulin sample's FTIR spectra (A), second derivatives (B), and spectrum positions associated with β-sheets, turns, loops, deuterated carboxyl groups, and each spectrum's band's width at its half-height (table inserted).

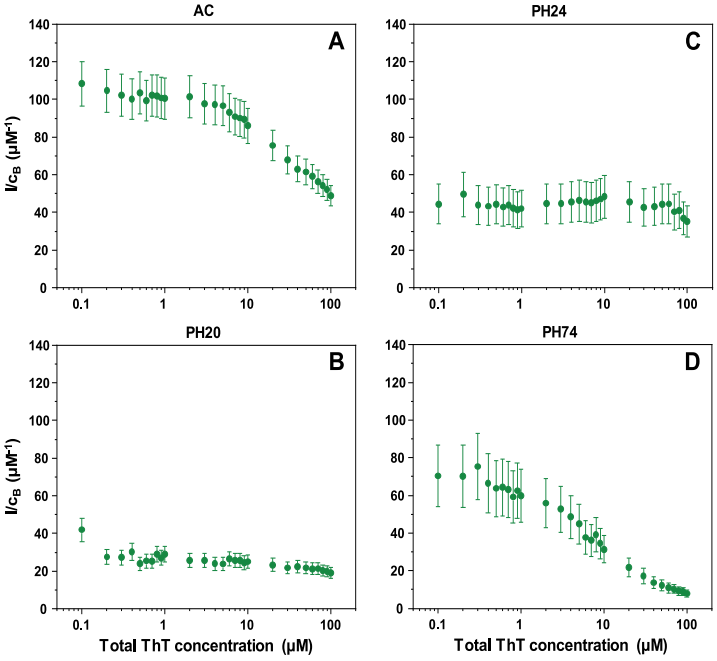

Figure 3. Insulin sample's ThT fluorescence intensity and bound ThT concentration ratios (I/c_B) at different total dye concentrations. Insulin fibrils were prepared under AC (A), PH20 (B), PH24 (C) and PH74 (D) conditions.

Fibril length was not used as a means of distinguishing between insulin fibril conformations due to fragmentation having a substantial effect on this factor, as can be seen in the case of PH74, where the sample was agitated during aggregation (Figure S2A,B). There were also no clear periodicity patterns observed for any of the fibrils, where such a parameter could be determined (Figure S4). Prior to further experiments, the samples were sonicated, which resulted in all four aggregates having a comparable length distribution (Figure S2B). The width distribution experienced a slight increase (Figure S1F), likely due to the lateral association of small fibril fragments.[45] Sonication had a very minimal influence on all four aggregate type height distributions (Figure S1E).

https://dx.doi.org/10.1021/acs.biomac.0c01178
Biomacromolecules 2020, 21, 4989−4997

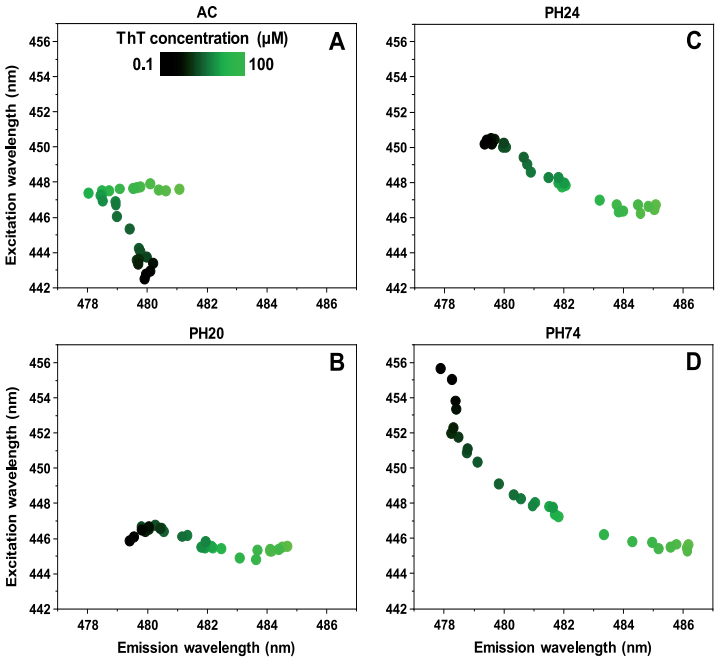

Figure 4. Insulin sample's ThT fluorescence EEM intensity center of mass positions at different total ThT concentrations. Insulin fibrils were prepared under AC (A), PH20 (B), PH24 (C), and PH74 (D) conditions.

Fibril Secondary Structure. FTIR was used to detect differences in the fibril secondary structure, relying on the amide I/I' region (Figure 2). The AC and PH20 samples share similarities in the fact that they both contain a small peak at 1729 cm^{-1}, which is associated with deuterated carboxyl groups. The appearance of this peak can be associated to the disappearance of salt bridge interactions and subsequent deuteration of the resulting carboxyl group.[46] They also both have the main minima in the second derivative at 1628 cm^{-1}, which can be associated with stronger hydrogen bonds in the β-sheet structure, while the bands at 1640 cm^{-1} for AC and 1641 cm^{-1} for PH20 are related to weaker hydrogen bonds. The difference between AC and PH20 fibrils lays in more expressed bands at 1659 and 1673 cm^{-1} (associated with turns and/or loops) in the second derivative spectrum of PH20. There is also a considerable difference between half-height band widths[43] of AC and PH20 amide I/I' bands (Figure 2). The PH24 sample displays the only main minimum at 1630 cm^{-1}, which suggests a single hydrogen bonding profile in the β-sheet structure. This spectrum also has no peak associated with deuterated carboxyl groups. The most distinct FTIR spectrum belongs to the PH74 sample, which has the main minimum at 1636 cm^{-1}, with smaller bands at 1628−1630 cm^{-1}, indicating a dominant presence of weaker and a smaller fraction of stronger hydrogen bonds in the β-sheet structure. Based on these observations, it is not difficult to separate the PH24 and PH74 samples from the rest; however, the AC and PH20 FTIR spectra have quite a few similarities and can only be accurately distinguished based on different HHBW values. All four types of fibrils contain parallel β-sheets, and there is no clear indication of the presence of antiparallel ones.[47]

Bound ThT Intensities. Before conducting experiments with ThT binding, all fibril samples were repeatedly resuspended into MilliQ water and sonicated to negate any effect that the solution's ionic strength, additives, or fibril superstructural organization may have on dye binding or fluorescence.

After measuring each sample's fluorescence EEMs and absorbance spectra under a range of ThT concentrations, the maximum fluorescence intensities, as well as bound ThT concentrations, were determined. Since fibrils may possess different dye binding modes or have parts of their surface covered due to cluster formation, the absolute fluorescence intensity could not be used to differentiate between samples. Instead, to accurately compare each sample, the ratios between ThT fluorescence intensities and bound dye concentrations (I/c_B) were calculated by dividing the fluorescence intensity with the concentration of bound dye molecules at each examined ThT concentration.

In the case of AC (Figure 3A), the I/c_B ratio is around 110 μM^{-1} when the total concentration of ThT is low. Once the dye's concentration reaches 3−4 μM, the ratio begins to decrease, eventually reaching 50 μM^{-1}. Such reductions in the fluorescence quantum yield are associated with self-quenching of dye molecules due to binding in close proximity on the fibril's surface.[48−50] For PH20 (Figure 3B), both the initial (30−40 μM^{-1}) and final (20−30 μM^{-1}) ratio values are quite low in comparison and they do not experience such a drastic drop upon an increase of ThT concentrations. The PH24 sample (Figure 3C) initial and final ratios are within the margin of error (35−50 μM^{-1}), and there is almost no reduction in values throughout the entire ThT concentration

https://dx.doi.org/10.1021/acs.biomac.0c01178
Biomacromolecules 2020, 21, 4989−4997

range. The PH74 (Figure 3D) ratio dependence on total ThT concentration has a sigmoidal shape, with initial values being 60−80 μM^{-1}, which then drop to 10 μM^{-1}. Based on I/c_B ratios, all four samples have distinct dependencies on the total ThT concentration. AC and PH74 have similar shapes but different initial and final values, as do PH20 and PH24 samples.

To verify the distinct ways of dye−fibril association, the bound ThT absorbance[29] and fluorescence spectra at 1 μM ThT (where most of the dye molecules are in their bound state) were compared (Figure S5A,B). The PH20 sample had the lowest absorbance values, as well as the lowest maximum absorbance wavelength (420 nm). PH24 had a wider peak, but the absorbance intensity was similar to PH20. Both AC and PH74 had the highest absorbance peaks, which were also shifted toward 445 nm. This partial similarity between PH20 and PH24, as well as between AC and PH74, is in line with the observed I/c_B ratio dependencies on total ThT concentration. Under these conditions, the fluorescence intensities correlate with the absorbance intensities (Figure S5B).

EEM Maxima Positions. Different modes of ThT binding may possess specific excitation and emission wavelength maximum positions, which was also used to differentiate between the four samples. In the case of AC (Figure 4A), at low ThT concentrations, the maximum positions are located at 443/480 nm excitation/emission wavelengths. As the dye's concentration increases, the excitation wavelength shifts toward 448 nm and the emission wavelength shifts to 478 nm. At higher ThT concentrations, the emission wavelength remains stable, but the excitation wavelength shifts toward 481 nm. This type of maximum position movement is a likely indicator of three ThT binding modes. For PH20 (Figure 4B), there is minimal variation in the excitation wavelength, which remains at 445−447 nm; however, there is a shift in the emission wavelength—from 479 to 485 nm. The PH24 sample's (Figure 4C) EEM maximum position moves from 450/479 to a similar position to the PH20 sample (446/485). This means that PH20 and PH24 fibrils likely have one different and one similar ThT binding mode. The PBS sample's (Figure 4D) EEM maximum position experiences the most significant movement, forming an arc-shape from 456/478 to 445/486. It has partial overlap with PH20 and PH24 sample positions at higher ThT concentrations, suggesting the existence of a similar binding mode for all three cases. The position at low ThT values, however, is different from all of the other samples. Such a significant movement and the arc-shape is also a likely indicator of more than two modes of ThT binding.

DISCUSSION

Using the two classical methods (AFM and FTIR) to compare insulin fibrils formed at different conditions, it can be identified that the four samples possess distinct morphologies and secondary structures. In some instances, there were similarities between AFM images or fibril heights and widths, and in others, there were similarities between FTIR spectra. Combining both methods, however, allows us to very clearly differentiate between the four insulin conformations.

When we examine the sample fluorescence intensity and bound ThT concentration ratios (I/c_B), we see that there are clear distinctions between the four samples. Besides the fact that this allows us to differentiate between the distinct conformations, there is also an interesting I/c_B ratio dependence on total ThT concentrations. In two of the cases, namely, AC and PH74, the ratio decreases with increasing ThT concentrations. Such an event is to be expected, as ThT is known to induce a self-quenching effect.[48] However, PH20 and PH24 samples do not experience such a significant decrease, even at the highest dye concentrations. It is possible that ThT binds in such a manner that it does not allow for a self-quenching effect to occur. The absorbance spectra of 1 μM bound ThT displays significant distinctions between all four samples, further supporting the idea that these four fibril conformations have specific ThT binding characteristics.

Comparing each sample's excitation−emission matrix and their intensity center of mass also leads to four different EEM maximum position distributions. At low ThT concentrations, all four samples have clearly distinct positions. In three of the cases, namely, PH20, PH24, and PH74, increasing the total ThT concentration leads to a maximum position convergence at 446/485 nm. This means that, while each fibril conformation possibly has unique ThT binding modes, some conformations may share a similar binding mode.

Since these ThT binding/fluorescence characteristics stem from either morphological or secondary structure variations, we have to examine which of them could be responsible for such dye−fibril association. In the case of morphology, the only real difference present between all four samples after sonication is their height distribution (Figure S1E). There does not seem to be any correlation between the I/c_B ratio and fibril height, as PH20 and PH24 samples have the largest height difference, yet similar shape I/c_B ratio distribution dependencies on the total ThT concentration. No correlation is also present in the case of fluorescence EEM positions. This leads to the idea that fibril morphology is not the main determining factor for ThT binding characteristics.

In the case of secondary structure, the relation between each structural motif and dye binding/fluorescence has to be considered. The deuterated carboxyl group, related to the loss of salt bridges[46] during insulin aggregation, does not appear to be a significant factor, as there is a massive difference in both I/c_B and EEM parameters between the two insulin conformations that have a peak at 1729 cm^{-1} in FTIR spectra. The turn/loop motives do not pertain to significant variations for them to be a factor, which leaves hydrogen bond strength in the β-sheet structure as the main suspect. The highest I/c_B ratio at low ThT concentrations is observed in the AC sample, where fibrils have the largest amount of stronger hydrogen bonds (as indicated by the major 1628 cm^{-1} band in the second derivative spectrum). The PH20 sample also has a peak at 1628 cm^{-1}, but in this case, the 1641 cm^{-1} band is relatively larger than in the case of AC. This sample has a significantly lower I/c_B ratio than AC, however, which may indicate that the weaker hydrogen bonds in the fibril's structure create binding positions with higher ThT binding affinity and lower fluorescence quantum yield. The PH24 FTIR spectrum has a single β-sheet-related band, and, coincidentally, the I/c_B ratio experiences the least amount of variation throughout the entire ThT concentration range. The PH74 FTIR spectrum is the most peculiar of all, displaying mostly weaker hydrogen bonds within the β-sheet structure but also some stronger ones. Its corresponding I/c_B ratio and EEM positions also experience the most drastic changes throughout the whole ThT concentration range. These observations hint at a possibility that weaker hydrogen bonds in the fibril's structure lead to binding positions with higher ThT binding affinity and lower

https://dx.doi.org/10.1021/acs.biomac.0c01178
Biomacromolecules 2020, 21, 4989−4997

fluorescence quantum yield, while stronger ones result in binding position with lower ThT binding affinity and higher quantum yield.

When we combine AFM with FTIR and I/c_B with EEM positions, it is clear that both pairs of methods are highly efficient at differentiating insulin fibrils prepared under different environmental conditions. Considering that a ThT binding examination has comparable efficiency to both AFM and FTIR, we have to discuss the advantages that this method has. In the case of FTIR, to acquire a high-quality spectrum and detect minor differences, a high concentration of fibrils has to be used. For AFM, the method of sample deposition can influence the overall fibril distribution (fibril clump formation, washing away smaller fibrils/oligomers, different aggregate/mica association propensities). Conversely, fibril–ThT fluorescence I/c_B ratio and EEM position profile outlines, as well as bound ThT absorbance spectra, can be acquired by scanning relatively low fibril concentration samples at four ThT concentrations (0.1, 1, 10, and 100 μM). This method also uses fibril resuspension into MilliQ water, which negates the effect that the initial solution's ionic strength or additives may have on ThT binding. The aggregates are also sonicated to both homogenize the sample, as well as disrupt any superstructural organization that may form during aggregation.

Despite insulin being a model for the study of amyloid aggregation and not considered as a neurodegenerative disease-associated protein, its ability to form multiple distinct fibril conformations serves as a means to display this method's effectiveness. As of this time, there have been reports showing that different strains of disease-related proteins, such as α-synuclein[33] or prion proteins,[34] also possess different ThT binding modes, resulting in distinct fluorescence profiles. This means that ThT binding could serve in conjunction with other commonly used methods to both identify and differentiate the large variety of conformations that amyloid fibrils can obtain.

CONCLUSIONS

ThT molecule interactions with insulin amyloid fibrils, prepared under different conditions, display a wide variety of bound ThT quantum yields, as well as distinct binding modes. Such interactions can be used to differentiate between fibrils to a similar extent as other widely used methods, such as AFM or FTIR. As this ThT binding assay requires minimal amounts of fibrils and is not affected by the initial aggregation solution or sample deposition, it can be applied as either an alternative or supplemental method in amyloid fibril research.

ASSOCIATED CONTENT

Supporting Information

The Supporting Information is available free of charge at https://pubs.acs.org/doi/10.1021/acs.biomac.0c01178.

Atomic force microscopy images of insulin fibrils, prepared in AC, PH20, PH24, and PH74 conditions after multiple rounds of resuspension into MilliQ H_2O and sonication (Figure S1); AC, PH20, PH24, and PH74 fibril length distributions before and after resuspension into MilliQ H_2O and sonication (Figure S2); comparison of total (bound + free) ThT concentration calculated from sample absorbance data and total ThT added to the sample (Figure S3); AC, PH20, and PH24 fibril surface height along the fibril axis (Figure S4); and absorbance spectra of free and fibril-bound ThT and fluorescence intensity of all four types of fibrils in the presence of 1 μM ThT (Figure S5) (PDF)

AUTHOR INFORMATION

Corresponding Author

Vytautas Smirnovas − *Institute of Biotechnology, Life Sciences Center, Vilnius University, Vilnius LT-10257, Lithuania;* orcid.org/0000-0002-1829-5455;
Email: vytautas.smirnovas@bti.vu.lt

Authors

Mantas Ziaunys − *Institute of Biotechnology, Life Sciences Center, Vilnius University, Vilnius LT-10257, Lithuania;* orcid.org/0000-0002-8368-6188

Andrius Sakalauskas − *Institute of Biotechnology, Life Sciences Center, Vilnius University, Vilnius LT-10257, Lithuania*

Complete contact information is available at: https://pubs.acs.org/10.1021/acs.biomac.0c01178

Author Contributions

M.Z. and V.S. designed the studies. M.Z. and A.S. undertook the experimental work. M.Z. and V.S. analyzed the data and prepared the manuscript.

Funding

This research was funded by Vilnius University, Grant No. MSF-JM-3.

Notes

The authors declare no competing financial interest.

REFERENCES

(1) Chiti, F.; Dobson, C. M. Protein Misfolding, Functional Amyloid, and Human Disease. *Annu. Rev. Biochem.* **2006**, *75*, 333–366.

(2) Knowles, T. P. J.; Vendruscolo, M.; Dobson, C. M. The Amyloid State and Its Association with Protein Misfolding Diseases. *Nat. Rev. Mol. Cell Biol.* **2014**, *15*, 384–396.

(3) Baker, K. R.; Rice, L. The Amyloidoses: Clinical Features, Diagnosis And Treatment. *Methodist DeBakey Cardiovasc. J.* **2012**, *8*, No. 3.

(4) Isik, A. T. Late Onset Alzheimer's Disease in Older People. *Clin. Interventions Aging* **2010**, *5*, 307.

(5) Hebert, L. E.; Weuve, J.; Scherr, P. A.; Evans, D. A. Alzheimer Disease in the United States (2010–2050) Estimated Using the 2010 Census. *Neurology* **2013**, *80*, 1778–1783.

(6) Arthur, K. C.; Calvo, A.; Price, T. R.; Geiger, J. T.; Chiò, A.; Traynor, B. J. Projected Increase in Amyotrophic Lateral Sclerosis from 2015 to 2040. *Nat. Commun.* **2016**, *7*, No. 12408.

(7) Chatani, E.; Yamamoto, N. Recent Progress on Understanding the Mechanisms of Amyloid Nucleation. *Biophys. Rev.* **2018**, *10*, 527–534.

(8) Meisl, G.; Kirkegaard, J. B.; Arosio, P.; Michaels, T. C. T.; Vendruscolo, M.; Dobson, C. M.; Linse, S.; Knowles, T. P. J. Molecular Mechanisms of Protein Aggregation from Global Fitting of Kinetic Models. *Nat. Protoc.* **2016**, *11*, 252–272.

(9) Fitzpatrick, A. W. P.; Debelouchina, G. T.; Bayro, M. J.; Clare, D. K.; Caporini, M. A.; Bajaj, V. S.; Jaroniec, C. P.; Wang, L.; Ladizhansky, V.; Muller, S. A.; MacPhee, C. E.; Waudby, C. A.; Mott, H. R.; De Simone, A.; Knowles, T. P. J.; Saibil, H. R.; Vendruscolo, M.; Orlova, E. V.; Griffin, R. G.; Dobson, C. M. Atomic Structure and Hierarchical Assembly of a Cross-β Amyloid Fibril. *Proc. Natl. Acad. Sci. U.S.A.* **2013**, *110*, 5468–5473.

(10) Fändrich, M.; Nyström, S.; Nilsson, K. P. R.; Böckmann, A.; LeVine, H.; Hammarström, P. Amyloid Fibril Polymorphism: A

Challenge for Molecular Imaging and Therapy. *J. Intern. Med.* **2018**, *283*, 218−237.
(11) Cummings, J.; Lee, G.; Ritter, A.; Sabbagh, M.; Zhong, K. Alzheimer's Disease Drug Development Pipeline: 2019. *Alzheimer's Dementia: Transl. Res. Clin. Interventions* **2019**, *5*, 272−293.
(12) Šneideris, T.; Baranauskienė, L.; Cannon, J. G.; Rutkienė, R.; Meškys, R.; Smirnovas, V. Looking for a Generic Inhibitor of Amyloid-like Fibril Formation among Flavone Derivatives. *PeerJ* **2015**, *3*, No. e1271.
(13) Srinivasan, E.; Rajasekaran, R. Probing the Inhibitory Activity of Epigallocatechin-Gallate on Toxic Aggregates of Mutant (L84F) SOD1 Protein through Geometry Based Sampling and Steered Molecular Dynamics. *J. Mol. Graphics Model.* **2017**, *74*, 288−295.
(14) Goyal, D.; Shuaib, S.; Mann, S.; Goyal, B. Rationally Designed Peptides and Peptidomimetics as Inhibitors of Amyloid-β (Aβ) Aggregation: Potential Therapeutics of Alzheimer's Disease. *ACS Comb. Sci.* **2017**, *19*, 55−80.
(15) Byeon, S. R.; Lee, J. H.; Sohn, J.-H.; Kim, D. C.; Shin, K. J.; Yoo, K. H.; Mook-Jung, I.; Lee, W. K.; Kim, D. J. Bis-Styrylpyridine and Bis-Styrylbenzene Derivatives as Inhibitors for Aβ Fibril Formation. *Bioorg. Med. Chem. Lett.* **2007**, *17*, 1466−1470.
(16) Konar, M.; Bag, S.; Roy, P.; Dasgupta, S. Gallic Acid Induced Dose Dependent Inhibition of Lysozyme Fibrillation. *Int. J. Biol. Macromol.* **2017**, *103*, 1224−1231.
(17) Ruggeri, F. S.; Šneideris, T.; Vendruscolo, M.; Knowles, T. P. J. Atomic Force Microscopy for Single Molecule Characterisation of Protein Aggregation. *Arch. Biochem. Biophys.* **2019**, *664*, 134−148.
(18) Podestà, A.; Tiana, G.; Milani, P.; Manno, M. Early Events in Insulin Fibrillization Studied by Time-Lapse Atomic Force Microscopy. *Biophys. J.* **2006**, *90*, 589−597.
(19) Streets, A. M.; Sourigues, Y.; Kopito, R. R.; Melki, R.; Quake, S. R. Simultaneous Measurement of Amyloid Fibril Formation by Dynamic Light Scattering and Fluorescence Reveals Complex Aggregation Kinetics. *PLoS One* **2013**, *8*, No. e54541.
(20) Zandomeneghi, G.; Krebs, M. R. H.; McCammon, M. G.; Fändrich, M. FTIR Reveals Structural Differences between Native β-Sheet Proteins and Amyloid Fibrils. *Protein Sci.* **2004**, *13*, 3314−3321.
(21) Malmos, K. G.; Blancas-Mejia, L. M.; Weber, B.; Buchner, J.; Ramirez-Alvarado, M.; Naiki, H.; Otzen, D. ThT 101: A Primer on the Use of Thioflavin T to Investigate Amyloid Formation. *Amyloid* **2017**, *24*, 1−16.
(22) Picken, M. M.; Herrera, G. A. Thioflavin T Stain: An Easier and More Sensitive Method for Amyloid Detection. In *Amyloid and Related Disorders*; Picken, M. M.; Herrera, G. A.; Dogan, A., Eds.; Humana Press: Totowa, NJ, 2012; pp 187−189.
(23) Wetzel, R.; Chemuru, S.; Misra, P.; Kodali, R.; Mukherjee, S.; Kar, K. An Aggregate Weight-Normalized Thioflavin-T Measurement Scale for Characterizing Polymorphic Amyloids and Assembly Intermediates. *Methods Mol. Biol.* **2018**, *1777*, 121−144.
(24) Groenning, M. Binding Mode of Thioflavin T and Other Molecular Probes in the Context of Amyloid Fibrils—Current Status. *J. Chem. Biol.* **2010**, *3*, 1−18.
(25) Lockhart, A.; Ye, L.; Judd, D. B.; Merritt, A. T.; Lowe, P. N.; Morgenstern, J. L.; Hong, G.; Gee, A. D.; Brown, J. Evidence for the Presence of Three Distinct Binding Sites for the Thioflavin T Class of Alzheimer's Disease PET Imaging Agents on β-Amyloid Peptide Fibrils. *J. Biol. Chem.* **2005**, *280*, 7677−7684.
(26) Ziaunys, M.; Smirnovas, V. Additional Thioflavin-T Binding Mode in Insulin Fibril Inner Core Region. *J. Phys. Chem. B* **2019**, *123*, 8727−8732.
(27) Sulatskaya, A. I.; Kuznetsova, I. M.; Belousov, M. V.; Bondarev, S. A.; Zhouravleva, G. A.; Turoverov, K. K. Stoichiometry and Affinity of Thioflavin T Binding to Sup35p Amyloid Fibrils. *PLoS One* **2016**, *11*, No. e0156314.
(28) Groenning, M.; Norrman, M.; Flink, J. M.; van de Weert, M.; Bukrinsky, J. T.; Schluckebier, G.; Frokjaer, S. Binding Mode of Thioflavin T in Insulin Amyloid Fibrils. *J. Struct. Biol.* **2007**, *159*, 483−497.
(29) Kuznetsova, I. M.; Sulatskaya, A. I.; Uversky, V. N.; Turoverov, K. K. Analyzing Thioflavin T Binding to Amyloid Fibrils by an Equilibrium Microdialysis-Based Technique. *PLoS One* **2012**, *7*, No. e30724.
(30) Kawai, R.; Araki, M.; Yoshimura, M.; Kamiya, N.; Ono, M.; Saji, H.; Okuno, Y. Core Binding Site of a Thioflavin-T-Derived Imaging Probe on Amyloid β Fibrils Predicted by Computational Methods. *ACS Chem. Neurosci.* **2018**, *9*, 957−966.
(31) Ivancic, V. A.; Ekanayake, O.; Lazo, N. D. Binding Modes of Thioflavin T on the Surface of Amyloid Fibrils Studied by NMR. *ChemPhysChem* **2016**, *17*, 2461−2464.
(32) Mao, X.; Guo, Y.; Wang, C.; Zhang, M.; Ma, X.; Liu, L.; Niu, L.; Zeng, Q.; Yang, Y.; Wang, C. Binding Modes of Thioflavin T Molecules to Prion Peptide Assemblies Identified by Using Scanning Tunneling Microscopy. *ACS Chem. Neurosci.* **2011**, *2*, 281−287.
(33) Sidhu, A.; Vaneyck, J.; Blum, C.; Segers-Nolten, I.; Subramaniam, V. Polymorph-Specific Distribution of Binding Sites Determines Thioflavin-T Fluorescence Intensity in α-Synuclein Fibrils. *Amyloid* **2018**, *25*, 189−196.
(34) Ziaunys, M.; Sneideris, T.; Smirnovas, V. Formation of Distinct Prion Protein Amyloid Fibrils under Identical Experimental Conditions. *Sci. Rep.* **2020**, *10*, No. 4572.
(35) Sakalauskas, A.; Ziaunys, M.; Smirnovas, V. Concentration-Dependent Polymorphism of Insulin Amyloid Fibrils. *PeerJ* **2019**, *7*, No. e8208.
(36) Sneideris, T.; Sakalauskas, A.; Sternke-Hoffmann, R.; Peduzzo, A.; Ziaunys, M.; Buell, A. K.; Smirnovas, V. The Environment Is a Key Factor in Determining the Anti-Amyloid Efficacy of EGCG. *Biomolecules* **2019**, *9*, No. 855.
(37) Gupta, Y.; Singla, G.; Singla, R. Insulin-Derived Amyloidosis. *Indian J. Endocrinol. Metab.* **2015**, *19*, 174−177.
(38) Foderà, V.; Cataldo, S.; Librizzi, F.; Pignataro, B.; Spiccia, P.; Leone, M. Self-Organization Pathways and Spatial Heterogeneity in Insulin Amyloid Fibril Formation. *J. Phys. Chem. B* **2009**, *113*, 10830−10837.
(39) Gong, H.; He, Z.; Peng, A.; Zhang, X.; Cheng, B.; Sun, Y.; Zheng, L.; Huang, K. Effects of Several Quinones on Insulin Aggregation. *Sci. Rep.* **2015**, *4*, No. 5648.
(40) Wang, J.-B.; Wang, Y.-M.; Zeng, C.-M. Quercetin Inhibits Amyloid Fibrillation of Bovine Insulin and Destabilizes Preformed Fibrils. *Biochem. Biophys. Res. Commun.* **2011**, *415*, 675−679.
(41) Jayamani, J.; Shanmugam, G. Gallic Acid, One of the Components in Many Plant Tissues, Is a Potential Inhibitor for Insulin Amyloid Fibril Formation. *Eur. J. Med. Chem.* **2014**, *85*, 352−358.
(42) Sneideris, T.; Darguzis, D.; Botyriute, A.; Grigaliunas, M.; Winter, R.; Smirnovas, V. PH-Driven Polymorphism of Insulin Amyloid-Like Fibrils. *PLoS One* **2015**, *10*, No. e0136602.
(43) Dzwolak, W.; Smirnovas, V.; Jansen, R.; Winter, R. Insulin Forms Amyloid in a Strain-Dependent Manner: An FT-IR Spectroscopic Study. *Protein Sci.* **2004**, *13*, 1927−1932.
(44) Iannuzzi, C.; Borriello, M.; Portaccio, M.; Irace, G.; Sirangelo, I. Insights into Insulin Fibril Assembly at Physiological and Acidic Ph and Related Amyloid Intrinsic Fluorescence. *Int. J. Mol. Sci.* **2017**, *18*, No. 2551.
(45) Milhiet, P.-E.; Yamamoto, D.; Berthoumieu, O.; Dosset, P.; Le Grimellec, C.; Verdier, J.-M.; Marchal, S.; Ando, T. Deciphering the Structure, Growth and Assembly of Amyloid-Like Fibrils Using High-Speed Atomic Force Microscopy. *PLoS One* **2010**, *5*, No. e13240.
(46) Surmacz-Chwedoruk, W.; Nieznańska, H.; Wójcik, S.; Dzwolak, W. Cross-Seeding of Fibrils from Two Types of Insulin Induces New Amyloid Strains. *Biochemistry* **2012**, *51*, 9460−9469.
(47) Barth, A. Infrared Spectroscopy of Proteins. *Biochim. Biophys. Acta* **2007**, *1767*, 1073−1101.
(48) Lindberg, D. J.; Wenger, A.; Sundin, E.; Wesén, E.; Westerlund, F.; Esbjörner, E. K. Binding of Thioflavin-T to Amyloid Fibrils Leads to Fluorescence Self-Quenching and Fibril Compaction. *Biochemistry* **2017**, *56*, 2170−2174.

(49) Ran, C.; Zhao, W.; Moir, R. D.; Moore, A. Non-Conjugated Small Molecule FRET for Differentiating Monomers from Higher Molecular Weight Amyloid Beta Species. *PLoS One* **2011**, *6*, No. e19362.
(50) Ziaunys, M.; Mikalauskaite, K.; Smirnovas, V. Amyloidophilic Molecule Interactions on the Surface of Insulin Fibrils: Cooperative Binding and Fluorescence Quenching. *Sci. Rep.* **2019**, *9*, No. 20303.

https://dx.doi.org/10.1021/acs.biomac.0c01178
Biomacromolecules 2020, 21, 4989−4997

SCIENTIFIC REPORTS
nature research

OPEN

Formation of distinct prion protein amyloid fibrils under identical experimental conditions

Mantas Ziaunys, Tomas Sneideris & Vytautas Smirnovas*

Protein aggregation into amyloid fibrils is linked to multiple neurodegenerative disorders, such as Alzheimer's, Parkinson's or Creutzfeldt-Jakob disease. A better understanding of the way these aggregates form is vital for the development of drugs. A large detriment to amyloid research is the ability of amyloidogenic proteins to spontaneously aggregate into multiple structurally distinct fibrils (strains) with different stability and seeding properties. In this work we show that prion proteins are capable of forming more than one type of fibril under the exact same conditions by assessing their Thioflavin T (ThT) binding ability, morphology, secondary structure, stability and seeding potential.

Prion proteins are cell surface glycoproteins, most widely known for their link to transmissible spongiform encephalopathies, such as Scrapie, Creutzfeldt-Jakob disease and Gerstmann-Straussler-Scheinker syndrome[1–4]. In their native form, prion proteins exist in a mostly alpha-helical conformation (PrP^{C})[5], however, conformational changes due to various environmental factors may induce the formation of an insoluble, β-sheet rich structure (PrP^{Sc})[6]. PrP^{Sc} acts as a template and an aggregation center for further fibril growth by incorporating monomers and changing them to the PrP^{Sc} form[7,8]. Such aggregation eventually leads to higher oligomers, protofibrils and eventually to fully formed amyloid fibrils[9].

Amyloid fibrils are highly structured, densely packed protein aggregates[10] which have been found in amyloid-plaques in patients with neurodegenerative disorders[11]. Their cytotoxic effect was also shown on numerous occasions with both *in vitro*[12–14] and *in vivo*[15,16] experiments. It has been observed that prion protein amyloid fibrils can exist in multiple distinct structural conformations[17–19]. *In vitro*, different strains can be formed based on the environmental conditions in which the aggregates are generated, such as sample agitation[20,21], pH[22], denaturant[23,24], and salt concentration[25]. While the process of how and why a protein with the exact same sequence can possess multiple different fibrillar structures is of great interest and is being widely examined[26–28], it does cause problems when analyzing and comparing data. The different strains have distinct morphologies[29,30] and secondary structures[22,31], replication rates[32], stability in denaturants[28,33]. This inevitably results in data obtained from heterogeneous mixtures[34,35]. There has been an ongoing effort to not only differentiate[36], but to purify strains of prion protein fibrils[37]. However, as of yet, single strain purification is still difficult[38].

A commonly used method for amyloid fibril detection is a ThT assay, in which the fluorescent dye molecules specifically bind to beta-sheet grooves on the fibril's surface, causing a red-shift in their excitation/emission spectra, as well as a large increase in fluorescence intensity[39]. ThT has been shown to have distinct binding capacity on different types of fibrils, most likely due to the structure and quantity of possible binding sites[40–42]. This specific affinity could potentially be used as a quick primary way of differentiating between samples that contain differently structured aggregates.

In this work we generated a range of mouse prion protein (MoPrP) fibril samples using the exact same conditions and attempted to separate the formed aggregate types by a ThT assay and further examine the structure, stability and seeding ability of the distinct samples. We show that under the selected conditions, there appear to be at least two mouse prion protein fibril types with different structural and seeding properties.

Methods

Amyloid fibril formation. Mouse recombinant prion protein C-terminal fragment (MoPrP89-230) was purified as described previously[43]. In short, the protein containing a His-tag was expressed in *E. coli*, inclusion bodies were dissolved in a 6 M guanidine hydrochloride (GuHCl) solution and the protein was loaded onto an immobilized metal affinity chromatography nickel column, refolded and eluted with a 700 mM imidazole

Institute of Biotechnology, Life Sciences Center, Vilnius University, Vilnius, Lithuania. *email: vytautas.smirnovas@bti.vu.lt

solution. The purified protein was dialyzed into 10 mM sodium acetate (pH 4) buffer at 4 °C, filtered, concentrated to 3 mg/ml and stored at −80 °C. Typically about 100 mg of the protein is purified in a single batch. The stock solution was mixed with 50 mM sodium phosphate buffers (pH 6.0) with or without 6 M GuHCl to a final 0.5 mg/ml protein and 2 M GuHCl concentration. The solution was then evenly distributed to 20 test tubes (Fisher, #15432545) (1 ml solution per tube). In order to confirm that the distribution process does not yield samples containing different types and amounts of oligomeric species or aggregates, light scattering and ThT fluorescence assays were carried out with aliquots from 20 test tubes (Fig. S1). The tubes were placed in a shaker incubator (IKA KS 4000i) parallel to the shaker's surface and incubated at 37 °C with constant shaking at 220 RPM for 72 hours to ensure the aggregation reaction is complete without having to periodically measure the ThT fluorescence of aliquots from each sample (typical time required is 20–30 hours (Fig. S2)). After fibril formation, an aliquot of each sample was taken for atomic force microscopy (AFM) examination, while the remaining samples were sonicated for 60 s (Bandelin Sonopuls 3100 ultrasonic homogenizer, MS-72 tip, 20% sonication strength) prior to further experiments.

ThT fluorescence assays. 99 µL aliquots of each sonicated fibril sample were mixed with 1 µL of 10 mM stock ThT solution to a final ThT concentration of 100 µM. The 100 µL sample fluorescence intensities were measured using a Varian Cary Eclipse spectrophotometer using 440 nm excitation and 460–500 nm emission range (excitation slit width – 10 nm, emission slit – 5 nm). Fluorescence intensities for each sample were the average of three measurements.

For the ThT affinity assay, 25 µL of each sample was diluted to 100 µL using a range of different concentration ThT solutions (containing 2 M GuHCl) to final ThT concentrations between 1 and 100 µM. ThT fluorescence intensity measurements were done as previously described.

Seeded aggregation. Aliquots of sonicated fibril samples were added to monomeric MoPrP (89–230) solutions (0.5 mg/ml protein, 2 M GuHCl, 50 mM sodium phosphate, pH 6.0) with ThT to a final fibril/monomer ratio of 1:10 and ThT concentration of 100 µM. During aggregation, the samples were incubated at a stable 60 °C temperature. The aggregation reaction was observed using a Qiagen Rotor-Gene Q real-time analyzer[43] for 1000 min, with measurements taken every minute.

Fibril dissociation assay. Sonicated fibril samples were diluted to 20% of their initial concentration to a range of different concentration GuHCl solutions using 50 mM sodium phosphate buffers (pH 6.0) with and without 6 M GuHCl. The samples were incubated for 1 hour at 25 °C, then ThT was added to a final concentration of 100 µM. Measurements of ThT fluorescence were done as previously described.

Atomic force microscopy. AFM images were acquired as described previously[44]. 20 µL of each sample was deposited on freshly cleaved mica and incubated for 1 minute. The samples were then rinsed with 1 mL of MilliQ water and dried under gentle airflow. AFM images were acquired using Dimension Icon (Bruker) atomic force microscope operating in tapping mode and equipped with a silicon cantilever RTESPA-300 (Bruker). All images were acquired at high-resolution (1024 × 1024 pixels). Three-dimensional AFM maps were flattened using SPIP or Gwyddion software. Height and width of the fibrils was determined from line profiles taken perpendicular to the fibril axes. Length was determined by tracing along the median axis of each aggregate.

Fourier-transform infrared spectroscopy (FTIR). MoPrP fibril samples were dialyzed into MilliQ water for 24 hours at 4 °C, then fibrils were separated from buffer solution by centrifugation at 20 000 x g for 30 min and resuspended in 1 mL of D_2O, the centrifugation-resuspension procedure was repeated three times. All samples were then sonicated for 60 s (MS-72 tip, 20% sonication strength). The FTIR spectra were recorded as described previously[44] using Bruker Vertex 80 v IR spectrometer equipped with mercury cadmium telluride (MCT) detector. For all measurements, CaF_2 transmission windows and 0.05 mm Teflon spacers were used. Spectra were recorded at room temperature under near-vacuum conditions (~2 mBar). For each spectrum, 256 interferograms of 2 cm^{-1} resolution were co-added. A D_2O spectrum was subtracted from each sample spectrum. All the spectra were normalized to the same area of amide I/I′ band (1700–1595 cm^{-1}). All data processing was performed using GRAMS software.

Results

Twenty MoPrP samples were aggregated under the exact same conditions and examined by a ThT fluorescence assay, which yielded a very uneven distribution of intensity values (Fig. 1A). The samples were then separated into low (LI), medium (MI) and high (HI) intensity groups and combined for further studies.

Seeding potential. All three groups were used in a seeded aggregation experiment to determine their aggregation kinetics. The results from all three samples presented both different fluorescence intensities, as well as distinct aggregation kinetic curves (Fig. 1B). The time needed for the fluorescence intensity to reach 50% of the maximum intensity value was 147 ± 11 min for LI, 108 ± 20 min for MI and 96 ± 6 min for HI samples. The fluorescence values at the end of the reaction had a similar intensity distribution (low, medium and high) as the initial samples (Fig. 1B). The MI and LI fibril seeding kinetic curves had an unusual "drop" at the early stages of the reaction (Fig. 1C), which is most evident in the case of MI fibrils.

ThT binding affinity. The fibril samples were examined for their ThT binding affinity by mixing the fibrils with a range of different ThT concentrations. We can see that in the case of both MI and LI fibrils (Fig. 2A), while the intensity of ThT fluorescence emissions is different, the ThT concentration at which the signal intensity midpoint is reached is within margin of error (5.8 ± 0.5 µM for LI and 5.7 ± 0.4 µM for MI). However, this value is

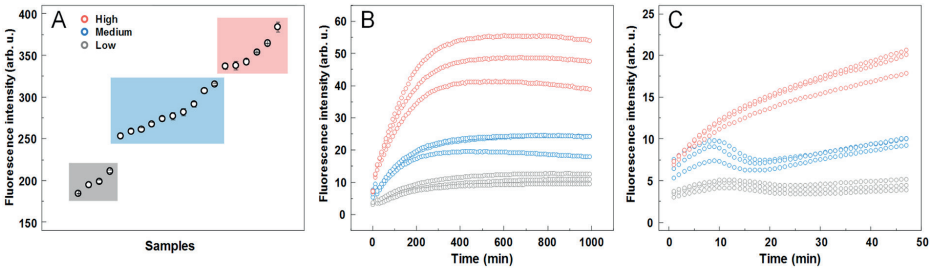

Figure 1. Separation of fibrils by ThT fluorescence intensity. (**A**) ThT fluorescence emission intensities of twenty MoPrP fibril samples prepared under identical conditions. The samples are grouped into three intensity regions, with some samples having low (grey), medium (blue) and high (red) emission intensities. (**B**) Seeded aggregation kinetics of the three intensity region fibrils using 10% of low, medium and high intensity fibrils. (**C**) Fluorescence intensity "drops" at the early stages of the aggregation process.

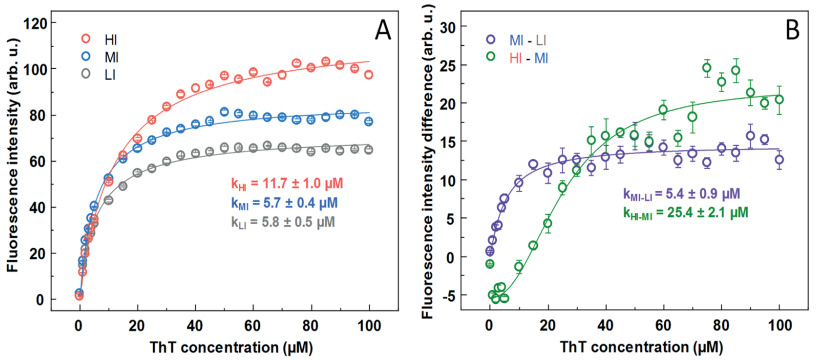

Figure 2. ThT binding to MoPrP amyloid fibrils probed by fluorescence assay. (**A**) ThT fluorescence emission intensity dependence on the concentration of ThT added to each fibril sample. (**B**) ThT fluorescence intensity differences between MI and LI samples and HI and MI samples. Hill equation fitting was done to determine the ThT concentration (k) at which the signal intensity midpoint is reached.

considerably higher (11.7 ± 1.0 μM) when examining the ThT binding affinity of fibrils in the HI sample (Fig. 2A). Subtracting the LI sample intensities from MI shows that the intensity midpoint ThT concentration of the resulting curve (Fig. 2B) is similar to both LI and MI values (5.4 ± 0.9 μM) seen in Fig. 2A, suggesting the higher intensity is the result of more ThT molecules bound in a similar mode. However, subtracting MI sample intensities from HI results in a completely different curve (Fig. 2B) with a much higher midpoint value (25.4 ± 2.1 μM). The signal intensity difference is also negative at low ThT values, suggesting that less ThT binds in the LI or MI mode, while more binds in a mode not present in the other two types of fibrils.

Fibril stability and secondary structure. Fibril dissociation under denaturing conditions was measured to determine possible structural differences between the three samples. There is a slight variation in the dissociation midpoint values (3.6 M for LI, 3.7 M for HI and 3.8 M for MI fibrils) when comparing normalized dissociation curves (Fig. 3A), however, such a minor difference does not constitute any substantial stability variations between the samples. This indicates that the formed aggregates do not have strain-specific structural stability. PK-digestion of all three samples also shows that there are no substantial variations in the size of the PK-resistant core (Fig. S3). In order to further examine the structure of these fibrils, FTIR spectra of all three samples were recorded.

The LI and MI sample fibrils appear to have a very similar FTIR spectra (Fig. 3B,C) in the amide I/I' region, both exhibit maxima at ~1627 (with the main minimum of the second derivative at ~1621 cm^{-1} and a weaker one at ~1629 cm^{-1}) and a shoulder which is reflected by the minimum of the second derivative at ~1662 cm^{-1}. However, there is a noticeable difference between them and the HI fibril sample, which exhibits a maximum at ~1627 (with the main minimum of the second derivative at ~1628 cm^{-1} and a weaker one at ~1621 cm^{-1}) and a shoulder which is reflected by the minimum of the second derivative at ~1660 cm^{-1}. (Fig. 3B,C). In all three cases, the band's shape and position are characteristic for the amyloid's parallel beta-sheet structure[45]. But the dramatic

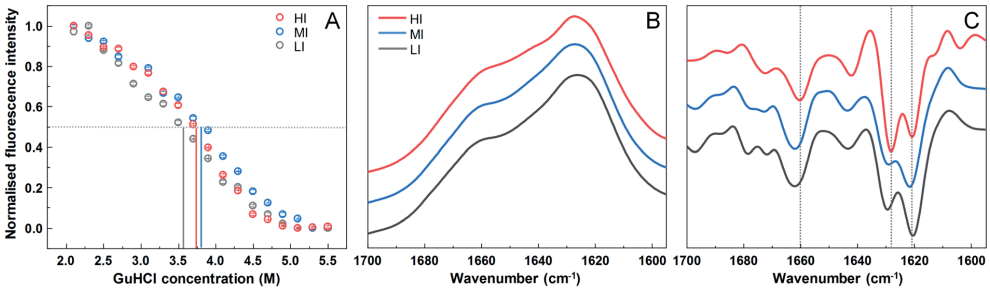

Figure 3. Dissociation assay of HI, MI, and LI fibrils and comparison of their secondary structures. (**A**) Normalized ThT fluorescence intensity values at different GuHCl concentrations, where the grey dotted line represents 50% of normalized fluorescence intensity and coloured lines correspond to each sample's GuHCl concentration at which the 50% intensity value is reached. (**B**) FTIR spectra of fibril samples and second order derivative spectra (**C**), where grey dotted lines show wavenumbers at which the differences between spectra can be observed.

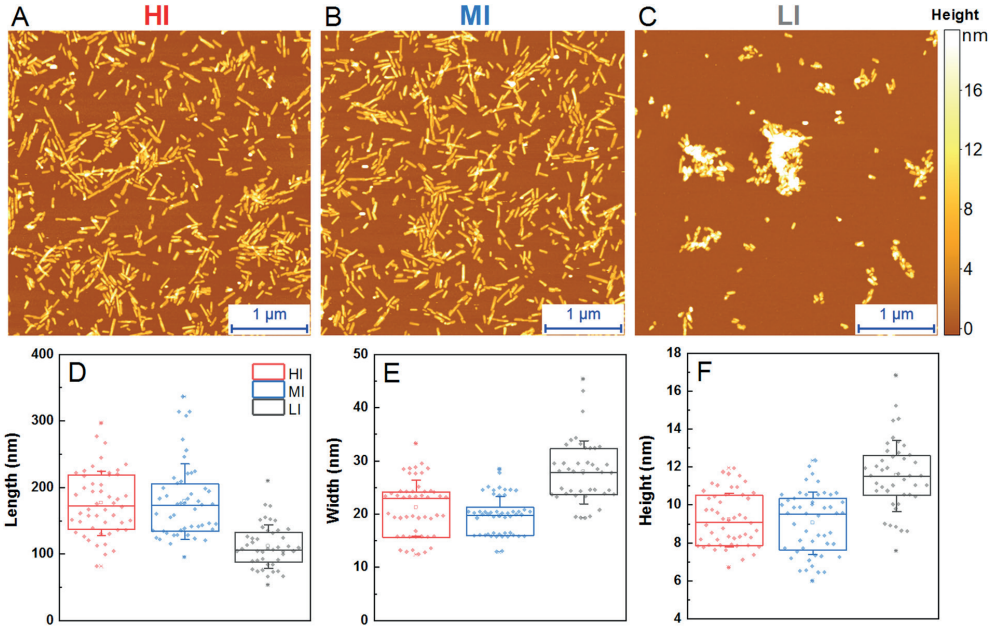

Figure 4. Atomic force microscopy of fibril samples and aggregate size distribution. Images of high intensity (**A**), medium intensity (**B**) and low intensity (**C**) fibrils. Length (**D**), width (**E**) and height (**F**) of single fibrils, where the box plot indicates the interquartile range, error bars are for one standard deviation.

reversal of the relative intensities of the two spectral components around 1621 and 1628–29 cm^{-1} in the second derivative spectra (Fig. 3C) of LI vs. HI fibrils confirms the difference between these aggregates in the level of secondary structure.

Fibril morphology. The fibrils from each sample were examined by atomic force microscopy to determine if there are any visible structural differences between them. The AFM images show small and completely dispersed fibril fragments in the case of HI (Fig. 4A) and MI (Fig. 4B) samples. Conversely, the LI (Fig. 4C) sample contains much larger aggregate clusters. Examining the length (Fig. 4D), width (Fig. 4E) and height (Fig. 4F) of single fibrils reveals that the LI aggregates are significantly shorter (~100 nm), wider (~27 nm) and higher (~11 nm), when compared to both MI and HI fibrils, which have a length of ~175 nm, width of ~20 nm and height of ~9 nm.

The surface of all samples appears to be relatively even, with no visible periodicity or twistedness (Fig. S4). Sample sonication has an insignificant effect on the dispersion of these aggregates, which indicates that the LI fibrils are highly prone to self-association and quickly reassemble into large clusters (Fig. S5).

Discussion

Comparison of all results leaves no doubts that LI and HI samples represent distinct amyloid fibril conformations. Besides almost a double difference in ThT fluorescence intensity (Fig. 1A), which gets even bigger in reseeded samples (Fig. 1B), different kinetic profiles of HI and LI fibril self-replication (Fig. 1B,C) were observed (ThT intensity drop at early stages of aggregation when LI fibrils were used as seeds, and no drop in case of HI seeds). Different major minima in FTIR second derivative suggests that two different populations of intra-fibrillar beta-strands are dominant in the structure of HI and LI fibrils (Fig. 3C), similar as were earlier observed in environment-induced polymorphism of amyloid fibrils[46]. Distinct conformations of HI and LI aggregates are also supported by the differences in ThT binding (Fig. 2A,B). Finally, in the AFM images (Fig. 4A–C) we can see that the LI fibrils are shorter, wider and higher than HI fibrils, and they are clumped together, as opposed to the HI sample. Such cluster formation was even observed by a simple visual inspection, with HI samples being almost completely clear and LI having cloudy precipitates. In fact, the HI fibrils were so dispersed, that their centrifugation had to be carried out after dialysis into Milli-Q water, in order to improve the rate of sedimentation. While the LI fibrils quickly associate back into such clusters (Fig. S5) even after sonication, which suggests that LI aggregates have different surface properties than HI aggregates.

The case of MI sample is less clear. Medium ThT fluorescence (Fig. 1A) may arise if MI samples would contain a mixture of LI and HI fibrils. Kinetic profiles of fibril self-replication (Fig. 1B,C) would also fit within the mixture hypothesis. FTIR spectral properties of MI samples are similar to LI (Fig. 3B,C), however there are some minor differences in peak positions and ratios between the minima of second derivative, so the possibility of a mixture cannot be completely excluded, but LI fibrils must be the major component of the mixture. ThT binding data also points to the similarities between LI an MI fibrils (Fig. 2A,B), but this experiment is not very precise, so we cannot completely reject the possibility of a mixture with the amount of LI aggregates several times higher than HI. But the AFM data shows opposite results (Fig. 4A–C). The appearance, length, width and height of MI fibrils are different from LI fibrils (Fig. 4D–F) but are very similar to HI fibrils. It means that the idea of the MI sample as a mixture of HI an LI aggregates may not be accurate. An alternative hypothesis would claim MI as an independent conformation of amyloid aggregates, different from both LI and HI conformations. In order to clear up the confusion regarding the MI sample, two additional aggregation experiments were carried out, using prion proteins from different purification batches (Fig. S6). In both cases, the difference between LI and HI was quite obvious in both the AFM (Fig. S7) and FTIR (Fig. S8) data, however, in one case, the MI sample was similar to LI and in another – to HI. This means that the intermediate samples are not composed of a different fibril conformation and are likely mixtures with varying degrees of LI and HI.

One can think of how different aggregate conformations may form under the same experimental conditions. According to the nucleated polymerization model, fibril formation starts from nucleation. To form a nucleus, a group of soluble protein molecules must get together and misfold into an amyloid structure. Once the nucleus is formed, it can rapidly grow into fibrils by capturing and refolding protein molecules from the solution. The number of fibrils can grow either via formation of new nuclei, or via fragmentation of the existing fibrils. Amyloid nucleation is a stochastic process[47], so if the protein can misfold into several different amyloid conformations, then it is probable that the structure of the first nucleus formed in one tube will be different from one in another tube. Fibril elongation rate is much higher than the nucleation rate, so once the first nucleus is formed, it can grow into a long fibril and, due to vigorous shaking, get fragmented into many short fibrils before the second nucleus is formed. In case of such scenario, once all protein in the tube gets aggregated, the majority of amyloid fibrils will have the same conformation as the first nucleus, and the stochastic nature of nucleation can be the reason for polymorphism of amyloid fibrils formed under identical conditions.

Conclusions

Our findings confirm that prion protein can misfold into at least two distinct amyloid conformations even under identical conditions and can be quickly distinguished by comparing ThT fluorescence emission intensities. Such stochastic polymorphism of amyloid fibrils may be the reason for low reproducibility in amyloid research. A quality-control of each sample by the comparison of ThT intensity could help to improve it.

Data availability

The datasets generated during and/or analysed during the current study are available from the corresponding author on reasonable request.

Received: 2 January 2020; Accepted: 28 February 2020;
Published online: 12 March 2020

References

1. González, L. *et al*. Pathogenesis of natural goat scrapie: modulation by host PRNP genotype and effect of co-existent conditions. *Vet. Res.* **41**, 48 (2010).
2. Prusiner, S. B. Prions. *Proc. Natl. Acad. Sci.* **95**, 13363–13383 (1998).
3. Collinge, J. Molecular neurology of prion disease. *J. Neurol. Neurosurg. Psychiatry* **76**, 906–919 (2005).
4. Norrby, E. Prions and protein-folding diseases. *J. Intern. Med.* **270**, 1–14 (2011).
5. Samson, A. O. & Levitt, M. Normal modes of prion proteins: from native to infectious particle. *Biochemistry* **50**, 2243–2248 (2011).
6. Chamachi, N. G. & Chakrabarty, S. Temperature-induced misfolding in prion protein: evidence of multiple partially disordered states stabilized by non-native hydrogen bonds. *Biochemistry* **56**, 833–844 (2017).
7. Mathias Jucker, L. C. W. Self-propagation of pathogenic aggregates in neurodegenerative diseases. *Nature* **501**, 45–51 (2013).

8. Stohr, J. *et al*. Mechanisms of prion protein assembly into amyloid. *Proc. Natl. Acad. Sci.* **105**, 2409–2414 (2008).
9. Verma, M., Taneja, V. & Vats, A. Toxic species in amyloid disorders: oligomers or mature fibrils. *Ann. Indian Acad. Neurol.* **18**, 138 (2015).
10. Fitzpatrick, A. W. P. *et al*. Atomic structure and hierarchical assembly of a cross-β amyloid fibril. *Proc. Natl. Acad. Sci.* **110**, 5468–5473 (2013).
11. Kitamoto, T. *et al*. Amyloid plaques in Creutzfeldt-Jakob disease stain with prion protein antibodies. *Ann. Neurol.* **20**, 204–208 (1986).
12. Canale, C., Oropesa-Nuñez, R., Diaspro, A. & Dante, S. Amyloid and membrane complexity: the toxic interplay revealed by AFM. *Semin. Cell. Dev. Biol.* **73**, 82–94 (2018).
13. Kim, J. *et al*. Rapid cytotoxicity screening platform for amyloid inhibitors using a membrane-potential sensitive fluorescent probe. *Anal. Chem.* **85**, 185–192 (2013).
14. Sorrentino, S. *et al*. Calcium binding promotes prion protein fragment 90–231 conformational change toward a membrane destabilizing and cytotoxic structure. *PLoS One* **7**, e38314 (2012).
15. Simoneau, S. *et al*. *In vitro* and *in vivo* neurotoxicity of prion protein oligomers. *PLoS Pathog.* **3**, e125 (2007).
16. Race, B., Jeffrey, M., McGovern, G., Dorward, D. & Chesebro, B. Ultrastructure and pathology of prion protein amyloid accumulation and cellular damage in extraneural tissues of scrapie-infected transgenic mice expressing anchorless prion protein. *Prion* **11**, 234–248 (2017).
17. Armiento, A. *et al*. The mechanism of monomer transfer between two structurally distinct PrP oligomers. *PLoS One* **12**, e0180538 (2017).
18. Le Dur, A. *et al*. Divergent prion strain evolution driven by PrPC expression level in transgenic mice. *Nat. Commun.* **8**, 14170 (2017).
19. Tixador, P. *et al*. The physical relationship between infectivity and prion protein aggregates is strain-dependent. *PLoS Pathog.* **6**, e1000859 (2010).
20. Petkova, A. T. *et al*. Self-propagating, molecular-level polymorphism in Alzheimer's β-amyloid fibrils. *Science* **307**, 262–265 (2005).
21. Pedersen, J. S. *et al*. The changing face of glucagon fibrillation: structural polymorphism and conformational imprinting. *J. Mol. Biol.* **355**, 501–523 (2006).
22. Sneideris, T. *et al*. pH-driven polymorphism of insulin amyloid-like fibrils. *PLoS One* **10**, e0136602 (2015).
23. Cobb, N. J., Apostol, M. I., Chen, S., Smirnovas, V. & Surewicz, W. K. Conformational stability of mammalian prion protein amyloid fibrils is dictated by a packing polymorphism within the core region. *J. Biol. Chem.* **289**, 2643–2650 (2014).
24. Sneideris, T., Milto, K. & Smirnovas, V. Polymorphism of amyloid-like fibrils can be defined by the concentration of seeds. *PeerJ* **3**, e1207 (2015).
25. Jain, S. & Udgaonkar, J. B. Salt-induced modulation of the pathway of amyloid fibril formation by the mouse prion protein. *Biochemistry* **49**, 7615–7624 (2010).
26. Savistchenko, J., Arellano-Anaya, Z. E., Andréoletti, O. & Vilette, D. Mammalian prions. *Prion* **5**, 84–87 (2011).
27. Thackray, A. M., Hopkins, L., Lockey, R., Spiropoulos, J. & Bujdoso, R. Emergence of multiple prion strains from single isolates of ovine scrapie. *J. Gen. Virol.* **92**, 1482–1491 (2011).
28. Pirisinu, L. *et al*. A new method for the characterization of strain-specific conformational stability of protease-sensitive and protease-resistant PrPSc. *PLoS One* **5**, e12723 (2010).
29. Diaz-Avalos, R., King, C.-Y., Wall, J., Simon, M. & Caspar, D. L. D. Strain-specific morphologies of yeast prion amyloid fibrils. *Proc. Natl. Acad. Sci.* **102**, 10165–10170 (2005).
30. Fändrich, M., Meinhardt, J. & Grigorieff, N. Structural polymorphism of Alzheimer Aβ and other amyloid fibrils. *Prion* **3**, 89–93 (2009).
31. Song, Y., Li, P., Liu, L., Bortolini, C. & Dong, M. Nanostructural differentiation and toxicity of amyloid-β25-35 aggregates ensue from distinct secondary conformation. *Sci. Rep.* **8**, 765 (2018).
32. Zampieri, M., Legname, G. & Altafini, C. Investigating the conformational stability of prion strains through a kinetic replication model. *PLoS Comput. Biol.* **5**, e1000420 (2009).
33. Choi, Y. P., Peden, A. H., Groner, A., Ironside, J. W. & Head, M. W. Distinct stability states of disease-associated human prion protein identified by conformation-dependent immunoassay. *J. Virol.* **84**, 12030–12038 (2010).
34. Nilsson, K. P. R., Joshi-Barr, S., Winson, O. & Sigurdson, C. J. Prion strain interactions are highly selective. *J. Neurosci.* **30**, 12094–12102 (2010).
35. Morales, R. *et al*. Strain-dependent profile of misfolded prion protein aggregates. *Sci. Rep.* **6**, 20526 (2016).
36. Magnusson, K. *et al*. Multimodal fluorescence microscopy of prion strain specific PrP deposits stained by thiophene-based amyloid ligands. *Prion* **8**, 319–329 (2014).
37. Wenborn, A. *et al*. A novel and rapid method for obtaining high titre intact prion strains from mammalian brain. *Sci. Rep.* **5**, 10062 (2015).
38. Taguchi, Y., Otaki, H. & Nishida, N. Mechanisms of strain diversity of disease-associated in-register parallel β-sheet amyloids and implications about prion strains. *Viruses* **11**, 110 (2019).
39. Xue, C., Lin, T. Y., Chang, D. & Guo, Z. Thioflavin T as an amyloid dye: fibril quantification, optimal concentration and effect on aggregation. *R. Soc. Open Sci.* **4**, 160696 (2017).
40. Mao, X. *et al*. Binding modes of thioflavin T molecules to prion peptide assemblies identified by using scanning tunneling microscopy. *ACS Chem. Neurosci.* **2**, 281–287 (2011).
41. Ivancic, V. A., Ekanayake, O. & Lazo, N. D. Binding modes of thioflavin T on the surface of amyloid fibrils studied by NMR. *Chem. Phys. Chem.* **17**, 2461–2464 (2016).
42. Krebs, M. R. H., Bromley, E. H. C. & Donald, A. M. The binding of thioflavin-T to amyloid fibrils: localisation and implications. *J. Struct. Biol.* **149**, 30–37 (2005).
43. Milto, K., Michailova, K. & Smirnovas, V. Elongation of mouse prion protein amyloid-like fibrils: effect of temperature and denaturant concentration. *PLoS One* **9**, e94469 (2014).
44. Sneideris, T. *et al*. The environment is a key factor in determining the anti-amyloid efficacy of EGCG. *Biomolecules* **9**, 1–17 (2019).
45. Moran, S. D. & Zanni, M. T. How to get insight into amyloid structure and formation from infrared spectroscopy. *J. Phys. Chem. Lett.* **5**, 1984–1993 (2014).
46. Dzwolak, W. *et al*. Template-controlled conformational patterns of insulin fibrillar self-assembly reflect history of solvation of the amyloid nuclei. *Phys. Chem. Chem. Phys.* **7**, 1349 (2005).
47. Foderà, V., Librizzi, F., Groenning, M., van de Weert, M. & Leone, M. Secondary nucleation and accessible surface in insulin amyloid fibril formation. *J. Phys. Chem. B* **112**, 3853–3858 (2008).

Acknowledgements

This research was funded by the grant no. TAP LLT-1/2017 from the Research Council of Lithuania.

Author contributions

M.Z., T.S. and V.S. designed the studies. M.Z. and T.S. undertook the experimental work. M.Z., T.S. and V.S. analyzed the data and prepared the manuscript.

Competing interests
The authors declare no competing interests.

Additional information
Supplementary information is available for this paper at https://doi.org/10.1038/s41598-020-61663-2.

Correspondence and requests for materials should be addressed to V.S.

Reprints and permissions information is available at www.nature.com/reprints.

Publisher's note Springer Nature remains neutral with regard to jurisdictional claims in published maps and institutional affiliations.

International Journal of
Molecular Sciences

MDPI

Article

Temperature-Dependent Structural Variability of Prion Protein Amyloid Fibrils

Mantas Ziaunys, Andrius Sakalauskas, Kamile Mikalauskaite, Ruta Snieckute and Vytautas Smirnovas *

Life Sciences Center, Institute of Biotechnology, Vilnius University, LT-10257 Vilnius, Lithuania; mantas.ziaunys@gmc.vu.lt (M.Z.); andrius.sakalauskas@gmc.vu.lt (A.S.); kamile.mikalauskaite@gmc.vu.lt (K.M.); ruta.snieckute@chgf.stud.vu.lt (R.S.)
* Correspondence: vytautas.smirnovas@bti.vu.lt

Abstract: Prion protein aggregation into amyloid fibrils is associated with the onset and progression of prion diseases—a group of neurodegenerative amyloidoses. The process of such aggregate formation is still not fully understood, especially regarding their polymorphism, an event where the same type of protein forms multiple, conformationally and morphologically distinct structures. Considering that such structural variations can greatly complicate the search for potential antiamyloid compounds, either by having specific propagation properties or stability, it is important to better understand this aggregation event. We have recently reported the ability of prion protein fibrils to obtain at least two distinct conformations under identical conditions, which raised the question if this occurrence is tied to only certain environmental conditions. In this work, we examined a large sample size of prion protein aggregation reactions under a range of temperatures and analyzed the resulting fibril dye-binding, secondary structure and morphological properties. We show that all temperature conditions lead to the formation of more than one fibril type and that this variability may depend on the state of the initial prion protein molecules.

Keywords: amyloids; prion proteins; protein aggregation; fibril structure

Citation: Ziaunys, M.; Sakalauskas, A.; Mikalauskaite, K.; Snieckute, R.; Smirnovas, V. Temperature-Dependent Structural Variability of Prion Protein Amyloid Fibrils. *Int. J. Mol. Sci.* **2021**, *22*, 5075. https://doi.org/10.3390/ijms22105075

Academic Editor: Vladimir N. Uversky

Received: 20 April 2021
Accepted: 9 May 2021
Published: 11 May 2021

1. Introduction

Amyloidogenic protein aggregation into insoluble, beta-sheet rich fibrils is linked with the onset of several neurodegenerative disorders, such as Alzheimer's, Parkinson's or prion diseases [1,2]. The way these structures form and propagate is still not fully understood, as evidence for new aggregation mechanisms or fibril structural features [3–5] keeps appearing on a regular basis. This lack of crucial information is likely one of the factors that has led to countless failed clinical trials [6] and to only a handful of effective, disease-modifying drugs [7]. Considering that amyloid diseases affect millions of people worldwide and the number is expected to continuously increase [8,9], it is of vital importance to gain a better understanding of the intricacies of amyloid aggregation.

One of the more interesting aspects of amyloid aggregation is the ability of a single type of protein to associate into multiple conformationally-distinct fibrils [10]. Such a phenomenon was observed with prion proteins, both in vivo and in vitro [11–14] and later–with other amyloidogenic proteins, such as amyloid beta [15], alpha-synuclein [16,17] and insulin [18,19]. These distinct conformation fibrils possess specific replication rates [20,21], morphologies [22], secondary structures [16,23] and stabilities [24]. In addition, some of these parameters are either codependent or change even after fibrils have been formed. It has been shown using computational methods that there is a correlation between the rate of self-replication and fibril symmetry, and stability [25,26]. It was also observed that oligomeric or protofibrillar intermediate aggregates gain mechanical stability when converting to fully formed fibrils [27].

Such a variation in their properties is likely one of the main aspects why potential drug candidates appear effective under a certain set of conditions, while being completely

inefficient in others [28]. It has been observed in multiple studies that the conformation of resulting fibrils depends highly on the environmental conditions, under which the protein is aggregated [29,30]. These conditions include temperature [31], agitation [32], pH [18], ionic strength [33], denaturant concentration [14] and protein concentration [34]. In our recent study, we have also shown that prion proteins are capable of forming two distinct conformation fibrils under identical conditions [23]. This hints at a possibility that primary nucleation, a process during which the initial aggregation centers from, may randomly generate distinct nuclei, only some of which can further propagate under the given environmental conditions.

Determining conformational differences between amyloid fibrils is typically done by evaluating their morphological features [35], such as aggregate height, width, length and periodicity patterns, and by acquiring information about their secondary structure [36]. The methods used for this, namely atomic force microscopy (AFM) [35] and Fourier-transform infrared spectroscopy (FTIR) [37], are difficult to apply in situations, where a large number of samples have to be differentiated. In recent years, both high-throughput screening platforms [38] and computer-aided molecule design systems [39] have advanced enough to identify neurodegenerative-disease related protein–ligand interactions and possible mechanisms of fibril formation. However, since protein aggregation is still not fully understood, such methods are not ideal for determining the highly complex structure of fully formed aggregates. As an alternative, the selective and conformation-specific binding of a fluorescent probe, thioflavin-T (ThT) [23,40,41], may be used to detect different types of aggregates. Such a method was applied in our aforementioned study with prion proteins and it was efficient at identifying different types of insulin fibrils as well [40]. Applying this type of initial screening would allow to sort out fibril samples with distinct conformations in a much larger scale assay.

Prion protein aggregation experiments are conducted under a variety of conditions in vitro, ranging from ambient temperature [42] to well-above physiological temperatures [43]. In order to determine if this environmental factor has an effect on prion protein fibril variability, we tracked the aggregation of a mouse prion protein under a range of different temperatures, using a large identical sample size to evaluate their seemingly random, conformational variations. To achieve complete fibrillization in a reasonable time frame, vigorous, fragmentation-inducing agitation was also used for every temperature condition. A ThT-assay was then employed as an initial means of sorting the distinct fibril types, which were then examined using FTIR and AFM.

2. Results

A large sample size of mouse prion protein fragment (89–230) was aggregated under a range of temperatures (from 25 to 65 °C) with all other conditions, such as buffer solution, protein concentration and volume remaining identical. Plotting the lag time (t_{lag}) dependence on aggregation temperature (Figure 1A) revealed a discontinuity in the linear trend at 45 °C. This is caused by the protein transitioning from being in mostly folded states (at temperatures below 45 °C) and mostly unfolded (above 45 °C) [43]. This is further supported by visualizing the data in an Arrhenius plot (Figure 1B), where the activation of nuclei formation was (78.7 ± 7.0) kJ/mol at low and (30.0 ± 5.0) kJ/mol at high temperatures. This transition temperature is in line with previously reported data, [43] where a shift in activation energy was also observed.

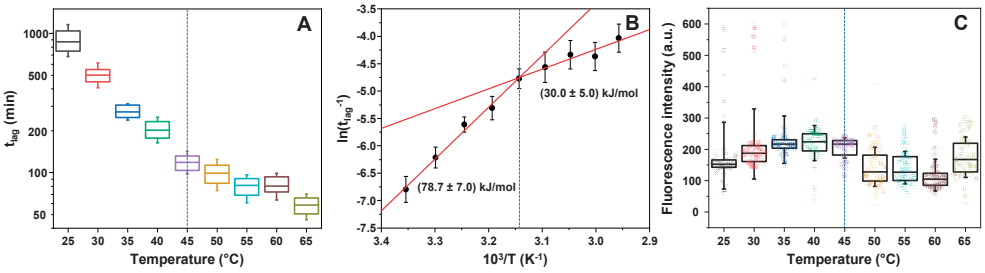

Figure 1. Prion protein aggregation t_{lag} and fibril-bound thioflavin-T (ThT) fluorescence intensity dependence on the aggregation reaction temperature. t_{lag} dependence on the reaction temperature (**A**) and the same data displayed in an Arrhenius plot (**B**), with reaction activation energies shown below linear fit curves. Sonicated and diluted fibril-ThT sample fluorescence intensity distribution (at 25 °C) dependence on the reaction temperature (**C**). Each sample set contained 90 data points, obtained by tracking the aggregation and fluorescence intensity of 90 prion protein aggregation reactions simultaneously at a set temperature. In A and C graphs, box plots indicate the interquartile range and error bars are for one standard deviation. Graph B points are the average $\ln(t_{lag}{}^{-1})$ values calculated from the t_{lag} values and error bars are one standard deviation. Dashed blue lines correspond to the temperature at which a non-linear change in t_{lag} and ThT fluorescence intensity is observed. Red lines (**B**) are linear fits of 25–45 °C and 45–65 °C temperature data points. Aggregation t_{lag} box plots (**A**) and their respective sample fluorescence intensities (**C**) are colour-coded.

When examining the fluorescence intensity of fibril-bound ThT molecules (when all samples were cooled down to 25 °C; Figure 1C), two interesting aspects are observed. First, there was a significantly larger amount of high fluorescence intensity samples (300–600 a.u.) when the protein was aggregated at temperatures below 45 °C, when compared to higher temperatures, where only a single high intensity sample was seen. Secondly, there was also a discontinuity of fluorescence intensity values occurring at 45 °C. The one-way analysis of variance (ANOVA) statistical analysis of the data (n = 90 for each case) using a Bonferroni means comparison (significance level–0.01) revealed that there was a difference between the 35–45 °C sample and 50–60 °C sample fluorescence intensity distributions, where 35–45 °C fibril-bound ThT possesses a considerably larger average signal intensity. Interestingly, there was no significant difference between the lowest and highest temperature sample sets (significance level–0.01), apart from the 25 °C samples having a greater standard deviation due to the existence of a few high fluorescence intensity samples. Both of these aspects could be explained by a larger fibril concentration or the formation of superstructural fibril assemblies, however, that is not the case. Each sample contained an identical concentration of prion protein and their aggregation kinetic curves reached a plateau, indicating a finished fibrillization process. Afterwards, each sample was diluted with the reaction buffer (containing 100 μM ThT) and sonicated, which removes the possibility of large aggregate structures entrapping the dye molecules [44] or certain samples having hydroxylated ThT [45]. This leaves the option of different samples containing distinct fibrils, which have conformation-specific dye-binding.

In order to separate and identify distinct fibril samples, an excitation–emission matrix (EEM) of each sample's fibril-bound ThT was scanned. The fluorescence emission intensity "centers of mass" were then compared for all temperature conditions (Figure 2). We can see that in all cases, there was a cluster of these positions with varying size and dispersion. In the case of samples from 25 to 45 °C (Figure 2A–E), the clusters were more compact than their higher temperature counterparts (Figure 2F–I), with the highest dispersion observed in the 50 °C sample set (Figure 2F).

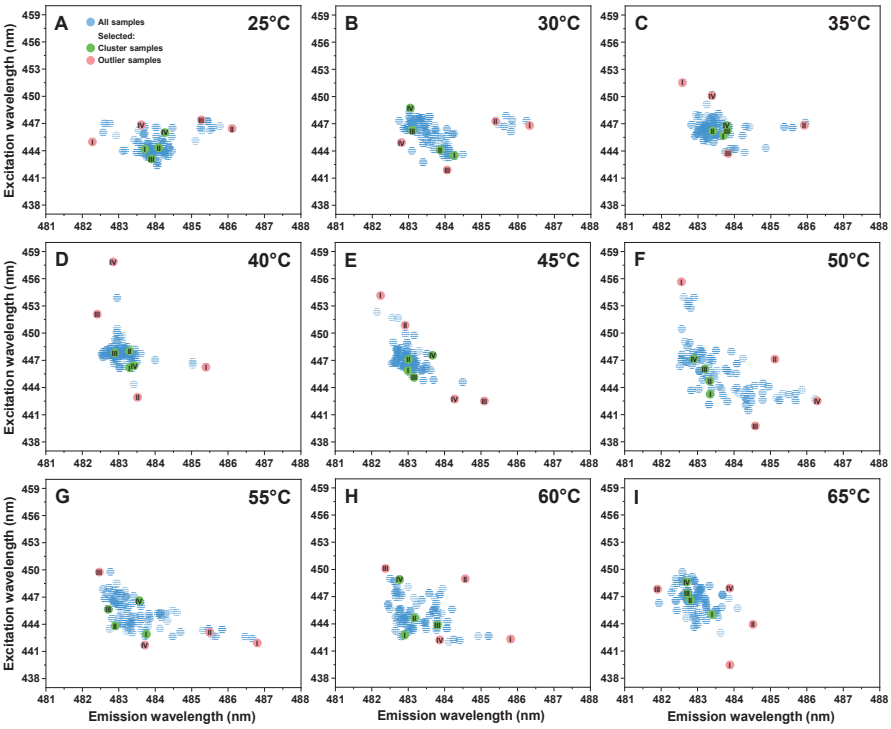

Figure 2. Prion protein fibril-bound thioflavin-T (ThT) fluorescence excitation-emission matrix "center of mass" distribution. Excitation-emission matrix (EEM) "centers of mass" were calculated for samples prepared under 25 °C (**A**), 30 °C (**B**), 35 °C (**C**), 40 °C (**D**), 45 °C (**E**), 50 °C (**F**), 55 °C (**G**), 60 °C (**H**) and 65 °C (**I**) temperature conditions as described in the Materials and Methods section. All samples are marked in blue, while samples selected for further analysis from the main cluster and outliers are marked green and red with Roman numerals respectively. Each EEM set was obtained by scanning 90 individual prion protein fibril samples after they were diluted, sonicated and set to 25 °C.

An important thing to notice is that each sample set contained several points, which did not belong to the main cluster. These outliers had quite extreme excitation/emission wavelength shifts when compared to their respective cluster, and very high or low fluorescence intensity values. In some of the sets, there were samples with 10 nm differences in their excitation wavelength (Figure 2D,G). Since there were multiple outliers in each case, and different fluorescence intensity samples within the main cluster, four most distinct EEM outliers (Figure 2 (red), Appendix A Table A1) and four main cluster samples from lowest to highest fluorescence (Figure 2 (green), Appendix A Table A1) were chosen for further structural examination. Each sample was then replicated to both increase the mass of available aggregates, and to test their self-replication propensity. In general, no significant variations in the rate of replication were observed (Appendix A, Figure A1A–I), however, most samples retained their conformation-specific fluorescence emission intensities after aggregation, especially visible in the case of lower temperature samples (Appendix A, Figure A1).

The replicated outlier (Figure 2 (red), Appendix A, Table A1) and cluster (Figure 2 (green), Appendix A, Table A1) samples were then examined using Fourier-transform infrared spectroscopy. In the case of the different fluorescence intensity cluster samples, three distinct secondary structures were observed. The second derivative FTIR spectra of aggregates prepared at low temperature conditions (Figure 3A,B, blue lines) display two

minima at 1628 cm^{-1} and 1615 cm^{-1}. The band at 1615 cm^{-1} is associated with stronger hydrogen bonding within fibril beta-sheets, while the band at 1628 cm^{-1} is associated with the presence of weaker hydrogen bonds [46]. The ratio between both of these positions is not identical for all samples, with the lower fluorescence intensity sample having a less expressed minima at 1628 cm^{-1}, suggesting that stronger hydrogen bonds within the fibril result in less bound-ThT or a lower fluorescence quantum yield.

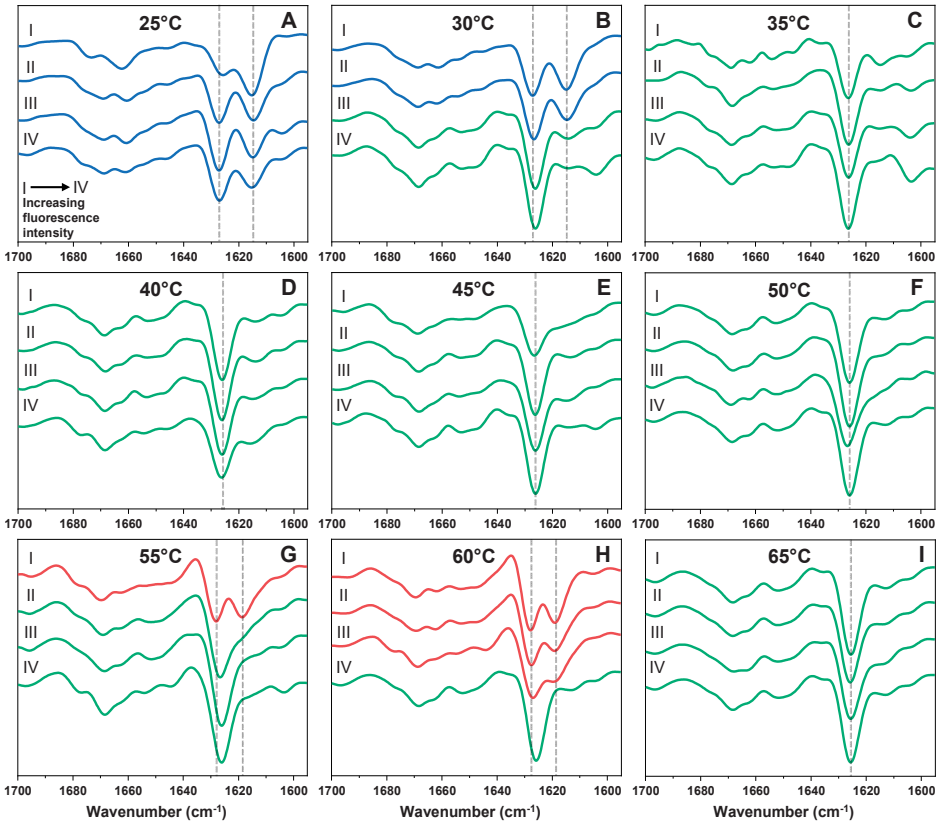

Figure 3. Second derivatives of Fourier-transform infrared spectra (FTIR) of prion protein fibril samples from their respective excitation-emission matrix (EEM) cluster. FTIR spectra were acquired for fibrils prepared under 25 °C (**A**), 30 °C (**B**), 35 °C (**C**), 40 °C (**D**), 45 °C (**E**), 50 °C (**F**), 55 °C (**G**), 60 °C (**H**) and 65 °C (**I**) temperature conditions. The roman numerals indicate the sample ThT-fluorescence intensity, with I being the sample with the lowest emission intensity and IV–the largest. Spectra are colour-coded blue, green and red based on their main minima position similarity. Dotted grey lines indicate the main spectra positions, where differences are observed.

The 30–65 °C sample set clusters (Figure 3B–I) contain a second type of fibrils, with the main second derivative FTIR spectrum minima located at 1626 cm^{-1}, which suggests a single dominant type of hydrogen bonding within the fibrils. This aggregate conformation was the most abundant, as it was observed in eight out of the nine cluster sample sets. The third fibril conformation was only observed at higher temperatures, namely 55 °C (Figure 3G) and 60 °C (Figure 3H). Similar to the low temperature fibril conformation, two minima associated with beta-sheet hydrogen bonding are observed, however, unlike in the

case of fibril prepared at low temperature, the second minima were at 1618 cm^{-1}, rather than 1615 cm^{-1}, which indicates a weaker mode of hydrogen bonding.

When the outlier fibril samples (Figure 2 (red), Appendix A, Table A1) were replicated and centrifuged, certain sample aggregate pellets were semitransparent and gel-like. Coincidentally, their FTIR spectra displayed a noticeable band associated with guanidine hydrochloride, despite multiple centrifugation and resuspension steps. Such abnormalities were only observed in the case of fibrils prepared under 25 °C and 30 °C temperatures. One likely explanation for this event is that this type of fibril conformation is capable of trapping some of the denaturant present in solution during aggregation, either in fibril cavities or by associating into this gel-like structure. While this, in itself, indicates a different type of aggregate, in order to acquire comparable FTIR spectra, the samples had to be washed three additional times (the second derivative FTIR spectra of these gel-like samples are marked with a * symbol in Figure 4). Certain low-temperature samples also contain a very small band at 1604 cm^{-1}, which means that they may contain a minor concentration of GuHCl as well.

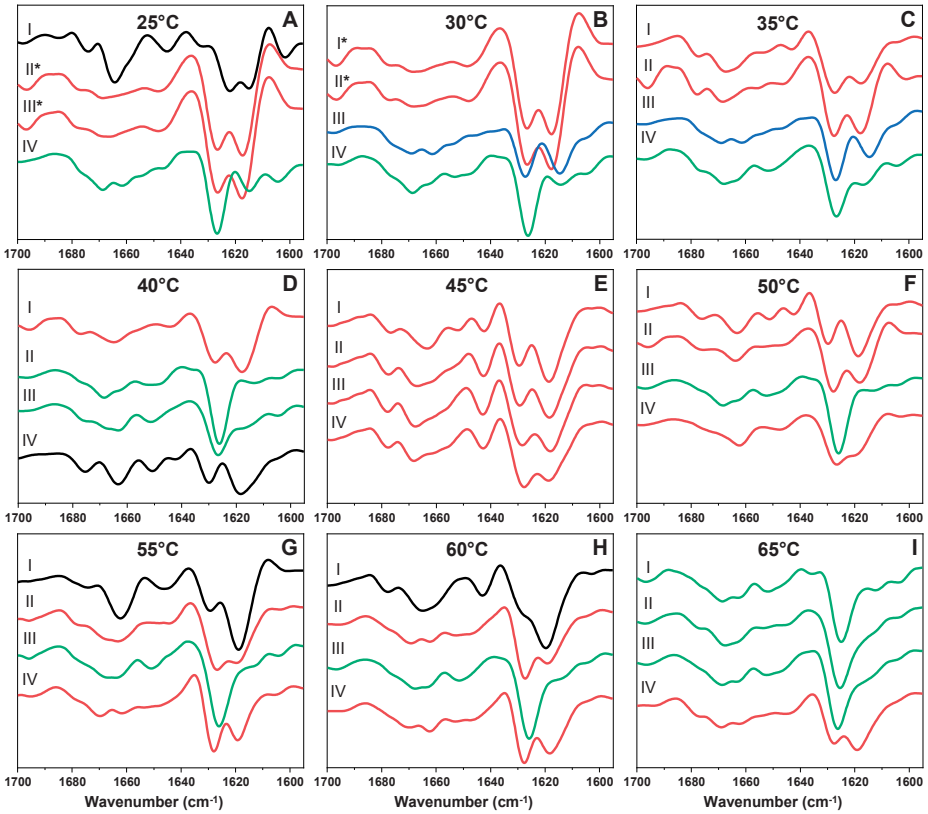

Figure 4. Second derivatives of Fourier-transform infrared spectra (FTIR) of prion protein fibril samples, which were outliers Figure. 25 °C (**A**), 30 °C (**B**), 35 °C (**C**), 40 °C (**D**), 45 °C (**E**), 50 °C (**F**), 55 °C (**G**), 60 °C (**H**) and 65 °C (**I**) temperature conditions. The Roman numerals indicate the outlier sample (list of outlier sample excitation-emission matrix (EEM) positions is located at the Appendix A Table A1). Spectra that share similarities to the main cluster samples are colour-coded accordingly (blue, green and red), while black spectra are unique outliers. The second derivative FTIR spectra of these gel-like samples are marked with a *.

The outlier sample second derivative FTIR spectra (Figure 4) were significantly more diverse than in the case of the main cluster samples. While most spectra shared similar minima positions to the three cluster fibril conformation spectra (Figure 4A–I), color-coded accordingly), the band intensity ratios experienced a considerably larger variation, which suggests the presence of multiple aggregates with distinct secondary structures. This is best seen in the case of 45 °C outliers (Figure 4E), where all spectra minima had similar positions, yet the 1628 cm^{-1} and 1618 cm^{-1} minima ratios were different. There was also a lot less temperature-dependent conformation distribution, as the structure associated with fibrils prepared under high temperatures was observed in the 35 °C outlier sample (Figure 4C), as was the structure associated with fibrils prepared under low temperatures.

Interestingly, there were four outliers that did not resemble any of the three main fibril conformations. The outlier generated at 25 °C (Figure 4A, black line) had a more significant minimum at 1664 cm^{-1}, which is associated with the presence of turn/loop motifs in the fibril structure [46]. It also had two minima at 1622 cm^{-1} and 1615 cm^{-1}, which means that, along with the strong type of hydrogen bonding, there was also a type of bonding that was dissimilar to all other fibrils. The outlier generated at 40 °C (Figure 4D, black line) shares some similarities to the high-temperature conformation, however, it has more minima associated with turn/loop motifs. The outlier generated at 55 °C (Figure 4G, black line) had a minimum at 1664 cm^{-1}, similarly to the 25 °C outlier, however, it has the most intense band at 1618 cm^{-1} with a smaller minimum at 1630 cm^{-1}, which means that the fibril structure had both a large amount of strong hydrogen bonds between beta-sheets, and some weak bonding. The 60 °C outlier (Figure 4H) had similarities to the 55 °C outlier, with both having significant minima at 1664 cm^{-1}, however, the 1630 cm^{-1} position is more of a shoulder, rather than a minimum, which indicates slightly less weak hydrogen bonds (these two samples were regarded as similar outliers). All four samples that had a gel-like appearance (marked with * in Figure 4) share minima positions with the high temperature conformation, however, their FTIR second derivative spectra minima are far more expressed when compared to their high-temperature counterparts, while the turn/loop motif minima are less expressed, suggesting a slightly different secondary structure.

The seven samples, which showed significant variations in their second derivative FTIR spectra, were further examined by atomic force microscopy. The first notable factor was the difference in fibril self-association (Figure 5A–G, Appendix A, Figures A2A–G and A3A–G). The 25 °C Cluster II, 25 °C Outlier I, 25 °C Outlier II, 45 °C Cluster II and 60 °C Cluster I samples contained aggregates that were highly prone towards binding to one another and forming large fibril clumps, while all other samples were more disperse. Despite the vigorous agitation during aggregation, the 25 °C Outlier II, 40 °C Outlier IV and 60 °C Cluster I samples had relatively long fibrils, suggesting a higher structural stability. Due to certain samples forming large superstructural clusters, conducting a statistical analysis was only possible on their height. A one-way ANOVA Bonferroni means comparison of the height data (n = 50, significance level–0.01) revealed that only the 60 °C Cluster I sample had a significantly different height distribution from all other samples, except for the 25 °C Outlier II sample (Figure 5H).

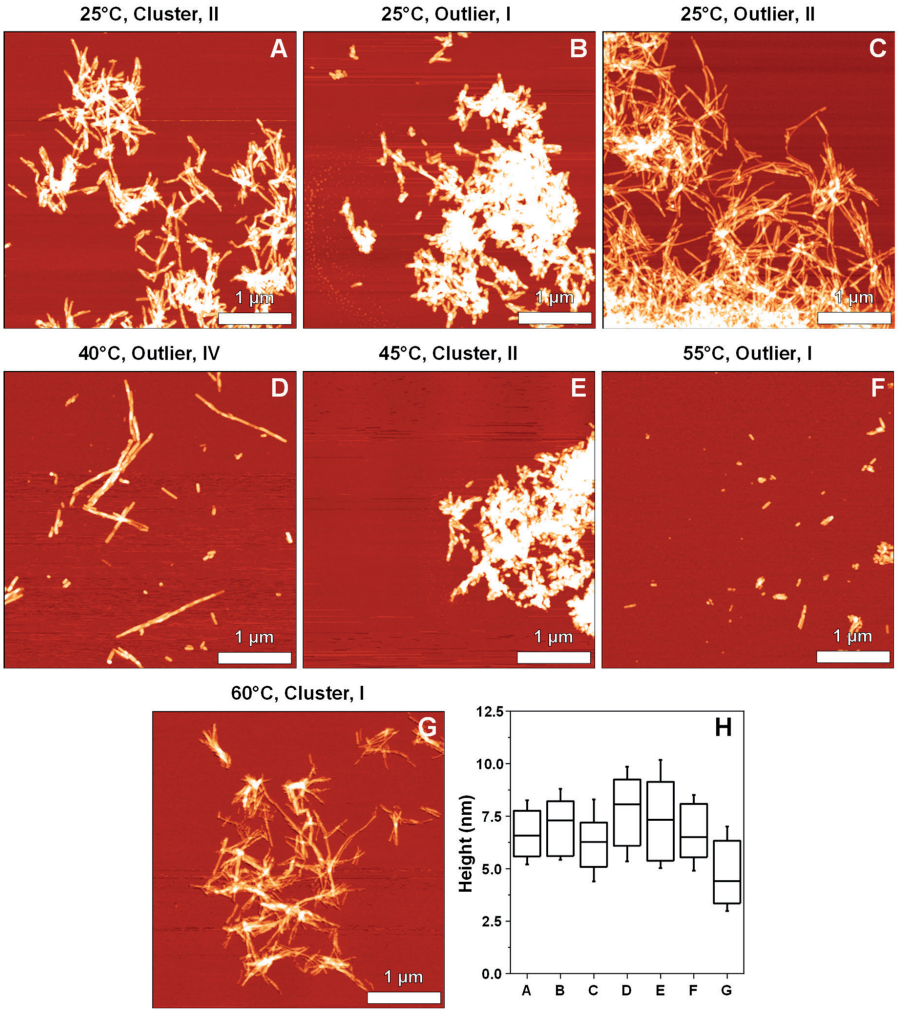

Figure 5. Atomic force microscopy images of prion protein fibrils possessing distinct Fourier-transform infrared (FTIR) spectra ((**A**–**G**), conditions and sample type shown above images). Fibril height (**H**) distribution, where box plots indicate the interquartile range and error bars are one standard deviation (n = 50). Fibril height values were obtained by tracing perpendicular to each fibril's axis (only separate, non-clumped aggregates were examined).

3. Discussion

Considering that a shift in sample secondary structure and the existence of high intensity samples coincide with the temperature, at which the prion protein switches between the folded and unfolded states, suggests that this factor is important in determining the type of fibril conformation. Since the temperatures under which the protein is in its mostly folded state also result in significantly slower aggregation, this provides two possibilities. First, certain nuclei may require a relatively long time to form and such stable aggregation centers simply do not have the required time to assemble during quick fibrillization at higher temperatures. Alternatively, it is also possible that distinct aggregates require a specific semifolded state of the protein to both form and grow, which makes their nu-

cleation/elongation events impossible when most of the protein is in a fully unfolded state. In addition, the tested prion protein (89–230 sequence with His-tag) had 54 polar amino acids (33% of the full sequence), 32 of which were charged, which may contribute to the appearance of distinct hydrogen bonds from polar–polar interactions under certain temperature conditions [47].

While such a temperature-dependent shift in fibril conformations can be expected, the truly peculiar aspect is the variation in aggregate secondary structure and morphology. Not a single sample set in the entire tested temperature range contained a well-defined and homogenous collection of fibrils. Each condition resulted in a variable bound-ThT fluorescence intensity, which was well beyond a standard deviation, different EEM maxima positions, FTIR spectra and even fibril morphologies. The large variation of all these factors suggests that prion proteins can form different conformation fibrils or non-homogenous aggregate mixtures under all tested temperatures and this event may encompass other conditions as well. In essence, this means that the assumption of identical conditions leading to identical samples is not correct for prion proteins and this factor has to be taken into account during assays which involve these proteins.

Another interesting observation is the existence of outliers in every set of samples. These outliers are few in number, suggesting that their aggregation pathways are either very complex or unlikely under the given conditions, however, they possess significantly different characteristics. Some of them are so distinct from other fibrils that they can be identified even with a simple visual inspection. While all other samples resulted in an opaque pellet after centrifugation, one type of outlier fibrils had a transparent, gel-like appearance and had a higher tendency of entrapping the buffer solution within itself. Other outliers seem to possess higher structural stabilities, as seen from AFM images. The differences in ThT binding characteristics also suggest a different surface morphology or charge, especially in the case of high fluorescence intensity samples.

Taking everything into consideration, it appears that the environmental conditions during prion protein aggregation do not have a strict control over the type of fibril that forms, but rather determine the dominant aggregate conformation with a certain level of variability. None of the tested conditions resulted in homogenous samples and this factor has to be taken into account, especially when conducting screenings for antiamyloid compounds, as different fibril types may have distinct responses to certain drug molecules.

4. Materials and Methods

4.1. Prion Protein Aggregation

Mouse recombinant prion protein (89–230) was purified as described previously [43], without the His-tag cleavage step, dialyzed in 10 mM sodium acetate (pH 4.0) for 24 h, concentrated to 3.0 mg/mL and stored at −80 °C prior to use. The protein solution was mixed with 50 mM sodium phosphate (pH 6.0) buffers, containing 0 M or 6 M guanidine hydrochloride (GuHCl) and a ThT stock solution (10 mM) to a final reaction solution, containing 2 M GuHCl, 100 μM ThT and 0.5 mg/mL protein concentration. The reaction solutions were distributed to 96-well half-area non-binding plates (cat. No 3881, Fisher Scientific, USA, Hampton, NH, USA) (100 μL final volume, each well contained a 3 mm bead), which were sealed with a Nunc sealing tape. The samples were incubated at a set temperature (range from 25 to 65 °C), with constant 600 RPM agitation (vigorous, fragmentation-inducing agitation was used to achieve complete fibrillization in a reasonable timeframe). Sample fluorescence was scanned every 5 min, using an excitation wavelength of 440 nm and an emission wavelength of 480 nm. Due to the stochastic nature of aggregation, a small number of samples displayed unusual aggregation kinetics (no detectable signal or signal jumps), which made it impossible to determine their kinetic parameters. Due to this reason, 6 samples were removed from every 96-well plate.

The aggregation lag time (t_{lag}) was calculated by applying a sigmoidal Boltzmann equation fit to the data. An example is provided as Appendix A, Figure A4. All aggregation kinetic data is available as Supplementary Material.

4.2. ThT-Assay

After aggregation had occurred, each sample was taken out of the 96-well plate and each well was additionally washed with the reaction solution (50 mM sodium phosphate buffer (pH 6.0) with 2 M GuHCl and 100 μM ThT) in order to collect all the fibrils. The samples were then further diluted using the reaction buffer solution to a final volume of 500 μL (5-fold dilution). Samples were then sonicated for 30 s using a Bandelin Sonopuls (Berlin, Germany) Ultrasonic homogenizer, equipped with a MS-72 tip (20% power). Each sample's excitation–emission matrix (EEM) was then scanned using a Varian Cary Eclipse (Agilent Technologies, Santa Clara, CA, USA) fluorescence spectrophotometer (excitation wavelength range was from 435 to 465 nm, emission wavelength range—from 460 to 500 nm; both excitation and emission slit widths were 5 nm) at 25 °C. Absorbance spectra were acquired from 300 to 600 nm using a Shimadzu (Kyoto, Japan) UV-1800 spectrophotometer. EEMs were then corrected for the inner filter effect and their signal intensity centre of mass was calculated as described previously [48]. All EEM data is available as Supplementary Material. Sample maximum fluorescence intensity distributions were compared using a one-way ANOVA Bonferroni means comparison with a significance level of 0.01 (Origin 2018 software, OriginLab Corporation, Northampton, MA, USA).

4.3. Fourier-Transform Infrared Spectroscopy

In order to obtain a larger quantity of fibrils for higher quality FTIR spectra, each sample was combined with a non-aggregated protein solution (identical to the one used for initial aggregation) in equal volumes. Final reaction solutions contained 0.25 mg/mL prion protein and 0.05 mg/mL fibrils (assuming a 100% fibrillization and complete aggregate recovery from wells). The lower non-aggregated protein concentration was used to minimize nucleation events and the relatively high concentration of fibrils assured quick self-replication [24]. The reaction solutions were then incubated under conditions, which were identical to their respective aggregate preparation conditions, in order to achieve effective self-replication.

The resulting aggregate solutions were centrifuged for 30 min at 10,000× *g*, after which the supernatant was removed and the fibril pellet was resuspended into 250 μL D_2O (D_2O was supplemented with 100 mM NaCl, which improves fibril sedimentation [49]). This centrifugation and resuspension procedure was repeated 4 times. After the final centrifugation step, the pellet was resuspended into 50 μL D_2O. The FTIR spectra were acquired as described previously [28]. A D_2O spectrum was subtracted from each sample spectrum, after which they were baseline corrected and normalized between 1595 and 1700 cm^{-1}. All data processing was done using GRAMS software and all FTIR data is available as Supplementary Material.

4.4. Atomic Force Microscopy

Fibril samples were agitated by mixing for 30 s in order to reduce aggregate clumping. Afterwards, 20 μL of each sample was deposited on freshly-cleaved mica and left to adsorb for 60 s. Then the mica were rinsed with 2 mL of H_2O and air-dried. AFM images were then acquired as previously described [28]. In short, 1024 pixel × 1024 pixel resolution three-dimensional maps were obtained for each sample using a dimension icon (Bruker, Billerica, MA, USA) atomic force microscope. The images were then flattened using Gwyddion 2.5.5 software. Fibril height was determined from line profiles taken perpendicular to the fibril axes. Fibril height distribution was compared using a one-way ANOVA Bonferroni means comparison with a significance level of 0.01 (Origin 2018 software, OriginLab Corporation, Northampton, MA, USA).

Supplementary Materials: Supplementary Materials can be found at https://www.mdpi.com/article/10.3390/ijms22105075/s1. Supplementary Materials contain the following: raw data of prion protein aggregation, FTIR spectra of prion protein fibrils, excitation-emission matrices of fibril-bound ThT and atomic force microscopy images in TIF format.

Author Contributions: Conceptualization, M.Z., A.S. and V.S.; investigation, M.Z., A.S., K.M. and R.S.; resources, V.S.; writing—original draft preparation, M.Z.; writing—review and editing, M.Z., A.S. and V.S.; supervision, V.S.; funding acquisition, V.S. All authors have read and agreed to the published version of the manuscript.

Funding: This research was funded by the grant no. S-SEN-20-3 from the Research Council of Lithuania.

Institutional Review Board Statement: Not applicable.

Informed Consent Statement: Not applicable.

Data Availability Statement: The data presented in this study are available in Supplementary Material.

Acknowledgments: The authors acknowledge G. Niaura from the Center of Physical Sciences and Technology for the access to FTIR.

Conflicts of Interest: The authors declare no conflict of interest.

Appendix A

Table A1. Excitation-emission matrix maximum position wavelengths (nm) and emission intensities of cluster and outlier samples.

T	Cluster	Excitation	Emission	Intensity	Outliers	Excitation	Emission	Intensity
25 °C	I	444.1	483.7	98.0	I	445.0	482.3	61.1
25 °C	II	444.3	484.1	145.6	II	446.4	486.1	440.6
25 °C	III	443.0	483.9	154.7	III	447.4	485.3	594.5
25 °C	IV	445.9	484.3	200.6	IV	446.8	483.6	187.6
30 °C	I	443.5	484.3	113.7	I	446.8	486.3	587.1
30 °C	II	444.2	483.9	164.8	II	447.2	485.4	590.8
30 °C	III	446.2	483.1	198.6	III	441.8	484.1	144.4
30 °C	IV	448.7	483.1	251.7	IV	444.9	482.8	201.4
35 °C	I	445.7	483.7	180.5	I	451.5	482.6	183.9
35 °C	II	446.2	483.4	210.9	II	446.8	485.9	465.7
35 °C	III	446.3	483.8	220.9	III	443.7	483.8	154.6
35 °C	IV	446.8	483.8	271.4	IV	450.1	483.4	236.4
40 °C	I	446.1	483.3	71.4	I	446.2	485.4	293.8
40 °C	II	448.0	483.3	207.0	II	442.8	483.5	38.8
40 °C	III	447.8	482.9	242.1	III	452.0	482.4	175.3
40 °C	IV	446.3	483.4	274.4	IV	457.8	482.9	141.3
45 °C	I	445.9	483.0	117.1	I	454.1	482.3	132.6
45 °C	II	447.1	483.0	212.0	II	450.8	482.9	142.8
45 °C	III	445.1	483.2	224.2	III	442.4	485.1	142.4
45 °C	IV	447.5	483.7	250.1	IV	442.7	484.3	111.8
50 °C	I	443.2	483.4	49.9	I	455.6	482.6	88.9
50 °C	II	444.6	483.3	107.6	II	447.1	485.1	404.2
50 °C	III	446.0	483.2	175.8	III	439.7	484.6	26.1
50 °C	IV	447.1	482.9	273.2	IV	442.5	486.3	79.3
55 °C	I	442.8	483.8	70.3	I	441.8	486.8	104.7

Table A1. *Cont.*

T	Cluster	Excitation	Emission	Intensity	Outliers	Excitation	Emission	Intensity
55 °C	II	443.7	482.9	112.2	II	443.0	485.5	119.2
55 °C	III	445.6	482.7	170.5	III	449.7	482.5	158.8
55 °C	IV	446.4	483.6	277.7	IV	441.6	483.7	62.8
60 °C	I	442.8	482.9	57.9	I	442.2	485.8	122.7
60 °C	II	444.7	483.2	92.2	II	448.9	484.6	108.3
60 °C	III	443.9	483.8	117.2	III	450.1	482.4	166.6
60 °C	IV	448.9	482.8	295.2	IV	442.1	483.9	106.6
65 °C	I	444.9	483.4	30.0	I	439.4	483.9	29.7
65 °C	II	446.6	482.8	146.3	II	443.9	484.5	112.0
65 °C	III	447.3	482.7	201.9	III	447.8	481.9	219.1
65 °C	IV	448.6	482.7	305.8	IV	447.9	483.9	127.6

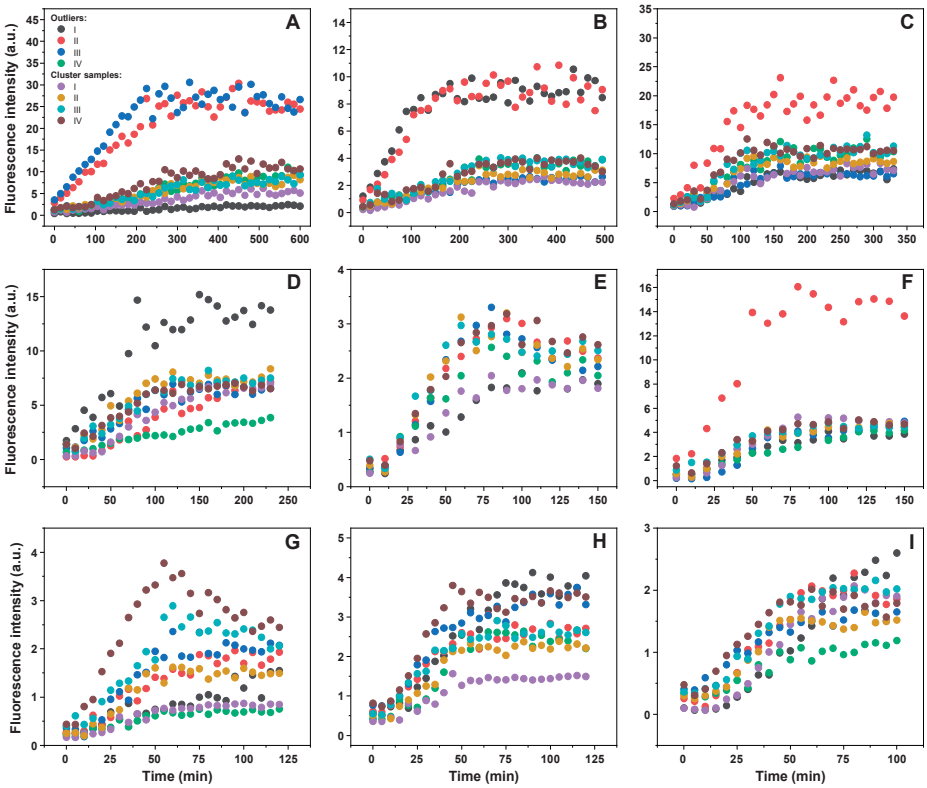

Figure A1. Reseeding aggregation kinetics of the selected cluster and outlier samples under 25 °C (**A**), 30 °C (**B**), 35 °C (**C**), 40 °C (**D**), 45 °C (**E**), 50 °C (**F**), 55 °C (**G**), 60 °C (**H**) and 65 °C (**I**) temperature conditions.

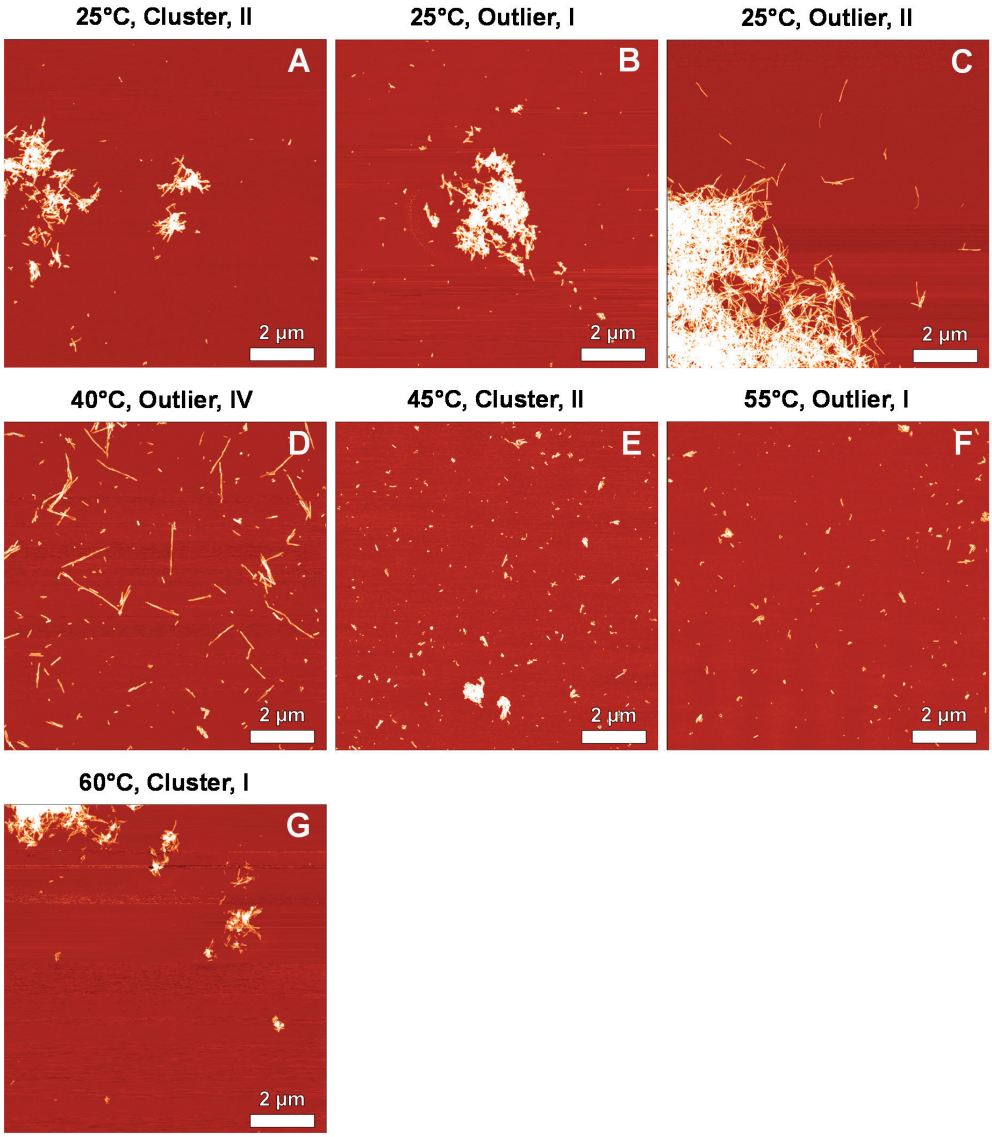

Figure A2. First set of larger scale atomic force microscopy images of prion protein fibrils possessing distinct Fourier-transform infrared (FTIR) spectra ((**A**–**G**), conditions and sample type shown above images).

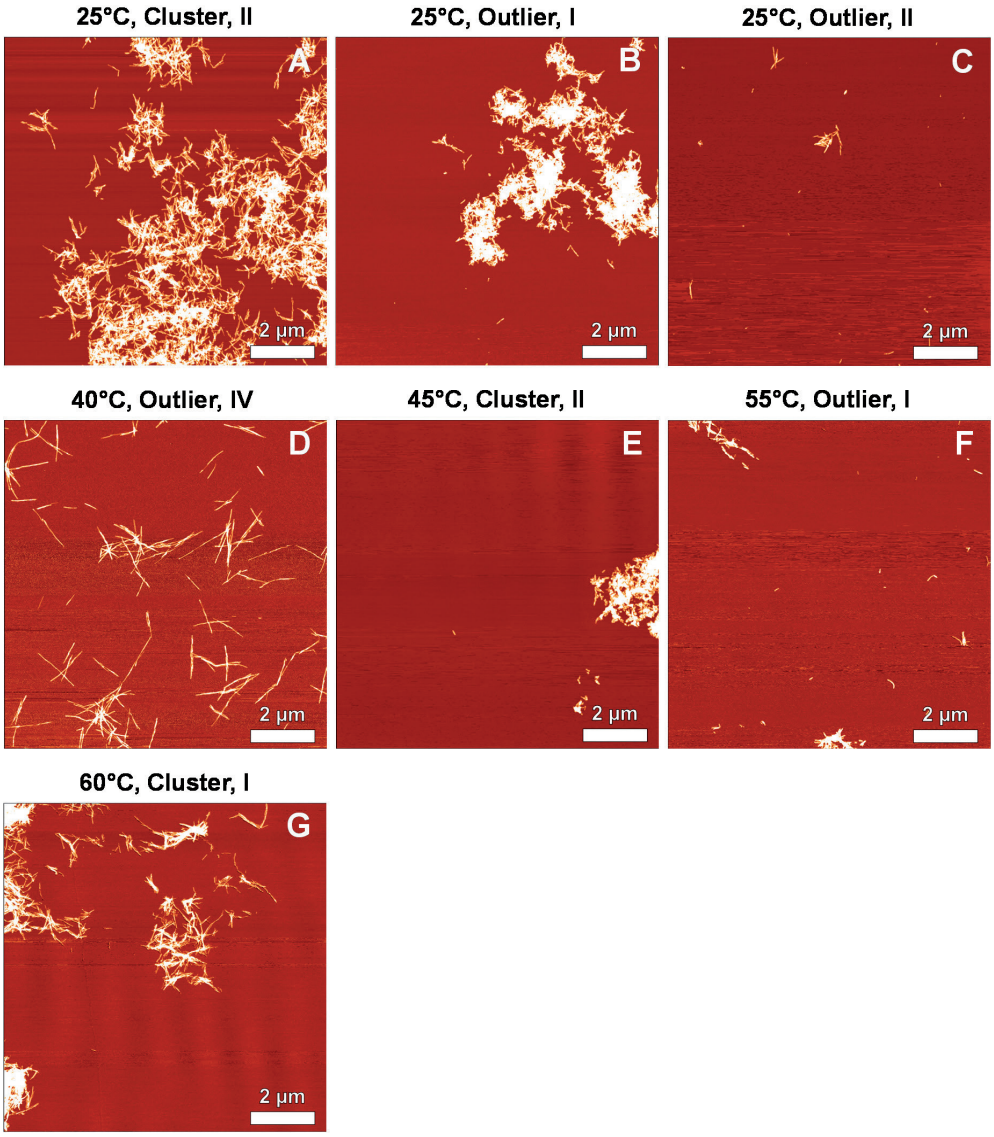

Figure A3. Second set of larger scale atomic force microscopy images of prion protein fibrils possessing distinct Fourier-transform infrared (FTIR) spectra ((**A**–**G**), conditions and sample type shown above images).

$$y = \frac{A_1 - A_2}{1 + e^{(x - x_0)/dx}} + A_2$$

$$t_{lag} = t_{50} - 2dx$$

A_1 – initial value
A_2 – final value
x_0 – center
dx – time constant
t_{lag} – lag time
t_{50} – time when $y = x_0$

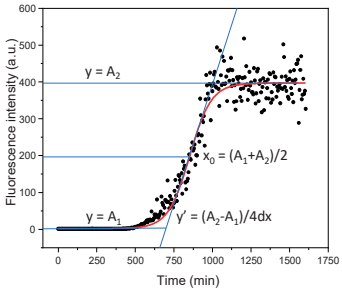

Figure A4. Boltzmann sigmoidal equation fit example and t_{lag} calculation. Data points were obtained by tracking the fluorescence intensity of thioflavin-T during prion protein aggregation. Horizontal blue lines indicate the lowest, intermediate and highest average fluorescence intensity. The red line is a Boltzmann sigmoidal equation fit (with a blue tangent line at the intermediate value of the fit).

References

1. Chiti, F.; Dobson, C.M. Protein Misfolding, Amyloid Formation, and Human Disease: A Summary of Progress Over the Last Decade. *Annu. Rev. Biochem.* **2017**, *86*, 27–68. [CrossRef] [PubMed]
2. Knowles, T.P.J.; Vendruscolo, M.; Dobson, C.M. The amyloid state and its association with protein misfolding diseases. *Nat. Rev. Mol. Cell Biol.* **2014**, *15*, 384–396. [CrossRef] [PubMed]
3. Meisl, G.; Kirkegaard, J.B.; Arosio, P.; Michaels, T.C.T.; Vendruscolo, M.; Dobson, C.M.; Linse, S.; Knowles, T.P.J. Molecular mechanisms of protein aggregation from global fitting of kinetic models. *Nat. Protoc.* **2016**, *11*, 252–272. [CrossRef]
4. Taguchi, Y.; Otaki, H.; Nishida, N. Mechanisms of Strain Diversity of Disease-Associated in-Register Parallel β-Sheet Amyloids and Implications About Prion Strains. *Viruses* **2019**, *11*, 110. [CrossRef]
5. Linse, S. Mechanism of amyloid protein aggregation and the role of inhibitors. *Pure Appl. Chem.* **2019**, *91*, 211–229. [CrossRef]
6. Mehta, D.; Jackson, R.; Paul, G.; Shi, J.; Sabbagh, M. Why do trials for Alzheimer's disease drugs keep failing? A discontinued drug perspective for 2010–2015. *Expert Opin. Investig. Drugs* **2017**, *26*, 735–739. [CrossRef] [PubMed]
7. Cummings, J.; Lee, G.; Ritter, A.; Sabbagh, M.; Zhong, K. Alzheimer's disease drug development pipeline: 2020. *Alzheimer's Dement. Transl. Res. Clin. Interv.* **2020**, *6*, 1–29. [CrossRef]
8. Arthur, K.C.; Calvo, A.; Price, T.R.; Geiger, J.T.; Chiò, A.; Traynor, B.J. Projected increase in amyotrophic lateral sclerosis from 2015 to 2040. *Nat. Commun.* **2016**, *7*, 12408. [CrossRef]
9. Hebert, L.E.; Weuve, J.; Scherr, P.A.; Evans, D.A. Alzheimer disease in the United States (2010-2050) estimated using the 2010 census. *Neurology* **2013**, *80*, 1778–1783. [CrossRef]
10. Tycko, R. Physical and structural basis for polymorphism in amyloid fibrils. *Protein Sci.* **2014**, *23*, 1528–1539. [CrossRef] [PubMed]
11. Collinge, J.; Clarke, A.R. A General Model of Prion Strains and Their Pathogenicity. *Science* **2007**, *318*, 930–936. [CrossRef] [PubMed]
12. Yang, S.; Thackray, A.M.; Hopkins, L.; Monie, T.P.; Burke, D.F.; Bujdoso, R. Polymorphisms at amino acid residues 141 and 154 influence conformational variation in ovine PrP. *Biomed Res. Int.* **2014**, *2014*, 372491. [CrossRef]
13. Fraser, H.; Dickinson, A.G. Scrapie in mice. *J. Comp. Pathol.* **1973**, *83*, 29–40. [CrossRef]
14. Cobb, N.J.; Apostol, M.I.; Chen, S.; Smirnovas, V.; Surewicz, W.K. Conformational Stability of Mammalian Prion Protein Amyloid Fibrils Is Dictated by a Packing Polymorphism within the Core Region. *J. Biol. Chem.* **2014**, *289*, 2643–2650. [CrossRef]
15. Petkova, A.T.; Leapman, R.D.; Guo, Z.; Yau, W.M.; Mattson, M.P.; Tycko, R. Self-propagating, molecular-level polymorphism in Alzheimer's β-amyloid fibrils. *Science* **2005**, *307*, 262–265. [CrossRef]
16. Heise, H.; Hoyer, W.; Becker, S.; Andronesi, O.C.; Riedel, D.; Baldus, M. Molecular-level secondary structure, polymorphism, and dynamics of full-length -synuclein fibrils studied by solid-state NMR. *Proc. Natl. Acad. Sci. USA* **2005**, *102*, 15871–15876. [CrossRef]
17. Bousset, L.; Pieri, L.; Ruiz-Arlandis, G.; Gath, J.; Jensen, P.H.; Habenstein, B.; Madiona, K.; Olieric, V.; Böckmann, A.; Meier, B.H.; et al. Structural and functional characterization of two alpha-synuclein strains. *Nat. Commun.* **2013**, *4*. [CrossRef]
18. Sneideris, T.; Darguzis, D.; Botyriute, A.; Grigaliunas, M.; Winter, R.; Smirnovas, V. pH-Driven Polymorphism of Insulin Amyloid-Like Fibrils. *PLoS ONE* **2015**, *10*, e0136602. [CrossRef]
19. Surmacz-Chwedoruk, W.; Nieznańska, H.; Wójcik, S.; Dzwolak, W. Cross-seeding of fibrils from two types of insulin induces new amyloid strains. *Biochemistry* **2012**, *51*, 9460–9469. [CrossRef]

20. Zampieri, M.; Legname, G.; Altafini, C. Investigating the Conformational Stability of Prion Strains through a Kinetic Replication. *Model. PLoS Comput. Biol.* **2009**, *5*, e1000420. [CrossRef] [PubMed]
21. Tixador, P.; Herzog, L.; Reine, F.; Jaumain, E.; Chapuis, J.; Le Dur, A.; Laude, H.; Béringue, V. The Physical Relationship between Infectivity and Prion Protein Aggregates Is Strain-Dependent. *PLoS Pathog.* **2010**, *6*, e1000859. [CrossRef]
22. Sidhu, A.; Segers-Nolten, I.; Raussens, V.; Claessens, M.M.A.E.; Subramaniam, V. Distinct Mechanisms Determine α-Synuclein Fibril Morphology during Growth and Maturation. *ACS Chem. Neurosci.* **2017**, *8*, 538–547. [CrossRef]
23. Ziaunys, M.; Sneideris, T.; Smirnovas, V. Formation of distinct prion protein amyloid fibrils under identical experimental conditions. *Sci. Rep.* **2020**, *10*, 4572. [CrossRef]
24. Sneideris, T.; Milto, K.; Smirnovas, V. Polymorphism of amyloid-like fibrils can be defined by the concentration of seeds. *PeerJ* **2015**, *3*, e1207. [CrossRef] [PubMed]
25. Poma, A.B.; Chwastyk, M.; Cieplak, M. Elastic moduli of biological fibers in a coarse-grained model: Crystalline cellulose and β-amyloids. *Phys. Chem. Chem. Phys.* **2017**, *19*, 28195–28206. [CrossRef] [PubMed]
26. Poma, A.B.; Guzman, H.V.; Li, M.S.; Theodorakis, P.E. Mechanical and thermodynamic properties of Aβ42, Aβ40, and α-synuclein fibrils: A coarse-grained method to complement experimental studies. *Beilstein J. Nanotechnol.* **2019**, *10*, 500–513. [CrossRef]
27. Ruggeri, F.S.; Adamcik, J.; Jeong, J.S.; Lashuel, H.A.; Mezzenga, R.; Dietler, G. Influence of the β-sheet content on the mechanical properties of aggregates during amyloid fibrillization. *Angew. Chemie Int. Ed.* **2015**, *54*, 2462–2466. [CrossRef] [PubMed]
28. Sneideris, T.; Sakalauskas, A.; Sternke-Hoffmann, R.; Peduzzo, A.; Ziaunys, M.; Buell, A.K.; Smirnovas, V. The Environment Is a Key Factor in Determining the Anti-Amyloid Efficacy of EGCG. *Biomolecules* **2019**, *9*, 855. [CrossRef] [PubMed]
29. Tycko, R. Amyloid Polymorphism: Structural Basis and Neurobiological Relevance. *Neuron* **2015**, *86*, 632–645. [CrossRef]
30. Close, W.; Neumann, M.; Schmidt, A.; Hora, M.; Annamalai, K.; Schmidt, M.; Reif, B.; Schmidt, V.; Grigorieff, N.; Fändrich, M. Physical basis of amyloid fibril polymorphism. *Nat. Commun.* **2018**, *9*, 699. [CrossRef]
31. Tanaka, M.; Chien, P.; Yonekura, K.; Weissman, J.S. Mechanism of cross-species prion transmission: An infectious conformation compatible with two highly divergent yeast prion proteins. *Cell* **2005**, *121*, 49–62. [CrossRef] [PubMed]
32. Makarava, N.; Ostapchenko, V.G.; Savtchenko, R.; Baskakov, I.V. Conformational switching within individual amyloid fibrils. *J. Biol. Chem.* **2009**, *284*, 14386–14395. [CrossRef]
33. Flynn, J.D.; McGlinchey, R.P.; Walker, R.L.; Lee, J.C. Structural features of α-synuclein amyloid fibrils revealed by Raman spectroscopy. *J. Biol. Chem.* **2018**, *293*, 767–776. [CrossRef] [PubMed]
34. Sakalauskas, A.; Ziaunys, M.; Smirnovas, V. Concentration-dependent polymorphism of insulin amyloid fibrils. *PeerJ* **2019**, *7*, e8208. [CrossRef]
35. Adamcik, J.; Mezzenga, R. Study of amyloid fibrils via atomic force microscopy. *Curr. Opin. Colloid Interface Sci.* **2012**, *17*, 369–376. [CrossRef]
36. Iannuzzi, C.; Borriello, M.; Portaccio, M.; Irace, G.; Sirangelo, I. Insights into insulin fibril assembly at physiological and acidic ph and related amyloid intrinsic fluorescence. *Int. J. Mol. Sci.* **2017**, *18*, 2551. [CrossRef] [PubMed]
37. Bouchard, M.; Zurdo, J.; Nettleton, E.J.; Dobson, C.M.; Robinson, C.V. Formation of insulin amyloid fibrils followed by FTIR simultaneously with CD and electron microscopy. *Protein Sci.* **2000**, *9*, 1960–1967. [CrossRef]
38. Aldewachi, H.; Al-Zidan, R.N.; Conner, M.T.; Salman, M.M. High-throughput screening platforms in the discovery of novel drugs for neurodegenerative diseases. *Bioengineering* **2021**, *8*, 30. [CrossRef]
39. Salman, M.M.; Al-Obaidi, Z.; Kitchen, P.; Loreto, A.; Bill, R.M.; Wade-Martins, R. Advances in Applying Computer-Aided Drug Design for Neurodegenerative Diseases. *Int. J. Mol. Sci.* **2021**, *22*, 4688. [CrossRef]
40. Ziaunys, M.; Sakalauskas, A.; Smirnovas, V. Identifying Insulin Fibril Conformational Differences by Thioflavin-T Binding Characteristics. *Biomacromolecules* **2020**, *21*, 4989–4997. [CrossRef]
41. Sidhu, A.; Vaneyck, J.; Blum, C.; Segers-Nolten, I.; Subramaniam, V. Polymorph-specific distribution of binding sites determines thioflavin-T fluorescence intensity in α-synuclein fibrils. *Amyloid* **2018**, *25*, 189–196. [CrossRef]
42. Kovachev, P.S.; Gomes, M.P.B.; Cordeiro, Y.; Ferreira, N.C.; Valadão, L.P.F.; Ascari, L.M.; Rangel, L.P.; Silva, J.L.; Sanyal, S. RNA modulates aggregation of the recombinant mammalian prion protein by direct interaction. *Sci. Rep.* **2019**, *9*, 1–12. [CrossRef]
43. Milto, K.; Michailova, K.; Smirnovas, V. Elongation of Mouse Prion Protein Amyloid-Like Fibrils: Effect of Temperature and Denaturant Concentration. *PLoS ONE* **2014**, *9*, e94469. [CrossRef] [PubMed]
44. Rodina, N.P.; Sulatsky, M.I.; Sulatskaya, A.I.; Kuznetsova, I.M.; Uversky, V.N.; Turoverov, K.K. Photophysical Properties of Fluorescent Probe Thioflavin T in Crowded Milieu. *J. Spectrosc.* **2017**, *2017*. [CrossRef]
45. Foderà, V.; Groenning, M.; Vetri, V.; Librizzi, F.; Spagnolo, S.; Cornett, C.; Olsen, L.; van de Weert, M.; Leone, M. Thioflavin T Hydroxylation at Basic pH and Its Effect on Amyloid Fibril Detection. *J. Phys. Chem. B* **2008**, *112*, 15174–15181. [CrossRef] [PubMed]
46. Barth, A. Infrared spectroscopy of proteins. *Biochim. Biophys. Acta Bioenerg.* **2007**, *1767*, 1073–1101. [CrossRef]
47. Ma, B.; Nussinov, R. Simulations as analytical tools to understand protein aggregation and predict amyloid conformation. *Curr. Opin. Chem. Biol.* **2006**, *10*, 445–452. [CrossRef] [PubMed]
48. Ziaunys, M.; Smirnovas, V. Additional Thioflavin-T Binding Mode in Insulin Fibril Inner Core Region. *J. Phys. Chem. B* **2019**, *123*, 8727–8732. [CrossRef]
49. Mikalauskaite, K.; Ziaunys, M.; Sneideris, T.; Smirnovas, V. Effect of Ionic Strength on Thioflavin-T Affinity to Amyloid Fibrils and Its Fluorescence Intensity. *Int. J. Mol. Sci.* **2020**, *21*, 8916. [CrossRef]

International Journal of
Molecular Sciences

MDPI

Article

Effect of Ionic Strength on Thioflavin-T Affinity to Amyloid Fibrils and Its Fluorescence Intensity

Kamile Mikalauskaite [1,†], Mantas Ziaunys [1,†], Tomas Sneideris [1,2] and Vytautas Smirnovas [1,*]

[1] Institute of Biotechnology, Life Sciences Center, Vilnius University, LT-10257 Vilnius, Lithuania; kamile.mikalauskaite@gmail.com (K.M.); mantas.ziaunys@gmail.com (M.Z.); sneideris.t@gmail.com (T.S.)
[2] Department of Chemistry, University of Cambridge, Cambridge CB2 1EW, UK
* Correspondence: vytautas.smirnovas@bti.vu.lt
† These authors contributed equally to this work.

Received: 5 November 2020; Accepted: 24 November 2020; Published: 24 November 2020

Abstract: The formation of amyloid fibrils is linked to multiple neurodegenerative disorders, including Alzheimer's and Parkinson's disease. Despite years of research and countless studies on the topic of such aggregate formation, as well as their resulting structure, the current knowledge is still fairly limited. One of the main aspects prohibiting effective aggregation tracking is the environment's effect on amyloid-specific dyes, namely thioflavin-T (ThT). Currently, there are only a few studies hinting at ionic strength being one of the factors that modulate the dye's binding affinity and fluorescence intensity. In this work we explore this effect under a range of ionic strength conditions, using insulin, lysozyme, mouse prion protein, and α-synuclein fibrils. We show that ionic strength is an extremely important factor affecting both the binding affinity, as well as the fluorescence intensity of ThT.

Keywords: amyloid; protein aggregation; ionic strength; thioflavin-T

1. Introduction

Protein aggregation into insoluble, highly structured amyloid fibrils is related to the onset and progression of many neurodegenerative disorders, such as Alzheimer's or Parkinson's diseases [1,2]. Despite an abundance of experiments conducted with both model [3,4] and disease-related proteins [5,6] there is still a limited understanding of how native proteins convert to these beta-sheet rich aggregates [7]. In addition, very few potential anti-amyloid compounds have passed the initial clinical trials, and none have been approved as effective in treating or curing patients [8,9]. These two factors are intertwined, as a limited comprehension of protein fibrillization and the methods used to track it ultimately led to the identification of seemingly potential, yet ineffective, disease-modulating compounds.

There are multiple methods used to track protein aggregation into amyloid fibrils. Changes in their secondary structure can be analyzed by circular dichroism [10] or Fourier-transform infrared spectroscopy [11]; aggregate morphology is commonly examined by transmission electron microscopy [12] or atomic force microscopy [13], while changes in fibril quantity are determined by sedimentation or amyloidophilic dye binding [14]. Despite the variety of methods, each one has its limitations, such as the inability to detect different types of aggregates or to quantify their concentration in solution. When examining a potential anti-amyloid compound, these drawbacks could lead to a false interpretation of the results and yield another failed clinical trial.

One of the more commonly used spectroscopic methods to track fibrillization reactions is a thioflavin-T (ThT) fluorescence assay [15]. This molecule binds to the beta-sheet grooves on the fibril's surface and attains a locked conformation, resulting in a significant increase in its fluorescence emission intensity [16,17]. Changes in this intensity are used as an indicator of fibril assembly or disassembly [18]. If a decrease in signal intensity is observed, it is attributed to the reduction of amyloid

assemblies [19,20], caused by the tested anti-amyloid compound. In recent years, such a correlation between the quantity of fibrils and ThT fluorescence intensity has come into question, as multiple reports displayed a variety of factors that can modulate this dye's fluorescence potential [21–23]. It was shown that distinct fibril conformations, originating from the same protein, can possess different bound ThT fluorescence intensities [24–26]. Moreover, the signal intensity can be modulated by other compounds present in solution, either by fluorescence quenching, an inner filter effect or interactions on the fibril's surface [22,27,28]. In addition, to complicate matters further, fibrils can bind ThT in more than one type of binding mode with different affinities [29,30]. The binding of ThT is also not limited to just amyloid fibrils, but to certain specific native state proteins [31].

One factor that was observed on a few occasions was that a change in the solution's ionic strength modulated ThT binding to lysozyme, prion protein fragment and amyloid beta fibrils [32–34]. A higher salt concentration resulted in a significant change to the dye's fluorescence intensity. Experiments with amyloid proteins are conducted in a wide variety of conditions and the addition of various salts, such as sodium chloride [10,35] or guanidine hydrochloride [36–38], are often used to initiate or speed up aggregation reactions. Because of this, the high variety of ionic strength conditions may also result in different types of ThT binding, making fluorescence intensity comparisons completely inaccurate and irrelevant.

In this work, we examine ThT binding to amyloid fibrils formed of either model amyloidogenic proteins–insulin [39] and lysozyme [3], or neurodegenerative disease-related prion protein [40] and α-synuclein [41] under a large range of ionic strength conditions. We compare the differences in total bound ThT concentration, its fluorescence intensity, self-quenching ability, and possible new binding modes and show that ionic strength has a significant effect on all of these factors.

2. Results

Before examining the interaction between amyloid fibrils and ThT under a range of NaCl concentrations, the effect of ionic strength was examined on the dye molecule itself. Based on the absorbance spectra and calculated extinction coefficient values at 412 nm, there does not seem to be any significant effect that NaCl has on non-bound ThT, even at the highest ionic strength conditions (Appendix A Figure A1). In the case of such small variations having any effect, the determined condition-specific ε_{412} values were used in all subsequent calculations.

When insulin fibrils are sonicated and resuspended into a range of NaCl and ThT concentration solutions, the first relevant observation is a difference in sample optical density at 600 nm (Figure 1A). When there is no NaCl present in solution, the optical density (OD_{600}) is relatively low (0.1). It then increases with the addition of NaCl to roughly 0.35 and reaches a plateau. This suggests that up to a certain ionic strength, insulin fibrils are less prone toward self-association. This is further supported by subsequent sample centrifugation, where a substantial concentration of residual fibrils was still present in the supernatant at low ionic strength conditions (0–10 mM NaCl). This has, in turn, made it difficult to accurately determine the concentration of free and bound ThT molecules for solutions containing 0 and 10 mM NaCl (Figure 1B).

Following centrifugation, the concentration of free and bound ThT was determined for samples containing a range of NaCl (from 20 mM to 2 M) and ThT (from 20 μM to 100 μM) concentrations (Figure 1B). There is a direct correlation between the concentration of bound ThT and the solution's ionic strength, as well as total ThT concentration. The dye-binding capacity of insulin fibrils increases from 4 μM at lower ionic strength and ThT concentrations, up to 55 μM at the highest NaCl and dye concentrations. The effect of ionic strength is most evident at the highest ThT concentration, where we observe a 4-fold increase in bound molecule concentration upon increase of NaCl concentration from 20 mM to 2 M (Figure 2B).

The fluorescence intensity follows a similar tendency, with higher ionic strength and ThT concentrations yielding a stronger signal (Figure 1C). However, the maximum fluorescence intensity values are not located at the same position as the highest concentration of bound dye, but rather at

the intermediate level. This suggests that there is a critical concentration of bound ThT molecules, after which the self-quenching effect [42] overcomes the increase in fluorescence-capable dye molecules. Dividing the signal intensity by the concentration of bound ThT reveals that the fluorescence quantum yield decreases in an arc shape (Figure 1D), suggesting that the more molecules are bound to the fibril's surface, the more they experience fluorescence self-quenching. Interestingly, the quantum yield values overlap with one another between different NaCl concentration conditions (Figure 1D), indicating that ionic strength itself does not influence the fluorescence intensity, but only the concentration of bound ThT molecules.

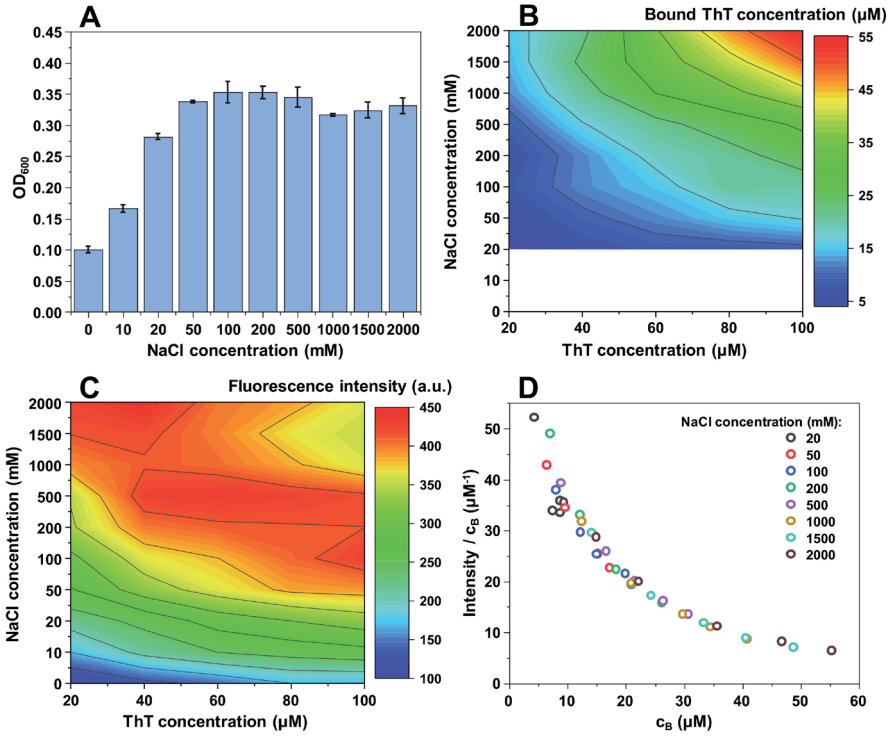

Figure 1. Insulin fibril and ThT solution optical density at 600 nm (**A**), bound ThT concentration (**B**), fluorescence intensity (**C**) and intensity/bound ThT (I/c_B) ratio (**D**) at different NaCl concentrations. Optical density and fluorescence spectra intensities are the result of three repeats. The white area in the bound ThT graph (**B**) represents conditions under which bound ThT concentration could not be determined accurately. Fluorescence intensity values are corrected for the primary and secondary inner filter effects.

When examining the ionic strength's effect on lysozyme fibrils (Figure 2A), similar tendencies are observed. When there is no NaCl present in solution, its OD_{600} is relatively low and, as in the case of insulin fibrils (Figure 1A), it rapidly rises with the increasing NaCl concentration, subsequently reaching a plateau. This change, however, appears to be more extreme than in the case of insulin fibrils, as the OD_{600} value goes from less than 0.1 to 0.5–0.6, while in the former case it was from 0.1 to 0.35. This suggests that lysozyme fibril self-association is more sensitive to changes in the solution's ionic strength. The plateau is also reached at a slightly lower solution's ionic strength than in the case of insulin fibrils.

While the dependence between bound ThT and ionic strength/total ThT concentration pertains a similar tendency (Figure 2B) as with insulin fibrils, the concentration of bound dye at the maximum

point is considerably higher (~70 μM as opposed to ~50 μM). The maximum fluorescence values are also shifted toward higher NaCl and ThT concentrations. The higher bound dye molecule concentrations result in a lower quantum yield, which shifts from 30 μM^{-1} to 10 μM^{-1} (Figure 2D), as opposed to insulin's 50 μM^{-1} to 10 μM^{-1} (Figure 1D) due to an increase in fluorescence self-quenching. In this case, there is a less precise overlap between fluorescence quantum yield values at different NaCl concentrations; however, they still follow a similar arc shape as with insulin fibrils.

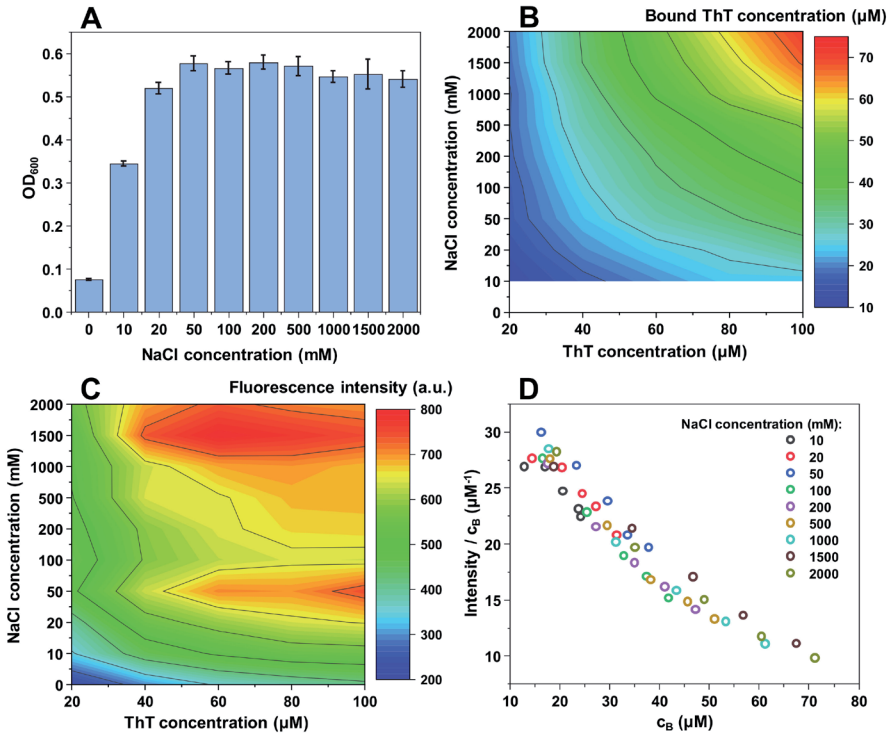

Figure 2. Lysozyme fibril and ThT solution optical density at 600 nm (**A**), bound ThT concentration (**B**), intensity/bound ThT (I/c_B) ratio (**C**) and fluorescence intensity (**D**) at different NaCl concentrations. Optical density and fluorescence spectra intensities are the result of three repeats. The white area in the bound ThT graph (**B**) represents conditions under which bound ThT concentration could not be determined accurately. Fluorescence intensity values are corrected for the primary and secondary inner filter effects.

Contrary to insulin and lysozyme, MoPrP fibrils appear to require a relatively high ionic strength (100 mM NaCl) to begin an effective self-association (Figure 3A). This makes it quite difficult to accurately determine the concentrations of bound ThT molecules (Figure 3B); however, there still seems to be a similar binding tendency as with both other protein fibrils, but with a lower maximum bound ThT concentration.

The fluorescence intensity value distribution also has a unique pattern, with intensity values being low up to 50–100 mM NaCl, after which the signal values suddenly increase (Figure 3C). This distribution is similar to the OD_{600} values (Figure 3A), indicating that there may be a correlation between fibril self-association tendencies and the maximum fluorescence intensity. The quantum yield values follow the same arc shape as in both other cases.

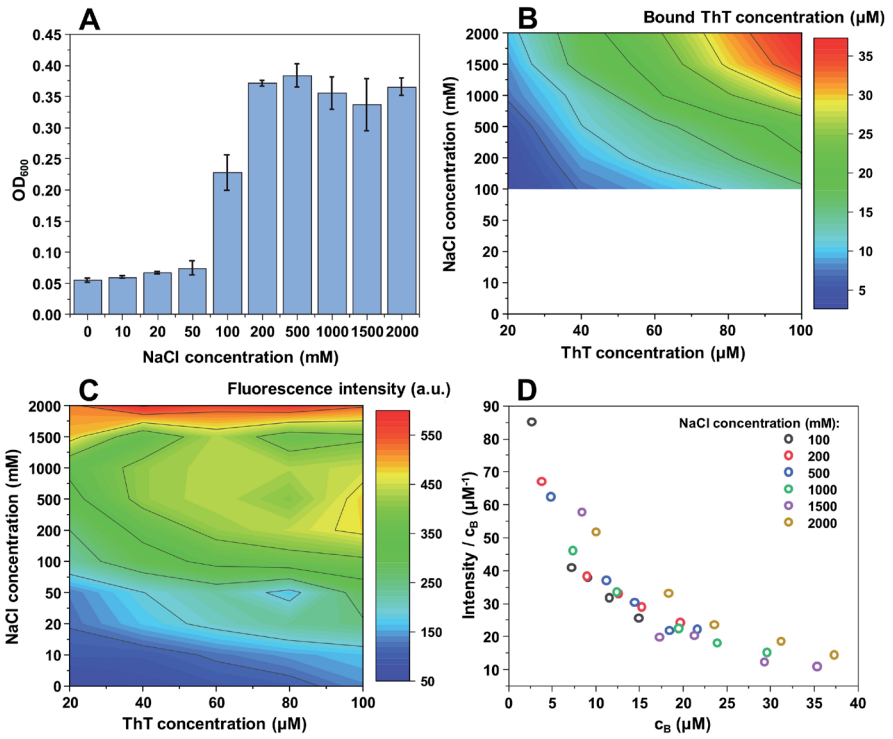

Figure 3. MoPrP fibril and ThT solution optical density at 600 nm (**A**), bound ThT concentration (**B**), intensity/bound ThT (I/c_B) ratio (**C**) and fluorescence intensity (**D**) at different NaCl concentrations. Optical density and fluorescence spectra intensities are the result of three repeats. The white area in the bound ThT graph (**B**) represents conditions under which bound ThT concentration could not be determined accurately. Fluorescence intensity values are corrected for the primary and secondary inner filter effects.

The most interesting effect of ionic strength appears in the case of α-synuclein fibrils. While the changes in OD_{600} (Figure 4A) and bound ThT concentration (Figure 4B) share similar tendencies to MoPrP fibrils, the fluorescence intensity itself is much higher than in all other three cases (Figure 4C), while OD_{600} is the lowest out of all four protein fibrils. This indicates that the fibrils are, in general, considerably less self-associated and bound ThT molecules have a significantly higher fluorescence quantum yield. Another interesting aspect is that the effect of ThT self-quenching appears to be much greater, as the fluorescence intensity decreases with increasing dye concentration even at the lowest NaCl concentrations (Figure 4C), opposite to what was observed for other protein fibrils.

An unusual distribution in ThT quantum yield values is also observed (Figure 4D). In the presence of 100 mM or 200 mM NaCl, the I/c_B values do not overlap with all the others, which were determined at higher ionic strength conditions. This indicates the possibility of a significant change in either ThT binding or the fibrils themselves. In fact, when all four aggregates were examined using Fourier-transform infrared spectroscopy (FTIR), the secondary structure of α-synuclein fibrils was affected by the change in NaCl concentration, while there were no substantial differences observed in the case of insulin, lysozyme of MoPrP fibrils (Appendix A Figure A2). The FTIR signal intensity at 1622 cm^{-1} (associated with beta-sheets) [43] is higher in the presence of 2 M NaCl. At low ionic strength, the aggregates appear to have a substantially larger disordered part, when compared to fibrils

at high ionic strength. This shift in FTIR spectra and the ThT quantum yield values suggests an ionic strength-induced conformational change.

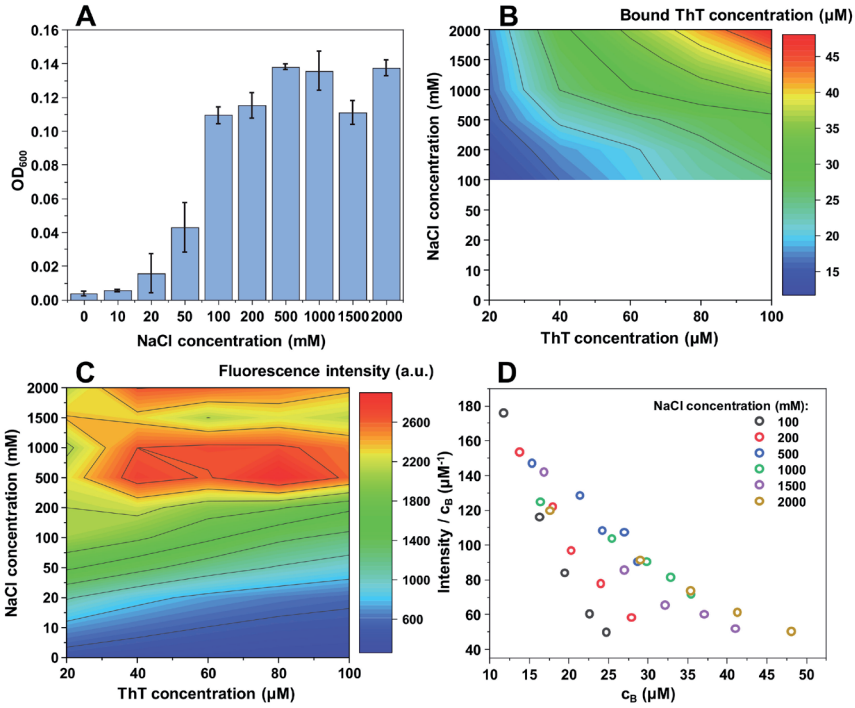

Figure 4. α-synuclein fibril and ThT solution optical density at 600 nm (**A**), bound ThT concentration (**B**), intensity/bound ThT (I/c_B) ratio (**C**) and fluorescence intensity (**D**) at different NaCl concentrations. Optical density and fluorescence spectra intensities are the result of three repeats. The white area in the bound ThT graph (**B**) represents conditions under which bound ThT concentration could not be determined accurately. Fluorescence intensity values are corrected for the primary and secondary inner filter effects.

The excitation-emission matrix (EEM) maximum signal intensity at low bound ThT concentrations is located at different excitation-emission wavelengths for all four types of fibrils (Figure 5A–D). This is to be expected, as distinct fibrils can possess specific ThT binding modes [17]. As the concentration of bound dye increases, the insulin, lysozyme and MoPrP EEM position shifts toward lower excitation and higher emission wavelengths, while in the case of α-synuclein, it experiences a very minor change toward a higher excitation wavelength. In general, such an observation can have two different explanations. One possibility is that an increase in the solution's ionic strength can result in ThT binding in a different mode on the fibril's surface, which has a specific maximum excitation/emission wavelength. The second viable explanation is that these amyloid fibrils have multiple binding modes with specific capacities. If the increase in the solution's ionic strength enhances ThT-fibril association, then certain binding modes may reach their capacity limit, causing more dye molecules to bind in a different mode and, in turn, result in a shift of the EEM maximum position. In the case of α-synuclein fibrils, a third possibility exists, where the change may be related to there being two different fibril conformations at both ends of the ionic strength spectrum.

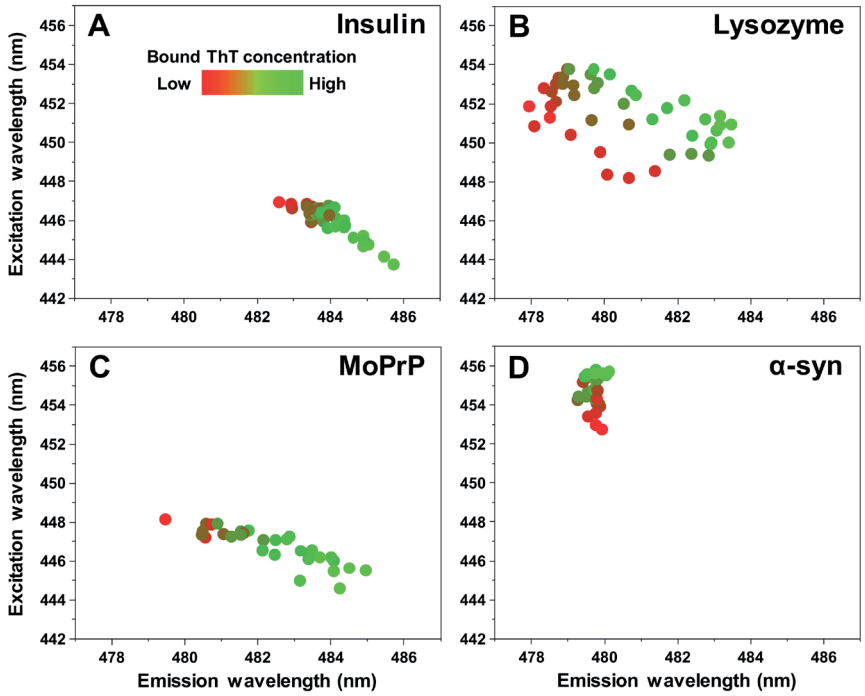

Figure 5. Insulin (**A**), lysozyme (**B**), mouse prion protein (**C**) and α-synuclein (**D**) fibril sample ThT fluorescence EEM intensity "center of mass" positions at different bound ThT concentrations.

3. Discussion

One of the more interesting events observed in this work is the apparent loss or reduction of fibril self-association properties at low ionic strength conditions. This could be attributed to being a generic feature of amyloid fibrils; however, both the change in OD_{600} values and the NaCl concentration at which the change occurs differ for all four protein fibrils. Lysozyme fibrils require the lowest ionic strength to self-associate, with insulin fibrils following a close second, while prion protein and α-synuclein fibrils need more than 50–100 mM NaCl present in solution to reach a plateau in solution OD_{600} values. This may be indicative of distinct fibrils with specific surface charges [44] that need to be shielded before effective association occurs. There also seems to be a correlation between when fibrils self-associate and the increase in ThT fluorescence intensity. This could be due to the same electrostatic repulsive forces acting upon both ThT molecules and other fibrils in solution.

Another interesting aspect is the massive effect ionic strength has on ThT binding and fluorescence properties. It is evident from this data that even minor variances in NaCl concentration result in major shifts of both fluorescence intensity, as well as the concentration of fibril-bound ThT molecules. This factor is important on two different fronts, both positive and negative. The negative aspect is that it makes comparisons of ThT fluorescence values, obtained at even slightly different ionic strength conditions, virtually impossible. Considering there are countless distinct conditions used to study amyloid formation and inhibition, a direct comparison between ThT fluorescence data sets becomes almost meaningless. The positive aspect, however, is the massive rise in ThT binding and fluorescence intensity upon the increase in ionic strength. If a certain type of fibrillar aggregate is difficult to track or detect due to its low dye affinity, one could achieve a several-fold rise in signal intensity by changing the solution's ionic strength. In addition, ionic strength itself does not seem to alter the spectral properties of ThT, but rather causes it to induce a self-quenching effect due to increased binding.

In two of the cases, namely insulin and lysozyme fibrils, there exists a cut-off point, where the fluorescence intensity reaches the highest point and then begins to decrease. This is most likely caused by ThT fluorescence self-quenching, as the concentration of bound dye molecules surpasses a certain value, where quenching effects dominate over fluorescence. As this maximum intensity position is different for all four tested fibrils, this indicates that each type of amyloid aggregate has certain ideal total ThT concentration and solution ionic strength for monitoring ThT fluorescence.

The EEM position shift observed in all four cases is also an indicator that ionic strength may modulate ThT binding modes on the fibril's surface. This may be due to certain positions with a maximum binding capacity, which causes the dye to associate with other, lower affinity positions. It could also directly affect the positions by altering the structure of the aggregate, as seen in the case of α-synuclein, or by increasing their affinity toward ThT by shielding charges between the fibril's surface and dye molecules. In either case, the bound ThT distribution on the fibril varies with the solution's ionic strength for all four types of aggregates examined in this work and such an effect may extend toward other amyloid aggregates as well. This ionic strength's effect on dye binding may also explain why some anti-amyloid compounds are extremely effective under certain conditions, yet fail to produce any meaningful results under others [45]. If affinity between drug molecules and amyloid fibrils is the driving force of aggregation-inhibition and we assume that the effect of ionic strength extends beyond just fibril-fibril or fibril-ThT interactions, then it may also be directly responsible for the potential of inhibition.

Finally, it seems that ionic strength is not only an important factor which modulates ThT binding, but it can also affect the secondary structure of certain types of aggregates. While insulin, lysozyme and prion protein fibrils were not affected by changes in the solution's ionic strength, α-synuclein fibrils displayed different amounts of disordered and beta-sheet structures at 0 and 2 M NaCl. Such an ionic strength-related structural shift is a clear indicator that the fibril environment is a determining factor in not just their formation, but their existence as well.

Taking everything into account, it appears that ionic strength is a highly important factor in fibril self-association events, structural aspects, ThT binding affinity and dye fluorescence intensity. It has a similar effect on distinct protein fibrils, including insulin, lysozyme, prion protein and α-synuclein amyloid aggregates. The significant dependence between ionic strength and fibril-dye interactions has both positive aspects, such as the ability to greatly enhance signal intensity, as well as negative ones—the diminished ability to compare fluorescence values between different conditions.

4. Materials and Methods

4.1. Fibril Formation

Human recombinant insulin powder (Sigma-Aldrich, St. Louis, MO, USA, cat. No. 91077C) was dissolved in a 100 mM sodium phosphate (pH 2.4) buffer, containing 100 mM NaCl. The final protein concentration was 200 μM (M = 5808 Da, ε_{280} = 6335 $M^{-1}cm^{-1}$). The solution was distributed to 1.5 mL test tubes (1.0 mL solution each) and incubated at 60 °C without agitation for 24 h. Afterwards, the test tubes were centrifuged at 10,000× *g* for 30 min and resuspended into MilliQ H_2O. This centrifugation/resuspension procedure was repeated 4 times. After the final centrifugation step, the fibrils were resuspended into a smaller volume of H_2O to result in a solution containing 400 μM fibrils.

Hen egg-white lysozyme powder (Sigma-Aldrich cat. No. L6876) was dissolved in a 50 mM sodium phosphate buffer (pH 6.0) containing 2 M guanidine hydrochloride (GuHCl) to a final protein concentration of 200 μM (M = 14,313 Da, ε_{280} = 37,970 $M^{-1}cm^{-1}$). The resulting solution was distributed to 1.5 mL test tubes (1.0 mL solution each, each containing two 3 mm glass-beads) and incubated at 60 °C for 72 h under 600 rpm agitation. Afterwards, the test tubes were centrifuged and resuspended into H_2O as described in the insulin fibril preparation section.

Mouse prion protein 89–230 (MoPrP 89–230) was purified as described previously [38] without the His-tag cleavage step and was stored at −80 °C prior to use. The protein solution was mixed

with 50 mM sodium phosphate (pH 6.0) buffers, which contained 0 or 6 M of GuHCl to a final protein concentration of 0.5 mg/mL and a GuHCl concentration of 0.5 M. The resulting solution was distributed to 2.0 mL test tubes (1.5 mL solution each) and incubated at 60 °C for 72 h under 600 rpm agitation. Afterwards, the test tubes were centrifuged and resuspended into H_2O as described in the insulin fibril preparation section and the protein concentration was set to 400 μM (M = 18,621 Da, ε_{280} = 27,515 $M^{-1}cm^{-1}$).

α-synuclein was purified as described previously [46] and was stored at −80 °C prior to use. The protein solution was mixed with 10× phosphate buffer saline (PBS) and MilliQ H_2O to a final protein concentration of 200 μM (PBS stock solution was diluted 10 times). The resulting solution was distributed to 1.5 mL test tubes (1.0 mL solution each, each containing 3 mm glass-beads) and incubated at 60 °C for 24 h under 600 rpm agitation. Afterwards, the test tubes were centrifuged and resuspended into H_2O as described in the insulin fibril preparation section and the final protein concentration was set to 400 μM (M = 14,460 Da, ε_{280} = 5,960 $M^{-1}cm^{-1}$).In all four cases, prior to further use, the fibril solutions of each protein were combined, sonicated for 1 min using a Bandelin Sonopuls (Berlin, Germany) ultrasonic homogenizer equipped with a MS73 tip at 40% total power in order to avoid variation between each sample. This procedure was done in case one or more of the tested proteins can form a heterogenous mixture of fibrils. Afterwards, 1 mL aliquots were taken and sonicated for an additional 10 min with 30 s sonication/rest intervals to fragment and homogenize the fibrils in solution [47].

4.2. ThT and NaCl Solution Preparation

ThT powder (Sigma-Aldrich cat. no. T3516) was dissolved in MilliQ H_2O to a concentration of 10 mM. The exact dye concentration was determined by diluting the solution 100 times and scanning the absorbance at 412 nm using a Shimadzu (Kyoto, Japan) UV-1800 spectrophotometer (ε_{412} = 23,250 $M^{-1}cm^{-1}$). The dye solution was then further diluted using H_2O to a range of ThT concentrations, before mixing with fibril solutions.

NaCl was dissolved in MilliQ H_2O to a final concentration of 4 M. The resulting solution was diluted to a range of NaCl concentrations using H_2O, before mixing with fibril solutions.

4.3. ThT Fluorescence Assay

Fibril solutions were mixed with ThT and NaCl stock solutions in a 1:1:2 ratio to result in a final fibril concentration of 100 μM and a range of NaCl (0–2 M) and ThT (0–100 μM) concentrations. Each sample's excitation/emission matrix (EEM) was scanned using a Varian Cary Eclipse spectrofluorometer (Agilent Technologies, Santa Clara, CA, USA) (excitation wavelength range was 435–465 nm with 1 nm steps, emission wavelength range was 460–500 nm with 1 nm steps). Excitation and emission slit widths were 5 nm and 2.5 nm respectively for insulin, lysozyme, and prion protein fibril samples and 2.5 nm/2.5 nm for α-synuclein samples. For each sample, three EEMs were recorded, averaged and a control EEM (without ThT) was subtracted. For an accurate comparison, the α-synuclein sample maximum fluorescence values were multiplied by a factor of 5, which is the intensity difference between scans when the excitation slit width is set to 5 nm or 2.5 nm.

4.4. Sample Absorbance and Optical Density Measurements

Each sample's absorbance spectrum was scanned in the range from 300 nm to 600 nm using a Shimadzu UV-1800 spectrophotometer. For each case, three absorbance spectra were recorded, averaged and a control (MilliQ H_2O) spectrum was subtracted. Afterwards, all samples were centrifuged at 10,000× *g* for 30 min, subsequently, a small aliquot (50 μL) of the supernatant was carefully removed (in order to not collect any pelleted fibrils) and diluted to 150 μL. The resulting sample absorbance spectra were also scanned as described previously. Optical density was measured at 600 nm using a 10 mm pathlength cuvette.

4.5. Inner Filter Correction and EEM Maxima Position Calculation

To account for the primary and secondary inner filter effect on fluorescence, caused by the sample's absorbance, each EEM was corrected as described previously [48] using the following equation:

$$I_m = I_c \times 10^{-(AEx+AEm)/2} \quad (1)$$

where AEx is the sample's absorbance at the excitation wavelength, AEm is the sample's absorbance at the emission wavelength, I_m is the signal intensity observed during measurement and I_c is the corrected signal intensity.

The exact EEM intensity maxima position cannot be accurately determined due to signal noise. For this reason, a signal intensity "center of mass" was calculated by selecting the top 10% intensity values and using the following equation:

$$\lambda = (\sum (\lambda_n \times \sum I_n)) / \sum I_a \quad (2)$$

where λ is the wavelength of either the excitation or emission center of mass, λ_n is an excitation or emission wavelength, $\sum I_n$ is the sum of all signal intensities at λ_n, $\sum I_a$ is the sum of all signal intensities.

To negate the effect of Rayleigh scattering on the "center of mass" position, the region located 8 nm or closer to the excitation wavelength was not taken into account in the calculation.

4.6. Fourier-Transform Infrared Spectroscopy

Fibril samples were centrifuged at 10,000× g for 30 min and resuspended into D_2O. This procedure was repeated 4 times. After the final centrifugation, the samples were resuspended into 200 µL D_2O and divided into two equal volume parts. The divided samples were then mixed with either 100 µL D_2O or D_2O containing 4 M NaCl. Sample FTIR spectra were recorded as described previously [45]. A D_2O spectrum was subtracted from the sample spectra, which was then baseline-corrected and normalized in the 1595–1700 cm^{-1} range. All data analysis was performed using GRAMS software.

Author Contributions: Conceptualization, K.M., M.Z. and V.S.; investigation, K.M., M.Z. and T.S.; resources, V.S.; writing–original draft preparation, M.Z., T.S. and V.S.; writing–review and editing, M.Z., T.S. and V.S.; supervision, V.S.; funding acquisition, M.Z. and V.S. All authors have read and agreed to the published version of the manuscript.

Funding: This research was funded by Vilnius University, grant No. MSF-JM-3.

Conflicts of Interest: The authors declare no conflict of interest.

Appendix A

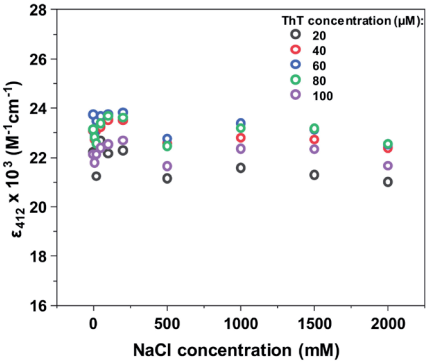

Figure A1. Dependence of ThT ε_{412} values on the concentration of NaCl present in solution at different ThT concentrations.

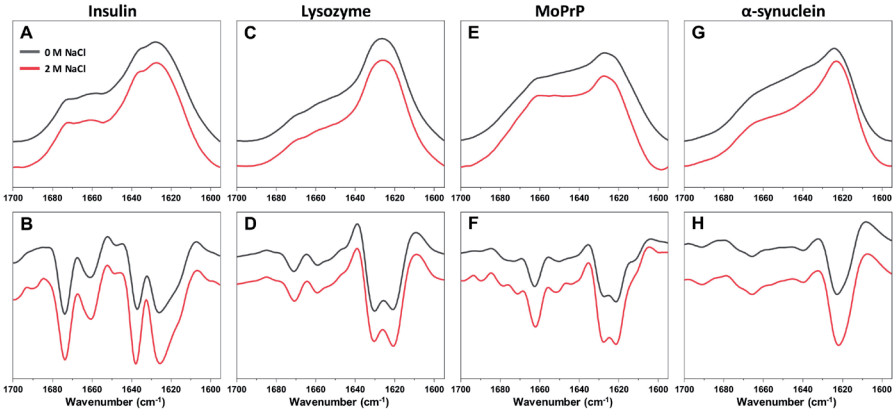

Figure A2. FTIR spectra and their second derivatives of insulin (**A**,**B**), lysozyme (**C**,**D**), MoPrP (**E**,**F**) and α-synuclein (**G**,**H**) fibrils.

References

1. Knowles, T.P.J.; Vendruscolo, M.; Dobson, C.M. The amyloid state and its association with protein misfolding diseases. *Nat. Rev. Mol. Cell Biol.* **2014**, *15*, 384–396. [CrossRef] [PubMed]
2. Chiti, F.; Dobson, C.M. Protein Misfolding, Amyloid Formation, and Human Disease: A Summary of Progress Over the Last Decade. *Annu. Rev. Biochem.* **2017**, *86*, 27–68. [CrossRef] [PubMed]
3. Swaminathan, R.; Ravi, V.K.; Kumar, S.; Kumar, M.V.S.; Chandra, N. Lysozyme: A model protein for amyloid research. *Adv. Protein Chem. Struct. Biol.* **2011**, *84*, 63–111. [CrossRef] [PubMed]
4. Mahdavimehr, M.; Katebi, B.; Meratan, A.A. Effect of fibrillation conditions on the anti-amyloidogenic properties of polyphenols and their involved mechanisms. *Int. J. Biol. Macromol.* **2018**, *118*, 552–560. [CrossRef] [PubMed]
5. Petkova, A.T.; Leapman, R.D.; Guo, Z.; Yau, W.-M.; Mattson, M.P.; Tycko, R. Self-propagating, molecular-level polymorphism in Alzheimer's beta-amyloid fibrils. *Science* **2005**, *307*, 262–265. [CrossRef]
6. Ono, K.; Takahashi, R.; Ikeda, T.; Yamada, M. Cross-seeding effects of amyloid β-protein and α-synuclein. *J. Neurochem.* **2012**, *122*, 883–890. [CrossRef]
7. Makin, O.S.; Serpell, L.C. Structures for amyloid fibrils. *FEBS J.* **2005**, *272*, 5950–5961. [CrossRef]
8. Cummings, J.; Lee, G.; Ritter, A.; Sabbagh, M.; Zhong, K. Alzheimer's disease drug development pipeline: 2019. *Alzheimer's Dement Transl. Res. Clin. Interv.* **2019**, *5*, 272–293. [CrossRef]
9. Mehta, D.; Jackson, R.; Paul, G.; Shi, J.; Sabbagh, M. Why do trials for Alzheimer's disease drugs keep failing? A discontinued drug perspective for 2010–2015. *Expert Opin. Investig. Drugs* **2017**, *26*, 735–739. [CrossRef]
10. Jain, S.; Udgaonkar, J.B. Salt-Induced Modulation of the Pathway of Amyloid Fibril Formation by the Mouse Prion Protein. *Biochemistry* **2010**, *49*, 7615–7624. [CrossRef]
11. Iannuzzi, C.; Borriello, M.; Portaccio, M.; Irace, G.; Sirangelo, I. Insights into insulin fibril assembly at physiological and acidic ph and related amyloid intrinsic fluorescence. *Int. J. Mol. Sci.* **2017**, *18*, 2551. [CrossRef] [PubMed]
12. Paravastu, A.K.; Leapman, R.D.; Yau, W.-M.; Tycko, R. Molecular structural basis for polymorphism in Alzheimer's -amyloid fibrils. *Proc. Natl. Acad. Sci. USA* **2008**, *105*, 18349–18354. [CrossRef] [PubMed]
13. Ruggeri, F.S.; Šneideris, T.; Vendruscolo, M.; Knowles, T.P.J. Atomic force microscopy for single molecule characterisation of protein aggregation. *Arch. Biochem. Biophys.* **2019**, *664*, 134–148. [CrossRef] [PubMed]
14. Wetzel, R.; Chemuru, S.; Misra, P.; Kodali, R.; Mukherjee, S.; Kar, K. An Aggregate Weight-Normalized Thioflavin-T Measurement Scale for Characterizing Polymorphic Amyloids and Assembly Intermediates. *Methods Mol. Biol.* **2018**, *1777*, 121–144. [CrossRef] [PubMed]
15. Gade Malmos, K.; Blancas-Mejia, L.M.; Weber, B.; Buchner, J.; Ramirez-Alvarado, M.; Naiki, H.; Otzen, D. ThT 101: A primer on the use of thioflavin T to investigate amyloid formation. *Amyloid* **2017**, *24*, 1–16. [CrossRef]

16. Robbins, K.J.; Liu, G.; Selmani, V.; Lazo, N.D. Conformational analysis of thioflavin T bound to the surface of amyloid fibrils. *Langmuir* **2012**, *28*, 16490–16495. [CrossRef]
17. Biancalana, M.; Koide, S. Molecular mechanism of Thioflavin-T binding to amyloid fibrils. *Biochim. Biophys. Acta Proteins Proteom.* **2010**, *1804*, 1405–1412. [CrossRef]
18. Manno, M.; Craparo, E.F.; Martorana, V.; Bulone, D.; San Biagio, P.L. Kinetics of Insulin Aggregation: Disentanglement of Amyloid Fibrillation from Large-Size Cluster Formation. *Biophys. J.* **2006**. [CrossRef]
19. Roy, S.; Bhat, R. Suppression, disaggregation, and modulation of γ-Synuclein fibrillation pathway by green tea polyphenol EGCG. *Protein Sci.* **2019**, *28*, 382–402. [CrossRef]
20. Zhang, J.; Zhou, X.; Yu, Q.; Yang, L.; Sun, D.; Zhou, Y.; Liu, J. Epigallocatechin-3-gallate (EGCG)-Stabilized Selenium Nanoparticles Coated with Tet-1 Peptide To Reduce Amyloid-β Aggregation and Cytotoxicity. *ACS Appl. Mater. Interfaces* **2014**, *6*, 8475–8487. [CrossRef]
21. Hudson, S.A.; Ecroyd, H.; Kee, T.W.; Carver, J.A. The thioflavin T fluorescence assay for amyloid fibril detection can be biased by the presence of exogenous compounds. *FEBS J.* **2009**, *276*, 5960–5972. [CrossRef] [PubMed]
22. Buell, A.K.; Dobson, C.M.; Knowles, T.P.J.; Welland, M.E. Interactions between Amyloidophilic Dyes and Their Relevance to Studies of Amyloid Inhibitors. *Biophys. J.* **2010**, *99*, 3492–3497. [CrossRef] [PubMed]
23. Foderà, V.; Groenning, M.; Vetri, V.; Librizzi, F.; Spagnolo, S.; Cornett, C.; Olsen, L.; van de Weert, M.; Leone, M. Thioflavin T Hydroxylation at Basic pH and Its Effect on Amyloid Fibril Detection. *J. Phys. Chem. B* **2008**, *112*, 15174–15181. [CrossRef]
24. Ziaunys, M.; Sneideris, T.; Smirnovas, V. Formation of distinct prion protein amyloid fibrils under identical experimental conditions. *Sci. Rep.* **2020**, *10*, 4572. [CrossRef] [PubMed]
25. Sakalauskas, A.; Ziaunys, M.; Smirnovas, V. Concentration-dependent polymorphism of insulin amyloid fibrils. *PeerJ* **2019**, *7*, e8208. [CrossRef]
26. Sidhu, A.; Vaneyck, J.; Blum, C.; Segers-Nolten, I.; Subramaniam, V. Polymorph-specific distribution of binding sites determines thioflavin-T fluorescence intensity in α-synuclein fibrils. *Amyloid* **2018**, *25*, 189–196. [CrossRef]
27. Ziaunys, M.; Mikalauskaite, K.; Smirnovas, V. Amyloidophilic Molecule Interactions on the Surface of Insulin Fibrils: Cooperative Binding and Fluorescence Quenching. *Sci. Rep.* **2019**. [CrossRef]
28. Sulatskaya, A.I.; Kuznetsova, I.M.; Belousov, M.V.; Bondarev, S.A.; Zhouravleva, G.A.; Turoverov, K.K. Stoichiometry and Affinity of Thioflavin T Binding to Sup35p Amyloid Fibrils. *PLoS ONE* **2016**, *11*, e0156314. [CrossRef]
29. Groenning, M.; Norrman, M.; Flink, J.M.; van de Weert, M.; Bukrinsky, J.T.; Schluckebier, G.; Frokjaer, S. Binding mode of Thioflavin T in insulin amyloid fibrils. *J. Struct. Biol.* **2007**, *159*, 483–497. [CrossRef]
30. Kuznetsova, I.M.; Sulatskaya, A.I.; Uversky, V.N.; Turoverov, K.K. Analyzing Thioflavin T Binding to Amyloid Fibrils by an Equilibrium Microdialysis-Based Technique. *PLoS ONE* **2012**, *7*, e30724. [CrossRef]
31. Halabelian, L.; Relini, A.; Barbiroli, A.; Penco, A.; Bolognesi, M.; Ricagno, S. A covalent homodimer probing early oligomers along amyloid aggregation. *Sci. Rep.* **2015**, *5*, 1–12. [CrossRef] [PubMed]
32. Wawer, J.; Szociński, M.; Olszewski, M.; Piątek, R.; Naczk, M.; Krakowiak, J. Influence of the ionic strength on the amyloid fibrillogenesis of hen egg white lysozyme. *Int. J. Biol. Macromol.* **2019**, *121*, 63–70. [CrossRef] [PubMed]
33. Sabaté, R.; Lascu, I.; Saupe, S.J. On the binding of Thioflavin-T to HET-s amyloid fibrils assembled at pH 2. *J. Struct. Biol.* **2008**, *162*, 387–396. [CrossRef] [PubMed]
34. LeVine, H. Stopped-flow kinetics reveal multiple phases of thioflavin T binding to Alzheimer β(1-40) amyloid fibrils. Arch. *Biochem. Biophys.* **1997**, *342*, 306–316. [CrossRef]
35. Kutsch, M.; Hortmann, P.; Herrmann, C.; Weibels, S.; Weingärtner, H. Dissecting ion-specific from electrostatic salt effects on amyloid fibrillation: A case study of insulin. *Biointerphases* **2016**, *11*, 019008. [CrossRef]
36. Vernaglia, B.A.; Huang, J.; Clark, E.D. Guanidine Hydrochloride Can Induce Amyloid Fibril Formation from Hen Egg-White Lysozyme. *Biomacromolecules* **2004**, *5*, 1362–1370. [CrossRef]
37. Ahmad, A.; Millett, I.S.; Doniach, S.; Uversky, V.N.; Fink, A.L. Partially Folded Intermediates in Insulin Fibrillation. *Biochemistry* **2003**, *42*, 11404–11416. [CrossRef]
38. Milto, K.; Michailova, K.; Smirnovas, V. Elongation of Mouse Prion Protein Amyloid-Like Fibrils: Effect of Temperature and Denaturant Concentration. *PLoS ONE* **2014**, *9*, e94469. [CrossRef]

39. Brange, J.; Andersen, L.; Laursen, E.D.; Meyn, G.; Rasmussen, E. Toward Understanding Insulin Fibrillation. *J. Pharm. Sci.* **1997**, *86*, 517–525. [CrossRef]
40. Norrby, E. Prions and protein-folding diseases. *J. Intern. Med.* **2011**, *270*, 1–14. [CrossRef]
41. Stefanis, L. α-Synuclein in Parkinson's Disease. *Cold Spring Harb. Perspect. Med.* **2012**, *2*, a009399. [CrossRef]
42. Lindberg, D.J.; Wenger, A.; Sundin, E.; Wesén, E.; Westerlund, F.; Esbjörner, E.K. Binding of Thioflavin-T to Amyloid Fibrils Leads to Fluorescence Self-Quenching and Fibril Compaction. *Biochemistry* **2017**, *56*, 2170–2174. [CrossRef]
43. Barth, A. Infrared spectroscopy of proteins. *Biochim. Biophys. Acta Bioenergy* **2007**, *1767*, 1073–1101. [CrossRef] [PubMed]
44. Lee, G.; Lee, W.; Lee, H.; Woo Lee, S.; Sung Yoon, D.; Eom, K.; Kwon, T. Mapping the surface charge distribution of amyloid fibril. *Appl. Phys. Lett.* **2012**, *101*. [CrossRef]
45. Sneideris, T.; Sakalauskas, A.; Sternke-Hoffmann, R.; Peduzzo, A.; Ziaunys, M.; Buell, A.K.; Smirnovas, V. The Environment Is a Key Factor in Determining the Anti-Amyloid Efficacy of EGCG. *Biomolecules* **2019**, *9*, 855. [CrossRef] [PubMed]
46. Šneideris, T.; Baranauskienė, L.; Cannon, J.G.; Rutkienė, R.; Meškys, R.; Smirnovas, V. Looking for a generic inhibitor of amyloid-like fibril formation among flavone derivatives. *PeerJ* **2015**, *3*, e1271. [CrossRef] [PubMed]
47. Chatani, E.; Lee, Y.-H.; Yagi, H.; Yoshimura, Y.; Naiki, H.; Goto, Y. Ultrasonication-dependent production and breakdown lead to minimum-sized amyloid fibrils. *Proc. Natl. Acad. Sci. USA* **2009**, *106*, 11119–11124. [CrossRef] [PubMed]
48. Ziaunys, M.; Smirnovas, V. Additional Thioflavin-T Binding Mode in Insulin Fibril Inner Core Region. *J. Phys. Chem. B* **2019**, *123*, 8727–8732. [CrossRef]

Interplay between epigallocatechin-3-gallate and ionic strength during amyloid aggregation

Mantas Ziaunys, Kamile Mikalauskaite, Andrius Sakalauskas and Vytautas Smirnovas

Institute of Biotechnology, Life Sciences Center, Vilnius University, Vilnius, Lithuania

ABSTRACT

The formation and accumulation of protein amyloid aggregates is linked with multiple amyloidoses, including neurodegenerative Alzheimer's or Parkinson's disease. The mechanism of such fibril formation is impacted by various environmental conditions, which greatly complicates the search for potential anti-amyloid compounds. One of these factors is solution ionic strength, which varies between different aggregation protocols during *in vitro* drug screenings. In this work, we examine the interplay between ionic strength and a well-known protein aggregation inhibitor—epigallocatechin-3-gallate. We show that changes in solution ionic strength have a major impact on the compound's inhibitory effect, reflected in both aggregation times and final fibril structure. We also observe that this effect is unique to different amyloid-forming proteins, such as insulin, alpha-synuclein and amyloid-beta.

Subjects Biochemistry, Biophysics
Keywords Amyloids, Protein aggregation, Aggregation inhibition, EGCG, Ionic strength, Amyloid beta, Alpha-synuclein, Insulin

INTRODUCTION

Protein aggregation into amyloid fibrils is associated with the onset and progression of many amyloidoses (*Baker & Rice, 2012*), including widespread neurodegenerative disorders, such as Alzheimer's or Parkinson's disease (*Knowles, Vendruscolo & Dobson, 2014*; *Chiti & Dobson, 2017*). Countless studies and years of research have resulted in very few disease-modifying drugs (*Maurer et al., 2018*; *Park et al., 2020*), with most potential aggregation-inhibiting compounds failing at various stages of clinical trials (*Mehta et al., 2017*; *Cummings et al., 2020*), which, in turn, has not allowed to slow down the ever-increasing occurrence of amyloid-related disorders and even more cases are projected for the upcoming decades (*Hebert et al., 2013*; *Arthur et al., 2016*). This makes it vitally important to obtain a better understanding of protein aggregation (*Cohen et al., 2012*), as well as their interaction (*Fusco et al., 2018*) with drug molecules. Currently, there are more than a hundred compounds which have shown potential in having either a direct or indirect effect on the appearance and accumulation of these disease-related protein/peptide aggregates (*Williams, Sorribas & Howes, 2011*). It was also shown that there are multiple modes of interaction between potential drug molecules and fibrils,

Submitted 28 July 2021
Accepted 4 October 2021
Published 22 October 2021

Corresponding author
Mantas Ziaunys,
mantas.ziaunys@gmc.vu.lt

Academic editor
Frances Separovic

Additional Information and Declarations can be found on page 11

DOI **10.7717/peerj.12381**

which include binding along their surface, inside cavities or by interacting with specific amino acids (*Landau et al., 2011*).

One of the main problems during anti-amyloid compound screenings is the impact of environmental conditions on both the aggregation rate and mechanism, as well as protein interaction. Multiple factors, such as protein concentration (*Sakalauskas, Ziaunys & Smirnovas, 2019*), temperature (*Tanaka et al., 2006*; *Colby et al., 2009*), agitation (*Petkova et al., 2005*), ionic strength (*Bousset et al., 2013*), pH (*Sneideris et al., 2015*) or denaturant concentration (*Colby et al., 2009*) can influence the initial amyloidogenic protein state (*Nettleton et al., 2000*), the course and rate of aggregation (*Morel et al., 2010*; *Noormägi et al., 2015*) and the resulting fibril conformation/morphology (*Morel et al., 2010*; *Zidar & Merzel, 2011*; *Nicoud et al., 2015*). Taking into consideration that amyloid-inhibitor interactions may be highly-selective (*Wang, Dong & Sun, 2012*; *Zhuang et al., 2016*; *Liu et al., 2018*; *Fusco et al., 2018*), distinct fibrillization intermediates or fibrils can have specific affinity to the drug molecules in question. This effect was demonstrated during alpha-synuclein and epigallocatechin-3-gallate (EGCG) experiments, where it was observed that changes to the solution's pH value or sample agitation drastically improve or impair the molecule's effectiveness at inhibiting alpha-synuclein aggregation (*Sneideris et al., 2019*; *Sternke-Hoffmann et al., 2020*).

One of these factors, which requires a more in-depth analysis, is ionic strength. It has been demonstrated that the solution's ionic strength (usually modulated by the addition of NaCl (*Jain & Udgaonkar, 2010*)) can influence the rate of aggregation by altering electrostatic interactions between protein molecules (*Ziaunys, Sneideris & Smirnovas, 2018*). It was also shown that this factor can determine the conformation and morphology of fibrils that form during aggregation (*Bousset et al., 2013*; *Gaspar et al., 2020*). In addition, ionic strength can influence compound interactions with fibrils and even cause conformation changes to preformed aggregates (*Mikalauskaite et al., 2020*). Taking all of this into account, it appears that ionic strength plays an important role in multiple stages of the amyloid formation process and could significantly alter experimental results and their conclusions regarding anti-amyloid compounds. Since there are many groups screening for potential aggregation-inhibiting drugs (*Findeis, 2000*; *Huang, Chao & Hu, 2020*) and each one has their own preferred/optimized fibrillization protocols (*Giorgetti et al., 2018*), there is a substantial number of different ionic strength conditions used. Considering the aforementioned effects that this factor may have on amyloid formation, as well as the possible highly-selective nature of anti-amyloid compounds, it is possible that certain potent drugs may appear ineffective under specific ionic strength conditions, leading to false-negative results.

In order to examine the magnitude of the effect that ionic strength has on anti-amyloid drug screening, one of the most well-known and commonly used compounds was chosen—epigallocatechin-3-gallate (EGCG). It has been shown on numerous studies, both *in vitro* and *in silico* (*Ngo et al., 2017*; *Tavanti, Pedone & Menziani, 2020*), that EGCG can alter the aggregation pathway of amyloidogenic proteins, leading to either off-pathway structures or slowing down the rate of fibril formation (*Andrich & Bieschke, 2015*). It is also known that this polyphenolic molecule undergoes autoxidation at neutral pH, which

increases its anti-amyloid potency and minimizes further structural changes during the aggregation reaction (*An, Feng & Zeng, 2017*; *Sneideris et al., 2019*).

In this work, the inhibitory effect of preoxidized EGCG was determined under a range of ionic strength conditions (below and above the typical physiological ionic strength; *Kawai, Wray & Güth, 1990*), using two neurodegenerative-disease-related proteins/peptides—amyloid-beta (Alzheimer's disease) and alpha-synuclein (Parkinson's disease), as well as insulin, which is associated with localized injection site amyloidosis (*Knowles, Vendruscolo & Dobson, 2014*), but is widely used as a model protein in amyloid studies. Due to the distinct amino acid sequences and aggregation conditions of the selected proteins/peptides, it was possible to gain a deeper insight into the effect that this factor has on EGCG inhibitory potential. We show how the interplay between ionic strength and EGCG has a unique effect on each protein/peptide aggregation kinetics and resulting fibril structures.

MATERIALS AND METHODS

Epigallocatechin gallate preparation

Epigallocatechin-3-gallate (Cat. No. M01719; Fluorochem, Derbyshire, UK) was dissolved in a 100 mM potassium phosphate (pH 7.4) buffer to a final concentration of 10 mM. Due to EGCG undergoing autoxidation at neutral pH under two of the three tested aggregation conditions, which changes the efficiency of its inhibition (*Sneideris et al., 2019*; *Wei et al., 2016*), the compound was preoxidized before being used in aggregation experiments by distributing the solution into 1.5 mL test-tubes (1 mL final volume) and incubating at 60 °C for 72 h without agitation (*Ziaunys et al., 2021a*). The solution's absorbance spectra were scanned every 24 h using a Shimadzu UV-1800 spectrophotometer in the range from 240 nm to 600 nm (1 nm steps, 3 mm pathlength cuvette) and baseline corrected. Prior to measurements, an aliquot of the solution was diluted 100 times by its initial reaction buffer. No significant changes to the absorbance spectra were observed after the 72 h mark, indicating that this time frame is sufficient for a complete oxidation process (Fig. S1). The final solution was then filtered through a 0.22 μm syringe filter and stored at 4 °C. Only the oxidized form of EGCG was used in all further experiments.

Aggregation reactions

Human recombinant insulin powder (Cat. No. 91077C; Sigma–Aldrich, St. Louis, MO, USA) was dissolved in 20% acetic acid (pH ~ 1.8, (*Foderà, Van De Weert & Vestergaard, 2010*)) solutions, containing a range of NaCl concentrations (from 100 mM to 800 mM) to a final protein concentration of 400 μM (ε_{280} = 6,335 M^{-1} cm^{-1}). The insulin stock solutions were then combined with 10 mM ThT (Cat. No. T3516; Sigma-Aldrich, St. Louis, MO, USA) and 10 mM EGCG stock solutions and diluted using their respective 20% acetic acid solutions to a final protein concentration of 200 μM, 100 μM ThT and 25 μM EGCG. Control samples contained an equal volume of 100 mM potassium phosphate (pH 7.4) buffer solution in place of EGCG. The reaction solutions were then distributed into 96-well non-binding plates (Cat. No. 3881; Fisher Scientific, Pittsburgh, PA, USA, final volume 100 μL, six repeats for each condition), which were sealed using Nunc sealing-tape.

Aggregation kinetics were monitored at 60 °C without agitation, using a ClarioStar Plus plate reader (440 nm excitation and 480 nm emission wavelengths) with measurements taken every 5 min. Samples were placed in the 96-well plate in an alternating style (Fig. S2) to avoid any possible non-homogenous temperature variations throughout the plate having an effect on the average aggregation kinetics.

Alpha-synuclein was purified as described previously (*Šneideris et al., 2015*), lyophilized and stored at −20 °C. Prior to aggregation experiments, alpha-synuclein powder was dissolved in 20 mM potassium phosphate (pH 7.4) buffers containing a range of NaCl concentrations (from 100 mM to 800 mM) and filtered through a 0.22 μm syringe filter, after which the protein solution was diluted to 250 μM (ε_{280} = 5960 M^{-1} cm^{-1}). The alpha-synuclein stock solutions were then combined with 10 mM ThT and 10 mM EGCG stock solutions and diluted using their respective buffer solutions to a final protein concentration of 100 μM, 100 μM ThT and 100 μM EGCG. The reaction solutions were distributed to 96-well plates as described previously (final volume 80 μL, each well contained a 3 mm glass bead). Aggregation kinetics were monitored at 37 °C with constant 600 RPM orbital agitation.

Amyloid beta (1–42) was purified as described in Supplemental Material, stored on ice (~5 min) until its concentration was determined by integrating the chromatographic UV absorbance peak (ε_{280} = 1,490 M^{-1} cm^{-1}), after which it was immediately diluted with a 20 mM sodium phosphate (pH 6.3) buffer solution in a 1:2 ratio to yield a pH 7.0 peptide solution. Afterwards, it was further diluted using a 20 mM sodium phopshate (pH 7.0) buffer to reach a peptide concentration of 5 μM. The peptide solution was then combined with 20 mM sodium phosphate (pH 7.0) buffers, containing either 0 or 1.6 M NaCl, 10 mM ThT and 10 mM EGCG stock solutions to a final peptide concentration of 2 μM, 20 μM ThT, 25 μM EGCG and a range of NaCl concentrations (from 0 mM to 700 mM). All buffer, ThT and EGCG solutions were kept at 4 °C prior to use. The reaction solutions were then distributed to a 96-well plate as described previously (final volume 80 μL). Aggregation kinetics were monitored at 25 °C without agitation.

For all three proteins/peptides, the EGCG concentrations were initially optimized to result in a 3 to 4-fold increase in the relative t_{50} values. The half-time (t_{50}), lag time (t_{lag}) and aggregation rate values were determined by fitting each curve with a Boltzmann sigmoidal equation as described previously (*Ziaunys et al., 2021b*).

Fourier-transform infrared (FTIR) spectroscopy

Each condition samples were collected from their respective 96-well plates and combined to a final volume of ~0.6 mL (insulin fibrils) or ~0.48 mL (alpha-synuclein). The combined samples were centrifuged at 12,500 RPM for 20 min, after which the supernatant was removed. The fibril pellets were resuspended into 0.5 mL D_2O with 400 mM NaCl (exchanging the solution to D_2O removes the H_2O-specific absorbance in the Amide I region, while the addition of NaCl improves aggregate sedimentation (*Mikalauskaite et al., 2020*)). This centrifugation and resuspension procedure was repeated 4 times. After the final centrifugation, the fibril pellets were resuspended into 0.1 mL D_2O without NaCl. Each sample was sonicated for 5 s using a Bandelin Sonopuls Ultrasonic homogenizer,

equipped with a MS-72 sonication tip (20% of maximum power, constant sonication). FTIR spectra were acquired as described previously (*Sneideris et al., 2019*) using a Bruker Invenio S FTIR spectrometer. A D_2O spectrum was subtracted from each sample's spectrum, which were then normalized between 1,595 and 1,700 cm^{-1}. All data processing was done using GRAMS software. In the case of amyloid beta, the resulting spectra did not meet the quality necessary for an accurate analysis due to the significantly lower concentration of fibrils and the resulting low signal-to-noise ratio.

ThT and EGCG absorbance assay

Insulin fibrils were prepared by incubating the previously described insulin aggregation reaction solutions in 2.0 mL non-binding test-tubes (2 mL final volume) at 60 °C without agitation for 24 h. The fibril samples were then centrifuged at 12,500 RPM for 20 min and resuspended into 2 mL of 20% acetic acid solutions, containing either 100 mM or 800 mM NaCl. This centrifugation and resuspension procedure was repeated 4 times. After this, both fibril samples were sonicated for 10 min on ice, using a MS-73 sonication tip (40% of maximum power, 30 s sonication/30 s rest intervals). The resulting sonicated fibril solutions were combined with 10 mM ThT and 10 mM EGCG stock solutions, resulting in a 2-fold diluted fibril sample, containing 0 μM, 50 μM or 100 μM ThT and 0 μM, 50 μM or 100 μM EGCG. For control samples, the fibril solution was replaced with a 20% acetic acid solution, containing either 100 mM or 800 mM NaCl.

All samples were then vigorously agitated and mixed for 10 s, incubated at room temperature without agitation for 20 min and centrifuged at 12,500 RPM for 20 min. From each sample, a portion of the supernatant was carefully removed. The supernatant was then scanned using a Shimadzu UV-1800 spectrophotometer in the wavelength range from 240 nm to 600 nm in a 10 mm pathlength cuvette. For each condition, three spectra were scanned, averaged and baseline corrected based on the absorbance value at 600 nm.

RESULTS

The inhibitory potential of oxidized epigallocatechin-3-gallate (further referred to as EGCG) was first examined on insulin, under a range of ionic strength conditions. At 0 mM NaCl, insulin aggregation in the presence of EGCG did not complete in a reasonable timeframe (the aggregation extended into time frames where sample evaporation and dye stability became an issue). When the concentration of NaCl was low (100 mM), the aggregation half-time (t_{50}) had an average value of ~1,700 min in the presence of EGCG, while the control sample's t_{50} was ~370 min (Fig. 1A). In this case, the relative t_{50} value was ~4, indicating a strong aggregation-inhibiting effect (Fig. 1B). When the concentration of NaCl was increased to 200 mM, the relative t_{50} value remained similar, however, both the control and EGCG samples aggregated significantly quicker. Further increase in ionic strength led to a considerable shift in the relative t_{50} values (from ~4 to ~1.5–2), while the half-times of samples continued to decrease with rising NaCl concentrations. A one-way ANOVA Bonferroni means comparison analysis displayed a significant difference between the 100–200 mM and 300–800 mM group relative t_{50} values ($p = 0.01$) with no significant variation within each group. The decreasing t_{50} values also greatly

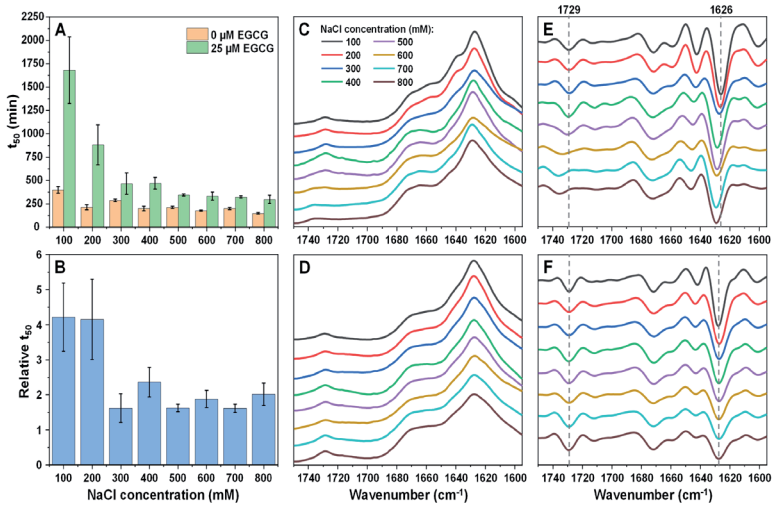

Figure 1 Insulin (200 μM) aggregation half-time (t_{50}) values and resulting fibril FTIR spectra. Insulin aggregation t_{50} values in the absence or presence of 25 μM EGCG (A) and relative t_{50} values (B). Relative t_{50} values were obtained by calculating the ratio between average t_{50} of samples with EGCG and average t_{50} without EGCG. FTIR spectra of insulin fibrils prepared under a range of NaCl concentrations in the absence (C) or presence (D) of 25 μM EGCG and their second derivatives (E and F respectively). Dotted lines show second derivative positions, which experience variation between different spectra. For each condition, half-time values were calculated from six repeats, error bars are for one standard deviation. All raw kinetic and FTIR data is available as Supplemental Information.

Full-size DOI: 10.7717/peerj.12381/fig-1

reduced the stochasticity of spontaneous aggregation (Fig. S3), which was quite large at lower ionic strength conditions (likely due to a significantly longer lag time, coupled with the spontaneous nature of unseeded aggregation (*Foderà et al., 2008b*)). The lag time (t_{lag}) of all reactions followed a similar tendency as the t_{50} values and the aggregation rate did not experience significant differences under all conditions (Fig. S6). Plotting a lag time dependence on the square root of NaCl concentration (*Zhou & Pang, 2018*; *Perez-Jimenez et al., 2004*) (Fig. S6) revealed that there was a discontinuity at 300 mM NaCl, after which the increasing ionic strength had a significantly lesser effect on the lag time.

The end-point fluorescence intensity values of fibril-bound ThT were not used as a means of identifying the inhibitory potential of EGCG for any of the three proteins/peptides used in this study. This was due to the fact that exogenous compounds may cause ThT fluorescence intensity variations by direct interaction, inner filter or non-conjugated FRET effects (*Hudson et al., 2009*; *Ran et al., 2011*; *Ziaunys, Sakalauskas & Smirnovas, 2020*). Differences in fibril secondary structure or morphology may also alter its signal intensity (*Ziaunys, Sakalauskas & Smirnovas, 2020*; *Bousset et al., 2013*).

The resulting fibril secondary structures were analysed using FTIR spectroscopy in order to determine whether EGCG and changes in ionic strength had any influence on insulin aggregate conformations. When the reaction solutions did not contain EGCG, insulin fibrils appear to have undergone a structural transition between low and high NaCl

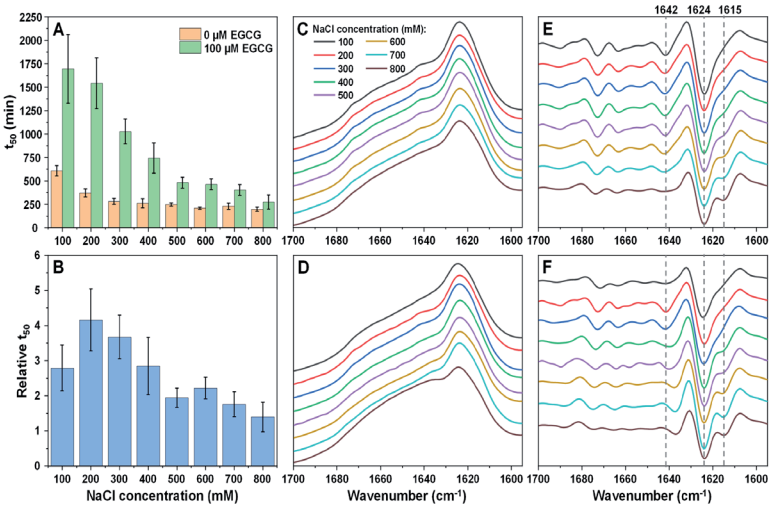

Figure 2 Alpha-synuclein (100 μM) aggregation half-time (t_{50}) values and resulting fibril FTIR spectra. Alpha-synuclein aggregation t_{50} values in the absence or presence of 100 μM EGCG (A) and relative t_{50} values (B). Relative t_{50} values were obtained by calculating the ratio between average t_{50} of samples with EGCG and average t_{50} without EGCG. FTIR spectra of alpha-synuclein fibrils prepared under a range of NaCl concentrations in the absence (C) or presence (D) of 100 μM EGCG and their second derivatives (E and F respectively). Dotted lines show second derivative positions, which experience variation between different spectra. For each condition, half-time values were calculated from six repeats, error bars are for one standard deviation. All raw kinetic and FTIR data is available as Supplemental Information. Full-size DOI: 10.7717/peerj.12381/fig-2

concentration conditions. At low ionic strength (100–200 mM NaCl), the FTIR spectra (Fig. 1C) main maxima are at 1,626 cm^{-1}, which is associated with the presence of beta-sheet hydrogen bonds (*Barth, 2007*). The second derivative spectra (Fig. 1E) also contain minima at 1,642 cm^{-1} (weaker beta-sheet hydrogen bonds), 1,659 cm^{-1} and 1,672 cm^{-1} (turn/loop motifs), as well as 1,729 cm^{-1} (deuterated carboxyl groups (*Surmacz-Chwedoruk et al., 2012*)). When ionic strength is higher, the main maximum shifts to 1,628–1,629 cm^{-1}, indicating weaker beta-sheet hydrogen bonding than in the lower ionic strength samples. The band associated with deuterated carboxyl groups (1,729 cm^{-1}) is also reduced at higher NaCl concentrations.

When the reaction solutions contained 25 μM EGCG, the main FTIR spectrum (Fig. 1D) maximum position is at 1,627–1,628 cm^{-1} under all ionic strength conditions. Unlike insulin fibrils without EGCG, the spectra of fibrils, prepared at different NaCl concentrations, are very similar and only a slight decreasing of 1,642 cm^{-1} band can be observed in second derivative spectra with increased ionic strength (Fig. 1F). This means that the presence of the inhibitor is also a factor in determining the conformation of the aggregate and it stabilises a certain secondary structure.

When alpha-synuclein was aggregated under a range of ionic strength conditions with and without EGCG, we observed a similar reduction in t_{50} values with increasing NaCl concentration (Fig. 2A), as was the case for insulin aggregation. However, the change in

relative t_{50} was quite different (Fig. 2B). When the solution's ionic strength was increased from 100 mM to 200 mM NaCl, the relative t_{50} value increased, indicating a stronger inhibitory effect of EGCG. After this point, the value gradually decreased with rising NaCl concentrations, eventually becoming within margin of error to the control. A Bonferroni means comparison revealed that the relative t_{50} values above 400 mM NaCl were significantly different ($p = 0.01$) from the 200 mM NaCl condition values. Unlike with insulin aggregation, there was no sudden shift in the relative t_{50} values, however, the higher stochasticity at low ionic strength conditions was quite similar (Fig. S4). As with insulin at 0 mM NaCl conditions, alpha-synuclein did not aggregate in a reasonable timeframe when in the presence of EGCG (the aggregation began to occur only after ~2,000 min for samples without EGCG, which created the issue of sample evaporation and ThT instability (*Foderà et al., 2008a*)). The aggregation rate values were mostly within margin of error without any major deviations, while t_{lag} values followed a similar tendency as t_{50} values (Fig. S6). Unlike with insulin, a discontinuity in the lag time dependence on the square root of NaCl concentration only appeared at 500 mM NaCl (Fig. S6).

The FTIR spectra of alpha-synuclein fibrils prepared in the absence (Figs. 2C and 2E) or presence (Figs. 2D and 2F) of EGCG show a gradual conformational shift with increasing NaCl concentration, reflected by the appearance of a minimum in the second derivative spectra at 1,615 cm^{-1}, which is related to stronger hydrogen bonds in the beta-sheet structure. While the main maxima (and the main minima in the second derivative spectra) all share the same position (1,624 cm^{-1}, related to hydrogen bonds in the beta-sheet structure), the minimum at 1,642 cm^{-1} (weak hydrogen bonds) disappears at the highest ionic strength conditions when there is no EGCG present in solution. When alpha-synuclein aggregates with the inhibitor, this minimum is almost undetectable at low ionic strength conditions (100 mM NaCl), then becomes visible (200–300 mM NaCl) and then shifts towards 1,637 cm^{-1}. EGCG also appears to cause minor variations in the region associated with turn/loop motifs (1,660–1,680 cm^{-1}) upon an increasing concentration of NaCl. Overall, the structural changes seem to be a lot less sudden than was the case with insulin fibrils, which falls in line with the gradual change to relative t_{50} values.

In the case of amyloid beta (1–42), it was possible to track the impact of ionic strength on its aggregation and the effect of EGCG from 0 mM NaCl due to the relatively quick aggregation reaction times (Fig. S5). The first notable thing is that the t_{50} values experienced a higher change when in the absence of EGCG, where they shifted from ~50 min at 0 mM NaCl to 20–30 min at higher NaCl concentrations (Fig. 3A). The t_{50} values in the presence of EGCG only appeared to experience minimal variations. The relative t_{50} values (Fig. 3B) did not follow any significant trend, as all values were mostly within margin of error. However, a Bonferroni means comparison analysis revealed that the 0 mM NaCl relative t_{50} values were significantly different ($p = 0.01$) from the 300–600 mM NaCl condition values. Unlike with both other proteins, the inhibitory effect of EGCG did not undergo considerable changes, as even 700 mM NaCl conditions resulted in ~2.5 times higher t_{50} values when compared to the control. The t_{lag} and aggregation rate values also did not display any significant variations, however, the lag time

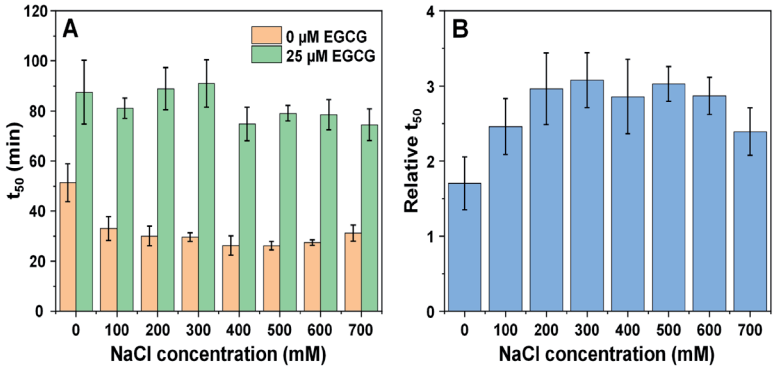

Figure 3 Amyloid-beta (1–42) (2 μM) aggregation half-time (t_{50}) (A) and relative t_{50} values (B) in the absence or presence of 25 μM EGCG. Relative t_{50} values were obtained by calculating the ratio between average t_{50} of samples with EGCG and average t_{50} without EGCG. For each condition, half-time values were calculated from six repeats, error bars are for one standard deviation. All raw kinetic data is available as Supplemental Information. Full-size DOI: 10.7717/peerj.12381/fig-3

dependence on the square root of NaCl concentration was distinct from both the insulin and alpha-synuclein cases. There was a positive trend up to 300 mM NaCl, followed by a linear decrease at increasing ionic strength conditions. This indicates that the charge screening effect of NaCl (up to 300 mM) had a positive effect on the lag time values (Fig. S6). In the case of amyloid beta, it was not possible to obtain high quality FTIR spectra due to the low peptide concentration (2 μM). Using a higher amount of each sample in the described FTIR method or exchanging the fibrils into D_2O with 10 kDa concentrators also did not yield sufficient quality results. Such a low concentration and the presence of a relatively high amount of EGCG also prohibited the use of other fibril characterization methods, such as CD spectroscopy or dye-binding assays.

Since it is known that the solution's ionic strength may influence fibril and amyloidophilic molecule interactions, the observed results could be caused by several ionic-strength-related factors, such as EGCG-fibril affinity and interaction or competitive binding with ThT. In order to examine if different NaCl concentrations have an effect ThT and EGCG interactions, the dye molecule absorbance spectra were scanned when they are separately (after which the spectra were combined) and together, as described in the Materials and Method section. When the combined spectra of ThT and EGCG are compared to the spectra of ThT-EGCG mixtures under 100 mM and 800 mM NaCl conditions, there do not appear to be any major differences (Figs. S7A and S7B). A change in their interaction would likely be seen as a shift in spectra maximum positions or lower/higher absorbance at their characteristic bands, however, this is not the case.

To test the competitive binding hypothesis, both ThT and EGCG were mixed with insulin fibrils under 100 mM and 800 mM NaCl conditions (separately and together), after which the fibril samples were centrifuged and their supernatant absorbance spectra were scanned. In the case of 50 μM ThT and 50 μM EGCG, we observed a lower absorbance value at 412 nm (characteristic maximum ThT absorbance peak) and an increase in

absorbance at 300 nm (position where both EGCG and ThT absorb light) when comparing low and high ionic strength conditions (Figs. S7C and S7D). A similar effect was seen when 100 μM ThT and 100 μM EGCG were used (Figs. S7E and S7F). This indicates that higher ionic strength leads to more bound ThT molecules (which is known to be the case for insulin and alpha-synuclein (*Mikalauskaite et al., 2020*)) and also results in less bound EGCG. These differences, however, are not significant enough to constitute this process as the sole reason for the loss of EGCG inhibitory potential at higher NaCl concentrations.

DISCUSSION

Taking all of these results into consideration, it is quite clear that ionic strength plays a major role in both amyloid aggregation, as well as determining the inhibitory potential of EGCG. However, the interplay between ionic strength, EGCG and amyloid proteins appears to be a lot more complex than one would initially assume. The first interesting aspect is that a different concentration of EGCG was required for each protein/peptide to achieve a 3 to 4-fold increase in relative t_{50} values. For insulin (pI ~ 5.3, condition pH = 2.4) the protein/EGCG ratio was 8:1, while for alpha-synuclein (pI ~ 4.7, condition pH = 7.4) it was 1:1. Despite an eight times different ratio, the highest increase in t_{50} values was 4-fold (with similar t_{50} values), indicating that either protein charge or the type of aggregation intermediates may play an important role in the inhibition process. Conversely, amyloid-beta (pI ~ 5.8, condition pH = 7.0) required a 0.08:1 ratio to even come close to similar inhibition. This may be due to the relatively fast aggregation of amyloid-beta when compared to both other proteins, thus significantly reducing the possibility of EGCG inhibiting the process.

The second factor is the effect that NaCl concentration has on fibril secondary structure. It is a known fact that the solution's ionic strength can lead to the formation of distinct fibril conformations (*Bousset et al., 2013*; *Gaspar et al., 2020*) and the potential inhibitor molecule may have a weaker or stronger effect, based on its interaction with the aggregate. In this case, we observe both gradual (alpha-synuclein) and quick (insulin) fibril structural variations with increasing ionic strength. The second factor is that EGCG, by itself, induces such structural variations, as seen in the case of insulin fibrils at 100 mM NaCl. Since both NaCl and EGCG can influence aggregate conformations, these factors are likely at play simultaneously, which increases the overall complexity of the fibrillization process.

Another interesting aspect is that there seems to be an optimal ionic strength, which showcases the best inhibitory potential of EGCG. Based on relative half-time values, low ionic strength conditions favour the strongest inhibition for insulin and alpha-synuclein, while for amyloid-beta (1–42) it appears to be almost identical at all NaCl concentrations above 0 mM. Conversely, certain conditions reduce the potency of EGCG to such a point, that it may almost appear as ineffective. Examining the charge screening of NaCl for each protein, it seems that alpha-synuclein is less susceptible to the screening effect when compared to insulin, while for amyloid-beta, an initial increase in ionic strength slightly improved the peptide-EGCG interaction (Fig. S6). Taking into account that this is just one

out of a whole plethora of potential anti-aggregation compounds, it is very likely that other compound effectiveness also depends on the solution's ionic strength. This leads to the possibility of certain drug molecules being classified as not having any effect on amyloid aggregation if the reaction conditions are not suitable for them specifically. A similar observation was also made with EGCG and environmental conditions, where the compound was only potent at certain solution pH values (*Sternke-Hoffmann et al., 2020*).

We also have to discuss the possible role that ionic strength has in determining EGCG effectiveness. The first possibility is that the increasing NaCl concentration makes it difficult for EGCG to interact with either the native state protein or the various aggregation intermediates through electrostatic effects. This does not appear to be an issue when it interacts with fibrils, as both 100 mM and 800 mM NaCl led to a similar number of bound EGCG molecules. The second possibility is that EGCG is only effective against certain types of aggregation intermediate species, as such interaction with intermediates has been shown previously (*Andrich & Bieschke, 2015*). If ionic strength changes what type of nuclei or protofibril species form, inhibition may not occur for the different type of aggregate. This does not explain, however, why EGCG seems to also change the conformation of aggregates, unless it does so by preventing certain nuclei from forming. The third probable cause is related to the aggregation kinetics. In general, amyloid fibril formation proceeds slower at low ionic strength conditions, as seen for all three proteins/peptides used in this study. If new nuclei appear less frequently, then the same concentration of EGCG would have a higher chance of preventing their formation and subsequent elongation into fibrils. It is also possible that multiple factors are at play simultaneously, resulting in a highly complex environment-based inhibitor-protein interaction.

CONCLUSIONS

These results show that each amyloidogenic protein/peptide may have specific ionic strength conditions where they are most susceptible to the inhibitory effect of EGCG. It appears that the inhibitor is generally most potent at lower ionic strength conditions for insulin and alpha-synuclein and an increasing concentration of NaCl reduces its effectiveness. This is not the case for amyloid-beta (1–42), where inhibition is quite similar under all ionic strength conditions above 100 mM NaCl. In addition, the interplay between ionic strength and the inhibitor molecule is highly complex, which affects multiple aggregation parameters, such as aggregation kinetics and fibril conformations. Considering that this is just one of the multiple possible variables in protein aggregation studies, it showcases the importance of taking into account every environmental factor during amyloid formation.

ADDITIONAL INFORMATION AND DECLARATIONS

Funding

This research was funded by the grant no. S-SEN-20-3 from the Research Council of Lithuania. The funders had no role in study design, data collection and analysis, decision to publish, or preparation of the manuscript.

Grant Disclosures

The following grant information was disclosed by the authors:
Research Council of Lithuania: S-SEN-20-3.

Competing Interests

The authors declare that they have no competing interests.

Author Contributions

- Mantas Ziaunys conceived and designed the experiments, performed the experiments, analyzed the data, prepared figures and/or tables, authored or reviewed drafts of the paper, and approved the final draft.
- Kamile Mikalauskaite performed the experiments, authored or reviewed drafts of the paper, and approved the final draft.
- Andrius Sakalauskas performed the experiments, authored or reviewed drafts of the paper, and approved the final draft.
- Vytautas Smirnovas conceived and designed the experiments, analyzed the data, authored or reviewed drafts of the paper, and approved the final draft.

Data Availability

The following information was supplied regarding data availability:

The raw data is available in the Supplemental Files.

Supplemental Information

Supplemental information for this article can be found online at http://dx.doi.org/10.7717/peerj.12381#supplemental-information.

REFERENCES

An T-T, Feng S, Zeng C-M. 2017. Oxidized epigallocatechin gallate inhibited lysozyme fibrillation more strongly than the native form. *Redox Biology* **11**:315–321 DOI 10.1016/j.redox.2016.12.016.

Andrich K, Bieschke J. 2015. The effect of (−)-epigallo-catechin-(3)-gallate on amyloidogenic proteins suggests a common mechanism. In: Vassallo N, ed. *Natural Compounds as Therapeutic Agents for Amyloidogenic Diseases: Advances in Experimental Medicine and Biology.* Vol. 863. Cham: Springer.

Arthur KC, Calvo A, Price TR, Geiger JT, Chiò A, Traynor BJ. 2016. Projected increase in amyotrophic lateral sclerosis from 2015 to 2040. *Nature Communications* **7(1)**:12408 DOI 10.1038/ncomms12408.

Baker KR, Rice L. 2012. The amyloidoses: clinical features, diagnosis and treatment. *Methodist DeBakey Cardiovascular Journal* **8(3)**:3–7 DOI 10.14797/mdcj-8-3-3.

Barth A. 2007. Infrared spectroscopy of proteins: biochimica et biophysica acta (BBA). *Bioenergetics* **1767(9)**:1073–1101 DOI 10.1016/j.bbabio.2007.06.004.

Bousset L, Pieri L, Ruiz-Arlandis G, Gath J, Jensen PH, Habenstein B, Madiona K, Olieric V, Böckmann A, Meier BH, Melki R. 2013. Structural and functional characterization of two alpha-synuclein strains. *Nature Communications* **4(1)**:2575 DOI 10.1038/ncomms3575.

Chiti F, Dobson CM. 2017. Protein misfolding, amyloid formation, and human disease: a summary of progress over the last decade. *Annual Review of Biochemistry* **86(1)**:27–68 DOI 10.1146/annurev-biochem-061516-045115.

Cohen SIA, Vendruscolo M, Dobson CM, Knowles TPJ. 2012. From macroscopic measurements to microscopic mechanisms of protein aggregation. *Journal of Molecular Biology* **421(2–3)**:160–171 DOI 10.1016/j.jmb.2012.02.031.

Colby DW, Giles K, Legname G, Wille H, Baskakov IV, DeArmond SJ, Prusiner SB. 2009. Design and construction of diverse mammalian prion strains. *Proceedings of the National Academy of Sciences of the United States of America* **106(48)**:20417–20422 DOI 10.1073/pnas.0910350106.

Cummings J, Lee G, Ritter A, Sabbagh M, Zhong K. 2020. Alzheimer's disease drug development pipeline: 2020. *Alzheimer's & Dementia: Translational Research & Clinical Interventions* **6(1)**:1–29 DOI 10.1002/trc2.12050.

Findeis MA. 2000. Approaches to discovery and characterization of inhibitors of amyloid β-peptide polymerization. *Biochimica et Biophysica Acta - Molecular Basis of Disease* **1502(1)**:76–84 DOI 10.1016/S0925-4439(00)00034-X.

Foderà V, Groenning M, Vetri V, Librizzi F, Spagnolo S, Cornett C, Olsen L, van de Weert M, Leone M. 2008a. Thioflavin T hydroxylation at basic pH and its effect on amyloid fibril detection. *The Journal of Physical Chemistry B* **112(47)**:15174–15181 DOI 10.1021/jp805560c.

Foderà V, Librizzi F, Groenning M, Van De Weert M, Leone M. 2008b. Secondary nucleation and accessible surface in insulin amyloid fibril formation. *Journal of Physical Chemistry B* **112(12)**:3853–3858 DOI 10.1021/jp710131u.

Foderà V, Van De Weert M, Vestergaard B. 2010. Large-scale polymorphism and auto-catalytic effect in insulin fibrillogenesis. *Soft Matter* **6(18)**:4413–4419 DOI 10.1039/c0sm00169d.

Fusco G, Sanz-Hernandez M, Ruggeri FS, Vendruscolo M, Dobson CM, De Simone A. 2018. Molecular determinants of the interaction of EGCG with ordered and disordered proteins. *Biopolymers* **109(10)**:e23117 DOI 10.1002/bip.23117.

Gaspar R, Lund M, Sparr E, Linse S. 2020. Anomalous salt dependence reveals an interplay of attractive and repulsive electrostatic interactions in α-synuclein fibril formation. *QRB Discovery* **1**:657 DOI 10.1017/qrd.2020.7.

Giorgetti S, Greco C, Tortora P, Aprile F. 2018. Targeting amyloid aggregation: an overview of strategies and mechanisms. *International Journal of Molecular Sciences* **19(9)**:2677 DOI 10.3390/ijms19092677.

Hebert LE, Weuve J, Scherr PA, Evans DA. 2013. Alzheimer disease in the United States (2010–2050) estimated using the 2010 census. *Neurology* **80(19)**:1778–1783 DOI 10.1212/WNL.0b013e31828726f5.

Huang LK, Chao SP, Hu CJ. 2020. Clinical trials of new drugs for Alzheimer disease. *Journal of Biomedical Science* **27(1)**:1–13 DOI 10.1186/s12929-019-0609-7.

Hudson SA, Ecroyd H, Kee TW, Carver JA. 2009. The thioflavin T fluorescence assay for amyloid fibril detection can be biased by the presence of exogenous compounds. *FEBS Journal* **276(20)**:5960–5972 DOI 10.1111/j.1742-4658.2009.07307.x.

Jain S, Udgaonkar JB. 2010. Salt-Induced modulation of the pathway of amyloid fibril formation by the mouse prion protein. *Biochemistry* **49(35)**:7615–7624 DOI 10.1021/bi100745j.

Kawai M, Wray JS, Güth K. 1990. Effect of ionic strength on crossbridge kinetics as studied by sinusoidal analysis, ATP hydrolysis rate and x-ray diffraction techniques in chemically skinned rabbit psoas fibres. *Journal of Muscle Research and Cell Motility* **11(5)**:392–402 DOI 10.1007/BF01739760.

Knowles TPJ, Vendruscolo M, Dobson CM. 2014. The amyloid state and its association with protein misfolding diseases. *Nature Reviews Molecular Cell Biology* **15(6)**:384–396 DOI 10.1038/nrm3810.

Landau M, Sawaya MR, Faull KF, Laganowsky A, Jiang L, Sievers SA, Liu J, Barrio JR, Eisenberg D. 2011. Towards a pharmacophore for amyloid. *PLOS Biology* **9(6)**:25–27 DOI 10.1371/journal.pbio.1001080.

Liu X, Zhou S, Shi D, Bai Q, Liu H, Yao X. 2018. Influence of EGCG on α-synuclein (αS) aggregation and identification of their possible binding mode: a computational study using molecular dynamics simulation. *Chemical Biology & Drug Design* **91(1)**:162–171 DOI 10.1111/cbdd.13067.

Maurer MS, Schwartz JH, Gundapaneni B, Elliott PM, Merlini G, Waddington-Cruz M, Kristen AV, Grogan M, Witteles R, Damy T, Drachman BM, Shah SJ, Hanna M, Judge DP, Barsdorf AI, Huber P, Patterson TA, Riley S, Schumacher J, Stewart M, Sultan MB, Rapezzi C. 2018. Tafamidis treatment for patients with transthyretin amyloid cardiomyopathy. *New England Journal of Medicine* **379(11)**:1007–1016 DOI 10.1056/NEJMoa1805689.

Mehta D, Jackson R, Paul G, Shi J, Sabbagh M. 2017. Why do trials for Alzheimer's disease drugs keep failing? A discontinued drug perspective for 2010–2015. *Expert Opinion on Investigational Drugs* **26(6)**:735–739 DOI 10.1080/13543784.2017.1323868.

Mikalauskaite K, Ziaunys M, Sneideris T, Smirnovas V. 2020. Effect of ionic strength on thioflavin-T affinity to amyloid fibrils and its fluorescence intensity. *International Journal of Molecular Sciences* **21(23)**:8916 DOI 10.3390/ijms21238916.

Morel B, Varela L, Azuaga AI, Conejero-Lara F. 2010. Environmental conditions affect the kinetics of nucleation of amyloid fibrils and determine their morphology. *Biophysical Journal* **99(11)**:3801–3810 DOI 10.1016/j.bpj.2010.10.039.

Nettleton EJ, Tito P, Sunde M, Bouchard M, Dobson CM, Robinson CV. 2000. Characterization of the oligomeric states of insulin in self-assembly and amyloid fibril formation by mass spectrometry. *Biophysical Journal* **79(2)**:1053–1065 DOI 10.1016/S0006-3495(00)76359-4.

Ngo ST, Truong DT, Tam NM, Nguyen MT. 2017. EGCG inhibits the oligomerization of amyloid beta (16–22) hexamer: theoretical studies. *Journal of Molecular Graphics and Modelling* **76(2321)**:1–10 DOI 10.1016/j.jmgm.2017.06.018.

Nicoud L, Lazzari S, Balderas Barragán D, Morbidelli M. 2015. Fragmentation of amyloid fibrils occurs in preferential positions depending on the environmental conditions. *The Journal of Physical Chemistry B* **119(13)**:4644–4652 DOI 10.1021/acs.jpcb.5b01160.

Noormägi A, Valmsen K, Tõugu V, Palumaa P. 2015. Insulin fibrillization at acidic and physiological pH values is controlled by different molecular mechanisms. *The Protein Journal* **34(6)**:398–403 DOI 10.1007/s10930-015-9634-x.

Park J, Egolum U, Parker S, Andrews E, Ombengi D, Ling H. 2020. Tafamidis: a first-in-class transthyretin stabilizer for transthyretin amyloid cardiomyopathy. *Annals of Pharmacotherapy* **54(5)**:470–477 DOI 10.1177/1060028019888489.

Perez-Jimenez R, Godoy-Ruiz R, Ibarra-Molero B, Sanchez-Ruiz JM. 2004. The efficiency of different salts to screen charge interactions in proteins: a hofmeister effect? *Biophysical Journal* **86(4)**:2414–2429 DOI 10.1016/S0006-3495(04)74298-8.

Petkova AT, Leapman RD, Guo Z, Yau W-M, Mattson MP, Tycko R. 2005. Self-propagating, molecular-level polymorphism in Alzheimer's beta-amyloid fibrils. *Science* **307(5707)**:262–265 DOI 10.1126/science.1105850.

Ran C, Zhao W, Moir RD, Moore A. 2011. Non-conjugated small molecule FRET for differentiating monomers from higher molecular weight amyloid beta species. *PLOS ONE* **6(4)**:e19362 DOI 10.1371/journal.pone.0019362.

Sakalauskas A, Ziaunys M, Smirnovas V. 2019. Concentration-dependent polymorphism of insulin amyloid fibrils. *PeerJ* **7(13)**:e8208 DOI 10.7717/peerj.8208.

Šneideris T, Baranauskienė L, Cannon JG, Rutkienė R, Meškys R, Smirnovas V. 2015. Looking for a generic inhibitor of amyloid-like fibril formation among flavone derivatives. *PeerJ* **3**:e1271 DOI 10.7717/peerj.1271.

Sneideris T, Darguzis D, Botyriute A, Grigaliunas M, Winter R, Smirnovas V. 2015. pH-Driven polymorphism of insulin amyloid-like fibrils. *PLOS ONE* **10(8)**:e0136602 DOI 10.1371/journal.pone.0136602.

Sneideris T, Sakalauskas A, Sternke-Hoffmann R, Peduzzo A, Ziaunys M, Buell AK, Smirnovas V. 2019. The environment is a key factor in determining the anti-amyloid efficacy of EGCG. *Biomolecules* **9(12)**:1–17 DOI 10.3390/biom9120855.

Sternke-Hoffmann R, Peduzzo A, Bolakhrif N, Haas R, Buell AK. 2020. The aggregation conditions define whether EGCG is an inhibitor or enhancer of α-synuclein amyloid fibril formation. *International Journal of Molecular Sciences* **21(6)**:1995 DOI 10.3390/ijms21061995.

Surmacz-Chwedoruk W, Nieznańska H, Wójcik S, Dzwolak W. 2012. Cross-seeding of fibrils from two types of insulin induces new amyloid strains. *Biochemistry* **51(47)**:9460–9469 DOI 10.1021/bi301144d.

Tanaka M, Collins SR, Toyama BH, Weissman JS. 2006. The physical basis of how prion conformations determine strain phenotypes. *Nature* **442(7102)**:585–589 DOI 10.1038/nature04922.

Tavanti F, Pedone A, Menziani MC. 2020. Insights into the effect of curcumin and (−)-epigallocatechin-3-gallate on the aggregation of aβ(1-40) monomers by means of molecular dynamics. *International Journal of Molecular Sciences* **21(15)**:1–15 DOI 10.3390/ijms21155462.

Wang S-H, Dong X-Y, Sun Y. 2012. Effect of (−)-epigallocatechin-3-gallate on human insulin fibrillation/aggregation kinetics. *Biochemical Engineering Journal* **63**:38–49 DOI 10.1016/j.bej.2012.02.002.

Wei Y, Chen P, Ling T, Wang Y, Dong R, Zhang C, Zhang L, Han M, Wang D, Wan X, Zhang J. 2016. Certain (−)-epigallocatechin-3-gallate (EGCG) auto-oxidation products (EAOPs) retain the cytotoxic activities of EGCG. *Food Chemistry* **204**:218–226 DOI 10.1016/j.foodchem.2016.02.134.

Williams P, Sorribas A, Howes MJR. 2011. Natural products as a source of Alzheimer's drug leads. *Natural Product Reports* **28(1)**:48–77 DOI 10.1039/C0NP00027B.

Zhou HX, Pang X. 2018. Electrostatic interactions in protein structure, folding, binding, and condensation. *Chemical Reviews* **118(4)**:1691–1741 DOI 10.1021/acs.chemrev.7b00305.

Zhuang X, Zhao B, Liu S, Song F, Cui F, Liu Z, Li Y. 2016. Noncovalent interactions between superoxide dismutase and flavonoids studied by native mass spectrometry combined with molecular simulations. *Analytical Chemistry* **88(23)**:11720–11726 DOI 10.1021/acs.analchem.6b03359.

Ziaunys M, Mikalauskaite K, Sakalauskas A, Smirnovas V. 2021a. Using lysozyme amyloid fibrils as a means of scavenging aggregation-inhibiting compounds. *Biotechnology Journal* **16(9)**:2100138 DOI 10.1002/biot.202100138.

Ziaunys M, Sakalauskas A, Mikalauskaite K, Snieckute R, Smirnovas V. 2021b. Temperature-dependent structural variability of prion protein amyloid fibrils. *International Journal of Molecular Sciences* **22(10)**:5075 DOI 10.3390/ijms22105075.

Ziaunys M, Sakalauskas A, Smirnovas V. 2020. Identifying insulin fibril conformational differences by thioflavin-T binding characteristics. *Biomacromolecules* **21(12)**:4989–4997 DOI 10.1021/acs.biomac.0c01178.

Ziaunys M, Sneideris T, Smirnovas V. 2018. Self-inhibition of insulin amyloid-like aggregation. *Physical Chemistry Chemical Physics* **20(43)**:27638–27645 DOI 10.1039/C8CP04838J.

Zidar J, Merzel F. 2011. Probing amyloid-beta fibril stability by increasing ionic strengths. *Journal of Physical Chemistry B* **115(9)**:2075–2081 DOI 10.1021/jp109025b.

International Journal of
Molecular Sciences

MDPI

Article

Polymorphism of Alpha-Synuclein Amyloid Fibrils Depends on Ionic Strength and Protein Concentration

Mantas Ziaunys *, Andrius Sakalauskas, Kamile Mikalauskaite and Vytautas Smirnovas

Institute of Biotechnology, Life Sciences Centre, Vilnius University, 10257 Vilnius, Lithuania; andrius.sakalauskas@gmc.vu.lt (A.S.); kamile.mikalauskaite@gmc.vu.lt (K.M.); vytautas.smirnovas@bti.vu.lt (V.S.)
* Correspondence: mantas.ziaunys@gmc.vu.lt

Abstract: Protein aggregate formation is linked with multiple amyloidoses, including Alzheimer's and Parkinson's diseases. Currently, the understanding of such fibrillar structure formation and propagation is still not sufficient, the outcome of which is a lack of potent, anti-amyloid drugs. The environmental conditions used during in vitro protein aggregation assays play an important role in determining both the aggregation kinetic parameters, as well as resulting fibril structure. In the case of alpha-synuclein, ionic strength has been shown as a crucial factor in its amyloid aggregation. In this work, we examine a large sample size of alpha-synuclein aggregation reactions under thirty different ionic strength and protein concentration combinations and determine the resulting fibril structural variations using their dye-binding properties, secondary structure and morphology. We show that both ionic strength and protein concentration determine the structural variability of alpha-synuclein amyloid fibrils and that sometimes even identical conditions can result in up to four distinct types of aggregates.

Keywords: alpha-synuclein; amyloid; aggregation; ionic strength; polymorphism

Citation: Ziaunys, M.; Sakalauskas, A.; Mikalauskaite, K.; Smirnovas, V. Polymorphism of Alpha-Synuclein Amyloid Fibrils Depends on Ionic Strength and Protein Concentration. *Int. J. Mol. Sci.* **2021**, *22*, 12382. https://doi.org/10.3390/ijms222212382

Academic Editor: Yuri Lyubchenko

Received: 4 November 2021
Accepted: 16 November 2021
Published: 17 November 2021

1. Introduction

Protein amyloid aggregation into insoluble fibrillar aggregates is linked with the onset and progression of multiple amyloidoses [1], including the widespread neurodegenerative Alzheimer's and Parkinson's diseases [2,3]. Despite years of research and growing number of such disorders [4], the overall process of protein aggregate formation is still not fully understood [5]. The complex nature of fibrillization and the resulting types of aggregates has led to the development of very few anti-amyloid drugs [6,7], with most potential compounds failing at various stages of clinical trials [8,9]. Since the number of patients affected by such protein aggregates is estimated to continue to rise over the next few decades [10,11], it is critically important to obtain a better understanding of protein fibrillization in the hopes of finding a potent cure or treatment.

Currently, it is known that multiple environmental factors can alter both the rate and mechanism of amyloid fibril formation. These include: temperature [12–14], agitation [15], protein concentration [16], ionic strength [17,18], denaturant concentration [19], pH [20], liquid-surface interfaces [21] and macromolecular crowding [22]. They affect primary nucleation, elongation, secondary processes (surface-mediated nucleation and fragmentation), fibril length and stability, as well as the structure of final aggregates [23]. Changes in solution pH value or ionic strength have been reported to affect fibril secondary structure/stability [24–26] and their interactions with amyloid-specific compounds, such as thioflavin-T, a fluorescent amyloid probe [26], or epigallocatechin-3-gallate, an aggregation inhibitor [27].

One of the most intensely studied amyloidogenic proteins is the Parkinson's disease-related alpha-synuclein (α-syn) [28]. During in vitro aggregation, it has been observed on multiple occasions that different ionic strength conditions affect the rate of aggregation and can lead to the formation of distinct types of α-syn fibrils [17,18,29,30]. It has also been

reported that α-syn aggregates can undergo slight structural rearrangements when they are resuspended into different ionic strength solutions [26]. Salt concentration also altered their capacity to bind ThT [26] and different fibril types have even been shown to possess distinct ThT-binding properties [31]. In addition, it has recently been observed that small variations in the solution's pH value can significantly alter the effectiveness of anti-amyloid compounds [27,32]. Considering all of these factors, it seems that α-syn amyloid aggregation and the resulting structures are highly susceptible to the environmental conditions, where even a small shift in certain parameters can have a major influence.

Since spontaneous α-syn aggregation is known to be a highly stochastic process [33], there exists a possibility of different types of fibrils forming under the same conditions, as was shown for prion proteins [34]. There may also not be a clear-cut line in the structural transition reported to occur between lower and higher reaction solution ionic strength. For this reason, we tracked the aggregation kinetics of α-syn under six different ionic strength and five different protein concentration conditions, using large sample sizes in each case. The fibril ThT-binding/fluorescence parameters were used as an initial means of identifying sample variations [34,35], which were then examined using Fourier-transform infrared spectroscopy and atomic force microscopy. We show a shift in fibril structure variability based on the initial ionic strength and protein concentration, as well as outlier samples, which contain distinct structural and morphological features.

2. Results

Alpha-synuclein aggregation was tracked under six different ionic strength conditions (0–500 mM NaCl), using five different protein concentrations (50–250 μM), resulting in a total of thirty conditions. In each case, a full 96-well plate of identical reaction mixtures was examined in order to obtain a considerable distribution of kinetic data and fibril samples. The lag time values (Figure 1A) have an expected dependence on both protein and NaCl concentration, where an increase in either parameter reduces the lag time. From a general overview of this data, three observations can be made. First, there is a massive shift in lag time values when going from 0 mM to 100 mM NaCl. Under most protein concentrations, this change is 2- to 4-fold and this tendency does not persist throughout higher NaCl concentrations, where much less significant reductions are seen. In the case of 50 μM α-syn, the 3-fold change occurs between 100 mM and 200 mM NaCl, as opposed to 0–100 mM NaCl, indicating that such a shift depends on both the protein and salt concentration. Secondly, we see that under most conditions, the standard deviation value is quite large, especially taking into consideration the sizable number of repeats. This illustrates the highly stochastic nature of spontaneous α-syn aggregation. Finally, the lag time appears to reach a saturation at higher α-syn concentrations (150–250 μM), where an increase in protein concentration has minimal effect on the time needed for primary nuclei to form.

After the aggregation reaction, all samples were cooled down to 25 °C and resuspended into equal ionic strength (500 mM NaCl) solutions, with equal protein concentrations (10 μM). After this, each sample's bound-ThT excitation-emission matrices (EEM) were scanned. Comparing the average fluorescence intensity of each set, we observe that the 0 mM NaCl sample intensity values are the lowest. They also have an extreme variation in intensity, as in some of the cases (Figure 1B, 200 μM, 250 μM), the standard deviation values are larger than the average value, which indicates a far-from-normal distribution (Figure A1). Under some conditions, there are even small subgroups of samples with either considerably smaller (50 μM α-syn, 500 mM NaCl) or larger (200 μM α-syn, 0 mM NaCl) fluorescence intensity values than the average value of their respective set (Figure A1). They also do not follow the same trend as lag time, with the highest average fluorescence values changing from lower ionic strength and high protein concentration to higher ionic strength and intermediate protein concentration (Figure 1B, green color-coded boxes).

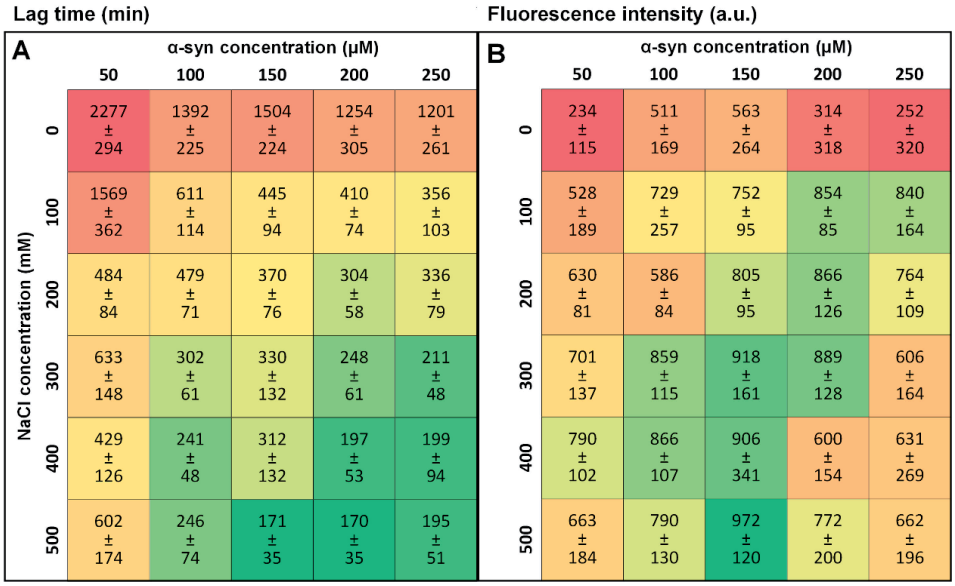

Figure 1. Alpha-synuclein aggregation lag time (**A**) and bound-ThT fluorescence intensity (**B**) dependence on protein concentration and solution ionic strength. Lag time and fluorescence intensity values and standard deviations were calculated from 90–96 repeats. Lag time color-coded boxes indicate a shift from long (red) to short lag times (green). Fluorescence intensity color-coded boxes indicate a shift from low (red) to high (green) intensity. Aggregation kinetic raw data are available as Supplementary Material.

Since there is a massive variance in bound-ThT fluorescence intensity and it is known that different α-syn fibrils can possess specific ThT-binding properties [31], each EEM's "center of mass" was calculated, in order to determine the maximum excitation and emission wavelengths. An overview of all the EEM matrices displays three distinct regions of variability (Figure 2). At low ionic strength conditions, the EEM maximum positions are spread out over a large area, with multiple outliers in each case (samples that do not belong to the main cluster). At intermediate ionic strength conditions, the variability is greatly reduced, with some sample sets having only a single EEM maximum position. Going further, higher ionic strength and protein concentrations increase the variability, but not to the same extent as low ionic strength conditions. Taking all of this into consideration, it appears that both low ionic strength and high ionic strength and protein concentrations lead to the formation of fibrils with distinct ThT-binding properties, while intermediate samples all seem to have one dominant type of binding.

Considering that each sample set has different bound-ThT intensity values and many sets have one or more outliers, the samples were divided into two groups. For the first, one sample was chosen from each condition, which had an average fluorescence intensity and belonged to the main EEM position cluster. For the second group, the lowest and highest fluorescence samples (fringe samples), as well as one or more outliers (very distinct EEM position) from each condition were selected. The aim of both groups was to determine the most common type of fibrils to occur at every given condition and also to analyze fringe samples and outliers.

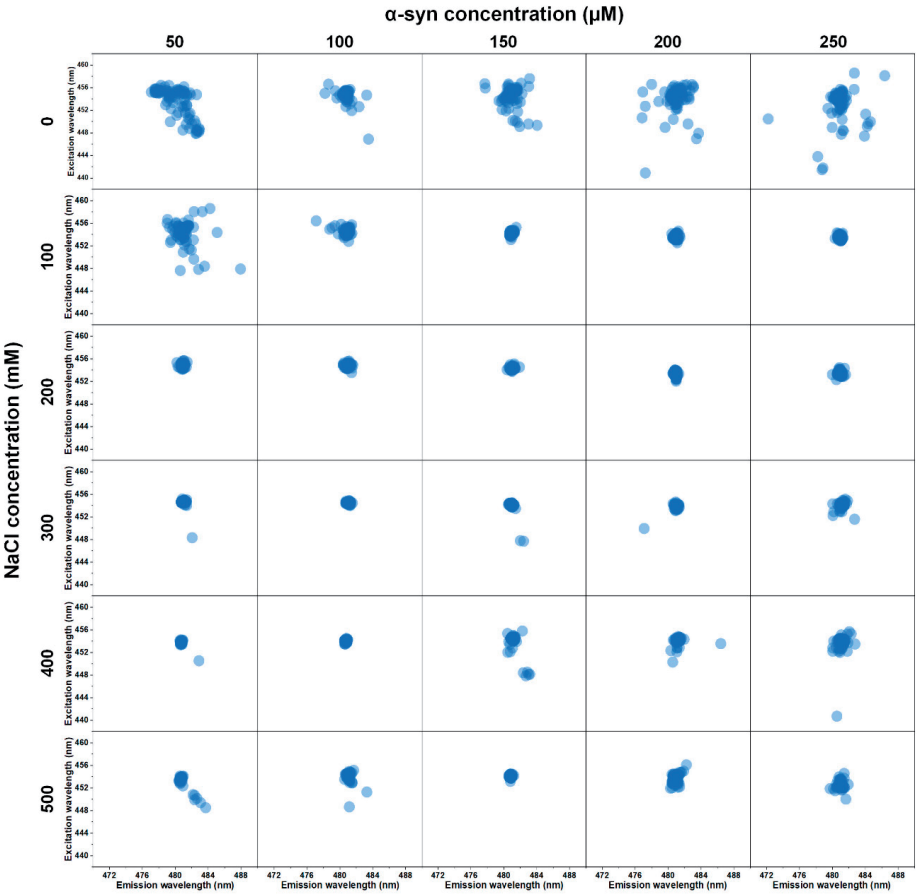

Figure 2. Excitation-emission matrix (EEM) maximum intensity positions of α-syn fibril-bound-ThT, determined for sample sets under thirty different environmental condition. Each position was calculated as described in the Materials and Methods section, at 25 °C, under identical ionic strength (500 mM NaCl) and protein concentration (10 μM) in order to have identical ThT binding conditions. EEM raw data are available as Supplementary Material.

The selected fibrils were replicated under their respective initial reaction conditions, in order to both increase the mass of aggregates for examination by FTIR, as well as to ensure that these structures are capable of self-replication. The FTIR spectra second derivatives of all average samples (first group) reveal that under many conditions, there are two dominant secondary structures (Figure 3). At higher ionic strength conditions, the most dominant type of fibril (Figure 3, light green) displays a main minimum at 1624 cm^{-1} in second derivative of FTIR spectra, which is related to beta-sheet hydrogen bonds [36]. The less pronounced band at 1615 cm^{-1} can be associated with stronger hydrogen bonds in the beta-sheet structure. There are also minima at 1641 cm^{-1} (weak hydrogen bonds), as well as 1663 cm^{-1} and 1673 cm^{-1} (turn/loop motifs). The other dominant structure appears at lower ionic strength conditions (Figure 3, dark green), whose second derivative FTIR spectrum is similar to the aforementioned fibrils, but contains only a minor shoulder at 1615 cm^{-1}, which indicates a lower amount of stronger hydrogen bonds in the beta-sheet structure.

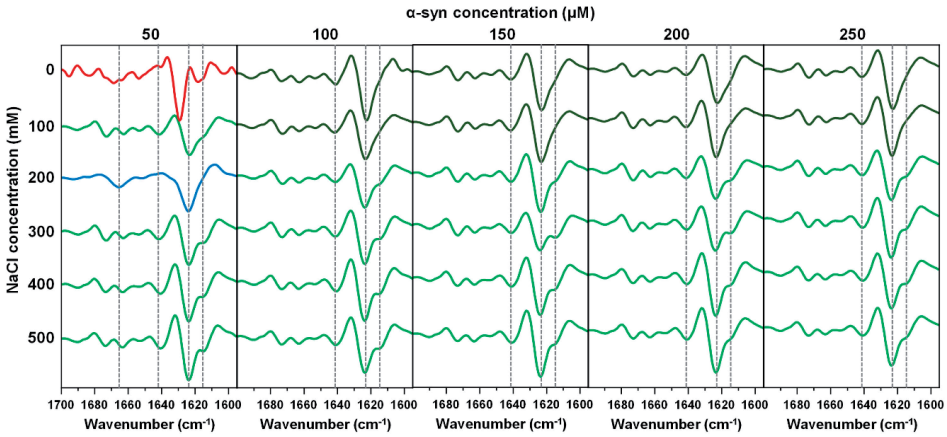

Figure 3. Second derivative FTIR spectra of α-syn fibril samples, which have an average fluorescence intensity and an EEM position in the main cluster. Samples from all thirty conditions were replicated in their respective initial reaction solutions in order to obtain higher quantity of fibrils for a better quality FTIR spectra and to ensure their replication. Spectra which contain significant similarities are color-coded identically. FTIR raw data are available as Supplementary Material.

Interestingly, there are two distinct types of fibrils at lower protein concentrations and ionic strength. In the case of 200 mM NaCl and 50 μM α-syn, we observe a second derivative FTIR spectrum, which has a main minimum at a similar position to both dominant fibril types, but which lacks stronger (1615 cm^{-1}) and weaker (1641 cm^{-1}) hydrogen bonds, and which only contains one minimum in the turn/loop motif region (1665 cm^{-1}). In the case of 0 mM NaCl and 50 μM α-syn, the second derivative spectrum contains a main minimum at 1629 cm^{-1}, which is related to weaker hydrogen bonds in the beta-sheet structure and a less expressed minimum at 1618 cm^{-1} (related to stronger hydrogen bonds), making it highly distinct from the rest.

Seeing as there were four distinct secondary structure aggregates present in the set containing the most likely-to-occur samples, the fringe and outlier fibrils were also examined and compared. In this case, four additional second derivative FTIR spectra were discovered (Figure 4V–VIII), which had different features from the initial four spectra (Figures 3 and 4I–IV). One spectrum, found among 0 mM NaCl samples (Figure 4V), had one main minimum at 1620 cm^{-1} and very few other features, indicating a dominant presence of one type of hydrogen bonds in the beta-sheet structure. Another spectrum, found among low ionic strength and protein concentration (Figure 4VI) had a main minimum at 1623 cm^{-1} and another minimum at 1637 cm^{-1}, which suggests two types of hydrogen bonding, which are dissimilar to other fibrils. The next spectrum, which was observed in many instances among outlier samples (Figure 4VII), shared some similarities to the IV spectrum; however, the main minimum was shifted towards lower wavenumbers, indicating stronger hydrogen bonds. The position at 1619 cm^{-1} was also more of a shoulder, rather than a separate minimum. Finally, the outlier, which only appeared at 500 mM NaCl and 50 μM α-syn, had similar minima to the dominant type fibril spectra (1615 and 1641 cm^{-1}), but had a shifted minima at 1636 cm^{-1}, as well as no clearly discernible turn/loop motifs.

Based on the distribution of these eight spectra (Figure 4B), it is quite clear that the most variability is present at low ionic strength and protein concentration, with 3–4 distinct conformations present in most cases. This variance in fibril secondary structures correlates with the EEM position variability, further solidifying the fact that low ionic strength and protein concentrations lead to not only distinct dominant type of fibril, but also to an abundance of different aggregates.

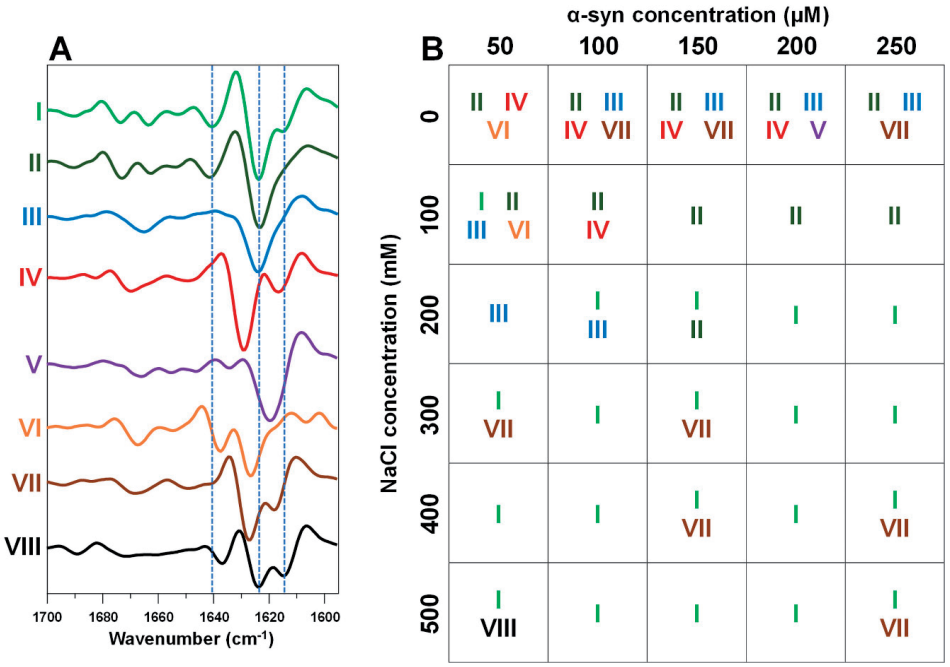

Figure 4. Second derivative FTIR spectra of fringe and outlier α-syn fibril samples (**A**). Samples from all thirty conditions were replicated in their respective initial reaction solutions in order to obtain higher quantity of fibrils for a better quality FTIR spectra and to ensure their replication. Conditions where these spectra were observed (**B**), with each spectrum assigned with a color-coded Roman numeral. FTIR raw data are available as Supplementary Material.

The eight different fibril types were further examined using AFM (Figure 5). Based on a simple visual inspection, the I, II and III samples appear to be quite similar; however, the II sample has significantly wider fibrils (32 nm, as opposed to 26–27 nm). Both IV and V fibrils form long, intertwined networks, which are not observed in any of the other samples and both their height and width are within the margin of error. The VI sample contains mostly aggregate clusters and the fibril height is the lowest out of all eight samples. The VII sample likely contains similar large clusters, as very few non-bound fibrils could be observed. They did, however, have a lower height when compared to most other aggregates, as well as a width similar to the II sample. Finally, the VIII sample had relatively short fibers, which form similar networks and clusters as IV and V fibrils, their height is also similar to the VII sample, while their width does not pertain any notable deviations.

To examine if different morphologies and secondary structures have an effect on fibril self-replication potential, the eight different aggregate types were resuspended into identical ionic strength (500 mM NaCl) and non-aggregated α-syn (50 μM) solutions. Their fibrillization was tracked as described in the Materials and Methods section. Comparing all fibril types, it appears that type IV and VII aggregates lead to the most significant reduction in lag time values (Figure A3A). Oppositely, III, V and VI fibrils have the least seeding potential, with the remaining types causing an intermediate reduction in lag time. The V and VI aggregates also have the lowest elongation rates (Figure A3B), while all other types have significantly higher values. Based on these observations, it appears that there is no clear correlation between seeding capacity and fibril morphology, secondary structure or initial preparation conditions.

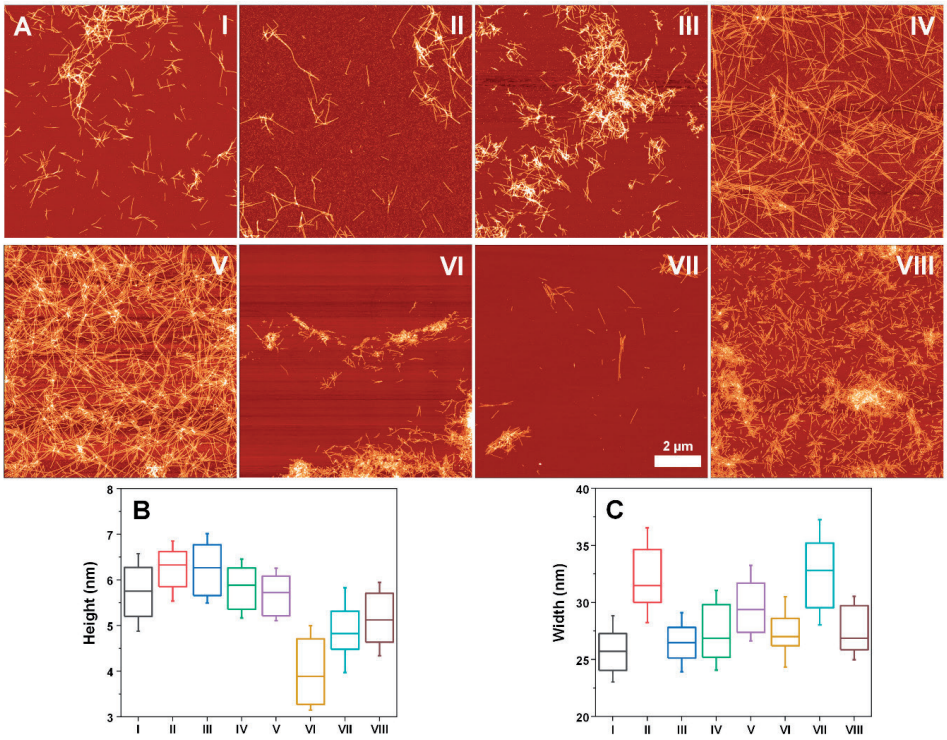

Figure 5. Atomic force microscopy images of α-syn fibrils, which had distinct second derivative FTIR spectra (**A**) and their height (**B**) and width (**C**) distribution (n = 50). Roman numerals correlate with Figure 4 FTIR spectra. Box plots indicate the interquartile range and the error bars are one standard deviation.

3. Discussion

Based on these data and previous reports, it is quite clear that both ionic strength and protein concentration play a significant role in determining the type of α-syn fibrils during spontaneous aggregation. In order to evaluate the effect of each factor, we have to discuss the correlation between all the present data, including aggregation kinetics, variation in conformations and aggregate morphology.

First, we can see that all protein concentrations at 0 mM NaCl and 50 µM α-syn at 100 mM NaCl experience significantly longer lag times, when compared to all other conditions. Such long time-frames could potentially allow for the formation of distinct nuclei, which, in turn, lead to structurally and morphologically different fibrils. These aforementioned conditions coincide with both the large variability of EEM maximum positions (Figure 2), secondary structure (Figure 4) and fibril morphology (Figure 5). However, the long aggregation times do not explain why there is a shift in the dominant type of aggregate, which occurs between 100 mM and 200 mM NaCl, rather than between 0 mM and 100 mM. In some cases, aggregation at 100 mM occurs quicker or similarly to 200 mM, but the resulting aggregates still pertain their ionic strength-specific secondary structure. Coincidentally, this transition in dominant fibril type occurs at an ionic strength similar to PBS, which is another buffer solution often used in alpha-synuclein studies and which also leads to the formation of a mixture of fibrils [37]. This means that ionic strength plays a crucial role during nuclei formation, where the presence of sodium and chloride ions alter the type of nucleus that forms, likely by influencing protein electrostatic interactions.

The concentration of α-syn also appears to play a role in determining the type of fibril, especially visible at lower ionic strength conditions. This factor, however, does not seem to have a significant effect at high protein and ionic strength conditions, where both the aggregation kinetics, as well as types of fibrils experience lower variation. This could be due to the reaction reaching the highest rate of nucleation and elongation, where the dominant type of fibril becomes the one that forms and elongates the quickest. This would leave no time for other nuclei formation and essentially limit the conformational variations.

One especially interesting and unexpected aspect of this work was the discovery of eight distinct fibril types, which have specific secondary structure motifs and, in some cases, morphologies. Based on previously reported α-syn aggregation experiments [18,29], one would expect to only observe a limited fibril variation, especially under similar conditions. On the one hand, it is quite interesting that α-syn is capable of forming up to four distinct types of fibrils under identical conditions (mostly seen at low ionic strength). This is a far greater variation than we have demonstrated in the case of prion proteins, which were capable of forming two different types of fibrils under identical conditions [34]. On the other hand, this means that during experimental procedures, α-syn can aggregate into more than one type of fibril. Taking into consideration the different secondary structures and morphologies, this random variation could significantly alter the outcome of any potential drug molecule assay or aggregation kinetic experiment. Another factor which may also complicate data interpretation is the vast dispersion of sample fluorescence intensities. Apart from distinct fibrils having significantly lower or higher bound-ThT fluorescence intensity, there were also substantial differences in intensity between fibrils that had similar secondary structures. This means that the assumption of ThT fluorescence relating to the concentration of fibers would be incorrect in the case of α-syn aggregation experiments.

The appearance of multiple distinct conformation α-syn fibrils under identical conditions may also be one of the steps in the complex mechanism of pathogenesis in Parkinson's disease and other synucleinopathies. Currently, the exact mode of alpha-synuclein-related disorder onset and propagation is not fully known, with multiple possible mechanisms proposed, such as prion-like spreading [38] and trans-synaptic α-syn propagation [39,40]. It has also recently been shown by Ferreira et al. [41] and Peng et al. [42] that certain α-syn fibril types have a considerably higher neurodegenerative potential than others. Combined with the findings in this work, it is possible that the polymorphism of α-syn fibrils at physiological ionic strength/protein concentration results in some of the aggregates having a significantly higher self-replication potential (Figure A3) and possible higher cytotoxicity.

As a positive note, the thirty different environmental conditions revealed certain sets of ionic strength and protein concentrations, which experienced minimal variation in the type of fibril that forms. As an example, the 200 mM NaCl and 200 μM α-syn conditions resulted in samples, which had identical EEM maximum positions, as well as a single type of secondary structure and morphology. Such conditions, which lead to homogenous fibrillization, can be used to avoid conformational variations during assays which employ α-syn aggregation and aid in amyloid research. Taking everything into consideration, spontaneous alpha-synuclein aggregation is a stochastic process, whose results depend highly on both the solution's ionic strength, as well as protein concentration. Conformational variation of the resulting fibrils depends on both parameters, with certain conditions leading to the formation of up to four structurally and morphologically distinct fibrils, while others result in all samples containing a single type of aggregate.

4. Materials and Methods

4.1. Alpha-Synuclein Aggregation

Alpha-synuclein was purified as described previously [43], lyophilized and stored at −20 °C prior to use. Before each aggregation reaction, α-syn powder was dissolved in a 20 mM potassium phosphate buffer (pH 7.4), containing 0–500 mM NaCl (further referred to as the reaction buffer) and filtered through a 0.22 μm syringe filter. The protein concentration was determined by scanning sample absorbance at 280 nm using a Shimadzu

(Kyoto, Japan) UV spectrophotometer (ε_{280} = 5960 $M^{-1}cm^{-1}$). The resulting solutions were then combined with their respective reaction buffers and a 10 mM thioflavin-T (ThT) stock solution to yield samples containing 50–250 μM final protein concentration and 100 μM ThT (10 mL total volume). The solutions were then distributed to 96-well non-binding plates, with each well containing 100 μL protein solution, a 3 mm glass-bead and sealed using Nunc sealing tape. The plates were then placed in a Clariostar Plus plate reader and incubated at 37 °C under constant 600 RPM orbital agitation. The presence of a 3 mm glass-bead and constant agitation minimized the possibility of alpha-synuclein liquid-liquid phase separation [44]. Measurements were taken every 5 min using excitation and emission wavelengths of 440 nm and 480 nm, respectively. After aggregation, the plates were stored at 4 °C.

For seeded aggregation, fibrils were centrifuged at 12,000 RPM for 15 min, after which the supernatant was removed and the fibril pellets were resuspended into a 20 mM potassium phosphate buffer (pH 7.4), containing 500 mM NaCl. The fibril solutions were then combined with a 100 μM α-syn solution (500 mM NaCl), ThT stock solution (10 mM) and 20 mM potassium phosphate buffer (pH 7.4), containing 500 mM NaCl to final solutions containing 50 μM α-syn, 2.5 μM fibrils (fibril concentration is based on aggregated monomer concentration, assuming 100% fibrillization) and 100 μM ThT. Solution aggregation was tracked as described in the non-seeded aggregation section.

Aggregation kinetic data were analyzed using Origin 2018 software (OriginLab Corporation, Northampton, MA, USA). Each kinetic curve was fit using a sigmoidal Boltzmann equation. The lag time was determined as shown in the Figure A2. In a rare set of cases, the aggregation curve data quality was not sufficient for analysis. In these instances, the samples were taken out of the batch.

4.2. Excitation-Emission Matrices

An aliquot of each sample was removed from the 96-well plates and diluted with 20 mM potassium phosphate buffers (pH 7.4), containing either 500 mM or 650 mM NaCl and 100 μM ThT, in order to make every sample contain 500 mM NaCl and 10 μM protein. An identical protein and NaCl concentration was required to compare ThT binding/fluorescence parameters, as both factors affect the concentration of bound ThT [26]. The addition of fresh ThT minimized the loss of the dye molecule due to hydroxylation during the aggregation experiment [45]. After the samples were prepared, they were placed into 96-well plates, and their bound-ThT excitation-emission matrices were scanned and generated using Clariostar Plus platereader and Clariostar MARS software. Emission intensity in the range from 470 nm to 490 nm was scanned using a set excitation wavelength of 450 nm. Afterwards, emission intensity at 480 nm was scanned using an excitation range from 440 nm to 460 nm. In each case, a 1 nm step size was used. The resulting data were combined into an EEM using Clariostar MARS software (3D spectrum function). The EEM "center of mass" was determined as described previously [46].

4.3. Fourier-Transform Infrared Spectroscopy (FTIR)

In order to prepare samples for FTIR, the selected fibril samples were first replicated by combining them with their respective reaction solutions (same NaCl and protein concentration as the initial samples) in a 1:4 ratio (20% fibril seed, assuming a complete fibrillization of the initial samples) and incubating them as described in the initial aggregate preparation section. The resulting samples were then centrifuged at 12,000 RPM for 15 min. The supernatant was removed and the fibril pellets were resuspended into 500 μL of D_2O, containing 500 mM NaCl (the addition of NaCl improved fibril sedimentation and created an equal ionic strength environment for all samples). The centrifugation and resuspension procedure was repeated four times. Finally, the fibril pellets were resuspended into 100 μL of D_2O, containing 500 mM NaCl and mixed vigorously for 10 s. For each sample, 256 interferograms of 2 cm^{-1} resolution were scanned using a Bruker (Billerica, MA, USA) Invenio S FTIR spectrometer (equipped with MCT detector) at room temperature. D_2O

and water vapor noise spectra were subtracted from each sample spectrum, which was then baseline corrected (1700–1595 cm^{-1}) and normalized to the area of Amide I' band. All data processing was done using GRAMS software.

4.4. Atomic Force Microscopy

Before depositing the fibril samples, the mica surface was modified with (3-aminopropyl)triethoxysilane (APTES). Then, 1% (% v.v) APTES solution (30 µL) was spread on the surface of the mica, incubated at room temperature for 5 min, gently washed with 2 mL of H_2O and dried using airflow. For AFM measurements, 30 µL aliquots of samples used in the EEM measurements were taken (identical protein and NaCl concentration) and placed on APTES-modified mica and left to adsorb for 60 s. The mica were then gently washed with 3 mL of H_2O and dried using airflow. AFM measurements were done as described previously [27]. In short, high-resolution AFM images were acquired using Dimension Icon (Bruker, Billerica, MA, USA)) atomic force microscope, operating in tapping-mode. The images were flattened and analyzed using Gwyddion 2.5.5 software. Fibril cross-sectional height and width were determined from line profiles, perpendicular to the fibril axes (only separate and non-clumped fibrils were measured).

Supplementary Materials: The following are available online at https://www.mdpi.com/article/10.3390/ijms222212382/s1.

Author Contributions: Conceptualization, M.Z., A.S. and V.S.; investigation, M.Z., A.S. and K.M.; resources, V.S.; writing—original draft preparation, M.Z.; writing—review and editing, M.Z., A.S., K.M. and V.S.; supervision, V.S.; funding acquisition, V.S. All authors have read and agreed to the published version of the manuscript.

Funding: This research was funded by the grant no. S-SEN-20-3 from the Research Council of Lithuania.

Institutional Review Board Statement: Not applicable.

Informed Consent Statement: Not applicable.

Data Availability Statement: The data presented in this study are available in Supplementary Material. It includes raw kinetic, EEM and FTIR data.

Conflicts of Interest: The authors declare no conflict of interest.

Appendix A

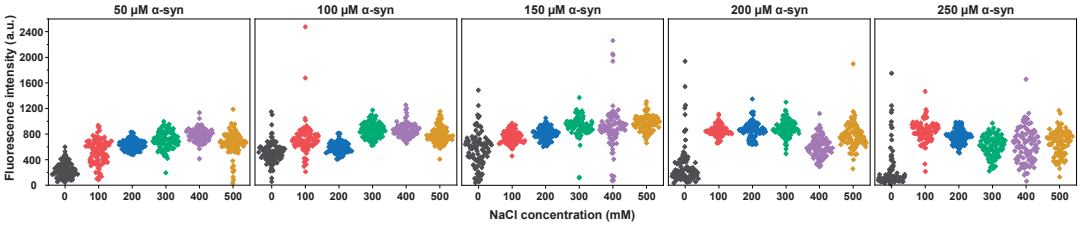

Figure A1. α-syn sample bound-ThT fluorescence intensity distribution at different ionic strength and protein concentration conditions.

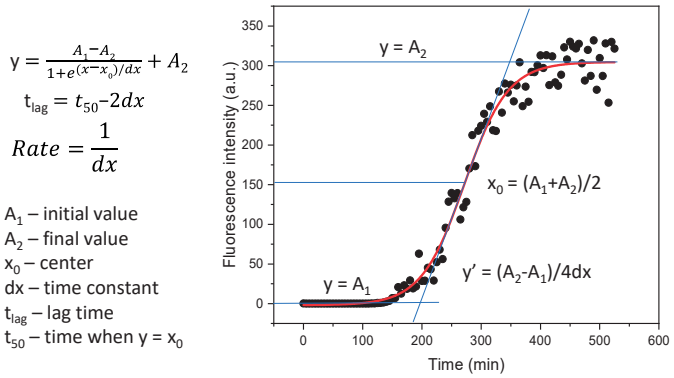

Figure A2. Boltzmann sigmoidal equation fit example with lag time (t_{lag}) and elongation rate calculation.

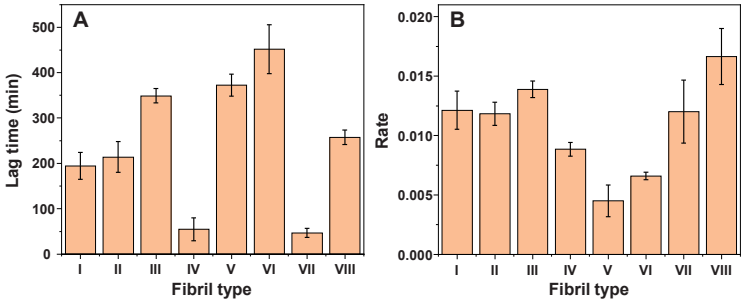

Figure A3. Lag time (**A**) and elongation rate (**B**) of all eight fibril types under identical ionic strength (500 mM NaCl), non-aggregated α-syn (50 μM) and initial fibril concentration (2.5 μM). Lag time and elongation rate values were calculated as shown in Figure A2.

References

1. Baker, K.R.; Rice, L. The Amyloidoses: Clinical Features, Diagnosis and Treatment. *Methodist Debakey Cardiovasc. J.* **2012**, *8*, 3–7. [CrossRef]
2. Knowles, T.P.J.; Vendruscolo, M.; Dobson, C.M. The amyloid state and its association with protein misfolding diseases. *Nat. Rev. Mol. Cell Biol.* **2014**, *15*, 384–396. [CrossRef] [PubMed]
3. Chiti, F.; Dobson, C.M. Protein Misfolding, Amyloid Formation, and Human Disease: A Summary of Progress over the Last Decade. *Annu. Rev. Biochem.* **2017**, *86*, 27–68. [CrossRef]
4. Savica, R.; Grossardt, B.R.; Bower, J.H.; Ahlskog, J.E.; Rocca, W.A.; Rocca, W. Time Trends in the Incidence of Parkinson's Disease: A 30-year Study born in the HHS Public Access. *JAMA Neurol.* **2016**, *73*, 981–989. [CrossRef] [PubMed]
5. Zhang, X.; Fu, Z.; Meng, L.; He, M.; Zhang, Z. The Early Events That Initiate β-Amyloid Aggregation in Alzheimer's Disease. *Front. Aging Neurosci.* **2018**, *10*, 359. [CrossRef]
6. Maurer, M.S.; Schwartz, J.H.; Gundapaneni, B.; Elliott, P.M.; Merlini, G.; Waddington-Cruz, M.; Kristen, A.V.; Grogan, M.; Witteles, R.; Damy, T.; et al. Tafamidis Treatment for Patients with Transthyretin Amyloid Cardiomyopathy. *N. Engl. J. Med.* **2018**, *379*, 1007–1016. [CrossRef] [PubMed]
7. Park, J.; Egolum, U.; Parker, S.; Andrews, E.; Ombengi, D.; Ling, H. Tafamidis: A First-in-Class Transthyretin Stabilizer for Transthyretin Amyloid Cardiomyopathy. *Ann. Pharmacother.* **2020**, *54*, 470–477. [CrossRef]
8. Cummings, J.; Lee, G.; Ritter, A.; Sabbagh, M.; Zhong, K. Alzheimer's disease drug development pipeline: 2020. *Alzheimers Dement.* **2020**, *6*, e12050. [CrossRef]
9. Mehta, D.; Jackson, R.; Paul, G.; Shi, J.; Sabbagh, M. Why do trials for Alzheimer's disease drugs keep failing? A discontinued drug perspective for 2010–2015. *Expert Opin. Investig. Drugs* **2017**, *26*, 735–739. [CrossRef]
10. Brookmeyer, R.; Gray, S.; Kawas, C. Projections of Alzheimer's disease in the United States and the public health impact of delaying disease onset. *Am. J. Public Health* **1998**, *88*, 1337–1342. [CrossRef]

11. Arthur, K.C.; Calvo, A.; Price, T.R.; Geiger, J.T.; Chiò, A.; Traynor, B.J. Projected increase in amyotrophic lateral sclerosis from 2015 to 2040. *Nat. Commun.* **2016**, *7*, 12408. [CrossRef]
12. Chamachi, N.G.; Chakrabarty, S. Temperature-Induced Misfolding in Prion Protein: Evidence of Multiple Partially Disordered States Stabilized by Non-Native Hydrogen Bonds. *Biochemistry* **2017**, *56*, 833–844. [CrossRef] [PubMed]
13. Milto, K.; Michailova, K.; Smirnovas, V. Elongation of Mouse Prion Protein Amyloid-Like Fibrils: Effect of Temperature and Denaturant Concentration. *PLoS ONE* **2014**, *9*, e94469. [CrossRef] [PubMed]
14. Tanaka, M.; Chien, P.; Yonekura, K.; Weissman, J.S. Mechanism of cross-species prion transmission: An infectious conformation compatible with two highly divergent yeast prion proteins. *Cell* **2005**, *121*, 49–62. [CrossRef]
15. Makarava, N.; Ostapchenko, V.G.; Savtchenko, R.; Baskakov, I.V. Conformational switching within individual amyloid fibrils. *J. Biol. Chem.* **2009**, *284*, 14386–14395. [CrossRef] [PubMed]
16. Sakalauskas, A.; Ziaunys, M.; Smirnovas, V. Concentration-dependent polymorphism of insulin amyloid fibrils. *PeerJ* **2019**, *7*, e8208. [CrossRef]
17. Munishkina, L.A.; Henriques, J.; Uversky, V.N.; Fink, A.L. Role of Protein-Water Interactions and Electrostatics in α-Synuclein Fibril Formation. *Biochemistry* **2004**, *43*, 3289–3300. [CrossRef]
18. Flynn, J.D.; McGlinchey, R.P.; Walker, R.L.; Lee, J.C. Structural features of -synuclein amyloid fibrils revealed by raman spectroscopy. *J. Biol. Chem.* **2018**, *293*, 767–776. [CrossRef]
19. Cobb, N.J.; Apostol, M.I.; Chen, S.; Smirnovas, V.; Surewicz, W.K. Conformational Stability of Mammalian Prion Protein Amyloid Fibrils Is Dictated by a Packing Polymorphism within the Core Region. *J. Biol. Chem.* **2014**, *289*, 2643–2650. [CrossRef]
20. Buell, A.K.; Galvagnion, C.; Gaspar, R.; Sparr, E.; Vendruscolo, M.; Knowles, T.P.J.; Linse, S.; Dobson, C.M. Solution conditions determine the relative importance of nucleation and growth processes in -synuclein aggregation. *Proc. Natl. Acad. Sci. USA* **2014**, *111*, 7671–7676. [CrossRef]
21. Keller, A.; Grundmeier, G. Amyloid aggregation at solid-liquid interfaces: Perspectives of studies using model surfaces. *Appl. Surf. Sci.* **2020**, *506*, 144991. [CrossRef]
22. Latshaw, D.C.; Cheon, M.; Hall, C.K. Effects of macromolecular crowding on amyloid beta (16-22) aggregation using coarse-grained simulations. *J. Phys. Chem. B* **2014**, *118*, 13513–13526. [CrossRef]
23. Morel, B.; Varela, L.; Azuaga, A.I.; Conejero-Lara, F. Environmental Conditions Affect the Kinetics of Nucleation of Amyloid Fibrils and Determine Their Morphology. *Biophys. J.* **2010**, *99*, 3801–3810. [CrossRef]
24. Zidar, J.; Merzel, F. Probing amyloid-beta fibril stability by increasing ionic strengths. *J. Phys. Chem. B* **2011**, *115*, 2075–2081. [CrossRef]
25. Shammas, S.L.; Knowles, T.P.J.; Baldwin, A.J.; MacPhee, C.E.; Welland, M.E.; Dobson, C.M.; Devlin, G.L. Perturbation of the stability of amyloid fibrils through alteration of electrostatic interactions. *Biophys. J.* **2011**, *100*, 2783–2791. [CrossRef]
26. Mikalauskaite, K.; Ziaunys, M.; Sneideris, T.; Smirnovas, V. Effect of Ionic Strength on Thioflavin-T Affinity to Amyloid Fibrils and Its Fluorescence Intensity. *Int. J. Mol. Sci.* **2020**, *21*, 8916. [CrossRef] [PubMed]
27. Sneideris, T.; Sakalauskas, A.; Sternke-Hoffmann, R.; Peduzzo, A.; Ziaunys, M.; Buell, A.K.; Smirnovas, V. The Environment Is a Key Factor in Determining the Anti-Amyloid Efficacy of EGCG. *Biomolecules* **2019**, *9*, 855. [CrossRef] [PubMed]
28. Stefanis, L. α-Synuclein in Parkinson's Disease. *Cold Spring Harb. Perspect. Med.* **2012**, *2*, a009399. [CrossRef]
29. Roeters, S.J.; Iyer, A.; Pletikapiä, G.; Kogan, V.; Subramaniam, V.; Woutersen, S. Evidence for Intramolecular Antiparallel Beta-Sheet Structure in Alpha-Synuclein Fibrils from a Combination of Two-Dimensional Infrared Spectroscopy and Atomic Force Microscopy. *Sci. Rep.* **2017**, *7*, 41051. [CrossRef]
30. Gaspar, R.; Lund, M.; Sparr, E.; Linse, S. Anomalous Salt Dependence Reveals an Interplay of Attractive and Repulsive Electrostatic Interactions in α-synuclein Fibril Formation. *QRB Discov.* **2020**, *1*, e2. [CrossRef]
31. Sidhu, A.; Vaneyck, J.; Blum, C.; Segers-Nolten, I.; Subramaniam, V. Polymorph-specific distribution of binding sites determines thioflavin-T fluorescence intensity in α-synuclein fibrils. *Amyloid* **2018**, *25*, 189–196. [CrossRef]
32. Sternke-Hoffmann, R.; Peduzzo, A.; Bolakhrif, N.; Haas, R.; Buell, A.K. The aggregation conditions define whether EGCG is an inhibitor or enhancer of α-synuclein amyloid fibril formation. *Int. J. Mol. Sci.* **2020**, *21*, 1995. [CrossRef]
33. Giehm, L.; Lorenzen, N.; Otzen, D.E. Assays for α-synuclein aggregation. *Methods* **2011**, *53*, 295–305. [CrossRef]
34. Ziaunys, M.; Sneideris, T.; Smirnovas, V. Formation of distinct prion protein amyloid fibrils under identical experimental conditions. *Sci. Rep.* **2020**, *10*, 4572. [CrossRef] [PubMed]
35. Ziaunys, M.; Sakalauskas, A.; Smirnovas, V. Identifying Insulin Fibril Conformational Differences by Thioflavin-T Binding Characteristics. *Biomacromolecules* **2020**, *21*, 4989–4997. [CrossRef] [PubMed]
36. Barth, A. Infrared spectroscopy of proteins. *Biochim. Biophys. Acta-Bioenerg.* **2007**, *1767*, 1073–1101. [CrossRef] [PubMed]
37. Toleikis, Z.; Ziaunys, M.; Baranauskiene, L.; Petrauskas, V.; Jaudzems, K.; Smirnovas, V. S100A9 Alters the Pathway of Alpha-Synuclein Amyloid Aggregation. *Int. J. Mol. Sci.* **2021**, *22*, 7972. [CrossRef]
38. Jan, A.; Gonçalves, N.P.; Vaegter, C.B.; Jensen, P.H.; Ferreira, N. The prion-like spreading of alpha-synuclein in parkinson's disease: Update on models and hypotheses. *Int. J. Mol. Sci.* **2021**, *22*, 8338. [CrossRef] [PubMed]
39. Van Den Berge, N.; Ferreira, N.; Gram, H.; Mikkelsen, T.W.; Alstrup, A.K.O.; Casadei, N.; Tsung-Pin, P.; Riess, O.; Nyengaard, J.R.; Tamgüney, G.; et al. Evidence for bidirectional and trans-synaptic parasympathetic and sympathetic propagation of alpha-synuclein in rats. *Acta Neuropathol.* **2019**, *138*, 535–550. [CrossRef]

40. Ferreira, N.; Gonçalves, N.P.; Jan, A.; Jensen, N.M.; van der Laan, A.; Mohseni, S.; Vægter, C.B.; Jensen, P.H. Trans-synaptic spreading of alpha-synuclein pathology through sensory afferents leads to sensory nerve degeneration and neuropathic pain. *Acta Neuropathol. Commun.* **2021**, *9*, 31. [CrossRef]
41. Ferreira, N.; Gram, H.; Sorrentino, Z.A.; Gregersen, E.; Schmidt, S.I.; Reimer, L.; Betzer, C.; Perez-Gozalbo, C.; Beltoja, M.; Nagaraj, M.; et al. Multiple system atrophy-associated oligodendroglial protein p25α stimulates formation of novel α-synuclein strain with enhanced neurodegenerative potential. *Acta Neuropathol.* **2021**, *142*, 87–115. [CrossRef] [PubMed]
42. Peng, C.; Gathagan, R.J.; Covell, D.J.; Medellin, C.; Stieber, A.; Robinson, J.L.; Zhang, B.; Pitkin, R.M.; Olufemi, M.F.; Luk, K.C.; et al. Cellular milieu imparts distinct pathological α-synuclein strains in α-synucleinopathies. *Nature* **2018**, *557*, 558–563. [CrossRef]
43. Šneideris, T.; Baranauskienė, L.; Cannon, J.G.; Rutkienė, R.; Meškys, R.; Smirnovas, V. Looking for a generic inhibitor of amyloid-like fibril formation among flavone derivatives. *PeerJ* **2015**, *3*, e1271. [CrossRef]
44. Ray, S.; Singh, N.; Kumar, R.; Patel, K.; Pandey, S.; Datta, D.; Mahato, J.; Panigrahi, R.; Navalkar, A.; Mehra, S.; et al. α-Synuclein aggregation nucleates through liquid–liquid phase separation. *Nat. Chem.* **2020**, *12*, 705–716. [CrossRef]
45. Foderà, V.; Groenning, M.; Vetri, V.; Librizzi, F.; Spagnolo, S.; Cornett, C.; Olsen, L.; van de Weert, M.; Leone, M. Thioflavin T Hydroxylation at Basic pH and Its Effect on Amyloid Fibril Detection. *J. Phys. Chem. B* **2008**, *112*, 15174–15181. [CrossRef] [PubMed]
46. Ziaunys, M.; Smirnovas, V. Additional Thioflavin-T Binding Mode in Insulin Fibril Inner Core Region. *J. Phys. Chem. B* **2019**, *123*, 8727–8732. [CrossRef] [PubMed]

THE JOURNAL OF PHYSICAL CHEMISTRY B

Article

Cite This: J. Phys. Chem. B 2019, 123, 8727−8732

pubs.acs.org/JPCB

Additional Thioflavin-T Binding Mode in Insulin Fibril Inner Core Region

Mantas Ziaunys and Vytautas Smirnovas*

Institute of Biotechnology, Life Sciences Center, Vilnius University, Vilnius LT-10257, Lithuania

Supporting Information

ABSTRACT: Amyloidogenic protein aggregation into fibrils is linked to several neurodegenerative disorders, such as Alzheimer's or Parkinson's disease. An amyloid specific fluorescent dye thioflavin-T (ThT) is often used to track the formation of these fibrils in vitro. Despite its wide application, it is still unknown how many types of ThT binding modes to amyloids exist, with multiple studies indicating varying numbers. In this work, we examine the binding of ThT to insulin fibrils generated at pH 2.4 and reveal a possible inner core binding mode which is not accessible to the dye molecule after aggregation occurs.

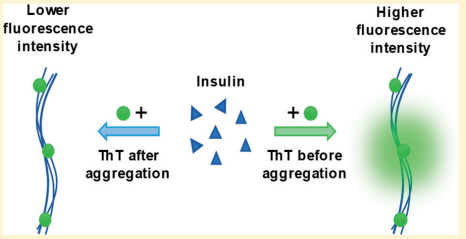

INTRODUCTION

Protein aggregation into highly structured amyloid fibrils is linked to multiple neurodegenerative disorders, such as Alzheimer's, Parkinson's, and Creutzfeldt-Jakob disease.[1,2] Such protein assembly into insoluble aggregates is being extensively studied in the hope of finding a possible inhibitor or cure[3−5] for the aforementioned disorders, which affect millions of people worldwide. Alongside in vivo amyloid investigations,[6,7] there is a plethora of aggregation experiments being conducted in vitro, by utilizing conditions that permit fast and easy-to-observe reactions, such as high temperature[8] or agitation.[9] While this does not reflect the conditions in live organisms, it does allow for a quick assessment of possible aggregation reaction inhibitors.

One of multiple possible methods used to track the formation of amyloid fibrils is a ThT assay.[10] The method is based upon selective binding of ThT molecules to the surface of amyloid fibrils,[11] resulting in both a red-shift of excitation and emission maxima wavelengths as well as a substantial increase in fluorescence intensity.[12] In some cases, the dye is added to the reaction mixture at the start in order to follow the fibrilization kinetics in real-time,[10,13] while in other cases it is added to aliquots of the aggregating sample at specific time points.[14] Usually, for the sake of simplicity, a couple of generalizations are made regarding the use of this amyloid dye. First, it is assumed that the increasing fluorescence intensity of the sample is correlated to the concentration of fibrils present in a linear way.[10] Second, the fluorescence intensity is measured using a certain set excitation wavelength and a range or single emission wavelength depending on the instrument used, which may not correspond to the exact maximum excitation or emission wavelengths. And for simple aggregate examinations, such as determining whether or not there are amyloids present[15] or checking if an aggregation reaction is occurring during inhibition experiments,[16] these simplifications have a minimal influence. However, for assays which investigate aggregation kinetic parameters[17−19] or rely on fluorescence measurements to determine fibril concentration changes,[20,21] this becomes extremely important due to the possibility of amyloids having more than one mode of binding ThT.

As of right now, there have been multiple studies conducted on the mechanism of ThT binding to the surface of amyloid fibrils,[11,22−26] especially on model amyloidogenic proteins, such as insulin.[27] Both theoretical[28,29] and experimental[22,27,30] data points toward a conclusion that insulin and certain other protein amyloid fibrils possess more than one mode of binding ThT. In a work by Sulatskaya et al.,[22] it is shown that not only do these binding modes have different affinities toward ThT molecules but also they modulate their absorbance and fluorescence parameters. This in itself can already lead to a problem when comparing data between similar experiments, as the concentrations of dye used by different research groups varies in quite a large range, from 1 nM[31] to hundreds of micromoles,[10] as do the excitation and emission wavelengths of the measurements based on the equipment used. Matters are even further complicated by the possibility of there being more than two binding modes on the surface of fibrils, with some reports suggesting four,[32] as well as potential fibril inner core region binding sites.[28] All of this makes it vitally important to better understand the ways ThT may incorporate itself into amyloids in order to improve the ThT assay.

The subject of ThT binding to the inner core region of a fibril is interesting, as there has been a report showing no difference between ThT binding to insulin under pH 1.6 conditions when it was added before or after aggregation,[27] but

Received: September 11, 2019
Revised: October 3, 2019
Published: October 3, 2019

DOI: 10.1021/acs.jpcb.9b08652
J. Phys. Chem. B 2019, 123, 8727−8732

the possibility could exist under different environmental conditions, such as a higher pH value, which yield differently structured fibrils.[33] And it is not impossible for this to occur, as there have been studies showing that amyloid aggregates contain pockets of water molecules inside their structure.[34,35] The ThT molecule would be shielded from interactions with the surrounding solution, therefore the possibility of a fluorescence quenching event should be greatly reduced. The molecule would also be in a relatively rigid environment, which has been shown to increase the quantum yield of ThT fluorescence.[12,36−38] And finally, such binding could only occur if ThT molecules were present in the solution during the aggregation process, otherwise the inner core region would be inaccessible. This would lead to different fluorescence intensities and excitation−emission maxima positions if the sample was tracked real-time or with the dye being added to aliquots of a ThT-free sample.

In this work, we measure the concentration of bound and free ThT molecules, as well as their fluorescence excitation−emission matrices when the dye is added to insulin samples before and after the aggregation process occurs. We compare the bound molecule relation to fluorescence intensity, excitation−emission maxima positions, as well as examine whether a new mode of ThT binding to the core of insulin fibrils occurs.

MATERIALS AND METHODS

Thioflavin-T Solution Preparation. Thioflavin-T powder (Sigma-Aldrich cat. no. T3516) was dissolved in Milli-Q water, and the concentration was determined by measuring the solution's absorbance at 412 nm, with $\varepsilon_{412} = 23.8 \times 10^3$ M^{-1} cm^{-1}. The extinction coefficient of ThT at the acidic conditions used in further experiments was determined to be 21.5×10^3 M^{-1} cm^{-1}. The ThT solution was diluted with the reaction buffer to final concentrations between 0.02 μM and 200 μM to be used in further experiments.

Insulin Aggregation. Human recombinant insulin (Sigma-Aldrich cat. no. 91077C) was dissolved in 100 mM sodium phosphate buffer (pH 2.4) with 100 mM NaCl to a concentration of 200 μM (1.16 mg/mL). For samples that were intended to be incubated with ThT present from the start, the 200 μM insulin solutions were mixed with varying concentrations of ThT to a final insulin concentration of 100 μM. Samples that did not contain ThT from the start were incubated at 200 μM. Incubation of all insulin samples was carried out in 1.5 mL test tubes (Fisher cat. no. 15432545) (solution volume was 1 mL) in a Ditabis thermomixer with no agitation at a constant 60 °C temperature for 24 h. The samples were placed in an ice bath and sonicated for 10 min using a Bandelin Sonopuls sonicator with a MS-73 tip at 40% power with 30 s sonication and 30 s rest intervals. Samples that did not contain ThT from the start were then mixed with the ThT solutions immediately after sonication to a final insulin concentration of 100 μM.

ThT Fluorescence Measurements. Thioflavin T fluorescence excitation−emission matrices (EEM) were measured using a Varian Cary Eclipse spectrophotometer with an excitation range from 435 to 465 nm and an emission range from 455 to 515 nm, with a wavelength step of 1 nm, excitation slit −5 nm and emission slit −2.5 nm. The solutions were measured 15 min after sonication without any additional dilution. For each condition, 3 excitation−emission matrices were scanned, averaged, and a control sample without ThT EEM was subtracted.

A calibration curve of fluorescence intensity based on ThT concentration was measured by mixing a range of different ThT concentration solutions with 200 μM insulin fibrils in a 1:1 ratio, and then the fluorescence intensity was scanned using a 450 nm excitation wavelength (slit −5 nm) and an emission range from 460 to 500 nm (slit −2.5 nm).

Free and Bound ThT Determination. Each sample (500 μL) was centrifuged at 20000*g* for 20 min, and then the absorbance of 150 μL of supernatant was measured and the concentration of free ThT determined using $\varepsilon_{412} = 21.5 \times 10^3$ $M^{-1}cm^{-1}$. This value was then subtracted from the total ThT present in the sample to calculate the concentration of bound ThT. In cases when the absorbance was too low to accurately measure, the supernatant was mixed with 200 μM insulin fibrils at a 1:1 ratio and the sample's fluorescence was measured as previously described. The fluorescence intensity was then used to determine the amount of ThT in the sample by comparing it to the ThT-fibril calibration curve. When both methods were unable to detect any ThT absorbance or fluorescence signals, it was assumed that all ThT was bound to fibrils.

Inner Filter Effect Correction. To correct for both the primary and secondary inner filter effects on each EEM matrix, absorption spectra of free ThT, fibrils without ThT, and fibrils with ThT were measured. Due to various possible dye binding modes, it was assumed that under conditions where the inner filter effect is prominent, the vast majority of ThT molecules would be bound in the most abundant binding mode, hence the measurements were performed with 60 μM ThT added to 200 μM insulin fibril samples in a 1:1 ratio and the resulting spectra was the sum of possible surface binding modes. The absorption spectra of bound ThT was determined by separating the fibrils with bound ThT from the sample by centrifugation, measuring the remaining free ThT concentration and subtracting the recalculated free ThT spectrum, as well as the fibril-without-ThT spectrum from the fibril-with-ThT spectrum. For each EEM, the inner filter effect was corrected by using each sample's corresponding free and bound ThT spectra by

$$I_m = I_c \times 10^{-(A_{ex}+A_{em})/2} \quad (1)$$

where A_{ex} is the sample's absorbance at the excitation wavelength, A_{em} is the sample's absorbance at the emission wavelength, I_m is the signal intensity observed during measurement, and I_c is the corrected signal intensity.

EEM Maxima Position Calculation. Due to background noise, it is difficult to discern the exact EEM maxima position, therefore in this case the top 1% intensity values were chosen from each EEM and their "center of mass" was calculated by

$$\lambda = \left(\sum \left(\lambda_n \times \sum I_n\right)\right) / \sum I_a \quad (2)$$

where λ is the wavelength of either the excitation or emission center of mass, λ_n is an excitation or emission wavelength, $\sum I_n$ is the sum of all signal intensities at λ_n, $\sum I_a$ is the sum of all signal intensities.

RESULTS AND DISCUSSION

By measuring the amount of ThT present in the supernatants of centrifuged samples, the concentration of bound ThT molecules can be calculated, as the amount of insulin fibrils remaining in the solution is minimal (Figure S1). The bound

DOI: 10.1021/acs.jpcb.9b08652
J. Phys. Chem. B 2019, 123, 8727−8732

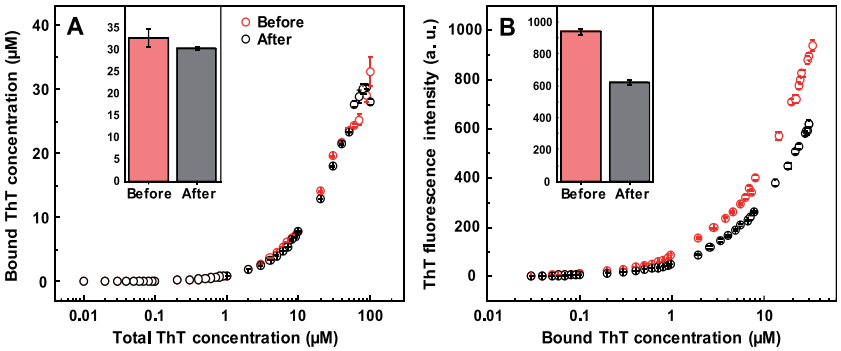

Figure 1. Concentrations of ThT bound to insulin fibrils and its fluorescence emission intensity when it was added before or after insulin aggregation. Bound ThT concentration dependence on total ThT concentration for samples that contained the dye before and after aggregation (A). ThT fluorescence intensity dependence on bound ThT concentration for insulin fibrils with dye added before and after aggregation (B). Inserts show the highest bound ThT concentration (A) and highest fluorescence intensity (B) for both conditions.

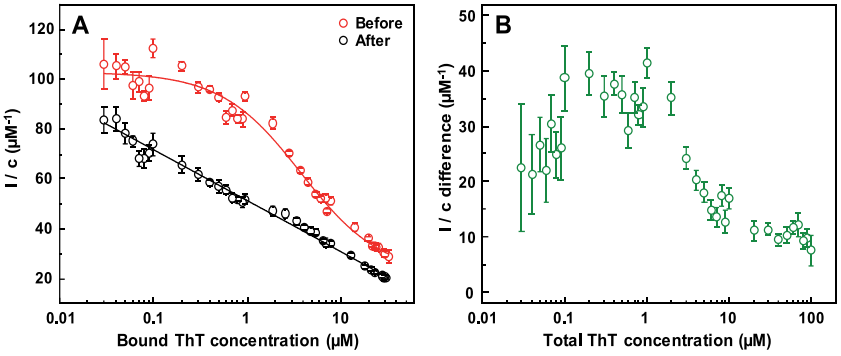

Figure 2. Insulin fibril ThT fluorescence intensity and concentration ratios and their differences throughout the entire ThT concentration range. Intensity/concentration dependence on bound ThT when the dye is added before and after the aggregation reaction (A). Intensity/concentration difference between both conditions in the entire tested ThT concentration range (B).

ThT concentration dependence on total dye added before or after aggregation occurs is similar in both cases (Figure 1A). The maximum bound dye concentration is slightly higher in the samples when it was added before aggregation; however, these maximum values are within margin of error between both cases. This suggests that if there is any additional ThT bound to fibrils when the dye is added before aggregation, this value is considerably lower than the total amount of bound ThT.

Considering that in both cases, the amount of bound ThT appears to be nearly identical, we would expect to observe a similar fluorescence intensity when comparing the samples. However, this is not the case, as the samples that contained ThT before aggregation have a considerably larger fluorescence signal than samples that had ThT added after fibril formation had occurred (Figure 1B), which was not observed by Groenning et al.[27] when examining a different insulin fibril strain formation at a lower pH value. In the tested ThT concentration range, when the dye is added before aggregation, the highest bound ThT concentration (32.7 ± 2.2 μM) has a fluorescence intensity of 938 ± 23 a. u., and when ThT was added after aggregation, 30.3 ± 0.3 μM bound ThT had a fluorescence intensity of 621 ± 14 a. u. The variation between total bound dye is negligible, while the signal intensity is 50% higher when ThT was added before aggregation. One obvious explanation for the discrepancy would be the ThT molecule self-quenching.[39] If there are enough dye molecules bound in close proximity and in the surrounding solution, energy transfer between them could cause a quenching effect and reduce the overall fluorescence intensity. In the case of samples, where ThT was added after aggregation and sonication, there would still be some small fibril clumps that would shield a portion of available surface area. However, the similar amount of bound ThT in both cases suggests that the difference between total surface area is insignificant. This also negates the possibility that an insulin fibril polymorph with higher ThT binding capacity forms in the presence of ThT.

In order to further examine this quenching effect, fluorescence intensity dependence on bound ThT concentration was calculated. We can see that in the case when ThT was added after the aggregation reaction, the dye's fluorescence potential decreases with increasing concentration in a linear way on a logarithmic scale (Figure 2A). This is not the case when the dye is added before aggregation. First, the intensity/μM values are considerably higher throughout the entire range. In addition, the curve is no longer linear but sigmoidal. Fluorescence self-quenching does not explain why there is a

DOI: 10.1021/acs.jpcb.9b08652
J. Phys. Chem. B 2019, 123, 8727−8732

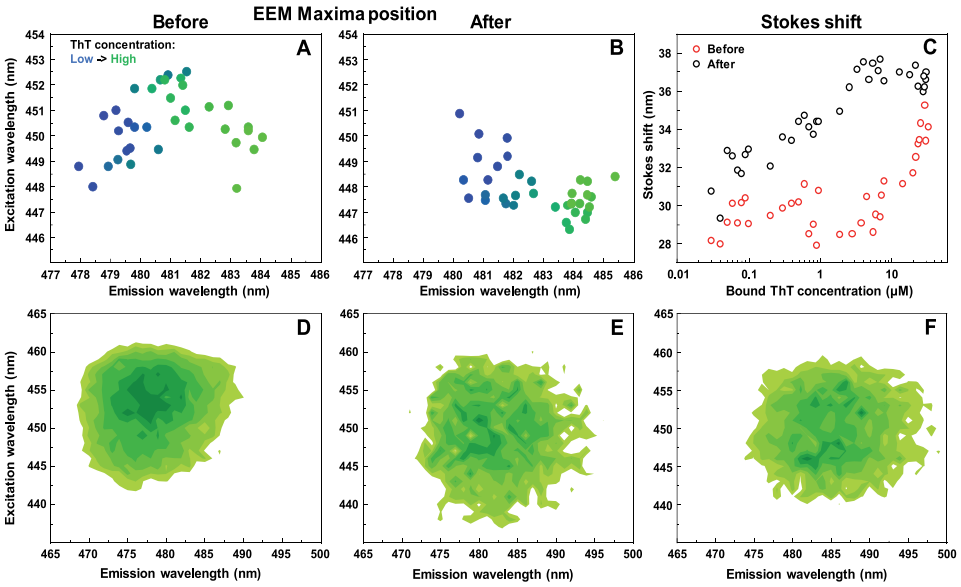

Figure 3. Excitation−emission matrix intensity distribution and Stokes shift of ThT bound to insulin fibrils. Position of EEM maxima with varying ThT concentrations when it is added to insulin before aggregation (A) and after (B). Stokes shift comparison between both conditions (C). EEM difference between insulin fibrils with ThT when the dye is added before and after aggregation when both samples have a similar bound ThT concentration (D). EEM difference between insulin fibrils with different ThT concentrations when dye is added after aggregation; 0.2 μM and 0.1 μM (E) and 40 μM and 20 μM (F). EEM images display the highest 20% intensity values with light green representing lower and dark green representing higher intensities.

difference in intensity/μM at low ThT concentrations or why the curve is sigmoidal. Subtracting one data set from the other (Figure 2B) reveals that the intensity/μM value divergence increases up to 1 μM of total dye concentration, and then the difference decreases to ∼10 au. Both of these factors point toward an idea that during fibril formation a ThT binding mode exists, which is not accessible from the outside of the aggregate after the reaction is complete. The 10 au intensity/μM difference continues to slowly decrease after 6 μM total ThT concentration, and the difference maximum is located between 0.1 and 2 μM. This would indicate that the core binding mode is nearly completely saturated when total ThT present in the solution is 6 μM and the largest difference between surface bound and core bound ThT is between 0.1 and 2.0 μM total ThT concentration. Comparing these values to the total amount of bound ThT, this core binding mode appears to account for only a small fraction of the fibril's total dye binding capacity. The bound molecules would also have a relatively high quantum yield, as this small amount would have to account for the 50% intensity difference at the highest bound ThT concentration. The core region would also not be affected by the increasing concentration of dye molecules outside of the fibrils.

As there appears to be another binding mode present in insulin fibrils and it causes ThT to have a higher quantum yield, it could also have different excitation and emission maxima wavelengths. Examining the EEM signal intensity center of mass reveals that when ThT is added before aggregation (Figure 3A), the maxima position shifts from 448/478 to 452/481 and then to 448/483 with increasing dye concentration, hinting that there are three types of ThT binding. In the case when ThT is added after aggregation (Figure 3B), we see the maxima position only shifts from 449/481 to 447/484 with increasing dye concentration, suggesting two types of ThT binding. Under both conditions, it is clear that at high bound ThT concentrations, the EEM maxima shifts toward a similar excitation and emission wavelength, likely caused by the most abundant binding mode. There is also a difference in both condition Stokes shift values (Figure 3C). When ThT was added after aggregation, the shift steadily increases from 29 nm to a plateau at 37 nm when the concentration of ThT rises to 6 μM. In the case when ThT was added before aggregation, the shift remains at 29 nm until 7−8 μM and then begins to converge to a similar value as the other condition samples. These observations fall in line with the differences seen in the intensity/μM graphs.

Seeing as 6 μM appears to be the point when the extra binding mode becomes almost completely saturated, an EEM of insulin fibrils with dye added after aggregation was subtracted from an EEM where the dye was added before aggregation (in both cases, the concentration of bound ThT was close to 6 μM). The resulting EEM highest signal intensities (Figure 3D) are shifted toward higher excitation and lower emission wavelengths, which explains why the lower concentration maxima positions seen in EEM of insulin fibrils with ThT added before aggregation (Figure 3A) are shifted in the same direction. Subtracting an EEM of insulin fibrils containing 0.1 μM ThT added after aggregation from an EEM with 0.2 μM (Figure 3E) reveals that the difference in intensity has a similar position as seen for low concentrations in Figure

DOI: 10.1021/acs.jpcb.9b08652
J. Phys. Chem. B 2019, 123, 8727−8732

3B. Subtracting an EEM with 20 μM ThT from one with 40 μM (Figure 3F) shows that the highest intensities move toward even higher emission wavelengths, similar to high concentration maxima positions in both Figure 3, panels A and B.

This indicates that when ThT is added after aggregation, it preferably binds in one mode at low dye concentrations and then in a second mode at high concentrations. On the other hand, when it is added before aggregation, it has a third binding mode which becomes nearly completely saturated at 6 μM of total ThT present in the sample and is accompanied by the other two binding modes.

CONCLUSIONS

Insulin fibril aggregates prepared at pH 2.4 with ThT present in the solution have a higher fluorescence intensity than ones with ThT added after fibrilization, and such a difference is not caused by a significantly larger amount of bound dye molecules. When ThT is added before aggregation, it appears to have access to an additional binding position, which becomes inaccessible after fibrils are fully formed. This specific binding mode accounts for a sizable portion of the total fluorescence intensity and causes the EEM maxima position to shift to different wavelengths, which should be taken into account when analyzing insulin amyloid aggregation.

ASSOCIATED CONTENT

Supporting Information

The Supporting Information is available free of charge on the ACS Publications website at DOI: 10.1021/acs.jpcb.9b08652.

Fibril sample supernatant absorbance spectrum (PDF)

AUTHOR INFORMATION

Corresponding Author

*Address: Sauletekio al. 7, Vilnius LT-10257, Lithuania. E-mail: vytautas.smirnovas@bti.vu.lt.

ORCID

Vytautas Smirnovas: 0000-0002-1829-5455

Author Contributions

M.Z. and V.S. designed the studies. M.Z. undertook the experimental work. M.Z. and V.S. analyzed the data and prepared the manuscript.

Notes

The authors declare no competing financial interest.

ACKNOWLEDGMENTS

This research was funded by Vilnius University, Grant MSF-JM-3.

REFERENCES

(1) Chiti, F.; Dobson, C. M. Protein Misfolding, Amyloid Formation, and Human Disease: A Summary of Progress Over the Last Decade. *Annu. Rev. Biochem.* **2017**, *86* (1), 27−68.

(2) Knowles, T. P. J.; Vendruscolo, M.; Dobson, C. M. The Amyloid State and Its Association with Protein Misfolding Diseases. *Nat. Rev. Mol. Cell Biol.* **2014**, *15* (6), 384−396.

(3) Belluti, F.; Rampa, A.; Gobbi, S.; Bisi, A. Small-Molecule Inhibitors/Modulators of Amyloid-β Peptide Aggregation and Toxicity for the Treatment of Alzheimer's Disease: A Patent Review (2010 − 2012). *Expert Opin. Ther. Pat.* **2013**, *23* (5), 581−596.

(4) Novick, P. A.; Lopes, D. H.; Branson, K. M.; Esteras-Chopo, A.; Graef, I. A.; Bitan, G.; Pande, V. S. Design of β-Amyloid Aggregation Inhibitors from a Predicted Structural Motif. *J. Med. Chem.* **2012**, *55* (7), 3002−3010.

(5) Šneideris, T.; Baranauskienė, L.; Cannon, J. G.; Rutkienė, R.; Meškys, R.; Smirnovas, V. Looking for a Generic Inhibitor of Amyloid-like Fibril Formation among Flavone Derivatives. *PeerJ* **2015**, *3*, e1271.

(6) Simoneau, S.; Rezaei, H.; Salès, N.; Kaiser-Schulz, G.; Lefebvre-Roque, M.; Vidal, C.; Fournier, J.-G.; Comte, J.; Wopfner, F.; Grosclaude, J.; et al. In Vitro and In Vivo Neurotoxicity of Prion Protein Oligomers. *PLoS Pathog.* **2007**, *3* (8), e125.

(7) Lu, J.-X.; Qiang, W.; Yau, W.-M.; Schwieters, C. D.; Meredith, S. C.; Tycko, R. Molecular Structure of β-Amyloid Fibrils in Alzheimer's Disease Brain Tissue. *Cell* **2013**, *154* (6), 1257−1268.

(8) Nielsen, L.; Khurana, R.; Coats, A.; Frokjaer, S.; Brange, J.; Vyas, S.; Uversky, V. N.; Fink, A. L. Effect of Environmental Factors on the Kinetics of Insulin Fibril Formation: Elucidation of the Molecular Mechanism. *Biochemistry* **2001**, *40* (20), 6036−6046.

(9) Batzli, K. M.; Love, B. J. Agitation of Amyloid Proteins to Speed Aggregation Measured by ThT Fluorescence: A Call for Standardization. *Mater. Sci. Eng., C* **2015**, *48*, 359−364.

(10) Xue, C.; Lin, T. Y.; Chang, D.; Guo, Z. Thioflavin T as an Amyloid Dye: Fibril Quantification, Optimal Concentration and Effect on Aggregation. *R. Soc. Open Sci.* **2017**, *4* (1), 160696.

(11) Ivancic, V. A.; Ekanayake, O.; Lazo, N. D. Binding Modes of Thioflavin T on the Surface of Amyloid Fibrils Studied by NMR. *ChemPhysChem* **2016**, *17* (16), 2461−2464.

(12) Freire, S.; De Araujo, M. H.; Al-Soufi, W.; Novo, M. Photophysical Study of Thioflavin T as Fluorescence Marker of Amyloid Fibrils. *Dyes Pigm.* **2014**, *110*, 97−105.

(13) Grigolato, F.; Arosio, P. Sensitivity Analysis of the Variability of Amyloid Aggregation Profiles. *Phys. Chem. Chem. Phys.* **2019**, *21* (3), 1435−1442.

(14) Chatani, E.; Inoue, R.; Imamura, H.; Sugiyama, M.; Kato, M.; Yamamoto, M.; Nishida, K.; Kanaya, T. Early Aggregation Preceding the Nucleation of Insulin Amyloid Fibrils as Monitored by Small Angle X-Ray Scattering. *Sci. Rep.* **2015**, *5* (1), 15485.

(15) Picken, M. M.; Herrera, G. A. Thioflavin T Stain: An Easier and More Sensitive Method for Amyloid Detection. In *Amyloid and Related Disorders*; Picken, M. M., Dogan, A., Herrera, G. A., Eds.; Humana Press: Totowa, NJ, 2012; pp 187−189.

(16) Zheng, Q.; Lazo, N. D. Mechanistic Studies of the Inhibition of Insulin Fibril Formation by Rosmarinic Acid. *J. Phys. Chem. B* **2018**, *122* (8), 2323−2331.

(17) Milto, K.; Botyriute, A.; Smirnovas, V. Amyloid-Like Fibril Elongation Follows Michaelis-Menten Kinetics. *PLoS One* **2013**, *8* (7), 8−11.

(18) Ziaunys, M.; Sneideris, T.; Smirnovas, V. Self-Inhibition of Insulin Amyloid-like Aggregation. *Phys. Chem. Chem. Phys.* **2018**, *20* (43), 27638−27645.

(19) Hortschansky, P.; Schroeckh, V.; Christopeit, T.; Zandomeneghi, G.; Fändrich, M. The Aggregation Kinetics of Alzheimer's β-Amyloid Peptide Is Controlled by Stochastic Nucleation. *Protein Sci.* **2005**, *14* (7), 1753−1759.

(20) Pujols, J.; Peña-Díaz, S.; Lázaro, D. F.; Peccati, F.; Pinheiro, F.; González, D.; Carija, A.; Navarro, S.; Conde-Giménez, M.; García, J.; et al. Small Molecule Inhibits α-Synuclein Aggregation, Disrupts Amyloid Fibrils, and Prevents Degeneration of Dopaminergic Neurons. *Proc. Natl. Acad. Sci. U. S. A.* **2018**, *115* (41), 10481−10486.

(21) Ono, K.; Hirohata, M.; Yamada, M. Ferulic Acid Destabilizes Preformed β-Amyloid Fibrils in Vitro. *Biochem. Biophys. Res. Commun.* **2005**, *336* (2), 444−449.

(22) Sulatskaya, A.; Rodina, N.; Sulatsky, M.; Povarova, O.; Antifeeva, I.; Kuznetsova, I.; Turoverov, K. Investigation of α-Synuclein Amyloid Fibrils Using the Fluorescent Probe Thioflavin T. *Int. J. Mol. Sci.* **2018**, *19* (9), 2486.

(23) Khurana, R.; Coleman, C.; Ionescu-Zanetti, C.; Carter, S. A.; Krishna, V.; Grover, R. K.; Roy, R.; Singh, S. Mechanism of Thioflavin T Binding to Amyloid Fibrils. *J. Struct. Biol.* **2005**, *151* (3), 229−238.

DOI: 10.1021/acs.jpcb.9b08652
J. Phys. Chem. B 2019, 123, 8727−8732

(24) Qin, Z.; Sun, Y.; Jia, B.; Wang, D.; Ma, Y.; Ma, G. Kinetic Mechanism of Thioflavin T Binding onto the Amyloid Fibril of Hen Egg White Lysozyme. *Langmuir* **2017**, *33* (22), 5398−5405.
(25) Lockhart, A.; Ye, L.; Judd, D. B.; Merritt, A. T.; Lowe, P. N.; Morgenstern, J. L.; Hong, G.; Gee, A. D.; Brown, J. Evidence for the Presence of Three Distinct Binding Sites for the Thioflavin T Class of Alzheimer's Disease PET Imaging Agents on β-Amyloid Peptide Fibrils. *J. Biol. Chem.* **2005**, *280* (9), 7677−7684.
(26) Wu, C.; Biancalana, M.; Koide, S.; Shea, J.-E. Binding Modes of Thioflavin-T to the Single-Layer β-Sheet of the Peptide Self-Assembly Mimics. *J. Mol. Biol.* **2009**, *394* (4), 627−633.
(27) Groenning, M.; Norrman, M.; Flink, J. M.; van de Weert, M.; Bukrinsky, J. T.; Schluckebier, G.; Frokjaer, S. Binding Mode of Thioflavin T in Insulin Amyloid Fibrils. *J. Struct. Biol.* **2007**, *159* (3), 483−497.
(28) Rodríguez-Rodríguez, C.; Rimola, A.; Rodríguez-Santiago, L.; Ugliengo, P.; Álvarez-Larena, Á.; Gutiérrez-de-Terán, H.; Sodupe, M.; González-Duarte, P. Crystal Structure of Thioflavin-T and Its Binding to Amyloid Fibrils: Insights at the Molecular Level. *Chem. Commun.* **2010**, *46* (7), 1156.
(29) Kawai, R.; Araki, M.; Yoshimura, M.; Kamiya, N.; Ono, M.; Saji, H.; Okuno, Y. Core Binding Site of a Thioflavin-T-Derived Imaging Probe on Amyloid β Fibrils Predicted by Computational Methods. *ACS Chem. Neurosci.* **2018**, *9* (5), 957−966.
(30) Sidhu, A.; Vaneyck, J.; Blum, C.; Segers-Nolten, I.; Subramaniam, V. Polymorph-Specific Distribution of Binding Sites Determines Thioflavin-T Fluorescence Intensity in α-Synuclein Fibrils. *Amyloid* **2018**, *25* (3), 189−196.
(31) Kutsch, M.; Hortmann, P.; Herrmann, C.; Weibels, S.; Weingärtner, H. Dissecting Ion-Specific from Electrostatic Salt Effects on Amyloid Fibrillation: A Case Study of Insulin. *Biointerphases* **2016**, *11* (1), 019008.
(32) Mao, X.; Guo, Y.; Wang, C.; Zhang, M.; Ma, X.; Liu, L.; Niu, L.; Zeng, Q.; Yang, Y.; Wang, C. Binding Modes of Thioflavin T Molecules to Prion Peptide Assemblies Identified by Using Scanning Tunneling Microscopy. *ACS Chem. Neurosci.* **2011**, *2* (6), 281−287.
(33) Sneideris, T.; Darguzis, D.; Botyriute, A.; Grigaliunas, M.; Winter, R.; Smirnovas, V. PH-Driven Polymorphism of Insulin Amyloid-Like Fibrils. *PLoS One* **2015**, *10* (8), e0136602.
(34) Kim, Y. S.; Liu, L.; Axelsen, P. H.; Hochstrasser, R. M. 2D IR Provides Evidence for Mobile Water Molecules in -Amyloid Fibrils. *Proc. Natl. Acad. Sci. U. S. A.* **2009**, *106* (42), 17751−17756.
(35) Wang, T.; Jo, H.; DeGrado, W. F.; Hong, M. Water Distribution, Dynamics, and Interactions with Alzheimer's β-Amyloid Fibrils Investigated by Solid-State NMR. *J. Am. Chem. Soc.* **2017**, *139* (17), 6242−6252.
(36) Singh, P. K.; Kumbhakar, M.; Pal, H.; Nath, S. Viscosity Effect on the Ultrafast Bond Twisting Dynamics in an Amyloid Fibril Sensor: Thioflavin-T. *J. Phys. Chem. B* **2010**, *114* (17), 5920−5927.
(37) Sulatskaya, A. I.; Maskevich, A. A.; Kuznetsova, I. M.; Uversky, V. N.; Turoverov, K. K. Fluorescence Quantum Yield of Thioflavin T in Rigid Isotropic Solution and Incorporated into the Amyloid Fibrils. *PLoS One* **2010**, *5* (10), e15385.
(38) Ziaunys, M.; Smirnovas, V. Emergence of Visible Light Optical Properties of L-Phenylalanine Aggregates. *PeerJ* **2019**, *7*, e6518.
(39) Lindberg, D. J.; Wenger, A.; Sundin, E.; Wesén, E.; Westerlund, F.; Esbjörner, E. K. Binding of Thioflavin-T to Amyloid Fibrils Leads to Fluorescence Self-Quenching and Fibril Compaction. *Biochemistry* **2017**, *56* (16), 2170−2174.

DOI: 10.1021/acs.jpcb.9b08652
J. Phys. Chem. B 2019, 123, 8727−8732

SCIENTIFIC REPORTS
nature research

OPEN

Amyloidophilic Molecule Interactions on the Surface of Insulin Fibrils: Cooperative Binding and Fluorescence Quenching

Mantas Ziaunys, Kamile Mikalauskaite & Vytautas Smirnovas*

Protein aggregation into insoluble fibrillar aggregates is linked to several neurodegenerative disorders, such as Alzheimer's or Parkinson's disease. Commonly used methods to study aggregation inhibition or fibril destabilization by potential drugs include spectroscopic measurements of amyloidophilic dye molecule fluorescence or absorbance changes. In this work we show the cross-interactions of five different dye molecules on the surface of insulin amyloid fibrils, resulting in cooperative binding and fluorescence quenching.

The aggregation of amyloidogenic proteins into highly structured amyloid fibrils is linked to several neurodegenerative disorders, such as Alzheimer's, Parkinson's and prion diseases[1–3]. The process of amyloid formation consists of native protein structural rearrangement and subsequent elongation into insoluble fibrillar aggregates[4]. Besides being cytotoxic[5], these fibrils possess the ability to self-replicate, a process which is being extensively studied in the hopes of understanding its mechanism and finding potential inhibitors[6,7]. However, as of yet, there is still no known cure or effective treatment available[8].

In vitro experiments of amyloid fibril formation and self-replication are often used when screening for potential inhibitory molecules or compounds that cause a disassembly of the aggregate structure. These observations are typically done by employing one or several methods, such as atomic force microscopy[9], extrinsic dye fluorescence spectroscopy[10], light scattering[11], Fourier-transform infrared spectroscopy[12], circular dichroism spectroscopy[13] and others[14]. While all these methods have their advantages and shortcomings, in this work we will focus on the use of absorbance and fluorescence spectroscopy. There is a growing amount of research being conducted on amyloid fibril aggregation and dissociation with the use of several amyloidophilic dye molecules. The most frequently utilized ones are thioflavin-T (ThT) and Congo red (CR) – which bind to grooves formed by beta-sheets on the fibril's surface[15–18], as well as 8-anilinonaphthalene-1-sulfonic acid (ANS) – which binds to the fibril's hydrophobic regions[19]. A common assumption made when using these dyes is that a change in their fluorescence signal or shift in their absorbance spectrum is the result of either amyloid fibril formation or dissociation[20–23].

A few recent reports allude to the fact that the use of such extrinsic fibril dyes is problematic when screening for potential aggregation inhibiting or fibril destabilizing substances. In the work done by Girych *et al.*[24] it is shown that when two of these amyloidophilic dyes are used in unison, namely ThT and CR, the fluorescence intensity of ThT is greatly reduced. CR is also known to quench other compound fluorescence, as shown by Patel *et al.*[25]. A report by Buell *et al.*[26] demonstrates that ThT and CR interact with one another at neutral pH and influence each other's binding to fibrils. The work by Hudson *et al.*[27] displays a ThT fluorescence quenching effect by polyphenolic anti-amyloid compounds. Another report by Lindberg *et al.*[28] has shown that when an increasing number of ThT molecules bind to the surface of fibrils, they cause a self-quenching effect. This indicates that the presence of another molecule, capable of binding to the fibril's surface, may alter the dye's fluorescence potential, thus leading to false conclusions that the compound's addition resulted in the inhibition or disassembly of amyloid fibrils.

Potential drugs that directly influence amyloid formation or dissociation have to, in one way or another, interact with either the native state protein (stabilizing the native state or changing the aggregation's path to non-fibrillar species[29,30]) or with the fibril (causing its dissociation or preventing it from incorporating native proteins[31,32]). In cases when it interacts with fibrils, it could act in a similar way as CR did with ThT in the previously

Institute of Biotechnology, Life Sciences Center, Vilnius University, Vilnius, Lithuania. *email: vytautas.smirnovas@bti.vu.lt

mentioned reports. This could lead to a false identification of the molecule in question as a potential anti-amyloid drug, while in actuality, its only function was as a fluorescence quencher.

In this work we examine five amyloidophilic dye molecules possessing very characteristic spectral properties – thioflavin-T, Congo red, 8-anilinonaphthalene-1-sulfonic acid, dapoxyl (Dap)[33] and methylene blue (MB)[34,35] in order to determine their cross-interactions when binding to insulin amyloid fibrils. We show the changes of absorbance spectra when these molecules interact with one another in solution and on fibrils, as well as how they influence each other's fibril binding affinity and the fluorescence intensity of ThT, ANS and Dap.

Methods

Fibril preparation. Human recombinant insulin (Sigma-Aldrich cat. No. 91077 C) was dissolved in PBS (pH 7.4) buffer to a final protein concentration of 300 μM (1.74 mg/ml). Insulin concentration was determined by measuring the sample's absorbance at 280 nm, with $\varepsilon = 6335\,M^{-1}cm^{-1}$ and M = 5808 Da. The protein solutions were distributed to test tubes (Fisher cat. No. 15432545) at a volume of 1 mL each and 2 glass beads (Merck, cat. No. 104015) were placed inside every tube. The samples were then mixed at a constant 600 rpm agitation at 60 °C in a Ditabis ThermoMixer MHR 23 for 24 hours. Formation of amyloids was confirmed by both atomic force microscopy (AFM) (Supplementary Fig. S1), which showed short insulin fibrils and Fourier-transform infrared spectroscopy (FTIR) (Supplementary Fig. S1), which revealed a beta-sheet secondary structure[36].

Dye solution preparation. ThT, CR, ANS, Dap and MB powders were dissolved in PBS (pH 7.4) buffer, filtered and diluted to a final concentration of 150 μM for ThT, CR, ANS, Dap and 20 μM for MB. Dye concentrations were determined by measuring a 10-fold diluted sample's absorbance at 412 nm for ThT ($\varepsilon = 22.1 \times 10^3\,M^{-1}cm^{-1}$), 486 nm for CR ($\varepsilon = 33.3 \times 10^3\,M^{-1}cm^{-1}$), 351 nm for ANS ($\varepsilon = 5.2 \times 10^3\,M^{-1}cm^{-1}$), 348 nm for Dap ($\varepsilon = 28.4 \times 10^3\,M^{-1}cm^{-1}$) and 664 nm for MB ($\varepsilon = 73.1 \times 10^3\,M^{-1}cm^{-1}$). The stock solutions were kept at 4 °C in the dark to prevent oxidation. Dye absorbance spectra before and after the experiments was measured to determine if there was no oxidation or loss of spectral properties.

Absorbance measurements. Samples for absorbance measurements were prepared by mixing dye, fibril and PBS solutions so that the dye and fibril solutions would be diluted 3 times, yielding 300 μL samples containing either a single dye, two dyes or dyes with 100 μM of insulin fibrils. The samples were then incubated at room temperature for 1 hour, after which they were scanned using a Shimadzu UV-1800 spectrophotometer (1 nm steps). The samples were diluted either 2 or 3 times when their absorbance was over the value of 2 in the scanned range. For each condition, three separate measurements were taken and a spectrum of insulin fibrils without dyes was subtracted. Then the samples were centrifuged at 20'000 g for 20 min. 150 μL of supernatant was carefully removed from each sample and its absorbance spectrum was scanned (1 nm steps). For each condition, three samples were scanned three times and the 9 spectra were averaged.

Absorbance difference and compensation curves. The absorbance spectra of two combined dyes were subtracted from the combined spectra when dyes were measured separately. In order to determine the contribution of each respective dye molecule to the resulting difference, the following system of equations was used:

$$\varepsilon_{11} \times x + \varepsilon_{12} \times y = A_1 \quad (1)$$

$$\varepsilon_{21} \times x + \varepsilon_{22} \times y = A_2 \quad (2)$$

where ε_{11} is the first dye's extinction coefficient at wavelength λ_1, ε_{12} is the second dye's extinction coefficient at wavelength λ_1, ε_{21} is the first dye's extinction coefficient at wavelength λ_2, ε_{22} is the second dye's extinction coefficient at wavelength λ_2, A_1 is the sample's absorbance at wavelength λ_1, A_2 is the sample's absorbance at wavelength λ_2, x is the concentration of the first dye and y is the concentration of the second dye. The specific wavelengths were chosen based on each molecule's specific absorbance maxima described in the dye solution preparation section, with an exception for the ANS and Dap pair, where the wavelength used for ANS was 265 nm ($\varepsilon = 16.2 \times 10^3\,M^{-1}cm^{-1}$), due to the close proximity of both absorbance maxima (351 nm and 348 nm for ANS and Dap respectively).

The contribution of each dye to the absorbance difference was then used to calculate a compensation curve, by combining each dye's respective absorbance fraction, i.e. if the difference was the result of a loss of 20% ThT and 10% ANS, then the compensation curve was the sum of 20% ThT and 10% ANS spectra. To correct for this difference in dye-fibril interaction experiments, the absorbance intensity at every wavelength is multiplied by the ratio between the absorbance intensities of dyes measured separately and together at the corresponding wavelength.

Fluorescence measurements. For fluorescence measurements, samples were prepared as described in the absorbance measurement section, apart from the last centrifugation step. Excitation-emission matrices (EEM) of each sample were then scanned using a Varian Cary Eclipse fluorescence spectrophotometer, using an excitation and emission range from 200 to 800 nm, with 10 nm excitation and 2 nm emission steps using 5 nm excitation and 2.5 nm emission slit widths. From each EEM, 100 nm x 100 nm regions containing fluorescence signals were scanned in greater detail with 1 nm excitation and 2 nm emission steps, using the same slit widths. For every condition, three detailed EEMs were scanned and averaged. The signal resulting from Rayleigh scattering was subtracted from each EEM.

Inner filter corrections. To correct for both the primary and secondary inner filter effects, the absorbance spectra of samples used in the fluorescence measurements were taken. In cases when the absorbance values were greater than 2, the samples were diluted either 2 or 3 times. Fibril absorbance spectra were then subtracted from

the dye-fibril spectra to determine the absorbance of free and bound dye present in the solution. Each EEM was corrected for the inner filter effect by using the following equation:

$$I_m = I_c \times 10^{-((AEx+AEm)/2)} \quad (3)$$

where AEx is the sample's absorbance at the excitation wavelength, AEm is the sample's absorbance at the emission wavelength, I_m is the signal intensity observed during measurement and I_c is the corrected signal intensity.

Titration of ThT-fibrils with CR. Insulin fibrils were combined with ThT and CR solutions to a final fibril concentration of 100 μM, ThT concentrations – 50, 100 and 150 μM and CR concentrations in the range from 0 to 50 μM. Samples were incubated for 1 hour, after which their fluorescence was measured with an excitation wavelength of 440 nm and 460–500 nm emission range using 5 nm excitation and 2.5 nm emission slits. Absorbance was measured after diluting a fraction of the solution 10 times. Non-bound ThT concentration was determined after sample centrifugation as described previously. Non-bound CR was determined to be less than 1 μM in all of the supernatants.

Results

Dye molecule interactions. Before any dye-fibril binding could be examined, the interactions between amyloidophilic molecules had to be evaluated. For each pair, a combined dye solution spectrum was measured and compared against a sum of corresponding separate dye solution spectra with identical concentrations. In some cases, we observed a massive disparity between the spectra, as seen with ThT-CR (Fig. 1a,b) and CR-MB (Fig. 1m,n). In other cases, there is a reduction in overall absorbance, as seen with ThT-ANS (Fig. 1c,d), ThT-Dap (Fig. 1e,f), ANS-MB (Fig. 1q,r) and Dap-MB (Fig. 1s,t). For other dye pairs, there is almost no difference between the spectra, as seen with ThT-MB (Fig. 1g,h), CR-ANS (Fig. 1I,j), CR-Dap (Fig. 1k,l) and ANS-Dap (Fig. 1o,p).

For each dye-pair absorbance spectra difference, a compensation spectrum was created by calculating what fraction of each dye is needed to compensate for the change in absorbance. In most cases, the difference and compensation spectra overlap, however, in the case of ThT-CR, CR-MB and to a lower extent ANS-MB and Dap-MB, there appears to be no way to compensate for this change. Examining how much of each dye is needed to create the compensation spectra, considerable fractions are required for ThT-CR, ThT-ANS, ThT-Dap, CR-MB, ANS-MB and Dap-MB pairs. In the case of ThT-MB, the combined dye solution creates the appearance that there is slightly more MB dye present than when measured separately. These interactions have to be taken into consideration in further dye-fibril binding experiments by correcting dye-pair spectra as described in the method section.

Dye interaction with fibrils. Examining single dye and dye-pair binding to insulin fibrils reveals that in every single case, there was an interference between these amyloidophilic molecules, even when the dye-dye interactions were accounted for. For ThT, the presence of every other dye increased its binding to fibrils (Fig. 2a–h), with the most notable change seen in the ThT-CR pair, where almost all ThT is bound. For CR (Fig. 2a,b,i–n), there were only very minimal changes in bound concentration and the vast majority of it remained on the fibril's surface, as it has a high binding affinity[37]. For ANS (Fig. 2c,d,i,j,o-r), there were small changes when paired with ThT or MB, but a noticeable decrease with CR and Dap. For Dap (Fig. 2e,f,k,l,o,p,s,t), there was an increase in bound concentration with ThT and MB, and a decrease with CR and ANS. For MB (Fig. 2g,h,m,n,q–t), there were small increases with ThT, ANS and Dap, and a larger one with CR. The compensation curves nearly perfectly mimicked the absorbance difference curves, except in the cases of ThT-MB, ANS-MB and Dap-MB.

The absorbance spectra of dyes when they are bound to fibrils was also examined (Fig. 3). When comparing the combined spectra of single dyes bound to fibrils with the spectra when both dyes are present, we see that in some of the cases, namely ThT-ANS (Fig. 3b), CR-ANS (Fig. 3e), CR-Dap (Fig. 3f) and ANS-Dap (Fig. 3h), there is virtually no difference between their peak wavelengths and only a small change in the case of ThT-Dap (Fig. 3c). However, there are very clear differences when comparing ThT-CR (Fig. 3a), ThT-MB (Fig. 3d), CR-MB (Fig. 3g), ANS-MB (Fig. 3i) and Dap-MB (Fig. 3j). In the ThT-CR pair, the ThT-related peak position shifts from 443 nm to 450 nm and in the ThT-MB pair - from 421 nm to 424 nm. In every case where MB is present, the MB-specific peaks experience a drastic change: from 643 nm to 665 nm in the ThT-MB pair, from 641 nm to 687 nm in the CR-MB pair, from 643 nm to 662 nm in the ANS-MB pair and from 643 nm to 665 in the Dap-MB pair.

Dye fluorescence. The excitation-emission matrices of ThT (Fig. 4a–e), ANS (Fig. 4f–j) and Dap (Fig. 4k–o), as well as single wavelength fluorescence spectra (Fig. 4p–r) with fibrils separately and in pairs were acquired and corrected for the primary and secondary inner filter effect in order to examine any possible effects of dye interference on their fluorescence intensity. In the case of ThT, when comparing the EEM of the dye alone with fibrils (Fig. 4a) and mixed with other amyloidophilic molecules, we observe an almost complete fluorescence quenching in the ThT-CR pair (Fig. 4b). There is also a substantial quenching effect seen with all other three tested molecules (Fig. 4c–e). In the case of ANS (Fig. 4f), CR completely quenches its fluorescence (Fig. 4h) and MB partially reduces its emission intensity (Fig. 4j). ANS-ThT (Fig. 4g) and ANS-Dap (Fig. 4i) pairs are more difficult to analyze, as their EEM spectra partially overlap, however, in the ANS-ThT pair we see the ANS EEM maxima position intensity is considerably reduced. The ANS-Dap pair has a similar intensity when compared against a sum of separate ANS and Dap spectra (327 and 334 a.u. respectively at the most intense EEM position). For Dap (Fig. 4k), the addition of ThT, CR or MB greatly quench its fluorescence (Fig. 4l,m,o) and there is virtually no effect when combined with ANS (Fig. 4n), as mentioned previously. There is no observable fluorescence emission intensity maxima shift in any of the cases, where these are no overlapping spectra from other dye molecules.

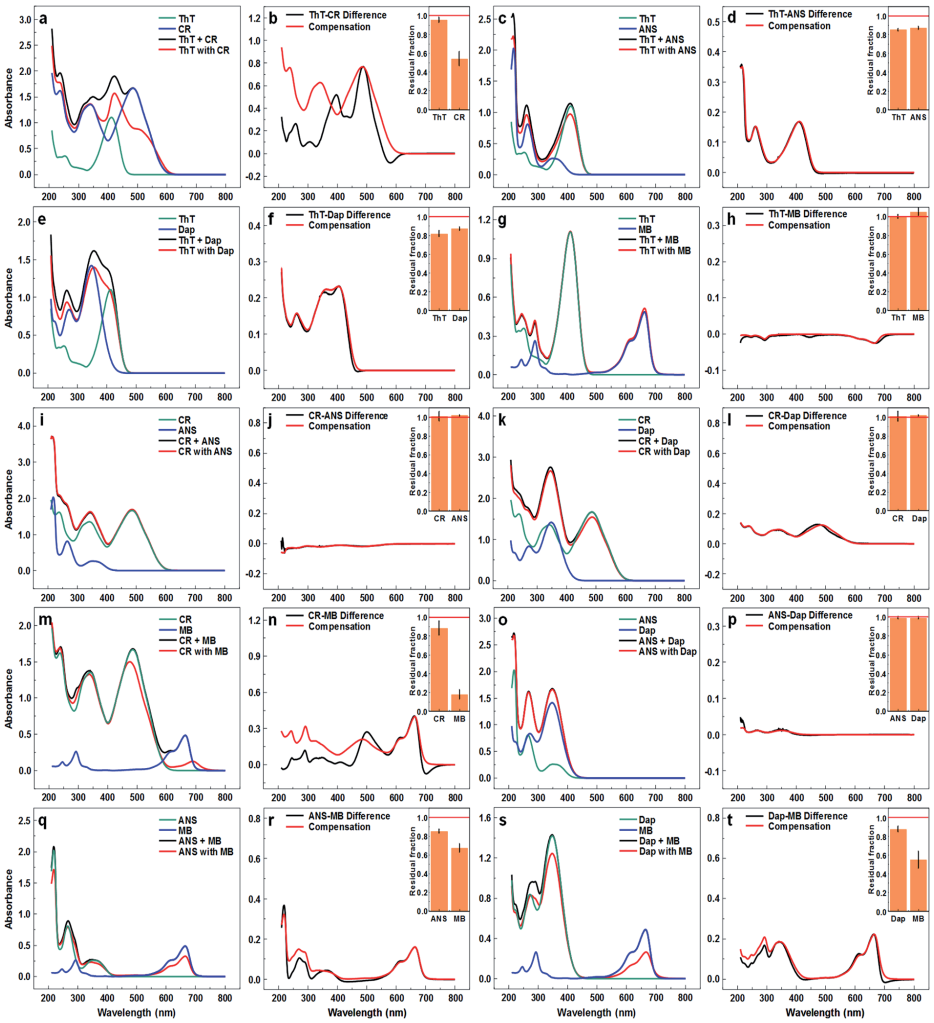

Figure 1. Absorbance spectra of ThT, CR, ANS, Dap and MB pairs. Comparison of absorbance spectra when dyes are measured separately and the spectra are combined (marked as Dye + Dye) and when they are measured together (marked as Dye with Dye), as well as the difference between both spectra and a calculated compensation curve for ThT and CR (**a**,**b**), ThT and ANS (**c**,**d**), ThT and Dap (**e**,**f**), ThT and MB (**g**,**h**), CR and ANS (**i**,**j**), CR and Dap (**k**,**l**), CR and MB (**m**,**n**), ANS and Dap (**o**,**p**), ANS and MB (**q**,**r**), Dap and MB (**s**,**t**). Inserts show the residual fraction of each dye's respective absorbance remaining when the dyes are combined as opposed to being scanned separately.

ThT and CR interaction. Seeing as the ThT-CR pair results in both the strongest quenching effect, as well as the most extreme change in ThT binding affinity, these dyes were subjected to further examinations. Fibril samples containing 50, 100 and 150 µM final ThT concentrations were titrated with CR. When the sample contains 50 µM ThT, rising the concentration of CR initially results in a linear increase in the concentration of bound ThT (Fig. 5a), followed by a gradual shift to a plateau, when almost all ThT molecules become bound. The slope of the linear part indicates that one CR molecule causes, on average, an additional binding of 1.3 ThT molecules. When the same titration experiment is conducted with 100 µM ThT (Fig. 5a), the linear section is longer and the slope value is 2.0, with all ThT eventually becoming bound. Finally, in the case of 150 µM ThT (Fig. 5a), the linear part is even further extended, with a slope value of 2.3. Now, however, 50 µM of CR does not cause all of ThT to become bound and it seems that more CR molecules would be needed for this to occur, as a plateau is not reached.

Examining how the gradual increase in CR concentration affects the fluorescence intensity of ThT (Fig. 5b) reveals that when the concentration of ThT is low, adding CR very quickly causes a massive drop in fluorescence

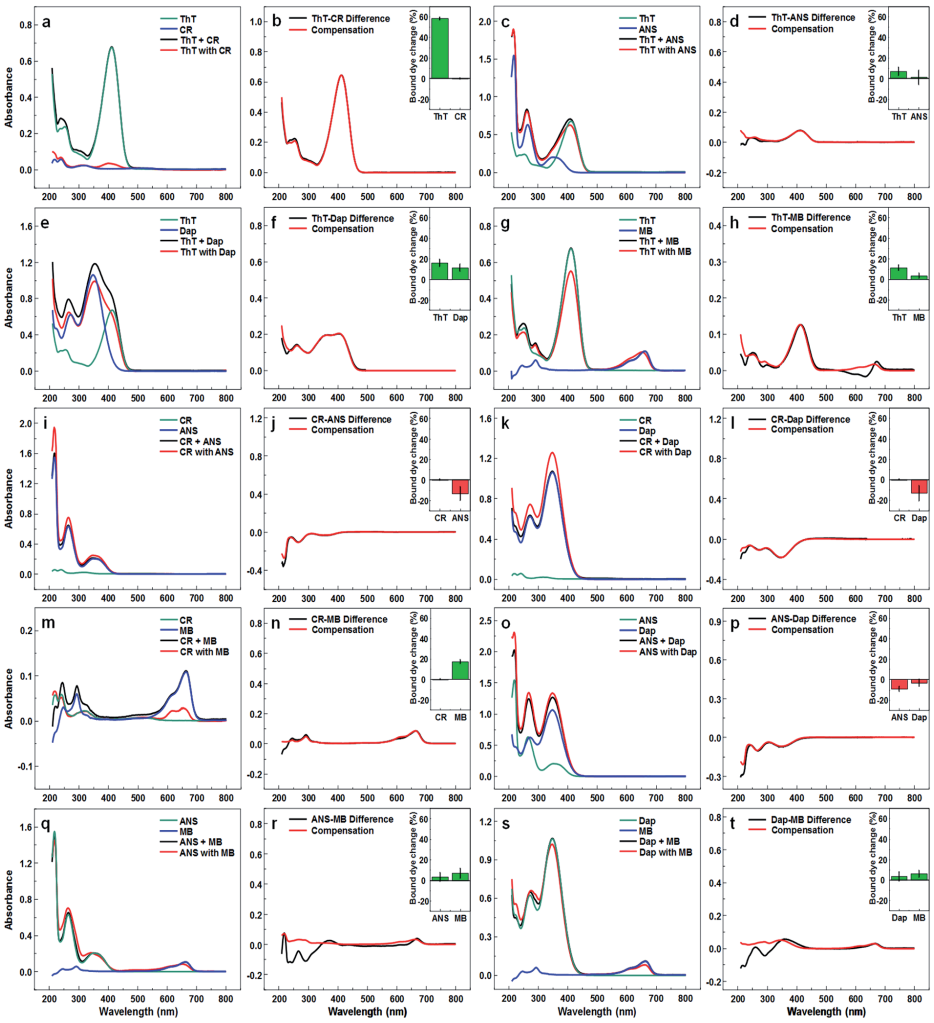

Figure 2. Absorbance spectra of ThT, CR, ANS, Dap and MB pairs remaining in supernatant after separation from fibrils. Comparison of dye supernatant absorbance spectra when the dyes were mixed with fibrils separately and the spectra were then combined (marked as Dye + Dye) and when both dyes were mixed with fibrils (marked as Dye with Dye), as well as the difference between both spectra and a calculated difference compensation curve for ThT and CR (**a**,**b**), ThT and ANS (**c**,**d**), ThT and Dap (**e**,**f**), ThT and MB (**g**,**h**), CR and ANS (**i**,**j**), CR and Dap (**k**,**l**), CR and MB (**m**,**n**), ANS and Dap (**o**,**p**), ANS and MB (**q**,**r**), Dap and MB (**s**,**t**). Inserts show the difference in bound dye concentration when they are both mixed with fibrils as opposed to being mixed separately. The difference is displayed as a percentage of total dye present in the initial sample.

emission intensity. When there is 100 µM ThT present, the fluorescence intensity dependence on CR concentration gains a sigmoidal shape and the intensity does not experience a significant drop at low CR concentrations. In the case of 150 µM ThT, there is an even longer initial plateau and the fluorescence intensity does not become completely quenched at the highest CR concentration. The total bound ThT at the highest ThT-CR concentrations tested is significantly higher than the amount of bound ThT when in the absence of CR (Fig. 5c).

Measuring the absorbance spectra of all samples used in the titration experiment reveals that in the case of 50 µM ThT (Fig. 5d), the absorbance maxima at 417 nm (when only free and bound ThT is present), begins to shift towards 450 nm after all ThT becomes bound. Such a shift is not evident under the two larger ThT concentrations (Fig. 5e,f), where the dye does not become fully bound at lower CR concentrations. This peak shift could be caused by an increasing amount of normally bound CR, which is not associated with ThT, as the ThT-CR interactions become saturated. If we calculate what the spectrum of bound ThT and CR was if they were bound separately with no interaction with one another and compare it to the highest ThT-CR concentration spectra, we

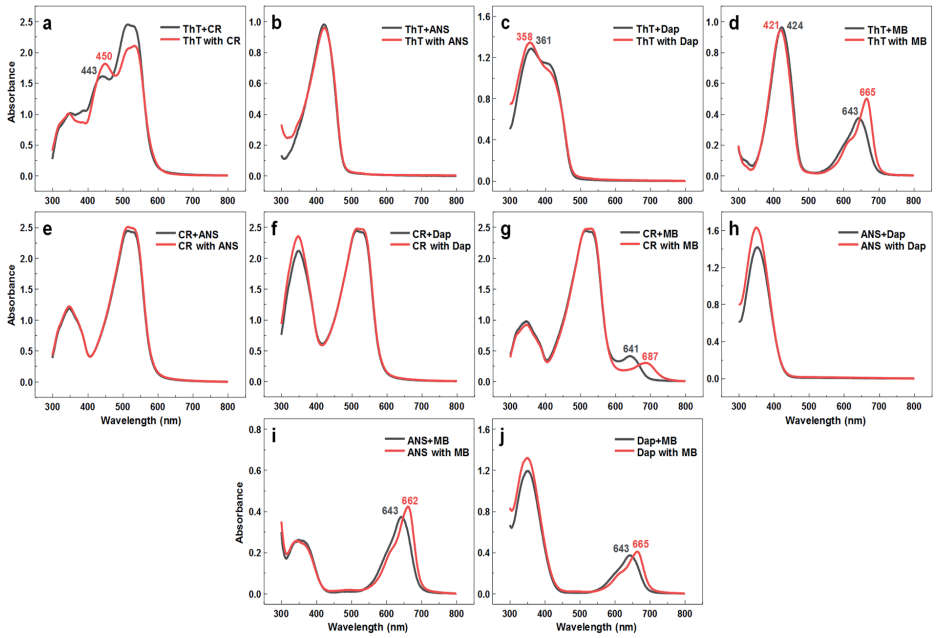

Figure 3. Absorbance spectra of dyes mixed with insulin fibrils. Comparison between absorbance spectra when the dyes were mixed with fibrils separately and then the spectra were combined (marked as Dye + Dye) and when both dyes were mixed with fibrils (marked as Dye with Dye) for ThT-CR (**a**), ThT-ANS (**b**), ThT-Dap (**c**), ThT-MB (**d**), CR-ANS (**e**), CR-Dap (**f**), CR-MB (**g**), ANS-Dap (**h**), ANS-MB (**i**) and Dap-MB (**j**) dye pairs. Color-coded numbers indicate the absorbance peak wavelengths (nm), where there is a shift in the peak's position.

observe an increasing disparity between them as the concentration of ThT rises. The most notable differences are observed for peaks in the 500–550 nm range associated with CR bound to insulin fibrils.

Discussion

The examination of dye molecule interactions reveals that no interference is seen in only a few select cases. In other cases, the combined solution absorbance spectra are lower or different than of summed separate dye solution spectra, suggesting the possibility that these molecules interact with one another in solution. In the case of ThT-CR and CR-MB we even see a shift in absorbance maxima positions, which may be due to dye-complex formation. This CR interaction with ThT and MB is interesting, as CR does not seem to interact with other dye molecules, such as ANS or Dap. Another interesting case is the considerable interference of MB, which is a potential amyloidosis inhibitor[35], with CR, ANS and Dap and to a lesser extent with ThT. These interactions have to be taken into account when examining amyloid fibril formation with more than one dye or when a potential inhibitor molecule possesses a similar scaffold to one that interferes with the dye molecule. Otherwise, a change in the optical properties of a sample could be falsely attributed to changes in fibril concentration.

When examining dye pair binding to fibrils, we observe a quite unusual result. Normally, it would be expected that if two amyloidophilic molecules bind to different parts of the fibril, then there would be no change in bound concentration when they are combined. If the molecules had the same or similar binding position, then there would be a reduction in each of their bound concentration, depending on each molecule's binding affinity. The strange thing here is that in 7 out of 10 cases, there is an increase in bound dye concentration, which means that the molecules actually aid one another in binding to the fibril's surface. This could potentially be achieved by either dye-dye interaction or complex formation, as seen in Fig. 1 or by fibril surface changes induced by the binding of dye molecules, such as subtle structural or charge alterations. The absorbance spectra of dyes bound to fibrils indicate that all pairs with MB and the ThT-CR pair experience significant changes. This supports the idea that there is some direct interaction between these molecules when they are located on the surface of fibrils. Examining the fluorescence of ThT, ANS and Dap, we see that in every single pair that contains ThT, its fluorescence is quenched quite dramatically, even though from dye-fibril interactions we know that there is more ThT bound in every case. These results are in line with previously reported observations of a quenching effect for the ThT-CR pair[24], however, it appears that this effect is not due to less ThT molecules binding, which would be the obvious first conclusion, but due to the existence of another amyloidophilic molecule. The same is true for both ANS and Dap, where the existence of other dye molecules quench their fluorescence emission intensity, except for when the two are paired together. This could be caused by either dye-dye interactions and weak complex

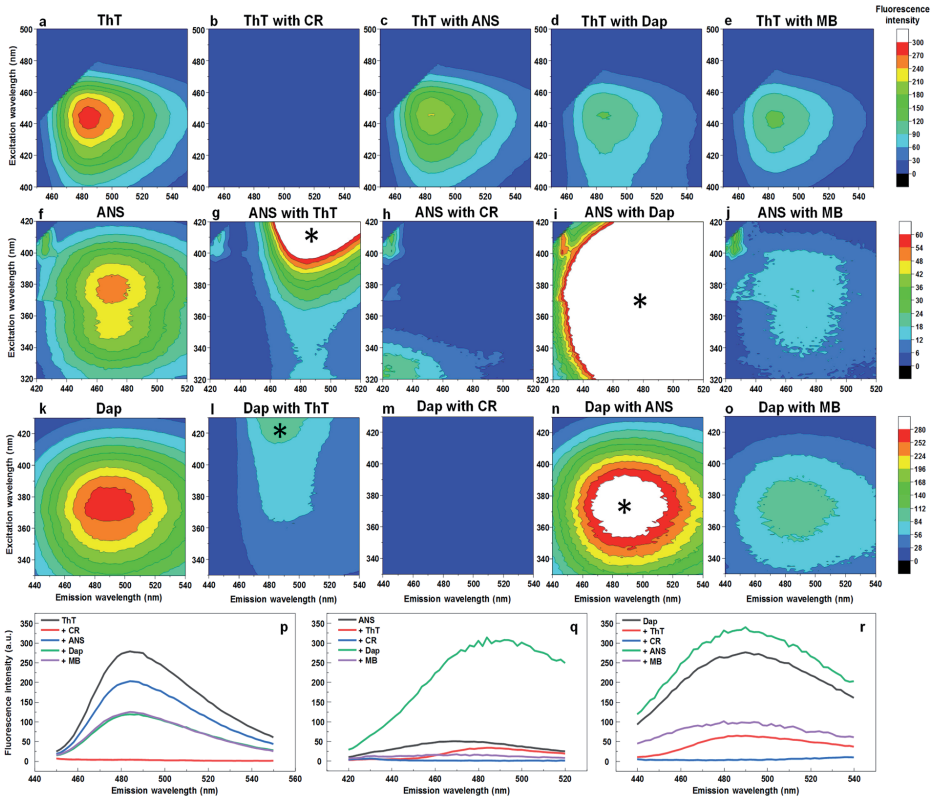

Figure 4. Excitation-emission matrices of ThT, ANS and Dap interacting with CR, MB and each other on insulin fibrils. EEM centered on the ThT emission signal maxima of single ThT (**a**) and in pairs with CR (**b**), ANS (**c**), Dap (**d**) and MB (**e**). EEM centered on the ANS emission signal maxima of single ANS (**f**) and in pairs with ThT (**g**), CR (**h**), Dap (**i**) and MB (**j**). EEM centered on the Dap emission signal maxima of single Dap (k) and in pairs with ThT (**l**), CR (**m**), ANS (**n**) and MB (**o**). Single excitation wavelength emission spectra of ThT at 440 nm (**p**), ANS at 380 nm (**q**) and Dap at 375 nm (**r**) mixed with other dyes. The * symbol represents fluorescence emission signals resulting from another dye in the solution.

formation or their interference while bound nearby on the surface of fibrils, possibly due to energy transfer between each other. There has been a report indicating that Forster-resonance energy transfer (FRET) is possible on amyloid fibrils even if the molecules are not conjugated[38]. Such an event would require the dye molecules to be in close proximity to one another (distances of less than 10 nm), as well as have an overlap between one molecule's excitation and another's emission spectra. CR absorbance overlaps with ThT, ANS and Dap emission spectra and the relatively high concentration of bound dye molecules at specific parts of the fibrils could bring them into close proximity. Now while this explains the quenching effect of CR on all three fluorescent dyes, as well as ThT's effect on ANS and Dap fluorescence and the non-existent quenching between ANS and Dap, this does not explain why ANS, Dap or MB quench the fluorescence of ThT. The emission spectrum of ThT does not match with the absorbance spectra of these three molecules, yet the fluorescence intensity is still considerably reduced. This unlikeliness of a FRET event leads to a conclusion that there has to be some interaction between these molecules, which induces a quenching effect without such energy transfer, which is likely due to a weak-complex formation which changes the dye's quantum yield.

A further examination of the interaction between ThT and CR on the surface of amyloid fibrils revealed that CR is extremely effective at increasing ThT's binding affinity. If this was the result of changes to the fibril's surface, which facilitated more positions for ThT binding, there would be minimal differences between the calculated sum absorbance spectra of bound ThT and CR when compared to the real spectra, which is not the case in either of the tested conditions. This leads to the hypothesis that ThT and CR interact quite effectively on the surface of fibrils, as their complex formation was already reported[26]. However, this complex formation is a lot more complicated, as our results show that one CR molecule can bind more than one ThT molecule. The CR-specific absorbance spectra also change quite drastically when there is a large concentration of available ThT, which suggests that the ThT-CR interaction may be quite strong when bound in close proximity.

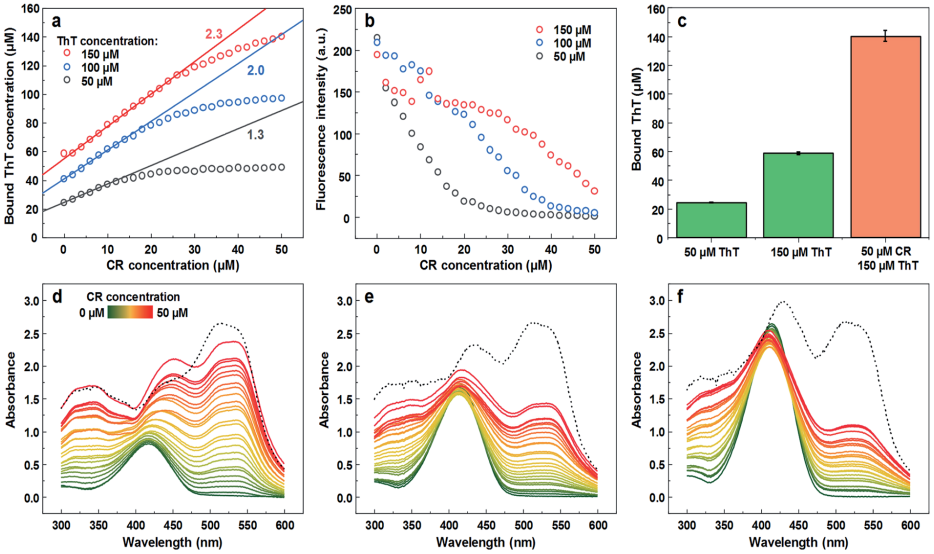

Figure 5. Titration of ThT-insulin fibril solutions by CR. Bound ThT concentration dependence on the concentration of CR present in solution (**a**), where color-coded numbers indicate slope values. ThT fluorescence intensity dependence on the concentration of CR present in solution (**b**). Bound ThT concentration when fibrils are mixed with different dye concentrations (**c**). Absorbance spectra of ThT-CR-insulin fibril solutions when 50 (**d**), 100 (**e**) and 150 (**f**) μM of ThT is present. The black dotted line represents the calculated sum absorbance spectra of separately bound ThT and CR. The absorbance spectra are corrected by subtracting a spectrum of insulin fibrils. Each data point is the average of three measurements.

One peculiar thing observed during these experiments is the sigmoidal shape of ThT fluorescence intensity dependence on the concentration of CR present. This could be explained by the fact that ThT molecules themselves are capable of self-quenching[28]. Here we can see that there is almost no difference between the fluorescence intensity between ~24 and ~60 μM of bound ThT, when accounted for the inner filter effect. The more ThT is bound, the higher the possibility of fluorescence exists, while at the same time the self-quenching effect becomes stronger and vice versa. This means that if CR forms a complex with some of the bound ThT molecules, the residual bound ThT would experience a smaller self-quenching effect, which would compensate for the decrease in bound dye. The fluorescence intensity begins to decrease only when the self-quenching effect becomes so little that its reduction does not compensate for the loss of normally bound ThT. Another interesting thing to note is that when such a large quantity of dye molecules binds to fibrils, the aggregates change their self-association properties. At higher CR concentrations, an even larger amount of ThT binds to fibrils and it becomes almost impossible to fully separate the dye-loaded aggregates from solution by centrifugation, as they quickly dissociate away from the pellet into solution. Due to this reason, all experiments were limited to a maximum CR concentration of 50 μM.

These results indicate that if a potential new aggregate formation inhibitor or fibril destabilizing drug was tested using amyloidophilic dye fluorescence spectra as a means to track their formation or dissociation, it could very easily lead to false conclusions that the molecule was effective. This is especially true if the molecule in question has a similar scaffold or spectral properties to the tested dyes or if it binds to the surface of amyloid fibrils.

Conclusions

In a majority of cases, amyloidophilic molecules, such as ThT, CR, ANS, Dap and MB appear to be able to aid each other in binding to the surface of insulin amyloid fibrils and only certain pairings interfere with one another. However, this additional binding does not result in an increased fluorescence of ThT, ANS or Dap. In fact, in most dye pairs, there is a sizeable fluorescence quenching effect, which could be attributed to the interaction of these molecules at the fibril's surface. Such an effect could lead to false identifications of anti-amyloid drugs if they possess a similar scaffold, spectral properties or binding propensity as the molecules used in this work.

Data availability

The datasets generated during and/or analysed during the current study are available from the corresponding author on reasonable request.

Received: 30 October 2019; Accepted: 16 December 2019;
Published online: 30 December 2019

References

1. Chiti, F. & Dobson, C. M. Protein misfolding, functional amyloid, and human disease. *Annu. Rev. Biochem.* **75**, 333–366 (2006).
2. Fitzpatrick, A. W. P. *et al*. Atomic structure and hierarchical assembly of a cross-β amyloid fibril. *Proc. Natl. Acad. Sci.* **110**, 5468–5473 (2013).
3. Chiti, F. & Dobson, C. M. Protein misfolding, amyloid formation, and human disease: a summary of progress over the last decade. *Annu. Rev. Biochem.* **86**, 27–68 (2017).
4. Meisl, G. *et al*. Scaling behaviour and rate-determining steps in filamentous self-assembly. *Chem. Sci.* **8**, 7087–7097 (2017).
5. Marshall, K. E., Marchante, R., Xue, W.-F. & Serpell, L. C. The relationship between amyloid structure and cytotoxicity. *Prion* **8**, 192–196 (2014).
6. Šarić, A. *et al*. Physical determinants of the self-replication of protein fibrils. *Nat. Phys.* **12**, 874–880 (2016).
7. Xiao, Y. *et al*. Aβ(1–42) fibril structure illuminates self-recognition and replication of amyloid in Alzheimer's disease. *Nat. Struct. Mol. Biol.* **22**, 499–505 (2015).
8. Cummings, J., Lee, G., Ritter, A. & Zhong, K. Alzheimer's disease drug development pipeline: 2018. *Alzheimer's Dement. Transl. Res. Clin. Interv.* **4**, 195–214 (2018).
9. Adamcik, J. & Mezzenga, R. Study of amyloid fibrils via atomic force microscopy. *Curr. Opin. Colloid Interface Sci.* **17**, 369–376 (2012).
10. Voropai, E. S. *et al*. Spectral properties of thioflavin T and its complexes with amyloid fibrils. *J. Appl. Spectrosc.* **70**, 868–874 (2003).
11. Streets, A. M., Sourigues, Y., Kopito, R. R., Melki, R. & Quake, S. R. Simultaneous measurement of amyloid fibril formation by dynamic light scattering and fluorescence reveals complex aggregation kinetics. *PLoS One* **8**, e54541 (2013).
12. Zandomeneghi, G., Krebs, M. R. H., McCammon, M. G. & Fändrich, M. FTIR reveals structural differences between native β-sheet proteins and amyloid fibrils. *Protein Sci.* **13**, 3314–3321 (2009).
13. Micsonai, A. *et al*. Accurate secondary structure prediction and fold recognition for circular dichroism spectroscopy. *Proc. Natl. Acad. Sci.* **112**, E3095–E3103 (2015).
14. Nilsson, M. Techniques to study amyloid fibril formation *in vitro*. *Methods* **34**, 151–160 (2004).
15. Yakupova, E. I., Bobyleva, L. G., Vikhlyantsev, I. M. & Bobylev, A. G. Congo Red and amyloids: history and relationship. *Biosci. Rep.* **39**, BSR20181415 (2019).
16. Xue, C., Lin, T. Y., Chang, D. & Guo, Z. Thioflavin T as an amyloid dye: fibril quantification, optimal concentration and effect on aggregation. *R. Soc. Open Sci.* **4**, 160696 (2017).
17. Gade Malmos, K. *et al*. ThT 101: a primer on the use of thioflavin T to investigate amyloid formation. *Amyloid* **24**, 1–16 (2017).
18. Mahdavimehr, M., Katebi, B. & Meratan, A. A. Effect of fibrillation conditions on the anti-amyloidogenic properties of polyphenols and their involved mechanisms. *Int. J. Biol. Macromol.* **118**, 552–560 (2018).
19. Nie, R., Zhu, W., Peng, J., Ge, Z. & Li, C. Comparison of disaggregative effect of A-type EGCG dimer and EGCG monomer on the preformed bovine insulin amyloid fibrils. *Biophys. Chem.* **230**, 1–9 (2017).
20. Ono, K. *et al*. Potent anti-amyloidogenic and fibril-destabilizing effects of polyphenols *in vitro*: implications for the prevention and therapeutics of Alzheimer's disease. *J. Neurochem.* **87**, 172–181 (2003).
21. Ono, K., Hirohata, M. & Yamada, M. Ferulic acid destabilizes preformed β-amyloid fibrils *in vitro*. *Biochem. Biophys. Res. Commun.* **336**, 444–449 (2005).
22. Byeon, S. R. *et al*. Bis-styrylpyridine and bis-styrylbenzene derivatives as inhibitors for Aβ fibril formation. *Bioorg. Med. Chem. Lett.* **17**, 1466–1470 (2007).
23. Zaman, M. *et al*. Amino group of salicylic acid exhibits enhanced inhibitory potential against insulin amyloid fibrillation with protective aptitude toward amyloid induced cytotoxicity. *J. Cell. Biochem.* **119**, 3945–3956 (2018).
24. Girych, M. *et al*. Combined thioflavin T–Congo red fluorescence assay for amyloid fibril detection. *Methods Appl. Fluoresc.* **4**, 034010 (2016).
25. Patel, B. R. & Kerman, K. Calorimetric and spectroscopic detection of the interaction between a diazo dye and human serum albumin. *Analyst* **143**, 3890–3899 (2018).
26. Buell, A. K., Dobson, C. M., Knowles, T. P. J. & Welland, M. E. Interactions between amyloidophilic dyes and their relevance to studies of amyloid inhibitors. *Biophys. J.* **99**, 3492–3497 (2010).
27. Hudson, S. A., Ecroyd, H., Kee, T. W. & Carver, J. A. The thioflavin T fluorescence assay for amyloid fibril detection can be biased by the presence of exogenous compounds. *FEBS J.* **276**, 5960–5972 (2009).
28. Lindberg, D. J. *et al*. Binding of thioflavin-T to amyloid fibrils leads to fluorescence self-quenching and fibril compaction. *Biochemistry* **56**, 2170–2174 (2017).
29. Ferreira, N., Saraiva, M. J. & Almeida, M. R. Natural polyphenols inhibit different steps of the process of transthyretin (TTR) amyloid fibril formation. *FEBS Lett.* **585**, 2424–2430 (2011).
30. Pullakhandam, R., Srinivas, P. N. B. S., Nair, M. K. & Reddy, G. B. Binding and stabilization of transthyretin by curcumin. *Arch. Biochem. Biophys.* **485**, 115–119 (2009).
31. Wang, J.-B., Wang, Y.-M. & Zeng, C.-M. Quercetin inhibits amyloid fibrillation of bovine insulin and destabilizes preformed fibrils. *Biochem. Biophys. Res. Commun.* **415**, 675–679 (2011).
32. Shvadchak, V. V., Afitska, K. & Yushchenko, D. A. Inhibition of α-synuclein amyloid fibril elongation by blocking fibril ends. *Angew. Chemie Int. Ed.* **57**, 5690–5694 (2018).
33. Yates, E. V., Meisl, G., Knowles, T. P. J. & Dobson, C. M. An environmentally sensitive fluorescent dye as a multidimensional probe of amyloid formation. *J. Phys. Chem. B* **120**, 2087–2094 (2016).
34. Wischik, C. M., Edwards, P. C., Lai, R. Y., Roth, M. & Harrington, C. R. Selective inhibition of Alzheimer disease-like tau aggregation by phenothiazines. *Proc. Natl. Acad. Sci.* **93**, 11213–11218 (1996).
35. How, S.-C. *et al*. Exploring the effects of methylene blue on amyloid fibrillogenesis of lysozyme. *Int. J. Biol. Macromol.* **119**, 1059–1067 (2018).
36. Sneideris, T. *et al*. pH-driven polymorphism of insulin amyloid-like fibrils. *PLoS One* **10**, e0136602 (2015).
37. Klunk, W. E., Pettegrew, J. W. & Abraham, D. J. Quantitative evaluation of congo red binding to amyloid-like proteins with a beta-pleated sheet conformation. *J. Histochem. Cytochem.* **37**, 1273–1281 (1989).
38. Ran, C., Zhao, W., Moir, R. D. & Moore, A. Non-conjugated small molecule FRET for differentiating monomers from higher molecular weight amyloid beta species. *PLoS One* **6**, e19362 (2011).

Acknowledgements

This research was funded by Vilnius University, Grant No. MSF-JM-3.

Author contributions

M.Z. and V.S. designed the studies. M.Z. and K.M. undertook the experimental work. M.Z., K.M. and V.S. analyzed the data and prepared the manuscript.

Competing interests
The authors declare no competing interests.

Additional information
Supplementary information is available for this paper at https://doi.org/10.1038/s41598-019-56788-y.

Correspondence and requests for materials should be addressed to V.S.

Reprints and permissions information is available at www.nature.com/reprints.

Publisher's note Springer Nature remains neutral with regard to jurisdictional claims in published maps and institutional affiliations.

Received: 17 March 2021 | Revised: 31 May 2021 | Accepted: 3 June 2021

DOI: 10.1002/biot.202100138

Biotechnology Journal

RESEARCH ARTICLE

Using lysozyme amyloid fibrils as a means of scavenging aggregation-inhibiting compounds

Mantas Ziaunys | Kamile Mikalauskaite | Andrius Sakalauskas | Vytautas Smirnovas

Institute of Biotechnology, Life Sciences Center, Vilnius University, Vilnius, Lithuania

Correspondence
Vytautas Smirnovas, Institute of Biotechnology, Life Sciences Center, Vilnius University, Sauletekio al. 7, Vilnius, LT-10257, Lithuania.
Email: vytautas.smirnovas@bti.vu.lt

Abstract

The aggregation of amyloidogenic proteins is linked to several amyloidoses, including neurodegenerative disorders, such as Alzheimer's or Parkinson's disease. Currently there are very few effective cures or treatments available, despite countless screenings and clinical trials. One of the most challenging aspects of potential anti-amyloid drug discovery is finding which molecules are the actual inhibitors out of mixtures, which may contain hundreds of distinct compounds. Considering that anti-amyloid compounds would interact with the aggregate, this affinity could be used as a means of separating such compounds from ineffective ones. In this work, we attempt to scavenge potential aggregation-inhibiting molecules out of four, different complexity mixtures, ranging from oxidized gallic acid to tea extract, using lysozyme amyloid fibrils. We show that these compounds bind to aggregates with high affinity and can be later separated from them by different methods.

KEYWORDS
aggregation-inhibitors, amyloid aggregation, amyloid fibrils, lysozyme fibrils

1 | INTRODUCTION

Protein amyloid aggregate formation is linked with several amyloidoses,[1] some of which are neurodegenerative, such as Alzheimer's or Parkinson's disease.[2,3] These disorders affect millions of people worldwide and the number of cases is projected to continue rising.[4,5] In order to halt the formation of these fibrillar structures, countless potential compounds have been tested, ranging from small molecules[6,7] to protein-specific antibodies.[8] Unfortunately, positive effects observed in vitro[9] are usually either non-existent or greatly diminished during clinical trials[10] and very few effective treatments are currently available.[11,12] This makes it important to obtain a better method of determining effective anti-amyloid compounds, which would be potent not only during in vitro testing.

One of the main issues when screening for potential aggregation-inhibiting compounds is identifying the actual effective molecule.[13] There have been multiple reports of tea[14] and plant extracts[15,16] or oxidation products of polyphenols[17] that reduce the rate of protein aggregation. However, they are usually comprised of a mixture of several distinct molecules,[18–20] rather than being one effective compound. This, in turn, makes it difficult to identify or acquire a high concentration of the inhibitor molecule without separating it from all the others, which is a considerable challenge in itself. First of all, it is not known which exact molecule is responsible for the anti-amyloid activity, which means that even after a successful separation procedure, each compound would have to be tested separately. Second, there can be a plethora of similar molecules, with the effective one only being minimally different from the rest; thus, complicating the separation procedure. Both of these factors point towards a need of a more effective drug identification/separation procedure.

For a potential anti-amyloid molecule to have any effect, it has to, in one way or another, interact with either the aggregate intermediate species[21] or the fibril itself,[22] without binding to/impeding the functions of the native protein.[23] This means that any compound which could alter the aggregation process, would have an affinity towards the non-native protein structures. It has been shown that

Abbreviations: DMSO, dimethyl sulfoxide; EGCG, epigallocatechin gallate; $EGCG_{ox}$, epigallocatechin gallate (oxidized); GA_{ox}, gallic acid (oxidized); GT, green tea extract; GT_{Inc}, green tea extract (incubated/oxidized); GuHCl, guanidine hydrochloride; GuSCN, guanidine thiocyanate; HPLC, High performance liquid chromatography; ThT, thioflavin-T

multiple molecules, such as thioflavin-T (ThT), Congo red or methylene blue have a high affinity towards the amyloid fibril surface[24,25] and also affect their rate of aggregation or self-association.[26–28] Taking these factors into consideration, it is possible that some of the potential drug molecules would also bind to the surface of amyloid fibrils, while compounds that do not affect aggregation—would not. If this affinity between amyloid fibrils and anti-aggregation compounds is a universal feature of protein aggregates, then any type of fibrils could potentially be used to separate the drug molecules. However, many amyloid proteins are either difficult/expensive to purify or have complex aggregation protocols, making them impractical for such a procedure. In this work, a model amyloidogenic protein—lysozyme was used due to its relatively low cost and simple fibrillization protocol.[29]

In order to examine the anti-amyloid molecule scavenging properties of lysozyme fibrils, four mixtures of increasing complexity, containing anti-aggregation compounds were generated. The most simple out of the set was gallic acid, a simple polyphenol, whose oxidation products have been reported to inhibit protein fibrillization.[16,30,31] The second one was epigallocatechin gallate (EGCG), whose inhibitory effects were demonstrated on many occasions[32–34] and whose oxidation/hydrolysis products include the aforementioned gallic acid. The third, most complex mixture, was green tea extract, which contains both gallic acid and EGCG, alongside many other distinct compounds.[14] And finally, the most complex mixture was generated by additional incubation of the tea extract, yielding even more oxidation/hydrolysis products.

In this work, we show that lysozyme fibrils are capable of scavenging amyloid-specific compounds out of all four tested mixtures and that these molecules may be later separated from the aggregates. Samples obtained prior to, during and after separation were examined using HPLC and UV-Vis spectroscopy, and their anti-aggregation effects were tested on insulin fibrillization.

2 | MATERIALS AND METHODS

2.1 | Lysozyme fibril preparation

Hen egg-white lysozyme powder (Sigma-Aldrich cat. No L6876) was dissolved in a 50 mM sodium phosphate buffer (pH 6.0), containing 2 M guanidine hydrochloride (GuHCl) to a final protein concentration of 1.0 mM (lysozyme MW = 14 313 Da, $\varepsilon_{280} = 37\,970\ M^{-1}\ cm^{-1}$). The solution was distributed to 1.5 mL test tubes (1.0 mL final volume) and incubated for 72 h at 60°C with 600 rpm agitation (two 3 mm glass beads in every test tube) in a MHR 23 ThermoMixer (Ditabis). The fibril solutions were then centrifuged for 15 min at 10,000 x *g* after which the supernatant was removed and the fibril pellets were resuspended into 100 mM potassium phosphate buffer (pH 7.4). This procedure was repeated four times to remove all non-aggregated lysozyme and replace the buffer solution. After the final centrifugation step, five fibril samples were combined to a final volume of 1 mL. The resulting highly concentrated fibril mass was then used for the following experiments.

2.2 | Oxidized gallic acid and EGCG preparation

In order to increase the inhibitory potential, as well as minimize oxidation or hydrolysis processes during separation and aggregation experiments, gallic acid and epigallocatechin gallate were oxidized before all further procedures.[17,31] oxidized gallic acid (GA_{ox}) and oxidized epigallocatechin gallate ($EGCG_{ox}$) were prepared by dissolving gallic acid (TCI Chemicals, cat. No. G0011) or EGCG (Fluorochem, cat. No. M01719) powders in a 100 mM potassium phosphate buffer (pH 7.4) to a final concentration of 10 mM, distributing the resulting solutions into 1.5 mL test tubes (1.0 mL final volume) and incubating them for 72 h at 60°C. After this procedure, the test tubes were stored at 4°C to prevent/slow down further oxidation processes.

2.3 | Green tea extract preparation and incubation

Generic brand dried green tea leaves (10 g) were mixed with 100 mL MilliQ H_2O and autoclaved for 20 min at 121°C. This procedure sterilizes the tea and changes the concentration of green tea components in solution, as described previously.[35] Part of the resulting solution (further referred to as GT) was stored at 4°C, while the other was further incubated at 60°C for 72 h to mimic the preparation of GA_{ox} and $EGCG_{ox}$ and result in a solution with multiple possible oxidation or hydrolysis products (further referred to as GT_{Inc}).

2.4 | Fibril-compound mixing, washing, and separation

The concentrated lysozyme fibril samples (1.0 mL) were combined with 1 mL of GA_{ox}, $EGCG_{ox}$, GT or GT_{Inc}. Each test tube contained two 3 mm glass beads, which were used to homogenize the mixture by constant vigorous agitation for 1 min. The samples were then continuously mixed by test-tube rotation at 20 rpm for 10 min. After the mixing procedure, the samples were centrifuged at 12,000 x *g* for 30 min and the supernatant (1 mL) was removed. This entire loading, mixing and centrifugation procedure (Figure 1A) was repeated five times.

After the final supernatant removal, the fibril-compound mixtures (1.0 mL) were combined with 1.0 mL of potassium phosphate buffer (pH 7.4). The samples were then homogenized, rotated and centrifuged as described previously. After centrifugation, 1 mL of the samples was removed and replaced with potassium phosphate buffer. This washing procedure (Figure 1B) was repeated 10 times.

After the final washing step, the samples were mixed with 1.0 mL of potassium phosphate buffer (pH 7.4) and rotated at 20 rpm for 72 h at 4°C in order for the highly-concentrated compounds on the fibril surface to diffuse into the solutions (Figure 1B). Afterwards, the samples

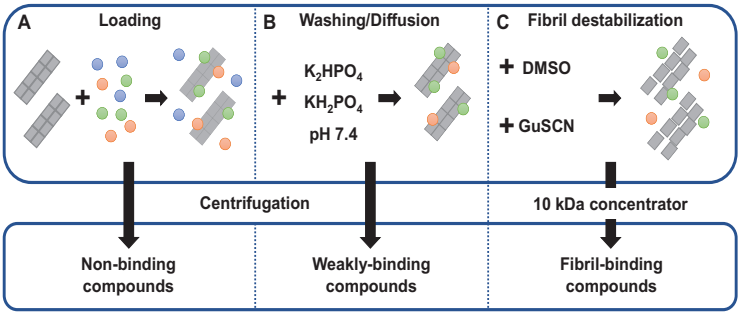

FIGURE 1 The stages of GA_{ox}, $EGCG_{ox}$, GT and GT_{Inc} loading onto fibrils (A) and subsequent separation by washing/diffusion (B) and fibril destabilization with DMSO or GuSCN (C)

were centrifuged and 1.6 mL of the supernatant was removed. All solutions collected during the loading, washing and diffusion steps were filtered through 0.22 μm syringe filters in order to remove any residual lysozyme fibrils. The remaining fibril pellets were resuspended to a final volume of 0.8 mL and split into two equal parts for further separation procedures.

The resuspended fibril mass (0.4 mL) was combined with either 1.6 mL 5 M guanidine thiocyanate (GuSCN) to a final GuSCN concentration of 4 M or with 1.6 mL 99.9% dimethyl sulfoxide (DMSO) to a final DMSO concentration of ~80%. The resulting mixtures were then homogenized and rotated at 20 rpm for 1 h at room temperature. Afterwards, the samples were centrifuged as described previously and 1.5 mL of supernatants were filtered through 10 kDa protein concentrators (Thermo Scientific, cat. No. 88513) to remove lysozyme monomers and any residual fibrils/aggregates.

2.5 | Sample absorbance measurements

Prior to absorbance measurements, each sample was diluted 100 times using a 100 mM potassium phosphate buffer (pH 7.4). Sample absorbance was scanned using a Shimadzu UV-1800 spectrophotometer in a wavelength range from 240 to 600 nm (3 mm pathlength cuvette). Each sample was scanned three times and the spectra were averaged. All spectra were baseline corrected using the absorbance value at 600 nm.

2.6 | Aggregation kinetics

Insulin powder was dissolved in a 100 mM sodium phosphate buffer (pH 2.4), containing 100 mM NaCl, to a final protein concentration of 400 μM. Thioflavin-T powder (Sigma-Aldrich cat. No T3516) was dissolved in MilliQ H_2O to a final concentration of ~11 mM. The solution was then filtered through a 0.22 μm syringe filter and the exact ThT concentration was determined by diluting an aliqout of the dye 200 times and scanning its absorbance at 412 nm ($\varepsilon_{412} = 23\,250\ M^{-1}\ cm^{-1}$), after which, the ThT solution was diluted to 10 mM. The aggregation reaction mixture was prepared by combining the insulin stock solution, ThT and inhibitor solution to yield a mixture with a final protein concentration of 200 and 100 μM ThT. The low pH value of the reaction solution minimized any further oxidation or hydrolysis of the tested compounds during the course of the aggregation experiments.

When examining the samples obtained during the loading procedure and diffusion (Figure 1), the aggregation reaction mixture (100 μL) contained 4 μL of the supernatant solution. Control samples contained 4 μL of 100 mM potassium phosphate (pH 7.4) buffer or 2 μL of the initial GA_{ox}, $EGCG_{ox}$, GT or GT_{Inc} solutions (during the loading procedure, the initial inhibitor solutions were diluted 2 times when mixing with fibrils, which is why 2 μL were used) and 2 μL 100 mM potassium phosphate buffer (pH 7.4). In the case of samples obtained during fibril destabilization with DMSO or GuSCN, the aggregation reaction mixtures contained 4 μL of the resulting inhibitor solutions (compounds in 80% DMSO or 4 M GuSCN). The control samples contained an equivalent concentration of either GuSCN or DMSO.

Insulin aggregation was tracked using a CLARIOstar Plus plate reader (BMG Labtech). The samples were placed into 96-well half-area non-binding plates (four repeats for each sample, 100 μL final volume). The plates were sealed using a Nunc sealing tape and incubated at 60°C without agitation. Measurements were taken every 5 min (excitation wavelength—440 nm, emission wavelength—480 nm).

Kinetic data was analyzed using Origin 2018 software. The aggregation half-time values were obtained by applying a Boltzmann sigmoidal equation fit. Sample fluorescence intensity was not used as an indicator of aggregation efficiency, as heterogeneous compounds can lead to fluorescence signal quenching, either by an inner filter effect or direct interaction with the fluorescent dye—ThT.[36]

2.7 | High performance liquid chromatography (HPLC)

The analytical separation of samples was done using a Shimadzu UFLC system with a CMB-20A communication module, two LC20AD quaternary and isocratic pumps, a SIL-20AC autosampler, a CTO-20A column compartment and a SPD-M20A DAD detector (Shimadzu Corp.,

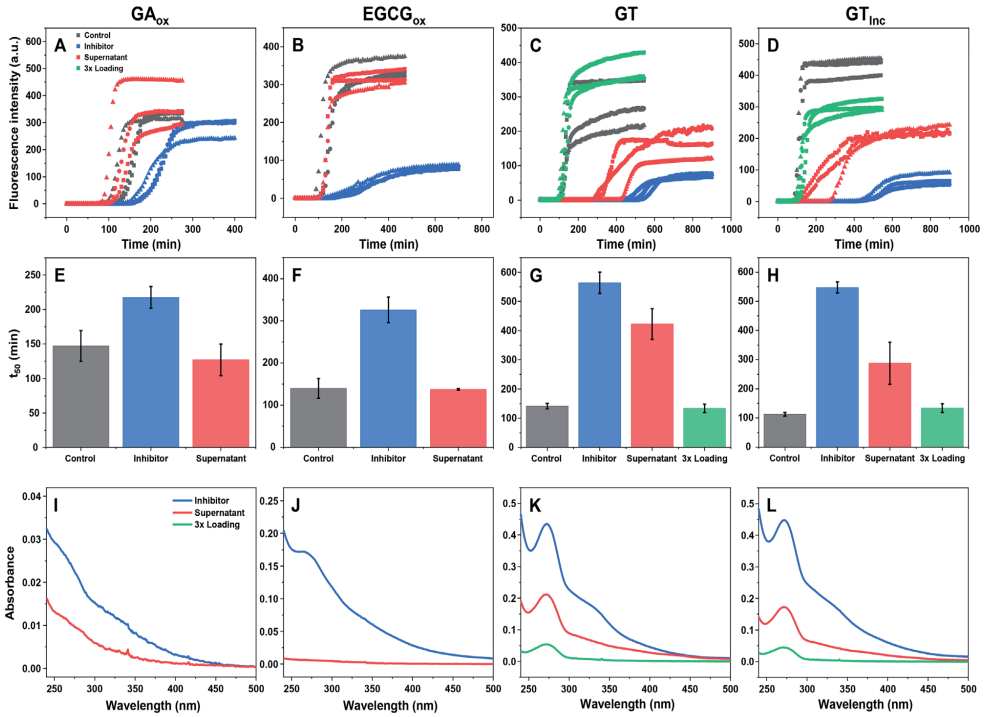

FIGURE 2 Insulin (200 μM) aggregation kinetics in the presence of GA_{ox} (A), $EGCG_{ox}$ (B), GT (C), GT_{Inc} (D) inhibitor or supernatant (initial or after three loading procedures) solutions and their t_{50} values (E–H, respectively). Absorbance values of GA_{ox} (I), $EGCG_{ox}$ (J), GT (K), GT_{Inc} (L) and their supernatants. For both kinetic and absorbance measurements, the initial inhibitor solutions were diluted with a 100 mM potassium phosphate buffer (pH 7.4) in a 1:1 ratio to mimic the supernatant dilution. Error bars are one standard deviation ($n = 3$)

Japan). The diode-array detector wavelength range was set from 190 to 400 nm with a data rate of 12.5 Hz. The C18-PFP HPLC separation column (10 cm x 4.6 cm, 3 μm, ACE) was used. The HPLC-grade MeCN (Fisher Scientific) and ultrapure water (18.2 MΩ cm^{-1}, Milli-Q Plus system, Millipore Bedford, MA, USA) were used for RP-HPLC separation.

The reverse-phase separation was performed in a C18-PFP column using a trinary mobile phase gradient consisting of ultrapure water (eluent A), MeCN (eluent B), and ultrapure water with 1% TFA (eluent C). Constant 10% flow of eluent C was used to contain 0.1% TFA concentration in the column, while the gradient conditions between eluents A and B were performed. To establish starting conditions, five column volume equilibration prior to each run was carried out (8.3 min). The column wash out after each run was performed using 90% B and 10% C isocratic conditions for 2 min. The gradient elution to separate samples was 5% B (0–1 min), 40.5% B (15 min) and 81% (16 min). The column thermostat was set to 40°C and the flow rate to 1 mL min^{-1}.

3 | RESULTS

In order to use lysozyme fibrils as a means of separating anti-amyloid compounds, it was first necessary to load the fibrils with a significant number of such molecules. Oxidized gallic acid (GA_{ox}), oxidized epigallocatechin gallate ($EGCG_{ox}$), green tea extract (GT) and incubated green tea extract (GT_{Inc}) were combined with lysozyme fibrils as described in the Section 2. The samples were then centrifuged, and the resulting supernatants were compared against the initial inhibitor solutions. Based on insulin aggregation kinetics (Figure 2A–D) and their half-time (t_{50}) values (Figure 2E–H) in the presence (blue curves) or absence (grey curves) of the initial inhibitor solutions, it is clear that all four have a significant inhibitory effect. However, when examining the supernatant obtained after combining the initial inhibitor solutions with lysozyme fibrils, it has completely lost all inhibitory effect in the case of GA_{ox} (Figure 2A,E) and $EGCG_{ox}$ (Figure 2B,F) and displayed a diminished effect with GT (Figure 2C,G) and GT_{Inc} (Figure 2D,H). This indicates that all or most of anti-amyloid compounds, present in GA_{ox} and $EGCG_{ox}$, became bound to lysozyme fibrils. The GT and GT_{Inc} solutions likely contained a much greater number of such molecules, which is why their inhibitory effect was still present when using their respective supernatants. In order to verify this, the loading procedure was repeated two additional times using GT and GT_{Inc} supernatants. After this was done, the supernatants were no longer capable of inhibiting insulin aggregation (Figure 2C,D, green curves), indicating that the initial supernatant did, in fact, contain more molecules that were able

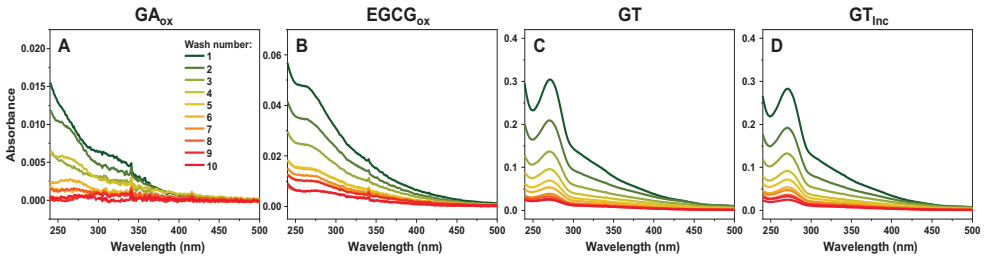

FIGURE 3 Absorbance spectra of GA_{ox} (A), $EGCG_{ox}$ (B), GT (C) and GT_{Inc} (D) supernatant solutions, obtained during ten rounds of washing the inhibitor-bound lysozyme fibrils. The color gradient from green to red indicates the number of washing steps. The washing procedure details are described in Section 2

to bind to one batch of lysozyme fibrils. The experiment was repeated using a different batch of insulin and inhibitor solutions in order to verify these observations (Figure S1). Since it is possible for amyloid inhibitor molecules to form chemical aggregates and be removed from the supernatant during centrifugation,[37] each initial inhibitor solution was centrifuged without the addition of lysozyme fibrils and their inhibitory potential was examined (Figure S1). The results show that the supernatants retained a similar effect against amyloid aggregation, which means that either the potent compounds do not form aggregates or they cannot be pelleted using this centrifugation protocol.

The absorbance spectra of initial inhibitor solutions and their supernatants were also scanned to determine the binding effectiveness and whether some compounds remained in solutions. In the case of GA_{ox} (Figure 2I), it seems that a portion of molecules, which have absorbance properties in the 240–500 nm range, remained in solution. However, the supernatant did not display any inhibitory effects on insulin aggregation, indicating that these remaining molecules may not have anti-aggregation properties. For $EGCG_{ox}$ (Figure 2J), practically everything that can absorb light in the scanned region became bound to lysozyme fibrils. Both GT (Figure 2K) and GT_{Inc} (Figure 2L) supernatants contained a significant portion of residual compounds, which is also evident by their inhibitory effect on insulin aggregation. After the loading procedure was repeated two additional times using GT and GT_{Inc} supernatants, their absorbance spectra (Figure 2K,L) displayed a small portion of light-absorbing molecules; however, they were not effective at inhibiting aggregation (Figure 2C,D). It is also worth noting that there may be a "hidden" group of molecules, which do not absorb light in the 240–500 nm region and they do not appear in the absorbance spectra, but which may also alter amyloid aggregation.

The loading procedure was repeated five times in order to saturate lysozyme fibrils with potential anti-amyloid compounds. All the non-binding or weakly associated molecules then had to be washed from the fibrils in order to diminish their presence during the separation procedures. Each aggregate sample was washed ten times, as explained in the Section 2, and all supernatant absorbance spectra were recorded. Based on these measurements (Figure 3A-D), it is evident that the vast majority of non-bound compounds were removed from the fibril solutions. However, taking into consideration that the washing procedure was repeated ten times and the solutions were diluted two times on each round, the final supernatant should contain only a minimal fraction of the initial molecules, but this is not the case. $EGCG_{ox}$, GT and GT_{Inc} (Figure 3B-D) absorbance spectra still show a small amount of light-absorbing compounds in the 240–400 nm range. This may indicate that some of the molecules diffuse into the solution during washing procedures and this process may be used as one of the means of separating them from lysozyme fibrils.

After all four fibril samples were washed from the majority of non-bound or weakly associated molecules, it was time to attempt to separate all fibril-bound compounds and test their effectiveness. To examine whether diffusion may be a good means of separation, the fibril solutions were mixed with a fresh buffer solution and agitated as described in the Section 2 for 3 days, after which they were centrifuged and their supernatants were tested. In the case of GA_{ox} (Figure 4A,D), there seems to be a minimal amount of anti-amyloid molecules present in the supernatant, as the t_{50} values are similar to the control sample (Figure 4D). $EGCG_{ox}$, GT and GT_{Inc} samples all contained a modest concentration of compounds, which inhibited insulin aggregation (Figure 4A,D) and the most effective supernatant was from GT.

A portion of lysozyme fibrils were mixed with a strong denaturant—GuSCN, which can dissociate amyloid aggregates[38] and the potential inhibitors were separated from residual fibrils and lysozyme monomers. In this case, the GA_{ox} sample (Figure 4B,E) displayed significant anti-aggregation potency, even larger than in the case of the initial inhibitor solution (Figure 2A,E). All other solutions also had a similar inhibitory effect (Figure 4B,E), while GT, conversely to the diffusion samples, had the lowest effect. The most diverse inhibitory effects were observed when lysozyme fibrils were resuspended into DMSO, which both causes lysozyme denaturation[39] and creates an organic solvent environment. When the potential inhibitory compounds were separated from the residual fibrils/monomers, their effect on insulin aggregation was examined (Figure 4C,F). Surprisingly, GA_{ox} had a lower effect on the t_{50} value, oppositely to what was observed during GuSCN separation. $EGCG_{ox}$ and GT_{Inc} had the most potent anti-aggregation properties, resulting in a four to five fold increase in the t_{50} values. GT had a similar effect as in both the diffusion and GuSCN separation cases. Taking into account all three methods of compound extraction from lysozyme fibrils, it seems that each one has its own strengths

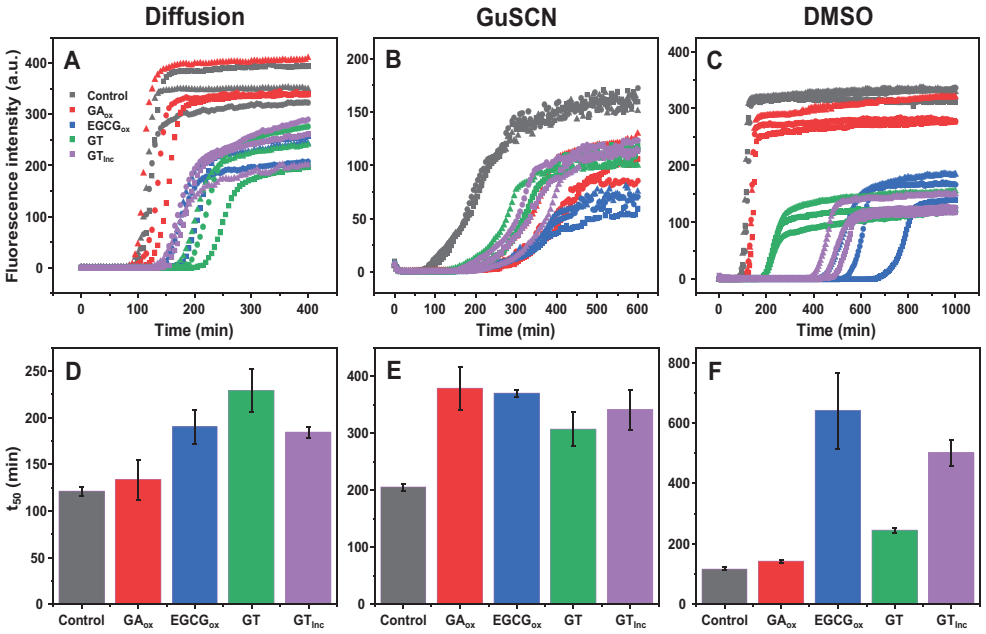

FIGURE 4 Insulin (200 μM) aggregation kinetics in the presence of all four potential inhibitor mixtures, obtained using diffusion (A), GuSCN (B), DMSO (C) and their respective t_{50} values (D–F). The separation details are described in Section 2. Error bars are one standard deviation ($n = 3$)

and weaknesses when dealing with specific inhibitor molecules. The experiment was repeated using a different batch of insulin and inhibitor solutions in order to verify these observations (Figure S2)

Finally, in order to determine the possible number/quantity of bound and separated compounds, the initial, supernatant and separated inhibitor solutions were examined using HPLC. In the case of GA_{ox}, the initial solution contains a significant number of compounds (Figure 5A, black line), a lot of which do not bind to lysozyme fibrils (Figure 5A, red line, elution time [2–7 min]) and remain in the supernatant, including the residual fraction of non-oxidized gallic acid. During diffusion, a small number of compounds separate from the fibrils; however, they do not possess significant inhibitory effects (Figure 5A, blue line). Both GuSCN and DMSO manage to separate a substantial number and quantity of components (Figure 5A, green and purple line, elution time [9–14 min]), which also possess anti-amyloid potency. Similar tendencies are observed in the case of $EGCG_{ox}$ (Figure 5B); however, the number of compounds is lower both in the initial sample and the separated ones. The $EGCG_{ox}$ sample also contains practically no residual non-oxidized EGCG, as opposed to the gallic acid sample. Another difference is that the diffusion sample (Figure 5B, blue line) has one notable peak at 10–11 elution min. There is also the appearance of a peak at elution time (13–14 min), which is not present in the initial samples. Since it is present in both the GuSCN and DMSO samples, it is likely not due to compound interaction with either of these molecules, but may be the result of some of the concentrated compounds interacting with each other.

In the case of GT and GT_{Inc}, the initial samples have a wide range of molecules and one massive peak at elution time (7–8 min) (Figure 5C,D), which is also present in the supernatant, indicating that this component has minimal affinity towards lysozyme. Samples, obtained using all three separation methods, also have this peak, however, it is greatly diminished. The GuSCN and DMSO samples also contain a small number of components observed at elution time (10–11 min). Despite the low quantity of notable peaks, the GuSCN and DMSO samples have a significant effect on the aggregation kinetics of insulin. This can be explained by one of three ways: either the separated compounds have a very potent effect at low concentrations; the components do not absorb light in the selected region or they cannot be separated using the selected method.

4 | DISCUSSION

Comparing the anti-amyloid effects of the initial inhibitor solutions and the supernatants remaining after they are mixed with lysozyme fibrils reveals that tested anti-amyloid compounds have a significant affinity towards fibrillar aggregates. This is most evident in the case of GA_{ox} and $EGCG_{ox}$, where the supernatant has practically no effect on the aggregation kinetics, meaning that everything that can inhibit aggregation became bound to lysozyme fibrils on the first loading procedure. For GT and GT_{Inc} supernatants, three loading procedures were required for all anti-amyloid compounds to become bound to fibrils.

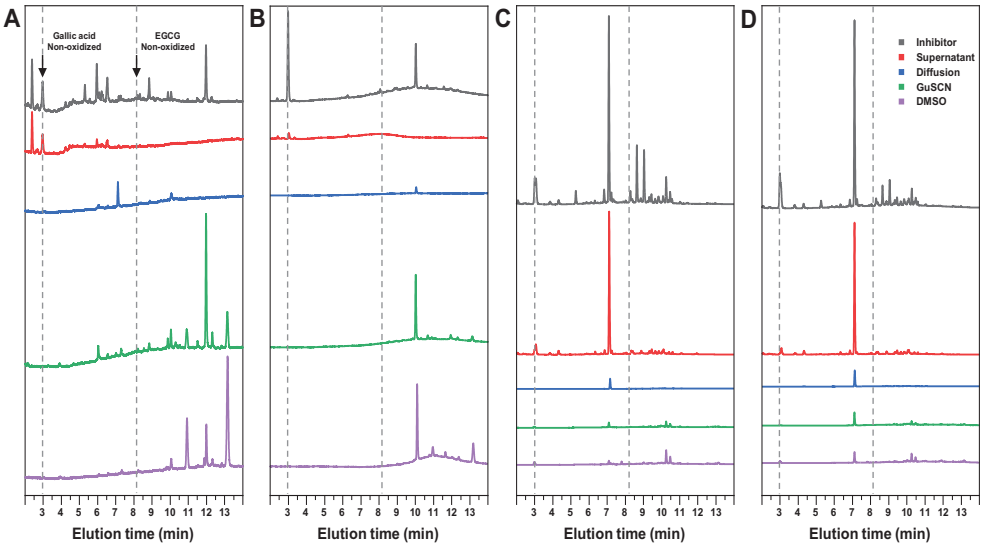

FIGURE 5 HPLC elution graphs of GA_{ox} (A), $EGCG_{ox}$ (B), GT (C) and GT_{Inc} (D) initial solution, supernatant and samples separated using diffusion, GuSCN and DMSO. The HPLC procedure details are described in Section 2. Absorbance was measured at 270 nm in the displayed graphs. Arrows and dashed lines indicate peaks related to non-oxidized gallic acid and EGCG

This created an opportunity to simply wash away the ineffective components and purify the effective ones.

In three of the four cases, the effective compounds were able to diffuse back into the solution, which makes it possible to use this process as a very simple method of extraction, without having to resort to strong denaturants or organic solvents. However, diffusion requires a relatively long time-frame when compared to both other methods and it can result in further chemical modifications to the present compounds, such as oxidation or hydrolysis. It may also be biased towards compounds with lower affinity, that is, components that strongly bind to fibrils may not diffuse into the solution to create an effective concentration and only weakly-bound molecules will be present in the supernatant. Using GuSCN or DMSO to destabilize aggregates and cause fibril-bound compounds to be detached is a relatively extreme method of separation; however, based on the aggregation kinetics, it is highly effective for some of the molecules, especially in the case of $EGCG_{ox}$ or GT_{Inc}. These methods do create a possibility of components undergoing chemical modifications, as 4 M of GuSCN or 80% DMSO greatly alter the environmental conditions and may directly interact with the compounds in question. Apart from denaturants and organic solvents, there are also other fibril-destabilizing approaches that can be used. As an example, insulin fibrils can be destabilized by raising the solution's pH value,[40] but this method may also induce further oxidation or hydrolysis of various components.

An interesting and unexpected result of the study is the large number of fibril-binding components, as observed in the HPLC examination. One would suspect that a single type of molecule would be the dominant particle, responsible for anti-aggregation effects in the tested mixtures; however, HPLC reveals that fibrils may bind several distinct compounds. It is possible that some of these particles simply bind to the fibril's structure without having any effect on the aggregation process. It is also not out of the realm of possibility that some compounds can associate with the aggregate and enhance fibrillization or surface-catalyzed nucleation by altering the fibril's surface properties. Some compounds may also form covalent bonds with the protein's amino acids, rather than associate with the aggregate's structure. This may also be observed in the present study, as some of the peaks seen in the initial inhibitor HPLC graphs are not present in any of the separation samples. This means that irreversibly bound compounds cannot be effectively identified using this procedure; however, such chemical modifications to native protein molecules may have adverse effects and the molecules in question might not be ideal anti-amyloid candidates.

Taking everything into consideration, it seems that lysozyme fibrils can be used to scavenge potential anti-amyloid compounds out of various complex mixtures. The effective components can then be separated from the fibrils using several different approaches, such as diffusion, denaturation by GuSCN or destabilization by DMSO.

ACKNOWLEDGMENTS

This research did not receive any specific grant from funding agencies in the public, commercial, or not-for-profit sectors.

CONFLICT OF INTEREST

The authors declare no conflict of interest.

AUTHOR CONTRIBUTIONS

Mantas Ziaunys and Vytautas Smirnovas designed the studies. Mantas Ziaunys, Kamile Mikalauskaite, and Andrius Sakalauskas undertook

the experimental work. Mantas Ziaunys and Vytautas Smirnovas analyzed the data and prepared the manuscript.

DATA AVAILABILITY STATEMENT

Data available on request from the authors.

REFERENCES

1. Baker, K. R., & Rice, L. (2012). The amyloidoses: Clinical features, diagnosis and treatment, diagnosis and treatment. *Methodist DeBakey Cardiovascular Journal*, *8*(3), 3–7.
2. Knowles, T. P. J., Vendruscolo, M., & Dobson, C. M. (2014). The amyloid state and its association with protein misfolding diseases. *Nature Reviews. Molecular cell biology*, *15*(6), 384–396.
3. Chiti, F., & Dobson, C. M. (2017). Protein misfolding, amyloid formation, and human disease: A summary of progress over the last decade. *Annual Review of Biochemistry*, *86*(1), 27–68.
4. Brookmeyer, R., Gray, S., & Kawas, C. (1998). Projections of Alzheimer's disease in the United States and the public health impact of delaying disease onset. *American Journal of Public Health*, *88*(9), 1337–1342.
5. Arthur, K. C., Calvo, A., Price, T. R., Geiger, J. T., Chiò, A., & Traynor, B. J. (2016). Projected increase in amyotrophic lateral sclerosis from 2015 to 2040 2015 to 2040. *Nature Communications*, *7*(1), 12408.
6. Belluti, F., Rampa, A., Gobbi, S., & Bisi, A. (2013). Small-molecule inhibitors/modulators of amyloid-β peptide aggregation and toxicity for the treatment of Alzheimer's disease: a patent review (2010–2012). *Expert Opinion on Therapeutic Patents*, *23*(5), 581–596.
7. Wobst, H. J., Sharma, A., Diamond, M. I., Wanker, E. E., & Bieschke, J. (2015). The green tea polyphenol (−)-epigallocatechin gallate prevents the aggregation of tau protein into toxic oligomers at substoichiometric ratios. *FEBS Letters*, *589*(1), 77–83.
8. Cummings, J., Lee, G., Ritter, A., Sabbagh, M., & Zhong, K. (2020). Alzheimer's disease drug development pipeline: 2020. *Alzheimer's & Dementia: Translational Research & Clinical Interventions*, *6*(1), 1–29.
9. Ono, K., Yoshiike, Y., Takashima, A., Hasegawa, K., Naiki, H., & Yamada, M. (2003). Potent anti-amyloidogenic and fibril-destabilizing effects of polyphenols in vitro: Implications for the prevention and therapeutics of Alzheimer's disease. *Journal of Neurochemistry*, *87*(1), 172–181.
10. Mehta, D., Jackson, R., Paul, G., Shi, J., & Sabbagh, M. (2017). Why do trials for Alzheimer's disease drugs keep failing? A discontinued drug perspective for 2010-2015. *Expert Opinion on Investigational Drugs*, *26*(6), 735–739.
11. Maurer, M. S., Schwartz, J. H., Gundapaneni, B., Elliott, P. M., Merlini, G., Waddington-Cruz, M., Kristen, A. V., Grogan, M., Witteles, R., Damy, T., Drachman, B. M., Shah, S. J., Hanna, M., Judge, D. P., Barsdorf, A. I., Huber, P., Patterson, T. A., Riley, S., Schumacher, J., … Rapezzi, C. (2018). Tafamidis treatment for patients with transthyretin amyloid cardiomyopathy. *New England Journal of Medicine*, *379*(11), 1007–1016.
12. Park, J., Egolum, U., Parker, S., Andrews, E., Ombengi, D., & Ling, H. (2020). Tafamidis: A first-in-class transthyretin stabilizer for transthyretin amyloid cardiomyopathy. *Annals of Pharmacotherapy*, *54*(5), 470–477.
13. Espargaró, A., Medina, A., Di Pietro, O., Muñoz-Torrero, D., & Sabate, R. (2016). Ultra rapid in vivo screening for anti-Alzheimer anti-amyloid drugs. *Scientific Reports*, *6*(1), 23349.
14. Mo, Y., Lei, J., Sun, Y., Zhang, Q., & Wei, G. (2016). Conformational ensemble of hIAPP dimer: Insight into the molecular mechanism by which a green tea extract inhibits hIAPP aggregation. *Scientific Reports*, *6*(1), 33076.
15. Andrich, K., & Bieschke, J. (2015). Natural compounds as therapeutic agents for amyloidogenic diseases. In N. Vassallo (Ed.), *Natural compounds as therapeutic agents for amyloidogenic diseases* (Vol. *863*, Issue 3). Springer International Publishing.
16. Jayamani, J., & Shanmugam, G. (2014). Gallic acid, one of the components in many plant tissues, is a potential inhibitor for insulin amyloid fibril formation. *European Journal of Medicinal Chemistry*, *85*, 352–358.
17. Sneideris, T., Sakalauskas, A., Sternke-Hoffmann, R., Peduzzo, A., Ziaunys, M., Buell, A. K., & Smirnovas, V. (2019). The environment is a key factor in determining the anti-amyloid efficacy of EGCG. *Biomolecules*, *9*(12), 1–17.
18. Lee, L.-S., Kim, S.-H., Kim, Y.-B., & Kim, Y.-C. (2014). Quantitative analysis of major constituents in green tea with different plucking periods and their antioxidant activity. *Molecules*, *19*(7), 9173–9186.
19. Altemimi, A., Lakhssassi, N., Baharlouei, A., Watson, D., & Lightfoot, D. (2017). Phytochemicals: Extraction, isolation, and identification of bioactive compounds from plant extracts. *Plants*, *6*(4), 42.
20. Konar, M., Bag, S., Roy, P., & Dasgupta, S. (2017). Gallic acid induced dose dependent inhibition of lysozyme fibrillation. *International Journal of Biological Macromolecules*, *103*, 1224–1231.
21. Ferreira, N., Saraiva, M. J., & Almeida, M. R. (2011). Natural polyphenols inhibit different steps of the process of transthyretin (TTR) amyloid fibril formation. *FEBS Letters*, *585*(15), 2424–2430.
22. Velander, P., Wu, L., Henderson, F., Zhang, S., Bevan, D. R., Xu, B., & Author, B. P. (2017). Natural product-based amyloid inhibitors. *Biochemical Pharmacology*, *139*, 40–55.
23. Ishii, T., Mori, T., Tanaka, T., Mizuno, D., Yamaji, R., Kumazawa, S., Nakayama, T., & Akagawa, M. (2008). Covalent modification of proteins by green tea polyphenol (-)-epigallocatechin-3-gallate through autoxidation. *Free Radical Biology and Medicine*, *45*(10), 1384–1394.
24. Ziaunys, M., Mikalauskaite, K., & Smirnovas, V. (2019). Amyloidophilic molecule interactions on the surface of insulin fibrils : Cooperative binding and fluorescence quenching. *Scientific Reports*, 1–10.
25. Buell, A. K., Dobson, C. M., Knowles, T. P. J., & Welland, M. E. (2010). Interactions between amyloidophilic dyes and their relevance to studies of amyloid inhibitors. *Biophysical Journal*, *99*(10), 3492–3497.
26. Lindberg, D. J., Wenger, A., Sundin, E., Wesén, E., Westerlund, F., & Esbjörner, E. K. (2017). Binding of thioflavin-T to amyloid fibrils leads to fluorescence self-quenching and fibril compaction. *Biochemistry*, *56*(16), 2170–2174.
27. Musteikyte, G., Ziaunys, M., & Smirnovas, V. (2020). Methylene blue inhibits nucleation and elongation of SOD1 amyloid fibrils. *PeerJ*, *8*, e9719.
28. Wu, C., Scott, J., & Shea, J. E. (2012). Binding of congo red to amyloid protofibrils of the Alzheimer Aβ9-40 peptide probed by molecular dynamics simulations. *Biophysical Journal*, *103*(3), 550–557.
29. Swaminathan, R., Ravi, V. K., Kumar, S., Kumar, M. V. S., & Chandra, N. (2011). Lysozyme: A model protein for amyloid research. In Advances in protein chemistry and structural biology (Vol. 84, pp. 63–111).
30. Liu, Y., Carver, J. A., Calabrese, A. N., & Pukala, T. L. (2014). Gallic acid interacts with α-synuclein to prevent the structural collapse necessary for its aggregation. *Biochimica et Biophysica Acta (BBA) – Proteins and Proteomics*, *1844*(9), 1481–1485.
31. Sakalauskas, A., Ziaunys, M., & Smirnovas, V. (2020). Gallic acid oxidation products alter the formation pathway of insulin amyloid fibrils. *Scientific Reports*, *10*(1), 1–9.
32. Roy, S., & Bhat, R. (2019). Suppression, disaggregation, and modulation of γ-Synuclein fibrillation pathway by green tea polyphenol EGCG. *Protein Science*, *28*(2), 382–402.
33. Xu, Y., Zhang, Y., Quan, Z., Wong, W., Guo, J., Zhang, R., Yang, Q., Dai, R., McGeer, P. L., & Qing, H. (2016). Epigallocatechin gallate (EGCG) inhibits alpha-synuclein aggregation: A potential agent for Parkinson's disease. *Neurochemical Research*, *41*(10), 2788–2796.
34. Visentin, C., Pellistri, F., Natalello, A., Vertemara, J., Bonanomi, M., Gatta, E., Penco, A., Relini, A., De Gioia, L., Airoldi, C., Regonesi, M. E., &

Tortora, P. (2017). Epigallocatechin-3-gallate and related phenol compounds redirect the amyloidogenic aggregation pathway of ataxin-3 towards non-toxic aggregates and prevent toxicity in neural cells and *Caenorhabditis elegans* animal model. *Human Molecular Genetics*, *26*(17), 3271–3284.
35. Rice-evans, C. A., Miller, N. J., Bolwell, P. G., Bramley, P. M., & Pridham, J. B. (1995). The relative antioxidant activities of plant-derived polyphenolic flavonoids. *Free Radical Research*, *22*(4), 375–383.
36. Hudson, S. A., Ecroyd, H., Kee, T. W., & Carver, J. A. (2009). The thioflavin T fluorescence assay for amyloid fibril detection can be biased by the presence of exogenous compounds. *The Febs Journal*, *276*(20), 5960–5972.
37. Feng, B. Y., Toyama, B. H., Wille, H., Colby, D. W., Collins, S. R., May, B. C. H., Prusiner, S. B., Weissman, J., & Shoichet, B. K. Small-molecule aggregates inhibit amyloid polymerization. *Nature Chemical Biology* 2008, *4*, 197–199, https://doi.org/10.1038/nchembio.65.
38. Sneideris, T., Milto, K., & Smirnovas, V. (2015). Polymorphism of amyloid-like fibrils can be defined by the concentration of seeds. *PeerJ*, *3*, e1207.
39. Voets, I. K., Cruz, W. A., Moitzi, C., Lindner, P., Arêas, E. P. G., & Schurtenberger, P. (2010). DMSO-induced denaturation of hen egg white lysozyme. *Journal of Physical Chemistry B*, *114*(36), 11875–11883.
40. Shammas, S. L., Knowles, T. P. J., Baldwin, A. J., MacPhee, C. E., Welland, M. E., Dobson, C. M., & Devlin, G. L. (2011). Perturbation of the stability of amyloid fibrils through alteration of electrostatic interactions. *Biophysical Journal*, 100, 2783–2791.

SUPPORTING INFORMATION

Additional supporting information may be found online in the Supporting Information section at the end of the article.

How to cite this article: Ziaunys, M., Mikalauskaite, K., Sakalauskas, A., & Smirnovas, V. (2021). Using lysozyme amyloid fibrils as a means of scavenging aggregation-inhibiting compounds. *Biotechnol. J*. e2100138. https://doi.org/10.1002/biot.202100138

NOTES

Vilniaus universiteto leidykla
Saulėtekio al. 9, III rūmai, LT-10222 Vilnius
El. p. info@leidykla.vu.lt, www.leidykla.vu.lt
bookshop.vu.lt, journals.vu.lt
Tiražas 15 egz.